Protein quality control and antibiotics:

The role of the small heat shock protein YocM and the disaggregase ClpC in *B. subtilis*

Von der Naturwissenschaftlichen Fakultät der

Gottfried Wilhelm Leibniz Universität Hannover

zur Erlangung des Grades

Doktor der Naturwissenschaften (Dr. rer. nat.)

genehmigte Dissertation von

Ingo Hantke, M. Sc.

2019

Diese Arbeit wurde am Institut für Mikrobiologie der Leibniz Universität Hannover im Rahmen der Hannover School for Biomolecular Drug Research (HSBDR) durchgeführt.

Referent: Prof. Dr. rer. nat. Kürşad Turgay

Korreferent: Prof. Dr. rer. nat. Jens Boch

Korreferent: PD. Dr. rer. nat. Axel Mogk

Tag der Promotion: 16.09.2019

Für meine Familie

Zusammenfassung

Schlagworte: Proteinqualitätskontrolle, bakterielle Stressantwort, Antibiotika, *Bacillus subtilis*

Alle lebenden Zellen müssen Fluktuationen von abiotischen Umweltfaktoren (z.B. Temperatur, Salzgehalt etc.) und daraus resultierendem proteotoxischen Stress entgegenwirken. Ein funktionales Proteom wird dabei durch die Aktivität verschiedener Chaperone und Proteasen gewährleistet. Dieses Proteinqualitätskontrollsystem (PQK) ist hoch konserviert. Einen Teil bilden kleine Hitzeschockproteine (*sHsp*), die Proteine vor Entfaltung schützen und deren Rückfaltung in Kooperation mit Chaperonsystemen begünstigen können. In dieser Arbeit wurde YocM als erstes Stress relevantes *sHsp* in *B. subtilis* identifiziert und dessen protektive Rolle während eines Salzschocks charakterisiert. Zudem wurde ein YocM-mCherry Fusionsprotein als *in vivo*-Aggregatmarker etabliert. Mittels dieses Markers wurde McsB als entscheidendes Adapterprotein für die vom Hsp100/Clp Protein ClpC vermittelte Disaggregation von Proteinaggregaten unter Hitzestress identifiziert und gleichzeitig dessen Proteinargininkinase als essentiell für ebenjene Aktivität erkannt. Dabei stellte sich generell die Disaggregation und Rückfaltung im Vergleich zu der Degradation von Proteinaggregaten als bedeutsamer heraus.

Kürzlich wurden einige Antibiotika charakterisiert, welche auf ClpC als zentralen Punkt in der PQK abzielen (z.B. Cyclomarin). In dieser Arbeit konnte gezeigt werden, dass der Austausch einer Aminosäure in ClpC (F436A) zu vermehrter Bildung von Proteinaggregaten sowie zu erheblich gestörtem Wachstum und sogar Zelltod führt. Diese durch ClpC vermittelte Toxizität untermauert die Eignung von ClpC als Ziel für Antibiotika. Im Folgenden wurde ein *target-based screen* in *B. subtilis* etabliert und als *proof of concept* validiert. Neue Antibiotika, die auf ClpC und die PQK abzielen, können so schnell selektiert und anschließend auf deren Effekt auf Gram-positive Pathogene weiter getestet werden.

Abstract

Keywords: protein quality control, bacterial stress response, antibiotics, *Bacillus subtilis*

All living cells have to deal with fluctuations of abiotic factors, such as temperature and salt content, which can cause different types of proteotoxic stress. A functional proteome depends on an intricate protein quality control network (PQC) of chaperones and proteases, which is highly conserved in all domains of life. As one part of the PQC system, small heat shock proteins (sHsp) protect proteins from unfolding and facilitate refolding in cooperation with molecular chaperons. During this work, YocM was identified as the first stress-related sHsp of *B. subtilis*, ensuring survival of cells during salt shock. Furthermore, a YocM-mCherry fusion protein was established as a protein aggregate marker. Thereby, McsB was identified as the main adaptor protein for disaggregation of subcellular protein aggregates by the Hsp100/Clp protein ClpC during heat stress, which was dependent on its protein arginine kinase activity. In general, protein disaggregation instead of degradation was observed to be the predominant process regarding protein aggregate removal in stress response in *B. subtilis*.

ClpC as a central player of PQC and stress response was recently identified as a target for various antibiotic compounds (e.g. cyclomarin). During this work it was demonstrated that a *clpC* F436A mutation led to severe formation of protein aggregates *in vivo* and substantially impaired survival of *B subtilis*, which was dependent on the presence of McsB. As this deregulation of ClpC by exchange of only one amino acid residue displayed such a toxic phenotype, ClpC was confirmed to be an adequate target for antibiotics. Consequently, a ClpC-target based screen was successfully established and validated in *B. subtilis* as proof of concept to discover and characterize novel antibiotics compounds that address the PQC system in Gram-positive pathogenic bacteria.

List of abbreviations

A	Adenosine
AAA+	ATPase associated with diverse cellular activities
AB	Antibody
Ac	Acetate
ACD	α-crystallin domain
Amp	Ampicillin
AP	alkaline phosphatase
APS	ammonium persulfate
ATP	adenosine triphosphate
BCIP	5-bromo-4-chloro-3-indoyl-phosphat
BGSC	*Bacillus* Genetic Stock Center
BSA	bovine serum albumin
C	Cytosine
Cat	chloramphenicol acetyltransferase
cfu	colony forming units
Cm	Chloramphenicol
CM	competence medium
CTD	carboxyl-(C)-terminal domain
CV	column volume
Da	Dalton
DEPC	diethylpyrocarbonate, diethyl dicarbonate
DNA	deoxyribonucleic acid
dNTP	deoxynucleotide triphosphate
DMF	Dimethylformamide
DMSO	dimethyl sulfoxide
DTT	1,4-dithio-D-threitol
ECF	enhanced chemifluorescence
ECF	enhanced chemoluminescence
EDTA	ethylenediaminetetraacetic acid
ery	Erythromycin
G	Guanosine
GB	glycine betaine
GFP	green fluorescent protein
HEPES	(4-(2-hydroxyethyl)-1-piperazineethanesulfonic acid)
(s)HSP	(small) Heat shock protein
IbpA	inclusion body protein A
IMAC	immobilized metal ion affinity chromatography
IPTG	isopropyl β-D-1 thiogalactopyranoside
Kan	Kanamycin
kb	Kilobases
kDa	Kilodalton
LB	Lysogeny Broth / Luria Bertani
MDH	malate dehydrogenase
MOPS	3-(N-morpholino)propanesulfonic acid
NADH	nicotinamide adenine dinucleotide
NBT	nitro blue tetrazolium chloride
NTA	nickel nitrilotriacetic acid
NTD	amino-(N)-terminal domain
OD$_{600}$	optical density at 600 nm
OV	overnight cell growth
PAGE	polyacrylamide gel electrophoresis
PBS	phosphate buffered saline
PC	phase contrast microscopy

PCR	polymerase chain reaction
PEP	phosphoenole pyruvate
PIPES	piperazine-N,N′-bis(2-ethanesulfonic acid)
PMSF	phenylmethanesulfonyl fluoride
ROS	reactive oxygen species
rpm	rotations per minute
RT	room temperature
SDS	sodium dodecyl sulfate
SMM	spizizen minimal medium
Spec	Spectinomycin
SSC	saline sodium citrate buffer
SUMO	small ubiquitin like modifier
T	Thymidine
TAM	triple adaptor mutant
TBS	tris buffered saline
TCA	trichloroacetic acid
TE	tris EDTA
TEMED	N,N,N',N'-tetramethylethane-1,2-diamine
TES	tris EDTA salt
tet	Tetracycline
TRIS	tris(hydroxymethyl)aminomethane
U	Uracil
Ulp	Ubiquitin like protease
UV	ultra violet
v/v	volume per volume
w/v	weight per volume
wt	Wildtype strain

Table of content

1. Introduction

Life is stressful. This applies to all living organisms known to – and including – mankind. Although many factors provoke different types of stress, e.g. oxidative stress, heat stress, salt stress, UV and starvation, one underlying aspect is the negative impact on the protein homeostasis (Figure 1). Hence, maintaining the dynamic equilibrium of the proteome by a functional protein homeostasis is a general and ubiquitous aim of all living cells. These protein quality control (PQC) systems consist of a network of chaperones and proteases to ensure a functional proteome and the viability of the cell. Molecular chaperones promote protein folding and simultaneously protect unfolded proteins from aggregation e.g. by holding, shielding and/or facilitating refolding. At the same time, proteases degrade unfolded and aggregated proteins to remove them from the system (Figure 1) (Bukau et al., 2006; Hartl and Hayer-Hartl, 2009, 2002; Wickner et al., 1999).
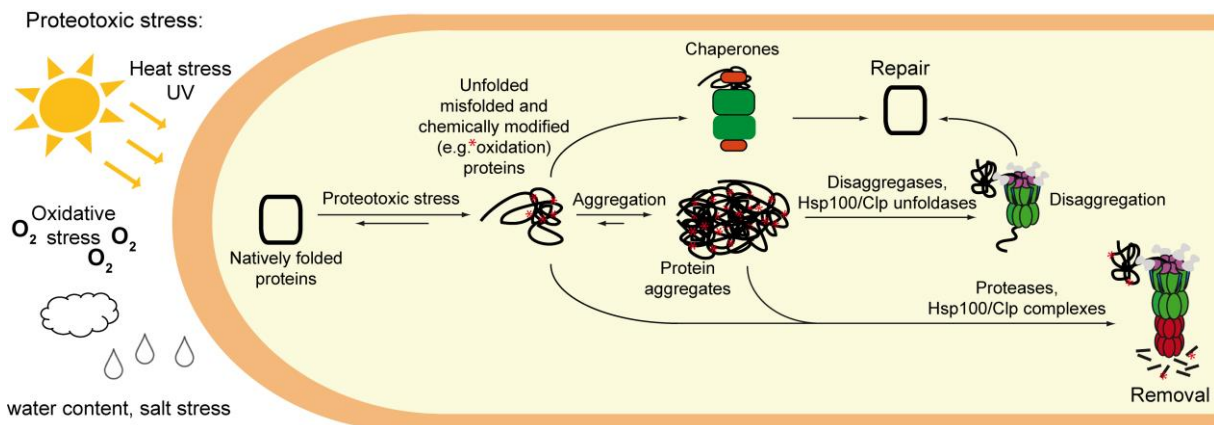
Figure 1: Simplified overview of general protein quality control mechanisms dealing with proteotoxic stress.

Fluctuations in abiotic factors (heat, UV, water content etc.) cause proteotoxic stress leading to unfolding and misfolding of proteins and their subsequent aggregation. The functionality of the proteome is maintained a) by chaperones (e.g. DnaK, GroEL), which refold their substrates into the native structure (Repair) and b) by proteases (e.g. ClpCP), which degrade them (Removal).

1.1.   High salinity and salt stress

Like all living cells, bacteria have to maintain and regulate their intracellular osmotic pressure, especially when facing a salt shock (Csonka, 1989). An increase of external salt concentrations leads to water efflux, which reduces the volume of the cytoplasm, thereby increasing the concentration of intracellular molecules (molecular crowding) and changing the turgor pressure. To deal with these circumstances, bacteria in general follow two main pathways: the salt-in and/or salt-out strategy (Kempf and Bremer, 1998; Oren, 2008).

The salt-in strategy follows the idea to realize an osmotic equilibrium by permanently increasing the cytoplasmic salt concentration. This mechanism is distributed among, but not limited to, members of the *Halobacteriaceae* (Martin et al., 1999). Living in an environment of elevated salinity leads to a constant passive efflux of water to restore an osmotic equilibrium. Thus, these organisms permanently possess high intracellular levels of K^+ ions to reduce and/or prevent this salt induced efflux of water. However, elevated levels of K^+ cause severe changes in the intracellular ion composition and therefore have a major influence on stability and interaction of macromolecules, e.g. by strengthening hydrophobic interactions. As these organisms do not exchange the K^+ ions with physiologically less interfering compounds such as compatible solutes (salt-out strategy), many halotolerant archaea have evolved their proteins towards acidic side chain residues, which then use K^+ ions as their respective counterparts. This enhances solvation, but simultaneously restricts optimal growth to a permanently elevated salinity (Lanyi, 1974; Mevarech et al., 1977). Collectively, the salt-in strategy describes life with increased amounts of intracellular ions such as K^+ and, as a consequence of the unfavorable ion composition, substantially adapted macromolecules.

Compared to the salt-in strategy, the salt-out strategy does not involve permanent adaptation towards increased salinity and is more common. As a fast response towards an osmotic upshift, the uptake of K^+ ions reduces the efflux of water and the decrease of turgor pressure. As a second phase and more long-term adaptation to an increased external osmolality, bacteria accumulate compatible solutes and excrete the previously accumulated K^+ ions (Kempf and Bremer, 1998; Roberts, 2005; Wood, 2015). These compatible solutes can be accumulated by *de novo* biosynthesis, uptake and transformation of an imported precursor, respectively. They are mostly small organic, polar and zwitterionic molecules like non-ionic carbohydrates, amino acids and their derivatives as well as polyols (Figure 2) and described as 'compatible' since cellular functions are not impaired even at substantially elevated intracellular concentrations. Simultaneously, they stabilize e.g. inter- and intramolecular protein-protein interactions and are often referred to as osmoprotectants (Boch et al., 1996; Ignatova and Gierasch, 2006; Low, 1985). Due to the underlying stabilizing effect, these molecules have, despite from salt stress, also been identified to protect macromolecules against heat and cold stress (Bashir et al., 2014b, 2014a; Boch et al., 1996; Diamant et al., 2003, 2001; Hoffmann and Bremer, 2011; Holtmann et al., 2003; Holtmann and Bremer, 2004; Kempf and Bremer, 1998; Moses et al., 2012; Plaza del Pino and Sanchez-Ruiz, 1995; Singer and Lindquist, 1998).
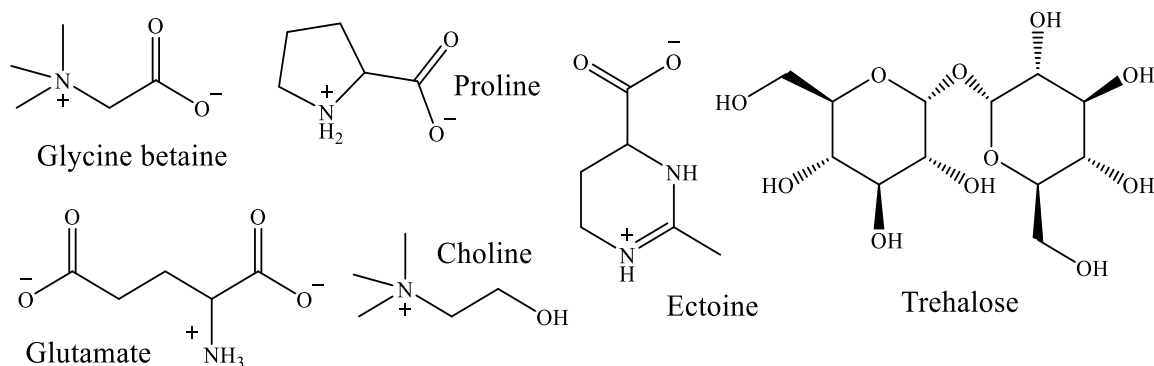
Figure 2: Selected compatible solutes.

Compatible solutes are generally small organic, polar and zwitterionic molecules like non-ionic carbohydrates and (derivatives of) amino acids. Especially glycine betaine and proline are the two major compatible solutes used by *B. subtilis*.

1.1.1. Salt stress defense strategies in *B. subtilis*

As a soil-dwelling organism, *B. subtilis* is exposed to frequent fluctuations in external salinity due to e.g. desiccation, rainfall or flooding. To protect itself from a potential salt shock, *B. subtilis* follows the described classic salt out two step process (see 1.1) starting, as a first response, with the fast uptake of K^+ ions from the environment, increasing its intracellular pool from about 350 mM to 720 mM in minimal medium (Whatmore et al., 1990; Whatmore and Reed, 1990). Thus, *B. subtilis* possesses three K^+ uptake systems with different KtrCD as a low-affinity and KtrAB as well as KimA as high-affinity K^+ transporters in order to allow the optimal response to various environmental circumstances (Figure 3) (Gundlach et al., 2017; Holtmann et al., 2003). Remarkably, transcription of the *ktrAB* and *kimA* is regulated by a riboswitch which is responsive to cyclic di-AMP (Gundlach et al., 2017; Nelson et al., 2013).
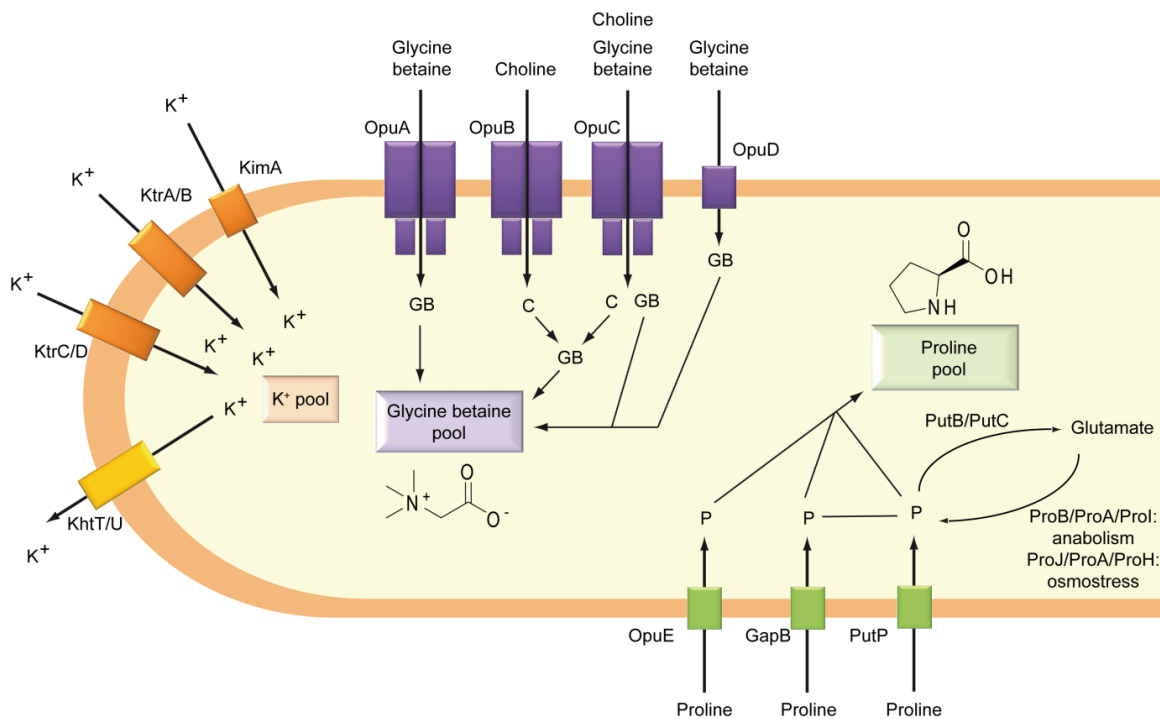
Figure 3: Overview of *B. subtilis* K$^+$, proline and glycine betaine uptake systems.

During osmotic stress, K$^+$ ions are taken up by *B. subtilis* as a first response by the three uptake systems KtrA/B, KtrC/D and KimA. Subsequently, K$^+$ is exchanged with compatible solutes to prevent the disturbance of cellular processes by K$^+$ ions. At that, export of K$^+$ is poorly understood and performed by cation-proton antiporter KhtT/U. As one of the two major compatible solutes in *B. subtilis*, glycine betaine (GB) can be taken up by the osmotically regulated transport systems OpuA, OpuC and OpuD, or synthesized from a precursor molecule like choline (C), which is imported by OpuB and OpuC. Proline (P) is the second major compatible solute and can, besides from being an osmoprotectant (imported by OpuE), be taken up as a nutrient by PutP and/or GabP. Furthermore it can be converted to glutamate by PutB/C and vice versa be generated from glutamate as precursor by either the ProH/A/J pathway (to serve as an osmoprotectant) or by the ProB/A/I pathway (during regular metabolism). Adapted from (Hoffmann and Bremer, 2016).

Uptake of high levels of intracellular K$^+$ is beneficial as a first line of defence to prevent substantial water efflux regarding osmotic stress, but would eventually affect viability of the cell by disturbing general processes such as protein-protein or protein-DNA interactions and enzyme activity in general. Thus, this first response is followed by the export of K$^+$ and simultaneous uptake and synthesis of compatible solutes. However, the export of K$^+$ in *B. subtilis* is only poorly understood with one cation-proton antiporter KhtTU, which is responsive to salt stress (Figure 3) (Fujisawa et al., 2007; Hahne et al., 2010).

On the contrary, the different pathways and mechanisms of synthesis and uptake of the various compatible solutes have been studied more extensively, where glycine betaine and proline have been identified as the two main compatible solutes regarding *B. subtilis* (Figure 2 and Figure 3) (Whatmore et al., 1990). When grown in the presence of 1 mM glycine betaine, *B. subtilis* is able to accumulate this compatible solute to intracellular concentrations reaching over 0.6 M upon salt shock (Whatmore et al., 1990). On the one hand this accumulation is the result of the three high-affinity transporters OpuA, OpuC or OpuD, albeit OpuC can import other osmoprotectants as well (Kappes et al., 1996; Kempf and Bremer, 1995). On the other hand it is important to note that besides from glycine betaine, its precursor molecule choline can be imported by OpuB and subsequently oxidized into glycine betaine (Boch et al., 1996; Kappes et al., 1999; Nau-Wagner et al., 1999).

Proline is the second major compatible solute used by *B. subtilis* and was observed to accumulate to levels up to 0.5 M upon salt shock starting from less than 20 mM in unstressed cells (Whatmore et al., 1990). It is imported by the OpuE transporter during osmotic stress or by PutP as a nutrient, albeit it can additionally be used as a nutrient when converted to glutamate by PutBC (Figure 3) (Moses et al., 2012; von Blohn et al., 1997). Vice versa, certain amino acids such as glutamate can be transformed into proline involving different biosynthetic pathways regarding either osmotic stress or during regular proline biosynthesis (Zaprasis et al., 2015). Furthermore, GabP as a third proline uptake system has been characterised, which belongs to the family of γ-amino butyrate (GABA) transport systems (Zaprasis et al., 2014). Collectively, *B. subtilis* has developed many ways to accumulate compatible solutes as part of their salt-out strategy such as uptake, conversion of a precursor or *de novo* synthesis.

In addition to their crucial role in salt stress, these compatible solutes were identified to play a minor role in heat stress as well. The addition of chemical chaperones relieved the thermosensitivity of a *dnaK* mutant and reduced the concurrent intracellular aggregate formation (Caldas et al., 1999; Chattopadhyay et al., 2004). Furthermore, glycine betaine was identified to positively affect the activity of different *E. coli* chaperone systems such as DnaK, GroEL or ClpB *in vitro* (Diamant et al., 2001).

In *B. subtilis*, this overlap of heat and salt stress related defensive mechanisms becomes apparent regarding salt and thermotolerance development, which describes the survival of a lethal heat or salt shock after a short exposure to a milder pre-shock. Thereby, a mild heat pre-shock can cross-protect against a severe salt stress and a mild salt stress pre-shock can cross-protect against a severe heat shock, suggesting that both stress response processes are intricately connected (Höper et al., 2005; Völker et al., 1992). This priming process depends on the ability of the cellular stress response and protein quality control system to prepare and protect their cells against otherwise lethal stresses (Runde et al., 2014; Völker et al., 1992). A connecting factor of heat and salt stress might be the general stress sigma factor SigB, which is important for *B. subtilis* heat shock response and is also directly involved in salt stress response, e.g. by controlling transcription of some osmoregulated transporter systems (Hahne et al., 2010; Hecker et al., 2007; Höper et al., 2006, 2005; Spiegelhalter and Bremer, 1998; Steil et al., 2003; von Blohn et al., 1997). These observations suggest a close connection of heat and salt stress in nature.

1.2.   Small heat shock proteins

Salt stress and heat stress can substantially affect the functionality of the proteome. Therefore, all organisms possess a protein quality control (PQC) system to counteract any kind of proteotoxic stress, continuously monitoring and maintaining protein homeostasis. One part of theses PQC systems are small heat shock proteins (sHsp), which occur ubiquitously in all domains of life and have even been detected in some marine viruses (Maaroufi and Tanguay, 2013). Although not every individual species has been identified to possess sHsps, their average number per organism ranges from 1-2 in most bacteria with up to 36 in plants (Haslbeck and Vierling, 2015; Waters, 2013; Waters et al., 2008).

As their name suggests, these sHsps are rather small in size with a range of 12 to 42 kDa. Despite their small size sHsps have the ability to form higher oligomeric structures, which is considered as crucial for their activity. These oligomeric structures can vary from the formation of dimers as the underlying building block up to large 36mers (Basha et al., 2013; Bepperling et al., 2012; Delbecq and Klevit, 2013). The formation of this underlying dimer is thought to be predominantly dependent on the highly conserved α-crystallin domain (ACD), which is embedded between the N-terminal domain (NTD) and the C-terminal domain (CTD) and the characteristic feature of the sHsp family. The flanking regions, especially a I-x-I/V motif in the CTD, are often considered as essential for the assembly of higher oligomers (Basha et al., 2012; Chen et al., 2010; McHaourab et al., 2012). However, although the number of available structures of sHsps is constantly increasing, exact recognition sites still remain elusive and the prediction of their oligomeric state based on their DNA or protein sequence has not been achieved yet (Jaspard and Hunault, 2016).

1.2.1. Molecular mechanisms of sHsps in protein quality control

The molecular mechanisms by which sHsps function as chaperones are not well understood. However, the emerging picture is that, as part of the PQC network, they can act alone, but in addition support and facilitate the activity of other ATP dependent chaperones, while sHsps *per se* act ATP independently (Figure 4). They interact with misfolding proteins, protecting them from irreversible aggregation. Furthermore, they stabilize early unfolding intermediates, which does not only maintain partial enzyme activity ('holdase' activity), but also allows spontaneous refolding (Figure 4) (Basha et al., 2012; Ehrnsperger et al., 1997; Horwitz, 1992; Mchaourab et al., 2002; Stromer et al., 2003).
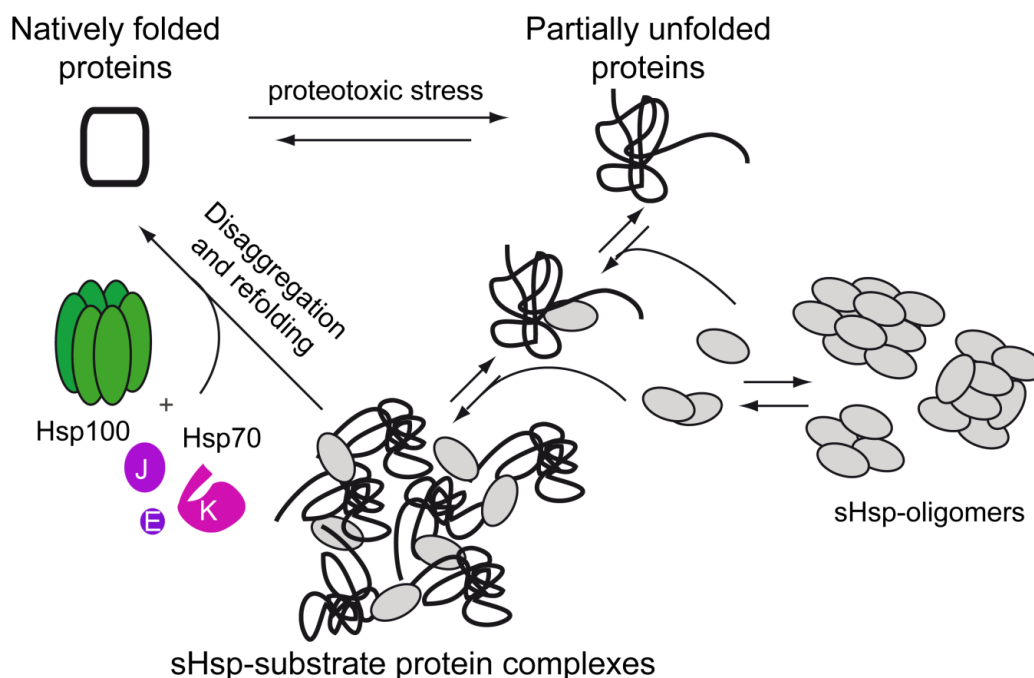
Figure 4: Model of the role of small heat shock proteins in protein homeostasis.

Small heat shock proteins (sHsp) occur in different oligomeric states. They interact with partially unfolded substrate proteins keeping them in an intermediate, partially active state. Concurrently they form higher oligomeric sHsp-substrate protein complexes, which facilitates disaggregation and refolding by molecular chaperones (e.g. Hsp100/ClpB and Hsp70/DnaK system) (adapted from (Haslbeck and Vierling, 2015)).

Moreover, disaggregation and refolding of misfolded proteins by chaperones systems like ClpB and/or DnaKJE can be enhanced by the presence of sHsp IbpA/B in protein aggregates in *E. coli*, as well as Hsp26 in yeast (Figure 4) (Haslbeck et al., 2005a, 2005b; Mogk et al., 2003b, 2003a; Żwirowski et al., 2017). The formation of these larger sHsp-substrate complexes is considered as part of their activity in general (Figure 4) (Basha et al., 2013; Bepperling et al., 2012). Recently, specific sHsps were observed to allow controlled protein sequestration to subcellular aggregates in eukaryotic cells, which entitled those sHsps as protein aggregases and broadens their role in PQC (Specht et al., 2011; Ungelenk et al., 2016). However, the exact recognition sites for binding of substrate proteins as well as oligomerisation *per se* have not been identified yet (Basha et al., 2006; Haslbeck and Vierling, 2015; Hochberg et al., 2014; van Montfort et al., 2001).

As their name suggests, sHsp are often involved in protection from heat stress (Giese and Vierling, 2002; Haslbeck et al., 2005a; Krajewski et al., 2014). As actual heat stress is relative, the activity range of sHsps depends on the physiological temperature of the organism (Kim et al., 1998; Laksanalamai and Robb, 2004; Lelj-Garolla and Mauk, 2006). In general, their mode of activation can be categorized into a) being synthesized upon stress or b) a simple change in equilibrium of already present sHsp oligomers, revealing substantially more substrate binding sites (Figure 4) (Haslbeck et al., 2008, 1999; McHaourab et al., 2009; Posner et al., 2012).

Some sHsps have also been identified to play a role in various other kinds of stress, including e.g. desiccation, osmotic stress and high salinity (Jiang et al., 2009; Khaskheli et al., 2015; Kuang et al., 2017; Mu et al., 2013; Ruibal et al., 2013). While some sHsps were shown to have a more specific role (e.g. salt stress) (Muthusamy et al., 2017), most take part in various

stress responses (Li et al., 2016; Paul et al., 2016; Ruibal et al., 2013; Sandhu et al., 2017; Sarkar et al., 2009; Wang et al., 2017a; Zhao et al., 2018). This is especially true for plants, which, as sessile organisms, always have to withstand the different types of stress without the possibility of simply avoiding it by moving away. Therefore, it appears reasonable that plants have developed a broader repertoire of different sHsps during evolution (Waters, 2013; Waters et al., 2008). Furthermore, it was demonstrated in many studies that both heterologous and homologous overexpression of sHsps led to a protective phenotype regarding multiple types of stress. This clearly indicates that although a sHsp may have evolved a more specific role under distinct circumstances, it can still contribute to protein protection in general (Kim et al., 2013; Salas-Muñoz et al., 2012; Tian et al., 2012; Wang et al., 2017b).

1.2.2. Potential sHsps in *B. subtilis*

Small heat shock proteins occur in all domains of life. In the Gram-positive model organism *B. subtilis*, three potential sHsp genes (*yocM*, *cotM*, *cotP*) encoding the sHsp-characteristic conserved α-crystallin domains were detected by sequence alignments (Reischl et al., 2001). Two of them (*cotM*, *cotP*) were identified as important in spore formation and it could subsequently be demonstrated that they participate in the formation of proteinaceous spore coat structures during spore development (Henriques et al., 1997; McKenney et al., 2013, 2010; McKenney and Eichenberger, 2012; Wang et al., 2009). The transcription of the remaining putative small heat shock *yocM* did not appear to be under heat shock control, thus it was not considered as part of the PQC (Reischl et al., 2001). Recently, whole genome transcriptome studies gave insights into the regulation pattern of *yocM*, revealing it to be substantially different compared to the more similar expression profiles of *cotM* and *cotP*, which both display strong bias towards upregulation upon sporulation conditions (Nicolas et

al., 2012). However, transcription of *yocM* was observed to be generally induced by salt stress (Nicolas et al., 2012) and additionally classified as part of SigW regulon, which is induced by cell wall and membrane stress and simultaneously responsive to salt stress (Zweers et al., 2012). However, it is not clear if and how YocM (or CotM and CotP) as a potential sHsp is part of the cellular chaperone network in *B. subtilis*.

1.3.   Chaperone systems

In addition to small heat shock proteins, whose protective activities are considered to be rather passive, the PQC system also consists of larger molecular chaperone systems to actively facilitate protein folding. These molecular chaperones have various operational areas ranging from the stabilization of nascent peptide chains during translation (trigger factor) to the prevention of protein aggregation and the active refolding of their substrate proteins (Hartl and Hayer-Hartl, 2002). The underlying substrate binding ('holding') activity of chaperones, which *per se* already prevents interaction of exposed hydrophobic peptide chains due to e.g. heat stress, is often ATP-independent, whereas active refolding of substrate proteins is energy-consuming and hence requires ATP (Hartl and Hayer-Hartl, 2002; Sauer and Baker, 2011).

One prominent example is the Hsp70/DnaK system, which performs an ATP dependent 'substrate bind and release' cycle to keep partially unfolded substrate proteins in an intermediate folded state that is prone to subsequent spontaneous refolding upon release (e.g. Hsp70/DnaK-system) (Hartl and Hayer-Hartl, 2002; Hesterkamp et al., 1996). As another example, chaperonins (Hsp60) bind and completely shield their substrate proteins from the cytoplasm favoring correct refolding by providing a beneficial environment (Hayer-Hartl et al., 2016). Furthermore, Hsp100/Clp proteins unfold misfolded and aggregated proteins by

translocating their substrate proteins through a barrel like structure. These chaperones often occur in a complex with of an additional downstream-acting protease to directly remove their substrates, e.g. damaged proteins or aggregates, from the cell (Figure 1, see 1.4).

1.4.   Protease complexes

The proteome is a dynamic equilibrium of synthesis and degradation, where every protein is synthesized with a certain purpose. After this purpose has been fulfilled it can be beneficial to actively remove the protein and re-use its amino acids to synthesize another peptide chain. However, this process at first glance might appear unfavorable regarding the energy needed for degradation in the first place (Hoffman and Rechsteiner, 1996; Sauer and Baker, 2011). Moreover, during the lifetime of a protein, its polypeptide chain can accumulate damages such as oxidations of amino acid residues, which impair or abolish its structure and/or function. Consequently, refolding by chaperones to restore its activity is not possible and the degradation by proteases becomes more important. The degradation of these non-functional and/or aggregated proteins is part of the PQC and termed general proteolysis. Remarkably, proteolysis is also performed as a regulatory mechanism. In this regulatory proteolysis, the same proteases involved in general proteolysis are responsible for adjusting the levels of substrate proteins e.g. to influence gene expression by modulating the amounts of a transcription factor or regulator (Battesti and Gottesman, 2013; Elsholz et al., 2017; Machiels et al., 1997; Wu et al., 2000).

1.4.1. AAA+ proteases and Hsp100/Clp proteins

In eukaryotes, the major protease is the proteasome. The proteasome is a compartmentalized proteolytic machinery consisting of a core particle flanked with two regulatory particles. As degradation of native proteins would be detrimental, the regulatory particles only detect specifically ubiquitin marked proteins and allow their subsequent translocation into the core particle (Hershko et al., 1983). The core particle consists of a barrel like structure, which guarantees a shielded environment for degradation of the substrate proteins, as the hydrolyzing amino acid residues are pointing inside (DeMartino and Slaughter, 1999; Voges et al., 1999).

The eukaryotic proteasome and the intracellular proteases of bacteria are part of the AAA+ (ATPase associated with various cellular activities) superfamily. These protease complexes form hexameric barrel-like structures, unfold and translocate their respective substrates into a central axial pore, thus functioning in an equivalent way to the heptameric proteasome (Figure 1 and Figure 5). This translocation of a substrate is driven by conformational changes due to cycles of ATP binding and hydrolysis (Martin et al., 2005). Interaction is especially facilitated by specific peptide loops that lay inside of the barrel like structure and transmit the generated force onto the substrate (Hinnerwisch et al., 2005).
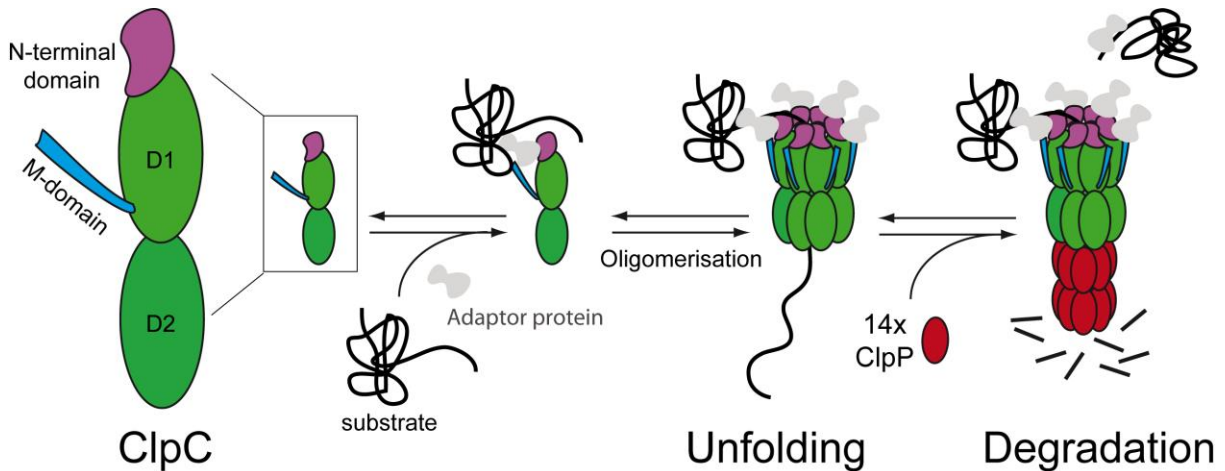
Figure 5: Adaptor protein mediated activation of *B. subtilis* ClpC.

Monomeric ClpC consists of an N-terminal domain (NTD, purple), two ATPase domains D1 and D2 (green) and a middle domain (M-domain, blue). By interaction with the NTD, adaptor proteins (grey) target substrate proteins (black line) towards ClpC and induce the oligomerisation. Subsequently, ClpP is able to constitute a double heptameric proteolytic chamber underneath the ClpC hexamer to form the now active ClpCP complex (adapted from (Elsholz et al., 2017)).

In general, these protease complexes contain one conserved 200-250 amino acid AAA+ module (D1) (e.g. Lon, FtsH, ClpX), but can consist of an additional one (D2), which leads to the formation of a double ring structure when oligomerized (e.g. ClpA, ClpC) (Figure 6) (Kirstein et al., 2009b; Sauer and Baker, 2011). It was observed, that the second ring owns a stronger unfoldase activity (Kress et al., 2009). Within one AAA+ module, there are specific Walker A and Walker B motifs to bind and hydrolyze ATP, respectively. A mutation within the Walker B motif, where the essential glutamate for hydrolysis of ATP is exchanged with e.g. an alanine residue, separates the event of ATP binding from subsequent hydrolysis and hence is often used as an ATP and substrate trapping mutant (Kirstein et al., 2006; Weibezahn et al., 2003).

Furthermore, theses protease complexes can be categorized by specific N-terminal and/or intermediate domains, which are only present in some subtypes of this larger family. One example is the zinc binding motif within the N-terminal domain of ClpX species, which is

absent in ClpA species and indicates a specific susceptibility towards oxidative stress (Figure 6) (Wojtyra et al., 2003). In addition, the linker or middle domain (MD), which intercepts the AAA+ modules in ClpC and ClpB species, is absent in protease complexes with only one AAA+ module and ClpA species (see 1.4.2 and Figure 6) (Haslberger et al., 2007; Kress et al., 2009; Sauer and Baker, 2011). Especially these structural features demonstrate that, although structurally rather similar, these protease complexes can be functionally quite diverse.

In general, AAA+ proteins can either consist of one polypeptide chain (e.g. AAA+ proteases Lon and FtsH) or are formed by an association of an unfoldase attached to a protease complex (Hsp100/Clp proteins). Remarkably, one protease can often associate with different Hsp100/Clp proteins to form a functional proteolytic complex (Figure 5 and Figure 6) (Sauer and Baker, 2011). However, the way these complexes are formed is quite diverse when comparing different bacterial species. In *B. subtilis*, the Hsp100/Clp proteins oligomerize only in the presence of the respective adaptor protein, subsequently allowing ClpP to also oligomerize and assemble to a complete double heptameric proteolytic complex attached to the hexameric unfoldase (Figure 5 and Figure 6) (Kirstein et al., 2006). In *E. coli*, a stable complex of the protease can already form without the presence of an oligomerized unfoldase to attach to (Kress et al., 2007).
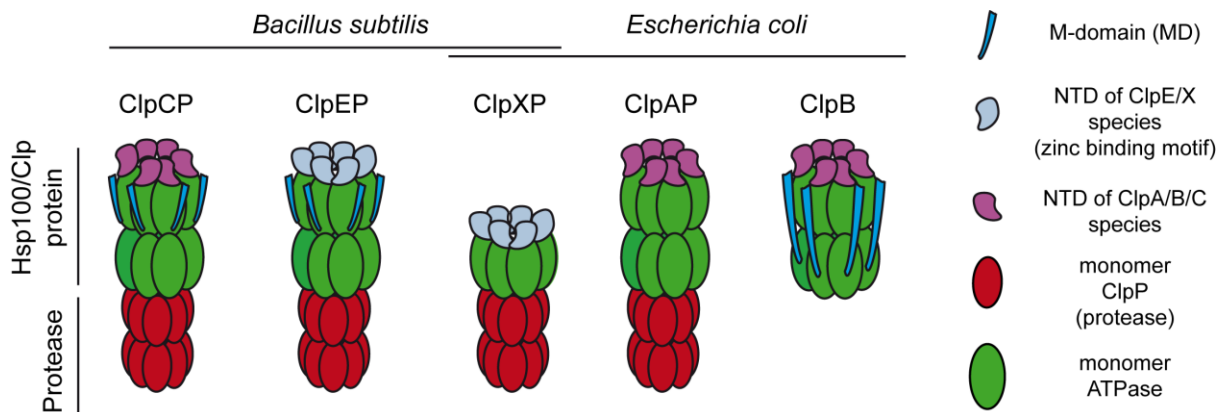
Figure 6: Structural organization of selected Hsp100/Clp proteins of *B. subtilis* and *E. coli*.

B. subtilis possesses, among others, the three Hsp100/Clp proteins ClpC, ClpE and ClpX, which can all associate with ClpP (red) to form a proteolytic complex. *E. coli* does also have a ClpX species, but lacks a variant of ClpE and ClpC. The stand-alone disaggregase ClpB of *E. coli* is absent in *B. subtilis*. Other proteases and protease complexes such as Lon and FtsH are not shown within this selection.

Regardless of the species, the interaction of the Hsp100/Clp protein and the respective protease such as ClpP is facilitated by specific surface loops containing a [LIV]-G-[FL] motif, which are pointing downwards (Kim et al., 2001; Liu et al., 2013). Regarding *B. subtilis*, the central protease ClpP associates with the different Hsp100/Clp unfoldases ClpC, ClpX and ClpE (Figure 6) (Gerth et al., 2004). For ClpC and ClpE species the interaction is predominantly based on the tripeptide sequence VGF, while ClpX species contain an analogous IGF motif (Kim et al., 2001). When comparing the three unfoldases regarding other their structural features it also becomes obvious that while both ClpC and ClpE possess a similar linker/middle domain (MD), ClpX and ClpE share a comparable N-terminal domain (Figure 6).

When attached to ClpP, all three Hsp100/Clp proteins take part in various kinds of general and regulatory proteolysis: ClpXP degrades ssrA-tagged substrate proteins and is involved in oxidative stress response (M. Nakano et al., 2002; S. Nakano et al., 2002; Wiegert and Schumann, 2001), ClpEP was observed to only play a role under severe heat shock conditions

(Gerth et al., 2004; Miethke et al., 2006), and ClpCP is a key player in competence development (see 1.4.3), heat shock response (see 1.4.4) and sporulation (Derré et al., 1999; Kirstein et al., 2007; Krüger et al., 2001; Msadek et al., 1994; Pan et al., 2001; Turgay et al., 1998).

1.4.2. The special case of the absent disaggregase ClpB in *B. subtilis*

When comparing the various AAA+ proteins from different bacterial species it becomes obvious that *B. subtilis* lacks a stand-alone disaggregase such as ClpB in *E. coli* or Hsp104 in yeast (Figure 6). These ClpB species lack the specific peptide surface loop to interact with ClpP and are thus *per se* incapable of forming a proteolytic complex (Gerth et al., 2004; Kirstein et al., 2009b; Mogk et al., 2015; Tanner et al., 2018). However, a genetically engineered variant where ClpB was fused to the ClpP protease was capable of substrate degradation indicating the possibility of a switch between disaggregation and proteolytic degradation of substrate proteins upon attachment of ClpP (Weibezahn et al., 2004, 2003). Remarkably, *B. subtilis* appears to be the only species within its genus that has been identified to possess ClpC, but not ClpB (Namy et al., 1999).

There are certain hints that *B. subtilis* ClpC has a functional role independent of ClpP, suggesting that ClpC might act as the *B. subtilis* 'ClpB'. *In vitro*, ClpC (+ its adaptor MecA, see 1.4.3) has been observed to bind to Spo0A thereby repressing its target promotors and inhibiting transcription independent of ClpP (Tanner et al., 2018). Furthermore, the occurrence of fewer ClpP tetradecamerix complexes (~1200 per cell) than hexameric ClpX, ClpC and ClpE complexes (~1750 per cell) was estimated in the cell (Gerth et al., 2004). However, as the individual ATPase complexes could presumably attach to both sides of ClpP as observed *in vitro* for ClpX and ClpA in *E. coli*, all unfoldases could at least hypothetically

be associated with a protease (Grimaud et al., 1998; Ortega, 2002). Regarding *B. subtilis*, hints towards a mixed ClpX-ClpP-ClpE complex were obtained *in vitro*, but not further characterized regarding physiological importance (Gerth et al., 2004).

Out of the three candidates that could represent ClpB in *B. subtilis*, ClpE (~100 per cell) only plays a subordinate role and becomes more important under severe heat shock conditions (Gerth et al., 2004; Miethke et al., 2006). On the contrary, ClpC is quite similar to ClpB regarding the presence of a coiled-coil middle domain (MD or linker domain) (Figure 5), which is in addition absent in ClpX species (Figure 6). This MD forms a ring-like structure around the active hexameric ClpB complex through head to tail interactions, which represses and controls its activity in tight cooperation with DnaK/Hsp70 (Carroni et al., 2014; Oguchi et al., 2012). Remarkably, the analogous MD of ClpC is only half the size of the MD of ClpB, which does not allow this specific head to tail interaction within an active hexamer (Figure 6). However, a head to head interaction within a decameric 'resting state' of ClpC was identified in *S. aureus* ClpC (Carroni et al., 2017). This observation still implies a major regulatory function for the MD.

Taken together, although some aspects point towards a role of ClpC independent of ClpP, it still remains elusive whether ClpC can act as a stand-alone disaggregase in protein quality control and if there is a regulatory switch between ClpC and ClpCP.

1.4.3. Adaptor proteins of ClpC

As the same proteolytic complexes are involved in both general and regulatory proteolysis, an accurate substrate recognition is crucial for all protease complexes in order to prevent mistargeting and malfunction. Besides from substrate recognition of N- or C-terminal

degrons, which are *per se* part of the substrate protein, many Hsp100/Clp disaggregases and AAA+ protease complexes enable or enhance their substrate recognition capabilities by interaction with various external adaptor proteins (Figure 5) (Kirstein et al., 2009b; Wiegert and Schumann, 2001). These adaptor proteins target substrate proteins to the respective protease complex, predominantly interacting with their N-terminal domains, thereby adding another layer of regulation to the intricate pathways of regulatory and general proteolysis (Kirstein et al., 2009b; Persuh et al., 1999).

Regarding *B. subtilis* ClpC, three adaptor proteins (MecA, YpbH and McsB) have been identified and characterized to date. Importantly, in *B. subtilis* the adaptor proteins completely modulate the activity of ClpC leaving it incapable of oligomerizing without an adaptor protein present (Kirstein et al., 2006, 2009b). The paralogs MecA and YpbH are about 26 kDa in size and facilitate ClpC mediated disaggregation and refolding of aggregated proteins generated by e.g. heat stress *in vitro* (Schlothauer et al., 2003). Furthermore, MecA is involved in regulatory proteolysis to control competence development of *B. subtilis*. At that, MecA constantly targets the master regulator of competence, ComK, for ClpCP degradation, which thereby represses competence development. The quorum sensing induced expression of *comS* leads to outcompetition of ComK by newly synthesized ComS. The now released positive auto-regulator ComK accumulates, which leads to the expression of all competence related genes and the development of a competent subgroup in the *B. subtilis* population (Prepiak and Dubnau, 2007; Turgay et al., 1998, 1997). This example of regulatory proteolysis demonstrates the importance of specific adaptor proteins, as the same protease complexes can simultaneously be involved in general proteolysis as well.

1.4.4. The protein arginine kinase McsB

The third adaptor protein of ClpC is the 40 kDa protein McsB, which is a protein arginine kinase and thereby substantially different from the other two, MecA and YpbH (Fuhrmann et al., 2009; Kirstein et al., 2007). At that, McsB is involved in the regulatory proteolysis of the heat shock repressor CtsR by ClpCP, controlling the heat stress response of *B. subtilis* (Derré et al., 1999; Fuhrmann et al., 2009; Krüger et al., 2001). Furthermore, McsB has been identified to delocalize and disassemble competence proteins from the cell poles (Hahn et al., 2009). Both activities were observed to be primarily dependent on its arginine kinase activity. Hence it is essential to determine the respective impact of its role as an adaptor protein and/or as an arginine kinase.

Under unstressed conditions, McsB is inhibited by interaction with ClpC as a result of their neighboring genome location and co-translation (Figure 7) (Elsholz et al., 2011a; Kirstein et al., 2005). Stress induced release of McsB, e.g. due to competition of ClpC with stress induced unfolded proteins, and subsequent activation by its activator protein McsA leads to auto-phosphorylation of McsB, which is dependent on the kinase activity of McsB (Elsholz et al., 2011a; Kirstein et al., 2005). This activated McsB species can now phosphorylate, among others, the class III heat shock repressor CtsR and target it for ClpCP degradation (Fuhrmann et al., 2009; Kirstein et al., 2005; Krüger et al., 2001). As CtsR represses the *clpC* operon (encoding *ctsR*, *mcsA*, *mcsB* and *clpC*) and the monocistronic genes *clpE* and *clpP*, removal of CtsR results in de-repression and upregulation of the class III heat shock genes, including CtsR (Figure 7). This negative feedback loop guarantees the shutdown of the stress response system after the cells are no longer exposed to stress.

As a regulator of this kinase activity of McsB, a specific arginine phosphatase YwlE was identified to dephosphorylate all phosphorylated arginine residues, including McsB *per se* (Figure 7) (Elsholz et al., 2010; Kirstein et al., 2005; Stannek et al., 2015). On one hand, overexpression of *ywlE* resulted in inhibition of McsB activity (Hahn et al., 2009). On the other hand, a full deletion of *ywlE* was observed to result in hyperactivation of McsB and simultaneously stabilized phosphorylated arginine residue (Elsholz et al., 2012). This effect allowed the identification of protein arginine phosphorylation sites, which could not be detected in the wildtype strain (Elsholz et al., 2012). The detection of phosphorylated arginine residues all over the proteome in this Δ*ywlE* mutant strain clearly indicated that this specific type of phosphorylation has a significant impact on cellular physiology (Elsholz et al., 2012). This is supported by the fact that the simultaneous deletion of both *clpC* and *ywlE*, as the two inhibitors of McsB activity, had a severe negative impact on viability of *B. subtilis* (Elsholz et al., 2011a).
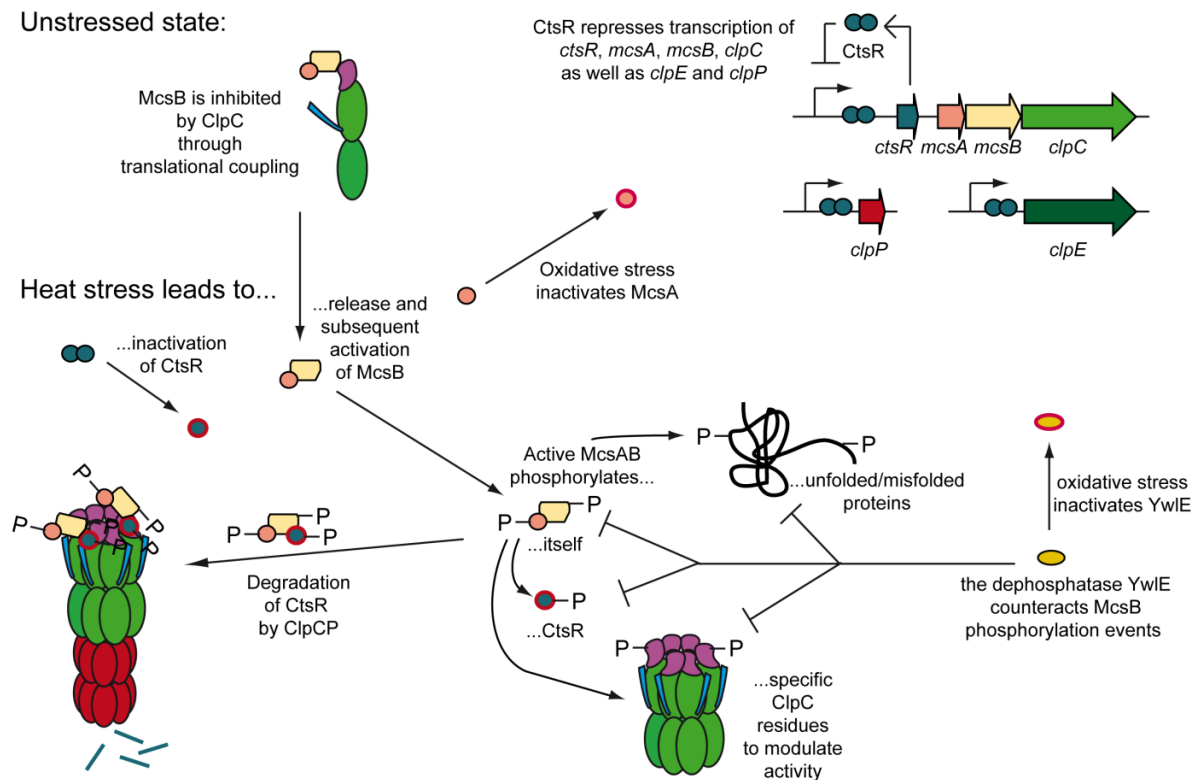
Figure 7: Simplified overview of regulation of CtsR activity by McsB.

CtsR inhibits the expression of class III heat shock genes (*ctsR*, *mcsA*, *mcsB*, *clpC*, *clpP*, *clpE*) and McsB is inhibited by specific interaction with ClpC due to translational coupling under non-stressed conditions. Heat stress leads to upregulation of class III heat shock genes due to a) inactivation of CtsR due to its intrinsic thermosensor and b) release and activation of McsB by its activator McsA with subsequent phosphorylation and targeting of CtsR for degradation by ClpCP. It is not completely understood how protein arginine phosphorylation is functional as a general degradation tag on unfolded and misfolded proteins. YwlE is the counterpart of McsB and dephosphorylates active McsB and its substrates. Both YwlE and McsA can be inactivated by oxidative stress, which links heat and oxidative stress conditions.

The specific role of arginine phosphorylation by McsB and the targeting of substrate proteins as an adaptor to ClpCP is still unclear (Figure 7). Regarding degradation of CtsR by ClpCP it has been shown that kinase active McsB is essential, although CtsR does not have to be phosphorylated (Elsholz et al., 2010, 2011a). However, kinase inactive McsB was identified to be still able to bind and thereby relieve CtsR-DNA interactions, which is sufficient to de-repress its target genes (Elsholz et al., 2010). In addition, certain arginine residues on ClpC were identified to be crucial for its activation by McsB, but not MecA, indicating that while acting as an adaptor protein, McsB might simultaneously modulate the activity of ClpC by

arginine phosphorylation as well (Elsholz et al., 2012). However, first hints were obtained that phosphorylated arginine residues on partially unfolded substrates might serve as a tag for ClpCP degradation without the presence of McsB as an adaptor protein and, instead, with specific binding pockets for phosphorylated arginine residues on the N-terminal domain of ClpC (Trentini et al., 2016). This is supported by the observations that binding of phosphorylated arginine was detected for *M. tuberculosis* ClpC1 (Weinhäupl et al., 2018). Taken together, the role of arginine phosphorylation in McsB dependent targeting of substrates to ClpC while modulating its activity is not completely understood. This is in particular due to the rather complicated discrimination between the arginine kinase activity of McsB and its role as an adaptor protein.

1.5.   *Hsp100/Clp complexes as novel target for antibiotics*

Classic approaches in antimicrobial therapy are based on targeting pathways which are of particular importance during cellular growth such as translation, transcription, cell-wall synthesis and replication. Following this strategy, antibiotics have saved millions of lives in the last decades. However, due to, among others, inappropriate prescribing and excessive overuse (in particular in agriculture), antibiotic resistant bacteria are continuously emerging worldwide (Kåhrström, 2013).

In addition to the problematic acquisition of resistance towards antibiotics, some bacteria have been identified to develop a specific, more antibiotic tolerant life style: persistence (Balaban et al., 2019; Lewis, 2012). While resistant bacteria are able to proliferate and replicate during antibiotic treatment without being negatively affected, persistence describes the ability of a minor part of the population to withstand and survive antimicrobial treatment, however, without being able to replicate during exposure of the drug. It is important to note

that a bacterial culture derived from a persistent subset of bacteria becomes as susceptible to the original drug as the parental culture. Persistence is in contrast to resistance not transferable (Balaban et al., 2019).

Although persister cells only represent a minor fraction of a bacterial population, they can become a serious threat. Since e.g. in these dormant cells all processes regarding proliferation are substantially downregulated they can tolerate all kinds of antibiotics that target processes associated with cellular growth such as transcription, translation and replication (Balaban et al., 2019; Fisher et al., 2017; Koul et al., 2008; Nathan, 2011). These observations, among others, emphasize the need for new targets in antimicrobial therapy, which additionally address the issue of persistence in bacteria.

Recently, some antibiotic compounds were observed to kill persisters of pathogenic bacteria such as *M. tuberculosis* and *S. aureus* and identified to target the protein quality control machinery (Conlon et al., 2013; Gao et al., 2015; Schmitt et al., 2011). At first glance, this approach appears to be promising as a functional proteome is obviously crucial for all cells. Furthermore, during infection, the pathogen has to deal with the host immune system and numerous types of stress, including reactive oxygen and nitrogen species (ROS/RNS), iron and general nutrient starvation, acidification and hypoxia, which all affect the functionality of its proteome (Kurthkoti et al., 2017; Lupoli et al., 2018; MacMicking et al., 1997; Nathan and Cunningham-Bussel, 2013; Vaubourgeix et al., 2015; Voskuil et al., 2011). Moreover, a defective Hsp100/Clp complex has often been observed to result in impaired virulence, pathogenicity, infectivity and/or viability of bacteria in general (Gaillot et al., 2000; Kwon et al., 2004; Ollinger et al., 2012; Rouquette et al., 1998, 1996; Sassetti et al., 2003; Wozniak et al., 2012). Both could be advantageous when addressing the PQC in antimicrobial therapy.

Furthermore, compounds that target the PQC machinery can help to elucidate the mechanism of action of their respective target in more detail since some of them were observed to display an unusual mode of action in comparison to a simple competitive or allosteric inhibition. One example are the acyldepsipeptides (ADEP), which simultaneously activate and uncouple their target ClpP from ClpCP leading to uncontrolled proteolysis and eventually cell death (Brötz-Oesterhelt et al., 2005; Famulla et al., 2016). Vice versa, the cyclic peptides ecumicin and lassomycin were identified to enhance the activity of their target ClpC1 in *M. tuberculosis* and were additionally postulated to uncouple it from the ClpP complex, leading to a potential toxic accumulation of no longer degraded substrate proteins (Figure 8) (Gao et al., 2015, 2014; Gavrish et al., 2014). ClpC1 is also the target of cyclomarin, which leads to enhanced and deregulated activity without uncoupling from the proteolytic complex (Figure 8) (Schmitt et al., 2011). Furthermore, a dihydrothiazepine derivative was shown to deoligomerize ClpX in *S. aureus* and thereby diminish virulence (Fetzer et al., 2017). All these compounds deregulate their target species in a special way, which might help gain more insight into the mechanism of e.g. ClpC activation.
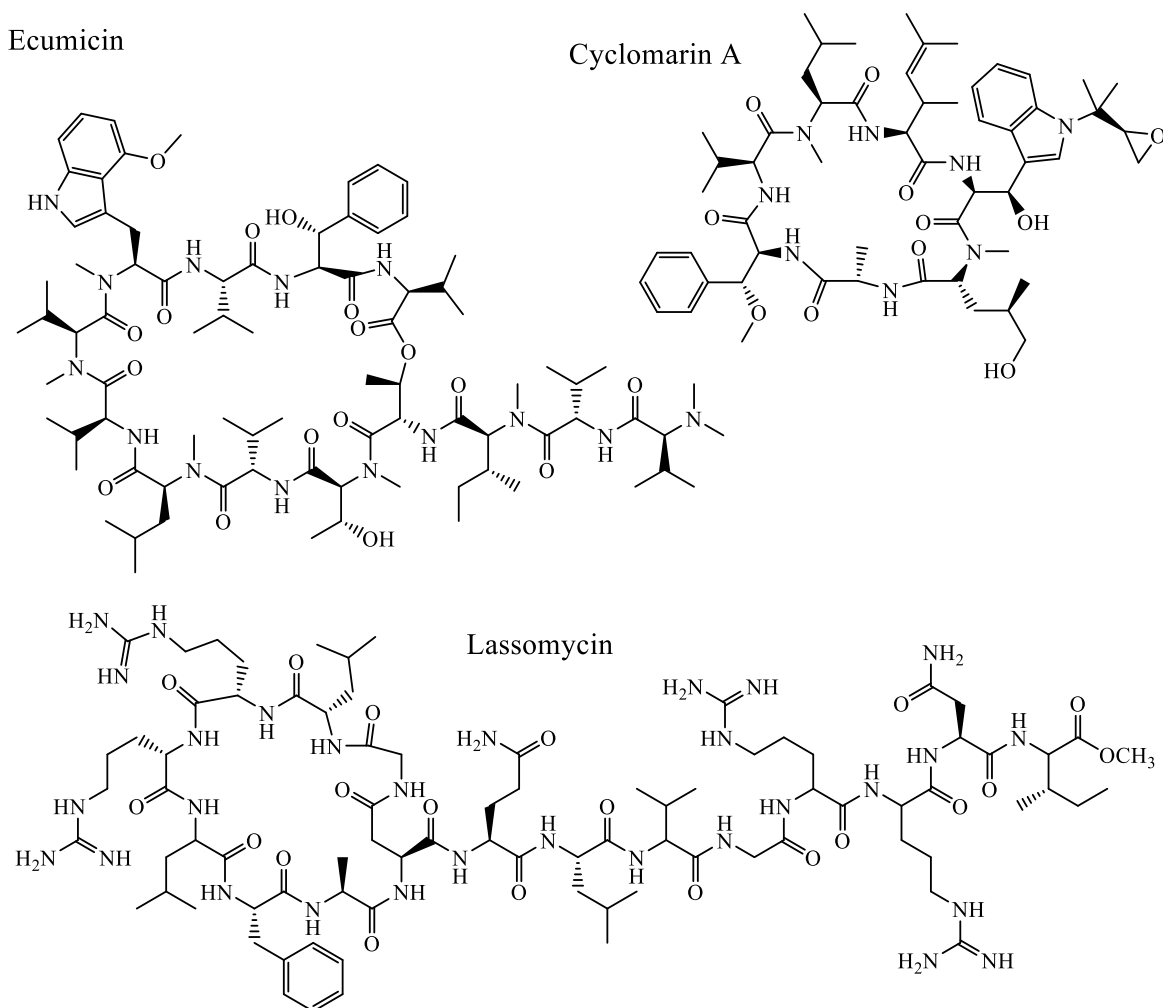
Figure 8: Structures of natural products cyclomarin A, ecumicin and lassomycin.

Binding sites of cyclomarin A, ecumicin and lassomycin on the N-terminal domain of ClpC1 of *M. tuberculosis* are indicated in Figure 9.

Remarkably, the natural products cyclomarin, ecumicin and lassomycin all bind to the N-terminal domain (NTD) of ClpC1 in *M. tuberculosis* to modulate its function (Culp and Wright, 2017; Gao et al., 2015; Gavrish et al., 2014; Vasudevan et al., 2013; Weinhäupl et al., 2018), which is similar to adaptor proteins that also interact with the NTD of e.g. *B. subtilis* ClpC (Figure 9) (Kirstein et al., 2009b). However, a mycobacterial adaptor protein for ClpC1 and ClpX has not been identified yet. Nevertheless there is a first hint towards an adaptor-protein like interaction of ClpC1 with ClpS *in vitro* (Marsee et al., 2018). Although crucial for

activity of *B. subtilis* ClpC (and ClpCP), the formation of an active proteolytic ClpC1 and ClpP1/ClpP2 complex does apparently not rely on the presence of an adaptor protein (Benaroudj et al., 2011; Kirstein et al., 2006; Kress et al., 2007; Marsee et al., 2018; Schlothauer et al., 2003; Schmitz and Sauer, 2014; Weinhäupl et al., 2018). Nevertheless, since their way of interacting with their target is comparable, a deeper understanding of the activation mechanism of Hsp100/Clp proteins such as ClpC by their respective adaptor proteins might help to understand the mode of action of antibiotic compounds that target similar Clp species.
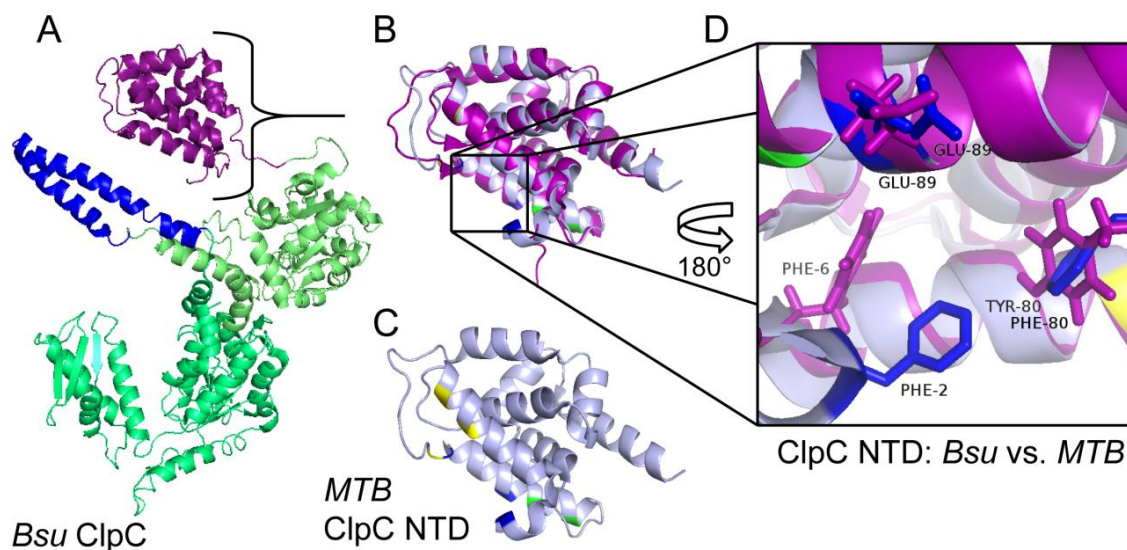

Figure 9: Natural products cyclomarin, lassomycin and ecumicin bind to the N-terminal domain of ClpC1 in *M. tuberculosis*.

A) Crystal structure of *B. subtilis* ClpC indicating the N-terminal domain (NTD, purple), the middle/linker-domain (blue) and the two ATPase domains D1 and D2 (green, light green, respectively) (PDB 3PXI). B) Superimposed structures of *B. subtilis* ClpC NTD (Bsu, purple) and *M. tuberculosis* ClpC1 (MTB, grey) (PDB 3WDC). C) Binding sites of lassomycin (yellow, Q17/R21/P79), cyclomarin (F2/E89/F80) and ecumicin (L92/L96) on the NTD of MTB ClpC1 (grey). D) Binding site of cyclomarin in MTB ClpC1 compared to Bsu ClpC: MTB Phe80 was observed to be essential for interaction, thus Bsu Tyr80 mutation confers resistance to cyclomarin (Vasudevan et al., 2013).

1.5.1. *B. subtilis* as a model and screening platform

Screening natural compounds for their bactericidal activity is a common approach in antibiotic research. Discovery of these drug-leads by screening natural product or synthetic libraries requires either advanced phenotypic screening systems or more specific target-based approaches, e.g. to identify compounds that specifically target Hsp100/Clp complexes (Cheng et al., 2007; Clardy and Walsh, 2004; Gao et al., 2014; Ozeki et al., 2015; Ulaczyk-Lesanko and Hall, 2005). As the principles and underlying mechanisms of the PQC are conserved in all three domains of life (Wickner et al., 1999) and handling of Gram-positive pathogens, such as *M. tuberculosis*, *S. aureus* or *L. monocytogenes*, requires specific safety precautions, the Gram-positive bacterium *Bacillus subtilis* is often used as a safe, genetically accessible and well-studied model organism when focusing on Gram-positive pathogenic bacteria (Figure 9). Furthermore, comparing different Gram-positive bacteria regarding their phenotype when treated with the same antimicrobial compound can substantially help to understand its function based on variations in the interaction sites. One example is cyclomarin, which has been identified to interact with the N-terminal domain of ClpC1 in *M. tuberculosis*. It has already been observed that Phe80 in ClpC1 is an essential residue for interaction with cyclomarin, as analogues Tyr80 in ClpC conferred resistance to *B. subtilis* by substantially decreasing binding affinity to cyclomarin (Figure 9) (Vasudevan et al., 2013). Thus, these observations can help to elucidate potential resistance mechanisms.

1.6. *Aim of this work*

The general aim of this work was to investigate different aspects of the bacterial protein quality control system. In particular it was intended to elucidate and characterize the potential role of YocM as the first small heat shock protein involved in PQC and stress response in *Bacillus subtilis*. Furthermore, YocM should be fused with a fluorescent protein and evaluated regarding its suitability as an aggregate marker protein in order to investigate the disaggregation activity of the Hsp100/Clp protein ClpC independent of the protease ClpP in more detail. Especially it was intended to further elucidate the role of the ClpC adaptor protein McsB and the particular impact of its arginine kinase activity in protein disaggregation.

Another objective was to establish a ClpC target-based screening system as proof of concept in *B. subtilis* to identify and characterize antibiotic compounds, while simultaneously evaluating ClpC as a promising target for antimicrobial therapy.

2. Materials and Methods

2.1. Basic methods

B. subtilis cells were grown in Lysogeny Broth medium (LB: 5 g l^{-1} yeast extract, 10 g l^{-1} tryptone-peptone, 5 g l^{-1} NaCl) at 37 °C if not otherwise indicated. Overnight cultures were inoculated from glycerol stock in presence of appropriate antibiotics, if necessary (Table 4). Table 7 exhibits the construction of all strains used during this work obtained from transformations with indicated plasmids (Table 6) or PCR products derived from cloning with primers/restriction enzymes (Table 5) with standard cloning and transformation procedures as described previously (Anagnostopoulos and Spizizen, 1961; Arnaud et al., 2004; Sambrook and Russell, 2001). Cloning was performed in *E. coli* DH5α (obtained from Invitrogen, Table 3) (ampicillin 100 µg ml^{-1}, kanamycin 50 µg ml^{-1}) with Phusion High Fidelity Polymerase (New England Biolabs, NEB) and chromosomal DNA (Table 7) or existing plasmids as template. Strains were stored frozen as glycerol stocks (glycerol final 15-20 % v/v) at -80 °C.

Table 1: Devices.

Device	Manufacturer
Äkta protein purification system FPLC	GE Healthcare
Autoclave VX150	Systec
AxioImager M2, fluorescence microscope	Zeiss
Centrifuge Sorvall RC 6+	Sorvall/Thermo Scientific
Epson Scanner	Eppendorf
Fastblot B44	Biometra
French Press	Heinemann
Heraeus Centrifuge	Thermo Scientific

Incubator MaxQ7000	Thermo Scientific
Micro centrifuge	Peqlab
Nanodrop spectrophotometer	Peqlab
Photometer	Eppendorf
Safe2020 Clean Bench	Thermo Scientific
SpectraMax M3	Molecular Devices
Spectrofluorometer FP6500	Jasco
Tecan Pro 200	Tecan
Thermocycler	Biometra
Thermo shaker	Eppendorf

Table 2: Reagents.

Reagents	Manufacturer
anti-rabbit IgG AP conjugate	GE Healthcare
antibodies, primary	Pineda
Basic chemicals	Carl Roth
MasterPure DNA purification Kit (Gram-positive)	Epicentre
NucleoSpin PCR clean-up Kit	Macherey & Nagel
peqGOLD plasmid Miniprep Kit	Peqlab
PCR/Cloning buffers/Restriction enzymes	New England Biolabs
Phusion Polymerase	New England Biolans
Primers	Biomers

Table 3: Basic *E. coli* strains.

Strain	Genotype	Reference	Use
DH5α	F⁻ Φ80*lac*ZΔM15 Δ(*lac*ZYA-*arg*F) U169 *rec*A1 *end*A1 *hsd*R17 (rK–, mK+) *pho*A *sup*E44 λ– *thi*-1 *gyr*A96 *rel*A1	Invitrogen	Cloning
BL21(DE3)	F⁻ *omp*T *hsd*S$_B$ (r$_B^-$, m$_B^-$) *dcm gal* λ(DE3) pLysS Cm^r	Invitrogen	Protein production

2.1.1. Media and antibiotics

LB medium (Miller) / agar	Yeast extract	5 g/L
	Tryptone	10 g/L
	NaCl	10 g/L
	±Agar	15 g/L

Belitsky minimal medium (BMM) (Stülke et al., 1993)	**10x Basics**	
	$(NH_4)_2SO_4$	20 g/L
	$MgSO_4 \cdot 7\ H_2OKCl$	20 g/L
	Na_3-citrat $\cdot 2\ H_2O$	20 g/L
	Tris	20 g/L
	ad dH_2O 1 L	60.6 g/L

1 L 1x Belitsky:	**Volume of stock:**	**Final concentration:**
KH_2PO_4	5 mL of 0.2 M	1 mM
$CaCl_2 \cdot 2\ H_2O$	2 mL of 1 M	2 mM
$FeSO_4 \cdot 7\ H_2O$ in 1 M HCl	2 mL of 0.5 mM	1 µM
NaOH	2 mL of 1 M	pH-adjustment
$MnSO_4 \cdot 1\ H_2O$	0.4 mL of 25 mM	10 µM
Glucose $\cdot 1\ H_2O$	10 mL of 20 % (w/v)	0.2 % (w/v)
L-glutamic acid (pH 7.5)	9 mL of 0.5 M	4.5 mM
L-tryptophan (pH 7.5)	1 mL of 0.039 M	39 µM

Table 4: Use of antibiotics.

Antibiotic	Stock	Use
Ampicillin (Amp)	100 mg/mL	100 µg/mL
Chloramphenicol (Cm)	25 mg/mL	10 µg/mL
Erythromycin (Ery)	1 mg/mL	1 µg/m
Lincomycin (Linc)	20 mg/mL	20 µg/mL
Kanamycin (Kan)	50 mg/mL	50 µg/mL *E. coli*, 10 µg/mL *B. subtilis*
Spectinomycin (Spec)	100 mg/mL	150 µg/mL
Tetracycline (Tet)	10 mg/mL	10 µg/mL

2.1.1. Primer, plasmids and strains

Table 5: Primer.

Nr.	Plasmid (Table 6)	Primer	Sequence
HS78	2	SacII_SpoVG_mecA$_{CTD}$_for	TCCCCGCGGTATAGGGAAAAGGTGGTGAACTACTGTGAAGCAAGAACCAGCATCTGAG
HS79	2 4	GFP_SpeI_rev	GGACTAGTGCTCGAATTCATTATTTGTATAGTTCATCCATGC
IH3	8	GFP_LCN_SpeI_rev	GGACTAGTTTAGTTGCAAAGTTTGTATAGTTCATCCATGCC
IH4	7 8	SacII_Strep_gfp_for	TGCCGCGGATGTGGTCTCATCCACAGTTCGAAAAAAGTAAAGGAGAAGAACTTTTC
IH5	7	GFP_SpeI_rev	GGACTAGTTTATTTGTATAGTTCATCCATGCC
IH7	7 8	SacII_SpoVG_Strep_for	TGCCGCGGTATAGGGAAAAGGTGGTGAACTACTGTGTGGTCTCATCCACAGTTC
IH8	4	SacII_SpoVG_GFP_for	TGCCGCGGTATAGGGAAAAGGTGGTGAACTACTGTGAGTAAAGGAGAAGAACTTTTC
IH39	6	SacII_RBS_mCherry_for	CCGCGGAGAGAACAAGGAGGGGCCTGCAGGATGGTGAGCAAGGGCGAGGAGG
IH41	6	SpeI_MecA$_{CTD}$_rev_IH	CGACTAGTCTACTATGATGCAAAGTGTTTTTTTATCG
IH42	6	mCherry_Link_MecA$_{CTD}$_IH	CAGATGCTGGTTCTTGCTTGGCGGAGCCCTTGTACAGCTCGTCCATGCCGCCGGTGG
IH43	63	GFP_Link_MecA$_{CTD}$_IH	CAGATGCTGGTTCTTGCTTGGCGGAGCCTTTGTATAGTTCATCCATGCCATGTGTAATC
IH44	6	MecA$_{CTD}$_Link_mCherry_IH	CGAGCTGTACAAGGGCTCCGCCAAGCAAGAACCAGCATCTGAGG
IH45	63	MecA$_{CTD}$_Link_GFP_IH	AACTATACAAAGGCTCCGCCAAGCAAGAACCAGCATCTGAGG
IH47	15 25 26	SalI_ClpC_for_IH	GCGTCGACAGAGAACAAGGAGGGGCTACAAATGATGTTTGGAAGATTTACAG

IH48	15 25-28	SphI_ClpC_rev_IH	GCGCATGCTTAATTCGTTTTAGCAGTCG
IH52	16	MecA$_{CTD}$_Mcherry_IH	CGATAAAAAAACACTTTGCATCACTTAAGG ACGTCATGGTGAGCAAGGGCGAGGAGGAT AACATGG
IH53	16	Mcherry_MecA$_{CTD}$_IH	CCTCCTCGCCCTTGCTCACCATGACGTCCTT AAGTGATGCAAAGTGTTTTTTTATCG
IH66	19	SphI_YocM_rev_IH	GCGCATGCTCAATCATCAATAACAATGGTT TTCGC
IH67	18	SalI_RBS_YocM_for	GCGTCGACAGAGAACAAGGAGGGGCTACA AATGGATTTCGAAAAGATGAAGC
IH70	3 5 7	SacII_RBS_mCherry_for	TCCCCGCGGTATAGGGAAAAGGTGGTGAAC TACTGTGGTGAGCAAGGGCGAGGAGG
IH76	52	ClpC_Phe80_rev	GACTTTTTTAGCTCTAGGAGTAAAATGAAT CGTTTGAGACATTTCC
IH77	52	ClpC_Phe80_for	GGAAATGTCTCAAACGATTCATTTTACTCCT AGAGCTAAAAAAGTC
IH78	34 36	SphI_GFP_rev_IH	GCGCATGCTCATTATTTGTATAGTTCATCCA TGC
IH81	16	mCherry_SphI_rev	GCGCATGCTCATTACTTGTACAGCTCGTCCA TGC
IH85	3 BIH360*	mCherry_SpeI_rev	GCACTAGTGGATCTTATTTATACAGTTCATC CATTCC
IH86	BIH359*	SacII_mcherry_for	TCCCCGCGGTAAGGAGGACAAACATGGTTA GCAAAGG
IH87	3 5	SacII_SpoVG_mCherry_for	TCCCCGCGGTATAGGGAAAAGGTGGTGAAC TACTGTGATGGTTAGCAAAGGCGAAGAGG
IH88	5 10	SpeI_ssrA_mCherry_rev	GGACTAGTTTAAGCAGCCAGAGCGTAGTTT TCGTCGTTAGCAGCTTTATACAGTTCATCC
IH95	60	XhoI_GFP_rev	TCGACTCGAGTCATCATTTGTAGGGCTCATC CATGCC
IH101	60	MecA$_{CTD}$_BsmBI_pCA_for	CCAGTGCGTCTCAGGTGGTATGAAGCAAGA ACCAGCATCTGAGG
IH108	19 20	KpnI_ACD_yocM_for	CGGGTACCATGGATATTGTAGATACCGTTG C
IH109	19 20	HindIII_ACD_yocM_rev	CGAAGCTTTTTTTTGAATAGTGATGTATAGG
IH110	17	HindIII_yocM_rev_IH	CGAAGCTTATCATCAATAACAATGGTTTTC G
IH160	BIH360*	SacII_RBS_FtsZ_IH	TCCCCGCGGTAAGGAGGACAAACATGTTGG AGTTCGAAACAAACA
IH161	BIH360*	Link_mCherry_FtsZ_I	CCTCTTCGCCCTTTGCTAACCATGCCGCGTTT ATTACGGTTTCTTAAG
IH162	BIH360*	Link_mCherry_FtsZ_II	CTTAAGAAACCGTAATAAACGCGGCATGGT TAGCAAAGGCGAAGAGG
IH171	BIH359*	Link1_mCherry_FtsZ_IH	CTATGTTTGTTTCGAACTCCAACATGCCTTT ATACAGTTCATCCATTCC
IH172	BIH359*	Link2_mCherry_FtsZ_IH	GGAATGGATGAACTGTATAAAGGCATGTTG GAGTTCGAAACAAACATAG
IH173	67	NcoI_mCherry_for_IH	CGCCATGGGCCATCATCATCATCATCACAT GGTTAGCAAAGGCGAAGAGG

IH174	67	XhoI_FtsZ_stop_rev_IH	CGCTCGAGTTATTAGCCGCGTTTATTACGGT TTCTTAAG
IH175	67	SpeI_FtsZ_stop_rev_IH	GCACTAGTTTATTAGCCGCGTTTATTACGGT TTCTTAAG
IH182	23 24	SalI_clpE_for_IH	GCGTCGACAGAGAACAAGGAGGGTACAAA TGCGTTGTCAACATTGTCATC
IH183	24	clpE_Y344A_fus_rev_IH	CGGAGTTTTGCCGCCAGTTCAGCATTTTCTT CTTCC
IH184	24	clpE_Y344A_fus_for_IH	GGAAGAAGAAATGCTGAACTGGCGGCAA AACTCCG
IH185	23 24	SphI_clpE_rev_IH	GCGCATGCTCATTATTTTGCTCGCACTTTGA TTTTATC
IH187	31	SphI_McsB_rev_IH	GCGCATGCTCATATCGATTCATCCTCCTGTC
IH197	51	BamHI_McsB_for_IH	CCCCGGATCCATGTCGCTAAAGCATTTTATT C
IH198	51	NcoI_McsB_rev_IH	CCCCCCATGGTCATATCGATTCATCCTCCTG TC
IH199	29 30	SalI_MicA_for_IH	GCGTCGACAGAGAACAAGGAGGGTACAAA TGTTATTTCTTCATGATGTG
IH201	29	SphI_MicA_rev_IH	GCGCATGCTCATTAGTTGACCTTTGATTCGT TTTCC
IH202	30	SphI_His_MicA_rev_IH	GCGCATGCTCATTAGTGGTGGTGGTGGTGG TGTGAGTTGACCTTTGATTCGTTTTCC
IH203	16 32	SalI_MecA_for_IH	GCGTCGACAGAGAACAAGGAGGGTACAAA TGGAAATTGAAAGAATTAACG
IH204	32	SphI_MecA_rev_IH	GCGCATGCCTATGATGCAAAGTGTTTTTTTA TCGTTTCTAGAGCGTGCTCTGAAAT
IH205	33	SalI_YpbH_rev_IH	GCGTCGACAGAGAACAAGGAGGGTACAAA TGCGGCTTGAGCGTCTGAA
IH206	33	SphI_YpbH_rev_IH	GCGCATGCTTATGAAAAATGAGTTTGTATC G
IH212	48	SalI_PorA_for_IH	GCGTCGACAGAGAACAAGGAGGGTACAAA TGCGAAAAAAACTTACCGCCC
IH213	48	SphI_PorA_rev_IH	GCGCATGCTTAGAATTTGTGGCGCAAACCG
IH220	65	NcoI_MecA_for_IH	TTCCATGGGCCATCATCATCATCATCATCAT GAAATTGAAAGAATTAACGAGCATAC
IH221	62 63 65	XhoI_MecA_rev_IH	ATCTCGAGTCACTATGATGCAAAGTGTTTTT TTATCG
IH222	61 62	NcoI_His_MecACTD_for	AGCCATGGGCCATCATCATCATCATCACAA GCAAGAACCAGCATCTGAGG
IH223	63	BsmBI_NcoI_His_GFP_for	CCAGTGCGTCTCCCATGGGCCATCATCATC ATCATCACATGAGTAAAGGAGAAGAACTT
IH230	46	AvrII_MicA_for_IH	TACCTAGGATGTTATTTCTTCATGATGTGTG GG
IH233	46	SpeI_MicA_stop_rev_IH	GCACTAGTACCTCAGTTGACCTTTGATTCGT TTTCC
IH234	46	GFP_MicA_rev_IH	CCCACACATCATGAAGAAATAACATTTTGT ATAGTTCATCCATGCCATGTG

IH235	46	GFP_MicA_for_IH	CACATGGCATGGATGAACTATACAAAATGT TATTTCTTCATGATGTGTGGG
IH236	55	MicA_xhoI_stop_rev_IH	TCGACTCGAGTCAGTTGACCTTTGATTCGTT TTCC
IH237	55	MicA_BsmBI_for_IH	CCAGTGCGTCTCAGGTGGTATGTTATTTCTT CATGATGTGTGG
IH278	35	McsB_Link_for_IH	AAAAGACAGGAGGATGAATCGATAGCAAG TGGAATGAGTAAAGGAGAAGAACTTTTC
IH279	35	McsB_Link_rev_IH	GAAAAGTTCTTCTCCTTTACTCATTCCACTT GCTATCGATTCATCCTCCTGTCTTTT
IH280	31 34 36	BsmBI_McsB_for_HindIII	CCAGTGCGTCTCAAGCTTAAGGAGGGGCTA CAAATGTCGCTAAAGCATTTTATTCAGG
IH283	58 59	NcoI_ClpC-NTD_for_IH	CATGCCATGGGGCTTGACAGCTTGGCAAGA GACTTAAC
IH284	27 28	SalI_ClpC-NTD_for_IH	GCGTCGACAGAGAACAAGGAGGGTACAAA TGGGGCTTGACAGCTTGGCAAGAGACTT
IH298	37	YwlE_SalI_for_IH	GCGTCGACAGAGAACAAGGAGGGTACAAA TGGATATTATTTTTGTCTGTACTGG
IH299	37 38	YwlE_SphI_rev_IH	GCGCATGCTCATTATCTACGGTCTTTTTTCA GC
IH300	38	YwlE_C7S_SalI_for_IH	GCGTCGACAGAGAACAAGGAGGGTACAAA TGGATATTATTTTTGTCTCTACTGGAAATAC
RK17	56-60 64	pET_ClpC_XhoI_rev	CCGCTCGAGATTCGTTTTAGCAGTCGTT
RK27	56 57 60 64	pET_ClpC_NcoI_for	CATGCCATGGGGTTTGGAAGATTTACAGA
NM318	49 50 52	BamHI_clpCORF for	CCCCGGATCCATGATGTTTGGAAGATTTAC AG
NM319	49 50 52	NcoI_clpCORF rev	CCCCCCATGGTTAATTCGTTTTAGCAGTCG
IH271		YpbH_mut1_for_IH	CCCACTTGGTTATAATCGGCGG
IH272		YpbH_mut2_rev_IH	ACTTAAGGGTAACTAGCCTCGCCGAACGTT CCCTCCTGCCTCTACTTGC
IH273	Construction of the *ypbH::cat* mutant	YpbH_mut3_cm_for_IH	TCAAATTTAAGGAGAATCTCATCGGCGAGG CTAGTTACCCTTAAGT
IH274		YpbH_mut4_cm_rev_IH	AAATCAGCAGTTTTCCGTTGCATTCCAATAG TTACCCTTATTATCAAG
IH275		YpbH_mut5_for_IH	CTTGATAATAAGGGTAACTATTGCGATACA AACTCATTTTTCATAA
IH276		YpbH_mut6_rev_IH	AATTCTTGAATACTCATCCATCATCC

*Ligation of pPG60 *ftsZ-mCherry* and *mcherry-fstZ* was directly transformed into *B. subtilis* (Strains BIH359 and BIH360, Table 7) due to unsuccessful transformation in *E. coli* DH5α.

Table 6: Plasmids.

Nr.	Plasmid	Description	Reference
1	pPG60	*amyE*-integrating plasmid, P_{veg}, *cm*^{R}	(Gamba et al., 2015)
2	pPG60 *mecA*$_{CTD}$-*gfp*	*mecA*$_{CTD}$-*gfp* fused into pPG60, *cm*^{R}	This work
3	pPG60 *mcherry*	Constitutive expression of *mcherry*, P_{veg}, *cm*^{R}	(Hantke et al., 2018)
4	pPG60 *gfp*	Constitutive expression of *gfp* A206K, P_{veg}, *cm*^{R}	This work
5	pPG60 *mcherry-ssrA*	Constitutive expression of *mcherry-ssrA*, P_{veg}, *cm*^{R}	This work
6	pPG60 *mcherry-mecA*$_{CTD}$	Constitutive expression of *mcherry-mecA*$_{CTD}$, P_{veg}, *cm*^{R}	This work
7	pPG60 *strep-gfp*	Constitutive expression of *strep-gfp*, P_{veg}, *cm*^{R}	This work
8	pPG60 *strep-gfp*-LCN	Constitutive expression of *strep-gfp*-LCN, P_{veg}, *cm*^{R}	This work
9	pBS2E	*lacA*-integrating plasmid, *ery*^{R}	(Radeck et al., 2013)
10	pBS2E *mcherry-ssrA*	Constitutive expression of *mcherry-ssrA*, P_{veg} *lacA*-integrating plasmid, *ery*^{R}	This work
11	pBS2E $P_{veg\ lac}Z$-*gfp*	$P_{veg\text{-}lac}Z$-*gfp* in pBS2E, *ery*^{R}	(Hantke et al., 2018)
12	pBS2E like pDR111	P_{lac} *gene of interest + lacI* in pBS2E backbone, *ery*^{R}	(Hantke et al., 2018)
13	pBS2E *ibpA gfp*A206K	P_{xyl} *ibpA-gfp*A206K in pBS2E, *ery*^{R}	(Hantke et al., 2018)
14	pBS2E *yocM-mCherry*	P_{xyl} *yocM-mCherry* in pBS2E, *ery*^{R}	(Hantke et al., 2018)
15	pBS2E P_{lac} *clpC*	*clpC* in pBS2E like pDR111, *ery*^{R}	This work
16	pDR111 *mecA*$_{CTD}$-*mcherry*	Expression of *mecA*$_{CTD}$-*mcherry*, P_{lac} promoter, *spec*^{R}	This work
17	pDR111 *yocM*	Expression of *yocM*, P_{lac} promoter, *spec*^{R}	(Hantke et al., 2018)
18	pDR111 *yocM* ΔCTD	Expression of *yocM* lacking the CTD, P_{lac} promoter, *spec*^{R}	This work
19	pDR111 *yocM* ΔNTD	Expression of *yocM* lacking the NTD, P_{lac} promoter, *spec*^{R}	This work
20	pDR111 *yocM* ACD	Expression of the ACD of *yocM*, P_{lac} promoter, *spec*^{R}	This work
21	pDR111 *clpC*	Expression of *clpC*, P_{lac} promoter, *spec*^{R}	(Hantke et al., 2018)
22	pDR111 *clpC* F436A	Expression of *clpC* F436A, P_{lac} promoter, *spec*^{R}	(Carroni et al., 2017)

23	pDR111 *clpE*	Expression of *clpE*, P$_{lac}$ promoter, *spec*[R]	This work
24	pDR111 *clpE* Y344A	Expression of *clpE* Y344A, P$_{lac}$ promoter, *spec*[R]	(Carroni et al., 2017)
25	pDR111 *clpC* loop	Expression of *clpC* VGF::GGR (671-673), P$_{lac}$ promoter, *spec*[R]	This work
26	pDR111 *clpC* F436A VGF::GGR	Expression of *clpC* F436A VGF::GGR (671-673), P$_{lac}$ promoter, *spec*[R]	This work
27	pDR111 ΔNTD-*clpC*	Expression of ΔNTD-*clpC*, P$_{lac}$ promoter, *spec*[R]	This work
28	pDR111 ΔNTD-*clpC* F436A	Expression of ΔNTD-*clpC* F436A, P$_{lac}$ promoter, *spec*[R]	This work
29	pDR111 *micA*	Expression of *micA*, P$_{lac}$ promoter, *spec*[R]	This work
30	pDR111 *micA-his₆*	Expression of *micA-his₆*, P$_{lac}$ promoter, *spec*[R]	This work
31	pDR111 *mcsB*	Expression of *mcsB*, P$_{lac}$ promoter, *spec*[R]	This work
32	pDR111 *mecA*	Expression of *mecA*, P$_{lac}$ promoter, *spec*[R]	This work
33	pDR111 *ypbH*	Expression of *ypbH*, P$_{lac}$ promoter, *spec*[R]	This work
34	pDR111 *mcsB-gfp*	Expression of *mcsB-gfp*A206K, P$_{lac}$ promoter, *spec*[R]	This work
35	pDR111 *mcsB* C167S	Expression of *mcsB* C167S, P$_{lac}$ promoter, *spec*[R]	This work
36	pDR111 *mcsB* C167S-*gfp*	Expression of *mcsB* C167S-*gfp* A206K, P$_{lac}$ promoter, *spec*[R]	This work
37	pDR111 *ywlE*	Expression of *ywlE*, P$_{lac}$ promoter, *spec*[R]	This work
38	pDR111 *ywlE* C7S	Expression of *ywlE* C7S, P$_{lac}$ promoter, *spec*[R]	This work
39	pSG1154-*gfp*A206K	*AmyE*-integrating plasmid, xylose inducible, *spect*[R]	(Lewis and Marston, 1999)
40	pSG1154 cotP-*mCherry*	*cotP-mCherry* in pSG1154, P$_{xyl}$, *spec*[R]	(Hantke et al., 2018)
41	pSG1154 cotM-*mCherry*	*cotM-mCherry* in pSG1154, P$_{xyl}$, *spec*[R]	(Hantke et al., 2018)
42	pSG1154 *ibpA gfp*A206K	*ibpA* in pSG1154-*gfp*A206K, P$_{xyl}$, *spec*[R]	(Runde et al., 2014)
43	pSG1154 *yocM gfp*A206K	*yocM* in pSG1154-*gfp*A206K, P$_{xyl}$, *spec*[R]	Provided by Noel Molière
44	pSG1154 *yocM-mCherry*	*yocM-mCherry* in pSG1154, P$_{xyl}$, *spec*[R]	(Hantke et al., 2018)
45	pSG1154 *mCherry*	*mCherry* in pSG1154, P$_{xyl}$, *spec*[R]	(Hantke et al., 2018)
46	pSG1154 *micA-gfp*A206K	*micA-gfp* A206K in pSG1154, P$_{xyl}$, *spec*[R]	This work

47	pKTH290 *porA*	Constitutive expression of *porA* from *Neisseria*, kan^R	(Nurminen et al., 1992)
48	pBS2E *porA*	Expression of *porA*, P$_{lac}$ promoter, *ery*^{R}	This work
49	pMAD *clpC* F436A	For *B. subtilis* markerless point mutation *clpC* F436A *in cis*, *ery*^{R}	This work
50	pMAD *clpC* F436A loop	For *B. subtilis* markerless point mutation *clpC* F436A VGF::GGR (671-673), *in cis*, *ery*^{R}	This work
51	pMAD *mcsB* C167S	For *B. subtilis* markerless point mutation *mcsB* C167S *in cis*, *ery*^{R}	This work
52	pMAD *clpC* Y80F	For *B. subtilis* markerless point mutation *clpC* Y80F *in cis*, *ery*^{R}	This work
53	pCA528	pET24a containing SMT3 from yeast (His$_6$-SUMO), *kan*^{R}	(Andréasson et al., 2008)
54	pCA528 *yocM*	Production of His-SUMO-YocM, *kan*^{R}	(Hantke et al., 2018)
55	pCA528 *micA*	Production of His-SUMO-MicA, *kan*^{R}	This work
56	pET28a clpC	Production of ClpC, *kan*^{R}	Provided by Regina Kramer
57	pET28a *clpC* F436A	Production of ClpC F436A, *kan*^{R}	This work
58	pET28a ΔNTD-*clpC*	Production of ΔNTD-ClpC, *kan*^{R}	This work
59	pET28a ΔNTD-*clpC* F436A	Production of ΔNTD-ClpC F436A, *kan*^{R}	This work
60	pET28a *clpC* DWB	Production of ClpC E280A E618A double walker B mutant, *kan*^{R}	This work
61	pET28a *mecA*$_{CTD}$-*gfp*	Production of MecA$_{CTD}$-GFP A206K, *kan*^{R}	This work
62	pET28a *mecA*$_{CTD}$	Production of MecA$_{CTD}$, *kan*^{R}	This work
63	pET28a *gfp*-*mecA*$_{CTD}$	Production of GFP A206K-MecA$_{CTD}$, *kan*^{R}	This work
64	pET28a *clpC* VGF::GGR	Production of ClpC VGF::GGR (671-673), *kan*^{R}	Provided by Regina Kramer
65	pET28a *mecA*	Production of MecA, *kan*^{R}	This work
66	pET28a *ftsZ*-*mCherry*	Production of FtsZ-mCherry, *kan*^{R}	This work
67	pET28a *mCherry*-*ftsZ*	Production of mCherry-FtsZ, *kan*^{R}	This work

Table 7: List of *B. subtilis* strains.

Nr.	Genotype / properties	Reference/ Construction
BIH1	*trpC2*	(Anagnostopoulos and Spizizen, 1961)
BT02	*trpC2 ΔdnaK::cat*	(Homuth et al., 1997)
BEK89	*trpC2 lys-3 ΔmcsB::kan*	(Krüger et al., 2001)
BEK90	*trpC2* lys-3 *ΔclpX::kan*	(Gerth et al., 2004)
BIH2	*trpC2 ΔyocM::spec*	(Hantke et al., 2018)
BIH11	*trpC2 amyE::P$_{veg}$ mecA$_{CTD}$-gfp* A206K *cm*	Plasmid 2 → BIH1
BIH19	*trpC2 ΔclpC::tet*	(Hantke et al., 2018)
BIH20	*trpC2 ΔmecA::tet*	Provided by Noel Molière (NM114, unpublished)
BIH23	*trpC2 amyE::P$_{veg}$ mecA$_{CTD}$-gfp* A206K *cm*	BIH20 → BIH11
BIH24	*trpC2 amyE::P$_{veg}$ mecA$_{CTD}$-gfp* A206K *cm*	Plasmid 2 → BIH217
BIH25	*trpC2 amyE::P$_{veg}$ mecA$_{CTD}$-gfp* A206K *cm*	BIH11 → BIH19
BIH27	*trpC2 amyE::P$_{veg}$ gfp* A206K *cm*	Plasmid 4 → BIH1
BIH35	*trpC2 amyE::Pveg strep-gfp*-LCN *cm*	Plasmid 11 → BIH1
BIH38	*trpC2 amyE::Pveg strep-gfp cm*	Plasmid 10 → BIH1
BIH39	*trpC2 amyE::Pveg strep-gfp*-LCN *cm ypbH::spec mcsB::kan mecA::tet*	Plasmid 11 → FS69
BIH47	*trpC2 amyE::P$_{xyl}$ yocM-gfp*A206K *spec*	(Hantke et al., 2018)
BIH48	*trpC2 amyE::P$_{xyl}$ ibpA-gfp*A206K *spec*	(Hantke et al., 2018)
BIH66	*trpC2 ΔmcsB::kan amyE::P$_{xyl}$ yocM-gfp*A206K *spec*	(Hantke et al., 2018)
BIH69	*trpC2 ΔmcsB::kan*	(Hantke et al., 2018)
BIH73	*trpC2 amyE::P$_{xyl}$ yocM-mCherry spec*	(Hantke et al., 2018)
BIH74	*trpC2 ΔmcsB::kan amyE::P$_{xyl}$ yocM-mCherry spec*	(Hantke et al., 2018)
BIH78	*trpC2 ΔclpX::kan*	(Hantke et al., 2018)
BIH79	*trpC2 ΔclpC::tet ΔdnaK::cat*	(Hantke et al., 2018)

BIH81	*trpC2 Δspx::kan*	(Hantke et al., 2018)
BIH82	*trpC2 amyE::P$_{xyl}$ mCherry spec*	(Hantke et al., 2018)
BIH84	*trpC2 Δspx::kan amyE::P$_{xyl}$ yocM-mCherry spec*	(Hantke et al., 2018)
BIH85	*trpC2 ΔclpX::kan amyE::P$_{xyl}$ yocM-mCherry spec*	(Hantke et al., 2018)
BIH88	*trpC2 ΔclpC::tet amyE::P$_{xyl}$ yocM-mCherry spec*	(Hantke et al., 2018)
BIH91	*trpC2 amyE::P$_{xyl}$ yocM-mCherry spec $_{lac}$A::P$_{xyl}$ ibpA-gfp*A206K *ery*	(Hantke et al., 2018)
BIH121	*trpC2 ΔclpC::tet ΔdnaK::cat ΔyocM::spec*	(Hantke et al., 2018)
BIH133	*trpC2 ΔclpC::tet amyE::P$_{veg}$ mcherry-mecA$_{CTD}$ cm*	BIH141 → BIH19
BIH140	*trpC2 clpC* E280A E618A (DWB)	(Kirstein et al., 2006)
BIH141	*trpC2 amyE::P$_{veg}$ mcherry-mecA$_{CTD}$ cm*	Plasmid 6 → BIH1
BIH143	*trpC2 clpC* E280A E618A *amyE::P$_{veg}$ mecA$_{CTD}$-gfp* A206K *cm*	Plasmid 2 → BIH140
BIH148	*trpC2 lacA::P$_{veg}$ $_{lac}$Z-gfp ery*	(Hantke et al., 2018)
BIH151	*trpC2 amyE::P$_{lac}$ clpC spec*	Plasmid 21 → BIH1
BIH152	*trpC2 amyE::P$_{lac}$ clpC spec ΔclpC::tet*	BIH19 → BIH151
BIH154	*trpC2 ΔclpC::tet amyE::P$_{lac}$ mecA$_{CTD}$ -mcherry cm*	Plasmid 16 → BIH19
BIH182	*trpC2 amyE::P$_{lac}$ yocM spec*	(Hantke et al., 2018)
BIH185	*trpC2 amyE::P$_{veg}$ mecA$_{CTD}$ –gfp* A206K *cm lacA::P$_{lac}$ clpC ery*	Plasmid 15 → BIH11
BIH186	*trpC2 ΔclpC::tet amyE::P$_{veg}$ mecA$_{CTD}$ –gfp* A206K *cm lacA::P$_{lac}$ clpC ery*	BIH19 → BIH185
BIH216	*trpC2 clpC* Y80F	Plasmid 52 → BIH1
BIH217	*trpC2 clpC* VGF::GGR	(Moliere, 2012)
BIH222	*trpC2 amyE::P$_{veg}$ mecA$_{CTD}$-gfp* A206K *cm clpC* Y80F	Plasmid 2 → BIH216
BIH239	*trpC2 amyE::P$_{veg}$ SpoVG mCherry cat*	Plasmid 3 → BIH1
BIH240	*trpC2 amyE::P$_{veg}$ RBS mCherry cat*	(Hantke et al., 2018)
BIH242	*trpC2 amyE::P$_{lac}$ yocM-mCherry spec*	(Hantke et al., 2018)
BIH243	*trpC2 amyE::P$_{lac}$ ibpA spec*	(Hantke et al., 2018)

BIH246	*trpC2 amyE::Pveg strep-gfp*-LCN *cat ΔclpC::tet*	BIH19 → BIH35
BIH254	*trpC2 amyE::P$_{veg}$ mecA$_{CTD}$-gfp* A206K *cm lacA::P$_{veg}$ mcherry-ssrA ery clpC* Y80F	Plasmid 7 → BIH222
BIH255	*trpC2 amyE::P$_{veg}$ mecA$_{CTD}$-gfp* A206K *cm lacA::P$_{veg}$ mcherry-ssrA ery*	Plasmid 7 → BIH11
BIH264	*trpC2 amyE::P$_{veg}$ mecA$_{CTD}$-gfp* A206K *cm lacA::P$_{veg}$ mcherry-ssrA ery clpX::kan*	NM107 → BIH255
BIH274	*trpC2 lacA::P$_{veg\ lac}$Z-gfp ery ΔyocM::spec*	(Hantke et al., 2018)
BIH286	*trpC2 lacA::P$_{lac}$ yocM ery ΔyocM::spec*	(Hantke et al., 2018)
BIH305	*trpC2 amyE::P$_{xyl}$ yocM-mCherry spec pSG1151mdh-gfp*A206K *cat*	(Hantke et al., 2018)
BIH309	*trpC2 ΔywlE::kan*	(Elsholz et al., 2010)
BIH331	*trpC2 ΔcotP::cat*	(Hantke et al., 2018)
BIH333	*trpC2 ΔcotP::cat ΔyocM::spec*	(Hantke et al., 2018)
BIH339	*trpC2 ΔcotM::tet*	(Hantke et al., 2018)
BIH348	*trpC2 ΔcotM::tet ΔyocM::spec*	(Hantke et al., 2018)
BIH351	*trpC2 ΔcotP::cat ΔcotM::tet*	(Hantke et al., 2018)
BIH352	*trpC2 ΔcotP::cat ΔyocM::spec ΔcotM::tet*	(Hantke et al., 2018)
BIH356	*trpC2 amyE::P$_{xyl}$ cotP-mCherry spec*	(Hantke et al., 2018)
BIH359	*trpC2 amyE::P$_{veg}$ mcherry-fstZ cat*	Transformation of ligation (no plasmid), see primer Table 5
BIH360	*trpC2 amyE::P$_{veg}$ ftsZ-mcherry cat*	Transformation of ligation (no plasmid), see primer Table 5
BIH369	*trpC2 lacA::P$_{xyl}$ yocM-mCherry ery*	(Hantke et al., 2018)
BIH375	*trpC2 lacA::P$_{xyl}$ yocM-mCherry ery amyE::P$_{lac}$ clpC spec*	(Hantke et al., 2018)
BIH381	*trpC2 amyE::P$_{lac}$ clpE spec*	Plasmid 23 → BIH1
BIH382	*trpC2 amyE::P$_{lac}$ mCherry-YocM$_{CTD}$ spec*	(Hantke et al., 2018)
BIH383	*trpC2 amyE::P$_{lac}$ clpE* Y344A *spec*	(Carroni et al., 2017)
BIH384	*trpC2 amyE::P$_{lac}$ clpC* F436A *spec*	(Carroni et al., 2017)
BIH385	*trpC2 amyE::P$_{lac}$ clpC* F436A VGF::GGR *spec*	Plasmid 26 → BIH1
BIH394	*trpC2 amyE::P$_{lac}$ clpC* F436A *spec ΔclpC::tet*	BIH19 → BIH384

BIH399	*trpC2 mcsB::kan lacA::P_{xyl} yocM-mcherry ery*	BIH69 → BIH369
BIH400	*trpC2 clpC* F436A	Plasmid 49 → BIH1
BIH407	*trpC2 amyE::P_{lac} mcsB spec clpC* VGF::GGR	Plasmid 31 → BIH217
BIH411	*trpC2 amyE::P_{lac} mcsB spec clpC* E280A E618A (DWB)	Plasmid 31 → BIH140
BIH413	*trpC2 amyE::P_{xyl} cotM-mCherry spec*	(Hantke et al., 2018)
BIH414	*trpC2 amyE::P_{lac} mcsB spec mcsB::kan lacA::P_{xyl} yocM-mcherry ery*	Plasmid 31 → BIH399
BIH420	*trpC2 amyE::P_{lac} clpC* F436A *spec ΔclpC::tet lacA::P_{xyl} yocM-mcherry ery*	BIH369 → BIH394
BIH423	*trpC2 amyE::P_{lac} mcsB spec mcsB::kan clpC* VGF::GGR	BIH69 → BIH407
BIH427	*trpC2 amyE::P_{lac} mcsB spec mcsB::kan clpC* E280A E618A (DWB)	BIH69 → BIH411
BIH432	*trpC2 lacA::P_{xyl} yocM-mCherry ery amyE::P_{lac} clpC spec ΔclpC::tet*	(Hantke et al., 2018)
BIH434	*trpC2 amyE::P_{lac} clpC* VGF::GGR *spec lacA::P_{xyl} yocM-mCherry ery*	Plasmid 25 → BIH369
BIH439	*trpC2 amyE::P_{lac} mcsB* C167S *spec mcsB::kan lacA::P_{xyl} yocM-mcherry ery*	Plasmid 35 → BIH399
BIH485	*trpC2 amyE::P_{lac} mcsB spec mcsB::kan lacA::P_{xyl} yocM-mcherry ery clpC* VGF::GGR	BIH369 → BIH423
BIH488	*trpC2 amyE::P_{lac} mcsB spec mcsB::kan lacA::P_{xyl} yocM-mcherry ery clpC* E280A E618A (DWB)	BIH369 → BIH427
BIH504	*trpC2 amyE::P_{lac} clpC* VGF::GGR *spec ΔclpC::tet lacA::P_{xyl} yocM-mCherry ery*	BIH19 → BIH434
BIH581	*trpC2 amyE::P_{lac} clpC* F436A *spec ΔmcsB::kan*	BIH69 → BIH384
BIH582	*trpC2 amyE::P_{lac} clpC* F436A VGF::GGR *spec ΔmcsB::kan*	BIH69 → BIH385
BIH587	*trpC2 amyE::P_{lac} clpC* F436A *spec ΔmecA::tet*	BIH20 → BIH384
BIH588	*trpC2 amyE::P_{lac} clpC* F436A VGF::GGR *spec ΔmecA::tet*	BIH20 → BIH385
BIH589	*trpC2 amyE::P_{lac} clpC* F436A *spec ΔmecA::tet ΔmcsB::kan*	BIH20 → BIH581
BIH590	*trpC2 amyE::P_{lac} clpC* F436A VGF::GGR *spec ΔmecA::tet ΔmcsB::kan*	BIH20 → BIH582
BIH599	*trpC2 lacA::P_{xyl} yocM-mCherry ery mcsB::mcsB* C167S	BIH369 → BIH694
BIH613	*trpC2 amyE::P_{lac} clpC* F436A *spec ΔypbH::ery*	MV210 → BIH384
BIH614	*trpC2 lacA::P_{xyl} yocM-mCherry ery amyE::P_{lac} clpC* F436A *spec mcsB::mcsB* C167S	Plasmid 2 → BIH599
BIH615	*trpC2 lacA::P_{xyl} yocM-mCherry ery amyE::P_{lac} clpC* F436A VGF::GGR *spec mcsB::mcsB* C167S	Plasmid 26 → BIH599

BIH618	*trpC2 amyE::P$_{lac}$ clpC* F436A VGF::GGR *spec* Δ*ypbH::ery*	MV210 → BIH385
BIH619	*trpC2 amyE::P$_{lac}$ clpC* F436A *spec* Δ*ypbH::ery* Δ*mcsB::kan*	MV210 → BIH581
BIH620	*trpC2 amyE::P$_{lac}$ clpC* F436A VGF::GGR *spec* Δ*ypbH::ery* Δ*mcsB::kan*	MV210 → BIH582
BIH621	*trpC2 amyE::P$_{lac}$ clpC* F436A *spec* Δ*mcsA::ery*	MV210 → BIH384
BIH622	*trpC2 amyE::P$_{lac}$ clpC* F436A VGF::GGR *spec* Δ*mcsA::ery*	MV210 → BIH385
BIH624	*trpC2 amyE::P$_{lac}$ clpC* F436A *spec* Δ*ypbH::ery* Δ*mecA::tet*	BIH20 → BIH613
BIH625	*trpC2 amyE::P$_{lac}$ clpC* F436A VGF::GGR *spec* Δ*ypbH::ery* Δ*mecA::tet*	BIH20 → BIH618
BIH627	*trpC2 amyE::P$_{lac}$ clpC* F436A *spec* Δ*ypbH::ery* Δ*mcsB::kan* Δ*mecA::tet*	BIH20 → BIH619
BIH628	*trpC2 amyE::P$_{lac}$ clpC* F436A VGF::GGR *spec* Δ*ypbH::ery* Δ*mcsB::kan* Δ*mecA::tet*	BIH20 → BIH620
BIH647	*trpC2 amyE::P$_{lac}$ clpE* Y344A *spec* Δ*mcsB::kan*	BIH69 → BIH383
BIH662	*trpC2 amyE::P$_{lac}$ mcsB-gfp* A206K *spec*	Plasmid 34 → BIH1
BIH663	*trpC2 amyE::P$_{lac}$ mcsB* C167S *-gfp* A206K *spec*	Plasmid 36 → BIH1
BIH671	*trpC2 lacA::P$_{xyl}$ yocM-mCherry ery amyE::P$_{lac}$ mcsB-gfp* A206K *spec*	BIH369 → BIH662
BIH672	*trpC2 lacA::P$_{xyl}$ yocM-mCherry ery amyE::P$_{lac}$ mcsB* C167S *-gfp* A206K *spec*	BIH369 → BIH663
BIH677	*trpC2 lacA::P$_{xyl}$ yocM-mCherry ery amyE::P$_{lac}$ mcsB-gfp* A206K *spec* Δ*mcsB::kan*	BIH662 → BIH399
BIH678	*trpC2 lacA::P$_{xyl}$ yocM-mCherry ery amyE::P$_{lac}$ mcsB* C167S *-gfp* A206K *spec* Δ*mcsB::kan*	BIH663 → BIH399
BIH681	*trpC2 lacA::P$_{xyl}$ yocM-mCherry ery* Δ*ywlE::kan amyE::P$_{lac}$ mcsB-gfp* A206K *spec* Δ*ywlE::kan*	BIH309 → BIH671
BIH682	*trpC2 lacA::P$_{xyl}$ yocM-mCherry ery* Δ*ywlE::kan amyE::P$_{lac}$ mcsB* C167S *-gfp* A206K *spec* Δ*ywlE::kan*	BIH309 →BIH672
BIH694	*trpC2 mcsB::mcsB* C167S	Plasmid 51 → BIH1
BIH695	*trpC2* Δ*ywlE::kan mcsB::mcsB* C167S	BIH309 → BIH694
BIH721	*trpC2 lacA::P$_{xyl}$ yocM-mCherry ery* Δ*ypbH::cat*	*ypbH::cat* (PCR) → BIH369
BIH735	*trpC2 lacA::P$_{xyl}$ yocM-mCherry ery* Δ*ypbH::cat* Δ*mcsB::kan*	BIH69 → BIH721
BIH737	*trpC2 lacA::P$_{xyl}$ yocM-mCherry ery* Δ*ypbH::cat* Δ*mcsB::kan* Δ*mecA::tet*	BIH20 → BIH735
BIH739	*trpC2 lacA::P$_{xyl}$ yocM-mCherry ery* Δ*ypbH::cat* Δ*mcsB::kan* Δ*mecA::tet amyE::P$_{lac}$ mcsB spec*	Plasmid 31 → BIH737

BIH740	*trpC2 lacA::P$_{xyl}$ yocM-mCherry ery ΔypbH::cat ΔmcsB::kan ΔmecA::tet amyE::P$_{lac}$ mecA spec*	Plasmid 32 → BIH737
BIH741	*trpC2 lacA::P$_{xyl}$ yocM-mCherry ery ΔypbH::cat ΔmcsB::kan ΔmecA::tet amyE::P$_{lac}$ ypbH spec*	Plasmid 33 → BIH737
BIH792	*trpC2 lacA::P$_{xyl}$ yocM-mCherry ery clpC::clpC* VGF::GGR (671-673)	BIH369 → BIH217
BIH805	*trpC2 lacA::P$_{xyl}$ yocM-mCherry ery ΔywlE::kan mcsB::mcsB* C167S	BIH369 → BIH695
BIH816	*trpC2 amyE::P$_{lac}$ ywlE spec*	Plasmid 37 → BIH309
BIH817	*trpC2 amyE::P$_{lac}$ ywlE C7S spec*	Plasmid 38 → BIH309
BIH819	*trpC2 lacA::P$_{xyl}$ yocM-mCherry ery ΔywlE::kan*	BIH369 → BIH309
BIH820	*trpC2 amyE::P$_{lac}$ ywlE spec ΔywlE::kan*	BIH309 → BIH816
BIH821	*trpC2 amyE::P$_{lac}$ ywlE C7S spec ΔywlE::kan*	BIH309 → BIH817
BIH824	*trpC2 lacA::P$_{xyl}$ yocM-mCherry ery amyE::P$_{lac}$ ywlE spec ΔywlE::kan mcsB::mcsB* C167S	BIH816 → BIH805
BIH825	*trpC2 lacA::P$_{xyl}$ yocM-mCherry ery amyE::P$_{lac}$ ywlE C7S spec ΔywlE::kan mcsB::mcsB* C167S	BIH817 → BIH805
BIH828	*trpC2 lacA::P$_{xyl}$ yocM-mCherry ery amyE::P$_{lac}$ ywlE spec ΔywlE::kan*	BIH369 → BIH820
BIH829	*trpC2 lacA::P$_{xyl}$ yocM-mCherry ery amyE::P$_{lac}$ ywlE C7S spec ΔywlE::kan*	BIH369 → BIH821
FS69	*trpC2 ypbH::spec mcsB::kan mecA::tet*	Provided by Franziska Schöttmer (unpublished)
NM107	*trpC2 clpX::kan*	(Gerth et al., 2004)
NM115	*trpC2 ypbH::spec*	(Persuh et al., 2002)
MV210	*trpC2 ypbH::ery*	(Koo et al., 2017) / BGSC
ORB3834	*trpC2 pheA1 Δspx::kan*	(Nakano et al., 2001)
QBP418	PY79 *ΔclpC::tet*	(Pan et al., 2001)

BGSC: Bacillus Genetic Stock Center

2.1.2. Transformation in *E. coli*

200 µL competent cells were thawed on ice before 50-200 ng plasmid DNA or ligation reaction was added. The mixture was kept on ice for 30 min and treated with a heat shock at 42 °C for 45 s. Afterwards the cells were shifted to ice for 5 min and subsequently 1 mL LB medium was added. The cells were incubated shaking at 37 °C for 1 h. After centrifugation for 3 min at 5,000 xg, the pellet was resuspended in 100 µL of the remaining supernatant. At last, the cells were plated on LB agar containing the appropriate antibiotics to select positive clones after incubation overnight at 37 °C.

2.1.2.1. Generating competent cells of *E. coli*

20 mL LB medium was inoculated with a single colony or glycerol stock as a pre-culture. That pre-culture was incubated shaking at 28 °C for 20 h. 4 mL pre-culture were used to inoculate 250 mL of SOB medium supplemented with $MgCl_2$ and $MgSO_4$. The main culture was kept shaking at 18 °C to an OD_{600} of 0.5 – 0.9, before being shifted to ice for 10 min. The cells were harvested at 4 °C and 5,000 xg for 10 min. The pellet was resuspended in 80 mL of TB buffer and incubated on ice for 10 min before re-centrifugation. The cells were resuspended in 20 mL ice-cold TB buffer. DMSO was added to a final concentration of 7 % (v/v). The cells were frozen in liquid N_2 and stored in 200 µL aliquots at -80 °C.

TB buffer	PIPES	10 mM
	$CaCl_2 \cdot 2H_2O$	15 mM
	KCl	250 mM
	$MnCl_2$	55 mM

SOB w/o Mg^{2+}	Tryptone	2 % (w/v)
	Yeast extract	0.5 % (w/v)
	NaCl	10 mM
	KCl	2.5 mM
SOB	SOB w/o Mg^{2+}	
	+ MgCl$_2$	10 mM
	+ MgSO$_4$	10 mM

2.1.3. Transformation in *B. subtilis*

Transformation of PCR-products, plasmids or gDNA into *B. subtilis* was performed by standard methods (Anagnostopoulos and Spizizen, 1961). *AmyE* insertion (pDR111, pPG60, pSG1154) in *B. subtilis* was checked by plating transformants on agar containing 0.4 % starch (w/v) in addition to appropriate antibiotics to check for successful loss of α-amylase by staining starch with Lugol's iodine. *LacA* insertion (pBS2E) was screened by PCR. Integrations into *lacA* instead of the *amyE* locus resulted in a lower expression level (Sauer et al., 2016; Slager and Veening, 2016), which was especially used to minimize a potential unspecific influence of YocM-mCherry in the *in vivo* disaggregation assays. Deletion mutant (*ypbH*::*cm*) was generated firstly fusing mut1/mut2, mut3/mut4 (resistance marker) and mut5/6, and secondly combining all PCR products in a standard overlap fusion PCR (Table 5). Successful gene integrations were re-confirmed by western blotting or fluorescence microscopy (depending on constructs).

2.1.4. Preparation of chromosomal DNA of *B. subtilis*

B. subtilis chromosomal DNA was prepared using the MasterPure Gram Positive DNA Purification Kit (Lucigen) according to instructions of the manufacturer. After cell lysis with ReadyLyse lysozyme in Gram Positive Lysis Solution, DNA precipitation was performed by adding MPC Protein Precipitation Reagent followed by isopropanol. DNA was dissolved in dH$_2$O. Concentrations were determined using the NanoDrop spectrophotometer and subsequently diluted to adequate concentrations for PCR and transformations (300-500 ng/µL).

2.2.   *Competition*

A *B. subtilis* pre-culture was inoculated with a fresh overnight culture to a mixed main culture with an OD of 0.05 each strain (Spizizen minimal medium or Belitsky Minimal Medium for salt stress and LB for heat competition) and grown to 0.4. Cultures were separated and either 0, 2.5, 5 or 15 % NaCl (w/v) was added (salt stress) or separated cultures were incubated at 37 °C, 48 °C and 53 °C (heat stress). At different time points, cells were plated on agar plates containing different antibiotics in serial dilution or analyzed by fluorescence microscopy to calculate the ratio of the chosen strains. Statistics were done with at least three biological replicates using unequal variances students' t-test (Welch's test), which is does not depend on equal variances or sample sizes and is consequently stricter than regular student's t-test. Standard deviations are indicated by error bars.

2.3.   *Spot test*

25 mL LB medium was inoculated 1:50 with overnight culture. Cells were incubated shaking at 37 °C to OD$_{600}$ 1 and kept on ice to stop growth before all samples were serially diluted

1:10 with saline. Starting at OD_{600} 1, 5 µL of each dilution step was put on agar plates containing 0, 0.05 or 2 mM IPTG. The plates were incubated either at 37 °C or 50 °C overnight.

2.4. *Northern blotting and RT-qPCR*

Northern blotting was performed as previously described (Hantke et al., 2018; Simard et al., 2001). 2 µg total RNA per sample was denatured and transferred to a positively charged nylon membrane by upwards capillary transfer overnight (16 h). The integrity and equal loading of the RNA was verified by staining the membrane with methylene blue dye (0.02 % methylene blue, 300 mM sodium acetate pH 5.5). Digoxigenin-labeled RNA probes were generated by *in vitro*-transcription with T7 RNA-polymerase (NEB) and labelled DIG RNA Labelling Mix (Roche). Membranes were hybridized overnight (Simard et al., 2001). The membrane was blocked by incubation in Blocking reagent (Roche Applied Sciences) for 1 h. Anti-digoxigenin antibodies conjugated to alkaline phosphatase (Roche Applied Sciences) were diluted 1:5000 in the same buffer and applied to the blot for 2 h. The membrane was washed. CDP-Star solution (Tropix Inc.) was used as substrate and signals were detected in a ChemiBIS 4.2 imaging system (DNR).

RT-qPCR was performed as previously described (Hantke et al., 2018). 500 ng total RNA was used for Protoscript® II reverse transcriptase (NEB) with 3.5 µM random hexamer primers for 1 h at 42 °C. qPCR was performed using Luna® Universal qPCR Master Mix (NEB) with cDNA equivalent to 5 ng RNA (or 0.5 ng RNA for rRNA targets). Primer efficiency was calculated using a standard curve with serial 10-fold dilutions of cDNA. 23S rRNA was used as the reference gene and the $2^{\Delta\Delta CT}$ Method was used to calculate relative gene expression (Livak and Schmittgen, 2001).

2.5.   *Fluorescence microscopy*

B. subtilis cells were inoculated with a fresh overnight culture to an OD of 0.05 in indicated medium + 0.25/0.5 % xylose (w/v) or 2 mM IPTG (indicated in figure, depending on construct P_{lac} / P_{xyl} and expression level), if not otherwise indicated. Cultures were treated according to experimental setup (e.g. thermotolerance or *in vivo* disaggregation). 1 µL samples were taken for microscopy performed on an object slide coated with 1 % agarose (w/v) in saline (0.9 % NaCl (w/v)). Oil immersion and 10x100 magnifications were used with an AxioImagerM2 Zeiss fluorescence microscope with common gfp and mCherry filters.

2.6.   *Aggregate preparation*

100 mL LB was inoculated with a fresh overnight culture to an OD of 0.05 and grown to 0.4. Cultures were separated and treated A) ± with a 15 min pre-shock of 48 °C or B) ± a 30 min pre-shock of 4 % NaCl w/v. Both were subsequently shifted to A) 53 °C or B) treated with 15 % NaCl w/v. 25 mL samples were taken by centrifugation at 5.000 xg for 10 min at indicated time points. Aggregate preparations were performed as previously described (Runde et al., 2014). Total amount of 2.5 or 5 µg protein, calculated by Bradford test from cellular extract 'CE'; was used for SDS Page analysis (PE: aggregate/enriched pellet fraction).

2.7.   *In vivo disaggregation assay*

B. subtilis cells were inoculated with a fresh overnight culture to an OD of 0.05 in LB + 0.5 % xylose (w/v) to induce P_{xyl} *yocM-mCherry*. At OD_{600} 0.25 – 0.3 cells were treated with a heat shock at 52 °C for 20 min or 50 °C for 30 min, depending on heat sensitivity of the strains used. Cultures were separated and ± 2 mM IPTG was added while shifting the cells to recover

at 37 °C. Samples were taken at indicated time points for aggregate preparations, western blotting and/or fluorescence microscopy.

2.8. *Salt and thermotolerance*

LB media (thermotolerance) or Belitsky minimal medium (salt tolerance) was inoculated with a fresh overnight culture to an OD of 0.05 and kept shaking at 37 °C. At OD_{600} 0.4 cultures were treated ± with a 15 min pre-shock of 48°C or ± 4 % NaCl (w/v) for 30 min. Both were shifted to 54°C or treated with 15 % NaCl (w/v). Samples were diluted and subsequently plated on LB agar at t_0, t_{30}, t_{60} and $t_{120 \text{ min}}$. Counted *cfu* were plotted against time after heat or salt shock. Statistics were done with at least three biological replicates using unequal variances students' t-test (Welch's test). Standard deviations are indicated by error bars.

2.9. *Growth curves*

25 mL LB was inoculated with a fresh overnight culture to an OD_{600} of 0.05 kept shaking at indicated temperature. The OD_{600} was measured every 30 min, if not otherwise indicated. For high throughput measurements, the SpectraMaxM3 or Tecan infinite 200Pro plate reader was used.

2.9.1. Growth curves / screening in plate reader

Pre-cultures were started in the morning 1:50 with fresh overnight cultures (LB medium). The pre and main cultures contained LB medium plus various supplements (e.g. xylose, IPTG), as indicated in each figure. When the exponential phase was reached, all strains were diluted to OD_{600} of 0.1 as OD_{start} of the main cultures. Afterwards, 200 µL of each sample was added into a sterile 96-well plate and growth curve was measured shaking at 37 °C in a SpectraMax M3 or Tecan infinite 200 Pro, if not otherwise indicated. At least four replicates were placed

on random positions on the 96-well plate to ensure reproducibility. For screening purposes, compounds dissolved in DMSO were added with different concentrations (0-64 µM) at the beginning of the growth curve (OD_{start}). A sample containing only DMSO was always used as control.

2.10.   *Biochemical methods*

SDS PAGE (15 % gels) and Blue native PAGE (3.5 – 15 % gradient gels) were performed as previously described (Laemmli, 1970; Schägger and von Jagow, 1991). In semi-dry blotting, proteins were blotted from gels onto nitrocellulose membranes soaked in 20 mM Tris-HCl pH 8, 150 mM glycine and 20 % methanol (v/v). Membranes were blocked afterwards in 1x TBS and 5 % skim milk powder (w/v). The membrane was incubated in 1x TBS + primary antibodies (Pineda Berlin), followed by three washing steps were performed before anti-rabbit or anti-mouse (for the anti-his_6 antibody) alkaline phosphatase conjugate was used as secondary antibody (1:10000). After 10 min equilibration in AP buffer, blots were developed in 10 mL AP buffer + 250 µL BCIP (5 % (w/v) in DMF) + 250 µL NBT (5 % (w/v) in 70 % DMF) or using the ECF western blotting reagent (GE Healthcare).

AP buffer	Tris-HCl pH 9.5	100 mM
	NaCl	100 mM
	$MgCl_2$	5 mM
1x TBS buffer	Tris-HCl pH 7.5	50 mM
	NaCl	150 mM

2.10.1. Protein production

Protein production was performed in *E. coli* BL21 (DE3) (Table 6). Cells were to grown at 37 °C to an OD_{600} of 0.7-0.9 and expression was started by adding 1 mM IPTG. Cells were shifted to 22 °C overnight for protein production. Purification of his_6-tagged proteins was performed by standard nickel affinity chromatography after cell lysis in lysis buffer by French press (Turgay et al., 1997). Lysis buffer was supplemented with 20 mM or 250 mM imidazole during washing and elution step, respectively. ClpC was purified as previously described (Turgay et al., 2001). His-Sumo-YocM was cleaved with Ulp-protease overnight at 4 °C according to manufacturer (ThermoFischer) in lysis buffer. Protein concentrations were calculated using Bradford test and, if necessary, enriched using Vivaspin® spin columns (Sartorius). Proteins were frozen in aliquots with liquid N_2 and stored at -80 °C in storage buffer.

Lysis buffer	Tris-HCl pH 8.0	50 mM
	NaCl	150 mM
	$MgCl_2$	5 mM
Storage buffer	Lysis buffer +	
	Glycerin	10 % w/v

2.10.2. Size exclusion chromatography

Size exclusion chromatography was performed with an ÄKTA FPLC system with a Superose6 Increase 10/300 column (CV: 24 mL) at 4 °C (GE Healthcare). The flowrate was kept constant at 0.5 mL · min^{-1}. For calibration purposes, different marker proteins were used: Thyroglobulin (669 kDa), Ferritin (440 kDa), Catalase (232 kDa), Aldolase (158 kDa),

Ovalbumin (44 kDa), Carbonic anhydrase (29 kDa) and Ribonuclease (13.7 kDa). For formation of hexameric ClpC complex (i.e. + MecA), the sample was incubated at 37 °C + 5 mM ATP for 10 min prior to chromatography. In addition, 0.5 mM ATP was added to the running buffer. ClpC E280A E618A (ATPase inactive Double Walker B mutant) was used instead of wildtype ClpC to increase stability of the oligomeric complex.

Running buffer	Tris-HCl pH 8.0	50 mM
	NaCl	150 mM
	$MgCl_2$	5 mM

2.10.2.1. Protein precipitation

After size exclusion chromatography, all peaks were collected in 1 mL fractions starting at 8 mL elution volume. 110 µL of TCA was added to each 1 mL fraction and the mixture was incubated for 10 min on ice. Samples were centrifuged for 15 min at 10,000 xg and the supernatant was discarded. The pellet was washed twice with 2 mL of acetone and kept on ice for 15 min before re-centrifugation. At last, the pellet was dried until all acetone was evaporated. 20 µL of 1x TBS was added and kept shaking at 37 °C for 5 min before being analyzed by SDS PAGE.

2.10.3. Malachite green ATPase and degradation assay

The staining solution was prepared in the described ratio and kept stirring under exclusion of light for 1 h before use. A calibration was performed with KH_2PO_4 as standard from 0 to 1000 µM. The reactions were performed in 1x ATPase assay buffer with a final 1 µM of protein samples in a total of 50 µL. Reactions were started by adding 1 µL ATP (200 mM, final 4 mM) and shifting of the mixture to 37 °C. At indicated time points, 10 µL of the

reaction mixture was added to 160 µL staining solution in a 96-well plate to stop the reaction. Afterwards 20 µL of sodium citrate (34 % (w/v)) was added and the released phosphate was measured at 660 nm in a SpectraMax M3 photometer. Degradation assay was performed in ATPase Assay buffer with an ATP regeneration system according to (Schlothauer et al., 2003) with all proteins diluted to a final 1 µM. Substrate αβ-casein was used with a final concentration of 3 µM. Reaction was started at 37°C by adding a final 4 mM ATP and samples were taken for SDS-Page at indicated time points.

5x ATPase assay buffer	Tris-HCl pH 8.0	250 mM
	KCl	250 mM
	$MgCl_2$	25 mM
Staining solution	Malachite Green hydrochloride	4.5 µg/mL, 30 mL
	Ammonium molybdate	4.2 % in 4 M HCl, 10 mL
	Triton X	100 %, 40 µL

2.10.4. Light scattering assays

2.10.4.1. Luciferase

5 µL of 1 mg · mL^{-1} luciferase (firefly luciferase, Roche) was denatured for 40 min at 25 °C in 200 µL 1x luciferase buffer + 114 mg GuHCl. 12.5 µL were added to 987.5 µL luciferase buffer (final 0.03 µM) containing proteins of interest at indicated concentrations and aggregation of luciferase was observed by light scattering at 360/360 nm in a Jasco FP6500 spectrofluorometer (sensitivity: medium) (Hantke et al., 2018).

5x luciferase buffer	HEPES/KOH pH 7.6	125 mM
	KCl	250 mM
	MgCl$_2$	25 mM
	DTT	1 mM

2.10.4.2. Malate dehydrogenase

Aggregation of Malate dehydrogenase (Mdh, final 2 μM) was performed in 1x refolding buffer at 47 °C containing different proteins of interest or other supplements at indicated concentrations. Light scattering was measured at 360/360 nm in a Jasco FP6500 spectrofluorometer (sensitivity: low) (Schlothauer et al., 2003). For Mdh refolding, Mdh was denatured with 6 M GuHCl and refolding was initiated by dilution 1:100 (final 0.5 μM) in 1x refolding buffer containing proteins of interest or other supplements at indicated concentrations. Samples were taken at indicated time points for activity measurements to follow refolding process. No increase in light scattering was observed at 360/360 nm under any tested conditions.

5x Mdh refolding buffer	Tris-HCl pH 7.5	500 mM
	KCl	750 mM
	Mg(OAc)$_2$	100 mM
	DTT	5 mM

The activity of Mdh was measured at indicated time points by adding 5 μL of the reaction mixture into 250 μL Mdh assay buffer. The reaction was followed at 340 nm in a SpectraMaxM3 (Figure 10) (Schlothauer et al., 2003). Standard deviations of at least three biological replicates are shown as error bars. p-values were calculated from Welch's test.
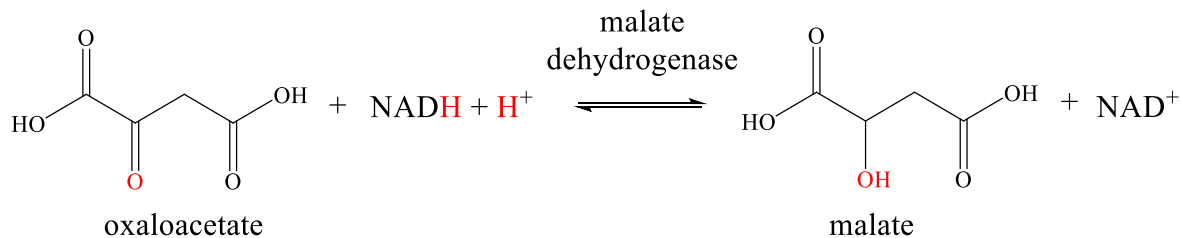
Figure 10: Enzymatic reactions of malate dehydrogenase (Mdh).

NADH is oxidized during the reaction of oxaloacetic acid to malate by Mdh. The reaction can be visualized by following the absorbance at 340 nm (NADH) in a spectrophotometer.

5 mL Mdh assay buffer	K^+-phosphate buffer pH 7.6	1 M, 750 µL
	DTT	1 mM
	NADH	0.931 mg
	Oxaloacetate	0.33 mg
	dH$_2$O	ad 5 mL

2.10.4.3. Citrate synthase

Citrate synthase was unfolded for 2 h in 0.1 M Tris HCl pH 8.0 by 6 M GuHCl. Refolding was induced by dilution 1:100 (Buchner et al., 1991) into reaction mixture (final 0.1 µM) containing proteins of interest and other supplements while measuring light scattering at 360/360 nm in a Jasco FP6500 spectrofluorometer (sensitivity: low). Activity was measured at indicated time points (5 µL samples, 30 °C) by conversion of Acetyl-CoA (0.047 mM) and oxaloacetate (0.023 mM) into citrate and CoA-SH, which reacts with the Ellman's reagent (0.1 mM DTNB) (Figure 11). The reaction was observed at 412 nm in a SpectraMaxM3 at 30 °C (Faloona and Srere, 1969; Hristozova et al., 2016).
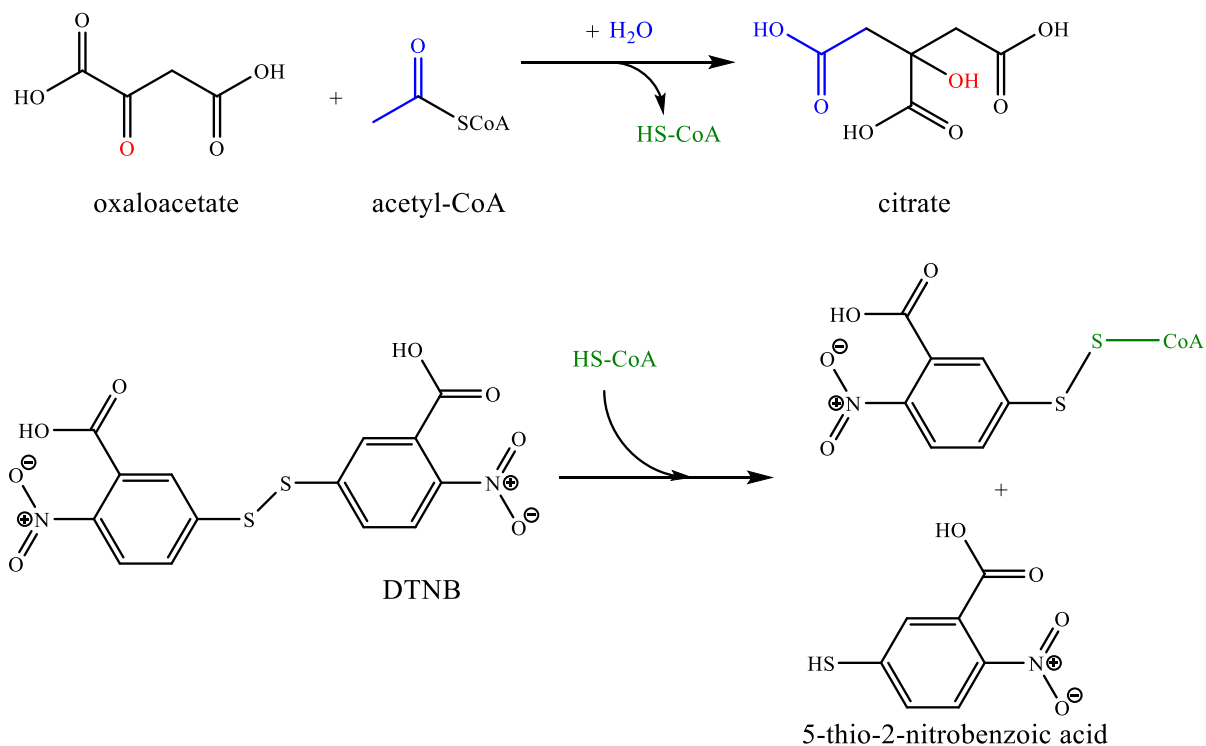
Figure 11: Enzymatic reactions of citrate synthase (CS).

While oxaloacetate is turned into citrate, acetyl-CoA is cleaved to CoA-HS, which reacts with the Ellman's reagent (DTNB). The reaction can be followed by observing the formation of 5-thio-2-nitrobenzoic acid at 412 nm.

3. Results

3.1. *The role of sHsp YocM during salt stress*

Despite the occurrence of small heat shock proteins in all domains of life, no sHsp has been identified as such in the Gram-positive model organism *B. subtilis* yet. In *B. subtilis*, the three genes *cotM*, *cotP* and *yocM* all encode for proteins containing the sHsp characteristic α-crystallin domain, but while CotM and CotP were observed to be part of the proteinaceous spore coat during spore development, YocM still lacks an assigned role in the cell (Henriques et al., 1997; McKenney et al., 2013, 2010; McKenney and Eichenberger, 2012; Wang et al., 2009). However, transcriptomics data gave a first hint towards a role of YocM during salt stress (Nicolas et al., 2012).

To further elucidate the stress mediated transcriptional and translational regulation of the potential sHsp YocM in more detail, RT-qPCR, northern and western blotting were performed (Figure 12). It was exhibited that the levels of the *yocM* transcript were significantly raised after 6 % NaCl salt shock, which was not as pronounced when looking at the translational level. S738, an asRNA to *yocM*, might additionally influence the efficient translation of YocM (Nicolas et al., 2012). However, a sHsp characteristic, significant heat mediated upshift in transcript or protein level, could not be observed for *yocM* and YocM, respectively (Figure 12).
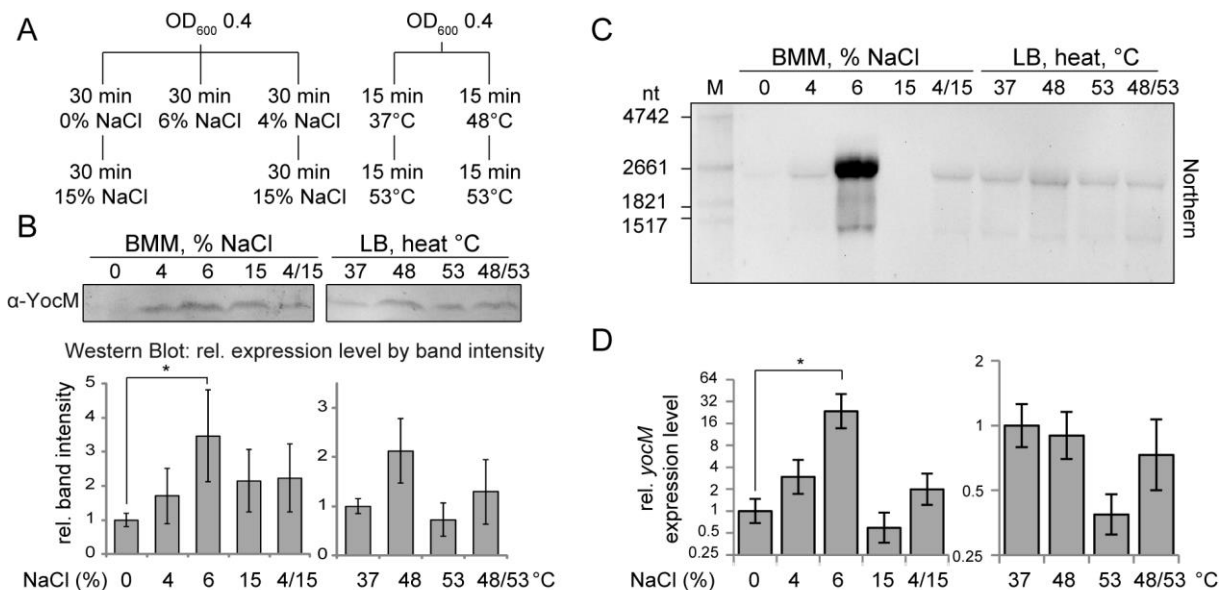
Figure 12: *yocM* is induced upon salt shock.

A) Sampling scheme. B) α-YocM western blotting according to sampling scheme (A) (salt, Belitsky minimal medium BMM / heat, LB medium). Translational level of YocM was calculated from western blot band intensity using ImageJ from at least three biological replicates with *: p<0.05. Error bars indicate standard deviations. 20 µg protein of whole cell extract was analyzed. C/D) Quantitative PCR analysis of *yocM* under indicated heat and salt stress conditions and northern blotting (of one representative sample to visualize qPCR results) were performed by Heinrich Schäfer (IFMB / LUH) with provided samples taken according to A. 2 µg RNA of whole cell extract was analyzed. Error bars (D) indicate standard deviations of at least three biological replicates. *: p < 0.05 (Kruskal-Wallis).

As *yocM* is upregulated upon salt shock, both a Δ*yocM* deletion mutant and a P$_{lac}$ *yocM* overexpression strain were examined towards salt sensitivity. The Δ*yocM* mutant appeared more sensitive towards higher NaCl concentrations, which was reversed in the P$_{lac}$ *yocM* strain (Figure 13AB). Additionally, elevated synthesis of the α-crystallin domain of YocM alone or in combination with either the NTD or the CTD did not positively affect growth at 5 % NaCl (Figure 13C). This truncation suggested the necessity of the full length YocM in the P$_{lac}$ *yocM* overexpression strain to display accelerated growth under higher salt concentrations (Figure 13C). To allow a direct comparison between the wildtype strain and the Δ*yocM* mutant, both strains were analyzed in a competition growth experiment where a mixed culture with equal amounts of both strains was examined (Figure 13DE). While the

Δ*yocM* mutant was slightly outcompeted by the wildtype strain when grown in SMM with 5 % NaCl (Figure 13D), the overexpression of *yocM* in the P$_{lac}$ *yocM* strain significantly enhanced growth under these conditions (Figure 13E).
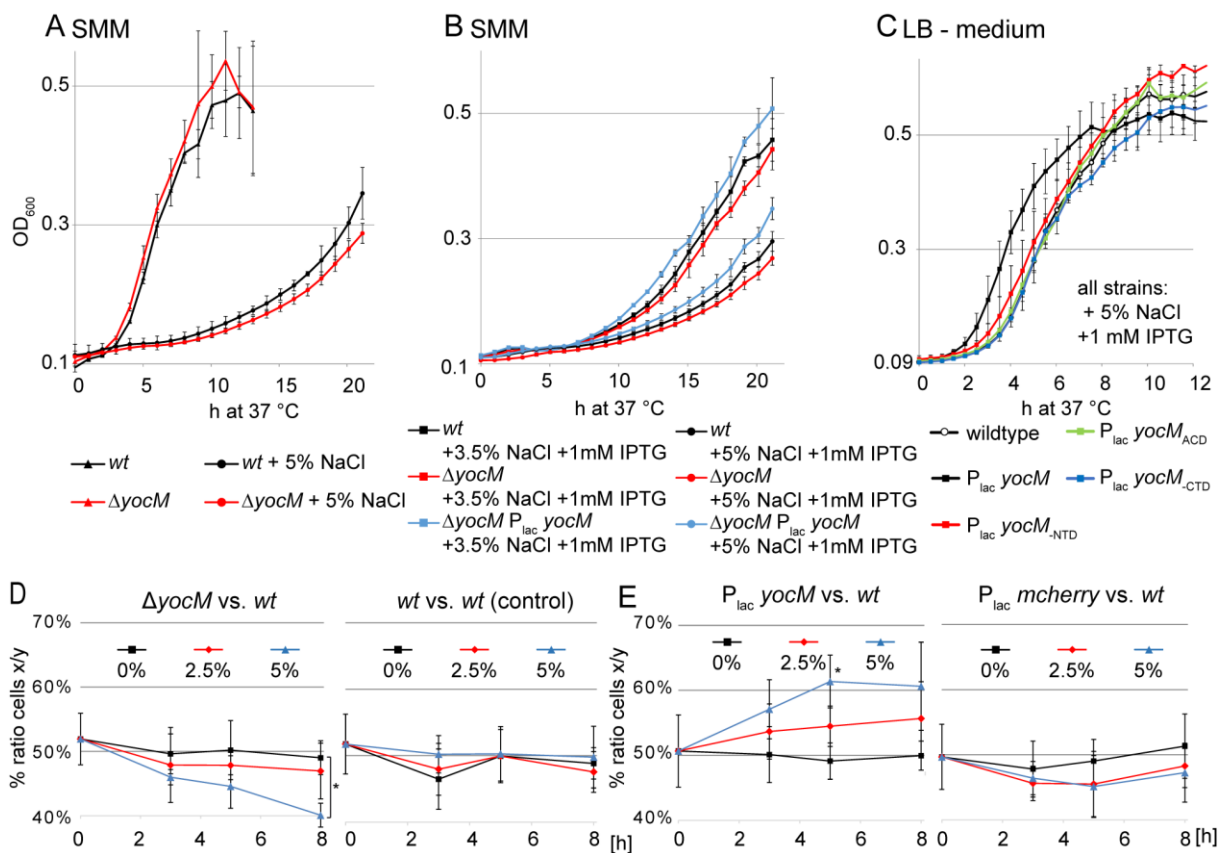
Figure 13: Levels of YocM correspond with salt sensitivity.

A) Growth of *B. subtilis* wt (black) and Δ*yocM* (BIH2, red) was compared in SMM ± 5% NaCl at 37 °C. B) Growth of *B. subtilis* wt (black), Δ*yocM* (BIH2, red) and Δ*yocM* P$_{lac}$ *yocM* (BIH286, blue) was compared in SMM ± 3.5/5% NaCl at 37°C + 1 mM IPTG. C) Growth of *B. subtilis* wt (white circle), P$_{lac}$ *yocM* (BIH182, black), P$_{lac}$ *yocM*$_{-NTD}$ (BIH343, red), P$_{lac}$ *yocM*$_{ACD}$ (BIH344, green) and P$_{lac}$ *yocM*$_{-CTD}$ (BIH345, blue) was compared in LB + 5% NaCl + 1 mM IPTG at 37°C. All growth curves were performed in a Tecan infinitePro200 plate reader. Error bars indicate standard deviations calculated from three biological replicates. D) *B. subtilis* wt constitutively expressing *mcherry* (BIH240) and Δ*yocM* constitutively expressing *gfp* (BIH274) were analyzed in a competition experiment in SMM with wt constitutively expressing *gfp* as control (BIH148). E) *B. subtilis* P$_{lac}$ *yocM* (BIH182) vs. wt were analyzed in a competition experiment under salt stress conditions with P$_{lac}$ *mcherry-yocM*$_{CTD}$ (BIH382) as control. Samples were taken at indicated time points for fluorescence microscopy and *cfu* counting on agar plates. Error bars indicate standard deviations (*: p<0.05 Welch's test) calculated from three biological replicates.

When examining a more severe salt shock of 15 % NaCl, the Δ*yocM* deletion mutant was significantly impaired in salt tolerance development (Figure 14A). However, artificially raised levels of YocM did only moderately improve both salt tolerance and resistance (Figure 14B). Nevertheless, the data suggests that YocM positively influences the ability of *B. subtilis* to deal with salt stress.
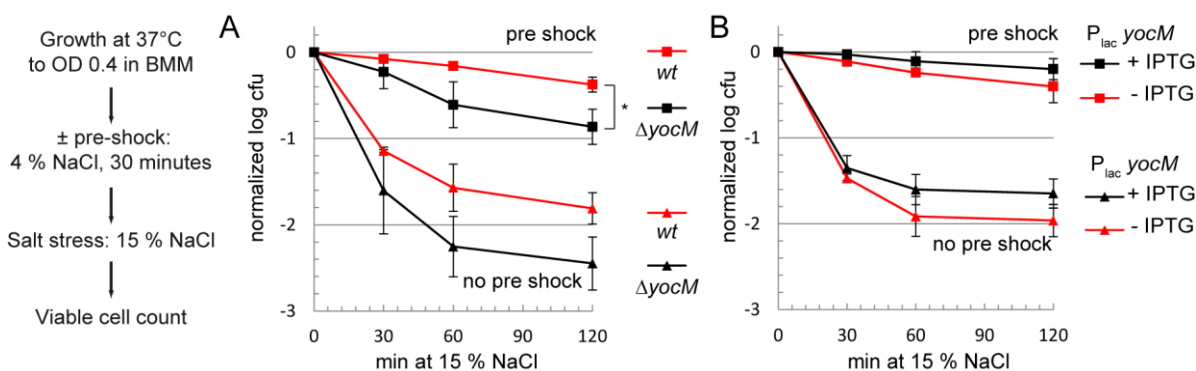

Figure 14: A *yocM* deletion mutant is impaired in salt tolerance development.

A) *B. subtilis* wt (red) and Δ*yocM* mutant (BIH2, black) were treated with a harsh 15 % salt shock and survival was measured by *cfu* at indicated time points. B) *B. subtilis* P$_{lac}$ *yocM* (BIH182) was analyzed as in A without IPTG (red) and with IPTG (black). Squares: with 30 min pre-shock at 4 % NaCl; triangles: without pre-shock. Log$_{10}$-values of viable cell count were normalized and standard deviations (indicated error bars) were calculated from three biological replicates (*: $p<0.05$ Welch's test).

As a member of the family of small heat shock proteins, the influence of varying levels of YocM regarding sensitivity towards heat stress was also investigated. The Δ*yocM* mutant and the wildtype strain were compared in a competition experiment regarding their ability to outgrow each other at elevated temperatures. It was observed that both strains behaved similarly (Figure 15A), albeit overexpression of *yocM* in the P$_{lac}$ yocM strain gave an advantage towards growth at 48 °C (Figure 15B). Furthermore, both thermoresistance and thermotolerance of the Δ*yocM* mutant were investigated. The overexpression of *yocM* in the P$_{lac}$ *yocM* strain led to a minor protective effect regarding heat stress while the deletion of *yocM* did not affect sensitivity towards heat stress (Figure 15CD).
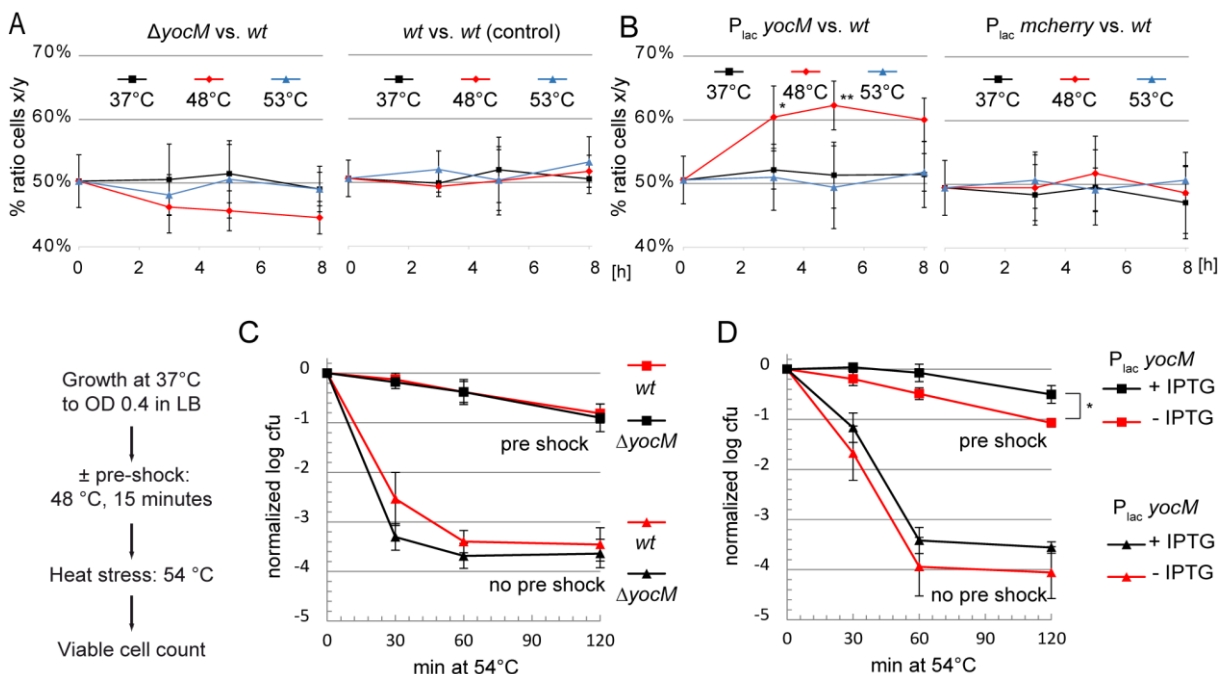
Figure 15: Deletion of *yocM* does not affect heat sensitivity.

A) *B. subtilis* wildtype constitutively expressing *mcherry* (BIH240) and Δ*yocM* constitutively expressing *gfp* (BIH274) were analyzed in a competition experiment in LB with a wildtype strain constitutively expressing *gfp* as control (BIH148) at indicated temperatures 37 °C (black) / 48 °C (red) / 53 °C (blue). B) *B. subtilis* P_{lac} *yocM* (BIH182) vs. wt were analyzed in a competition experiment with P_{lac} *mcherry-yocM$_{CTD}$* (BIH382) as control at indicated temperatures 37 °C (black) / 48 °C (red) / 53 °C (blue). Samples were taken at indicated time points for fluorescence microscopy and *cfu* on agar plates. C) *B. subtilis* wt (red) and Δ*yocM* mutant (BIH2, black) were treated with a 54 °C heat shock and survival was measured by *cfu* at indicated time points. D) *B. subtilis* P_{lac} *yocM* (BIH182) was analyzed (see A) without IPTG (red) / with IPTG (black). Squares: with 15 min pre-shock at 48 °C; triangles: no pre-shock. Log$_{10}$-values of viable cell count were normalized and standard deviations (indicated error bars) were calculated from three biological replicates (*: p<0.05, **: p<0.01, Welch's test).

3.1.1. YocM-mCherry as a marker for protein aggregation

As YocM was detected in the aggregate fraction, the subcellular localization of YocM was additionally determined *in vivo* with a xylose inducible P_{xyl} *yocM-mcherry* strain and verified by co-localization with malate dehydrogenase fused to GFP (Mdh-GFP), a known aggregate marker protein (Runde et al., 2014). Under non-stressed conditions both YocM-mCherry and Mdh-GFP were homogenously distributed throughout the cell (Figure 16). After salt or heat shock distinct fluorescent YocM-mCherry foci were formed, which were localized and distributed similar to subcellular protein aggregates (Kirstein et al., 2008; Runde et al., 2014).
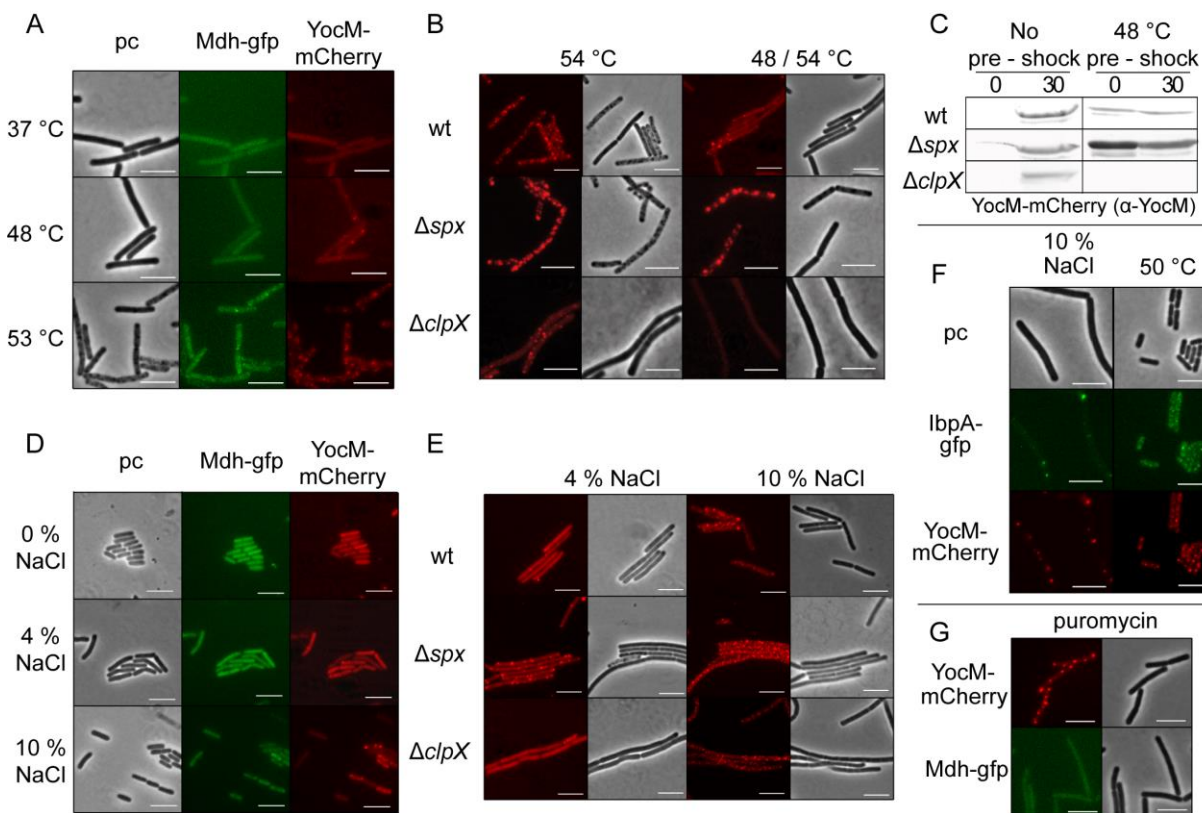
Figure 16: YocM-mCherry targets subcellular protein aggregates *in vivo*.

A/D) Strain *mdh::mdh-gfp P$_{xyl}$ yocM-mCherry* (BIH305) was grown in A) LB or D) BMM + 0.25 % xylose and treated with a 15 min shock at indicated temperature or salt concentration. B/E) Strain *P$_{xyl}$ yocM-mCherry* in Δ*spx* and Δ*clpX* background (BIH73, BIH84, BIH85) was grown in LB with 0.25 % xylose and treated with B) 15 min 54 °C heat shock ± a 15 min 48 °C pre-shock or E) with indicated salt concentration for 30 min. C) Corresponding western blot of aggregate fractions of B) after 30 min of 54 °C heat shock of *P$_{xyl}$ yocM-mCherry* (BIH73) compared with Δ*spx* and Δ*clpX* mutants (BIH84, BIH85). Western blot α-YocM shows band of YocM-mCherry in aggregate fraction indicating amount of aggregates in comparison to wt. F) Strain *P$_{xyl}$ ibpA-gfp P$_{xyl}$ yocM-mCherry* (BIH91) was grown with 0.25 % xylose and either treated with 15 min heat shock at 50 °C or 30 min salt shock with 10 % NaCl. G) Strain *mdh-gfp P$_{xyl}$ yocM-mCherry* (BIH305) treated with 20 µg/mL puromycin for 15 min in LB medium. Grey: phase contrast; red: mCherry; green: gfp (standard mCherry/gfp filter). Scale bar: 5 µm

When elucidating the distribution of YocM-mCherry in different background mutant strains, which are known to accumulate more (Δ*spx*) or less (Δ*clpX*) subcellular protein aggregates than the wildtype (Runde et al., 2014), it was observed that the degree of YocM-mCherry marked aggregates reflected and confirmed those phenotypes of a Δ*spx* and a Δ*clpX* strain (Figure 16BE). At the same time, the expression of *yocM-mcherry* did not affect heat stress resistance per se (Figure 17). Moreover, comparing the sHsp fusion protein YocM-mCherry

to the *E. coli* sHsp IbpA fused to GFP resulted in a similar distribution *in vivo* (Figure 16F) (Lindner et al., 2008; Runde et al., 2014). Furthermore, after treatment with puromycin, which leads to pre-termination of peptide chain during translation, only YocM-mCherry instead of Mdh-GFP was observed to co-localize with emerging subcellular protein aggregates (Figure 16G). While YocM-Cherry associated with protein aggregates consisting of puromycin induced, unfinished protein fragments, Mdh-GFP was only appropriate as an aggregation marker protein at elevated temperatures due to unfolding of Mdh *per se* (Runde et al., 2014).
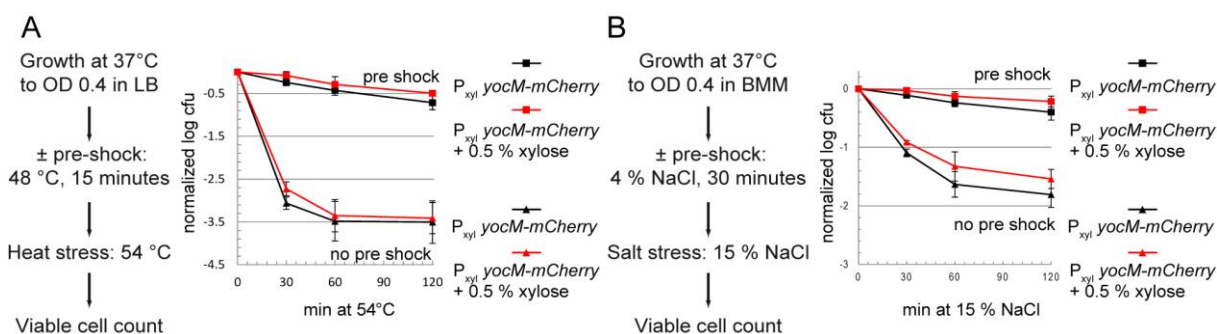
Figure 17: Elevated levels of YocM-mCherry do not affect heat and salt resistance.

B. subtilis strain P_{xyl} *yocM-mcherry* was grown ± 0.5 % xylose and treated at OD_{600} 0.4 with A) a 54 °C heat shock or B) a 15 % salt shock according to the respective scheme and survival was measured by *cfu* at indicated time points. Squares: A) with 15 min 48 °C pre-shock / B) with 30 min pre-shock at 4 % NaCl; triangles: without pre-shock. Log_{10}-values of viable cell count were normalized and standard deviations (indicated error bars) were calculated from three biological replicates.

For further characterization, the *yocM* overexpressing strain (P_{lac} *yocM*) was examined with the new established *yocM-mcherry* marker. Surprisingly, the formation of polar fluorescent foci was observed when, besides from *yocM-mcherry*, *yocM* was overexpressed (Figure 18A). It is important to note that overexpression of *yocM* did not result in the formation of more insoluble protein aggregates and protected *B. subtilis* cells to a certain agree against salt and heat stress, while expression of *yocM-mcherry in trans* affected the heat sensitivity and thermotolerance of *B. subtilis* to a much lesser extent than *yocM*, suggesting only partial

YocM activity (Figure 13, Figure 15, Figure 17 and Figure 19). When IPTG was removed and P$_{lac}$ *yocM* no longer induced, the foci disappeared within 180 min (Figure 18A). After heat shock and subsequent recovery at 37 °C, all heat induced subcellular aggregates were cleared, but YocM based foci were still apparent (Figure 18B). It was tempting to speculate that the formation of those sHsp clusters at the polar region might be an artifact due to overexpression and interaction of both a sHsp and a sHsp-fusion protein. Hence, the sHsp IbpA from *E. coli* was compared to YocM. As expected, whenever YocM-mCherry or IbpA-GFP was present in the cell and subsequently *yocM* or *ibpA* was overexpressed, fluorescent foci were formed at the cellular pole (Figure 18C).
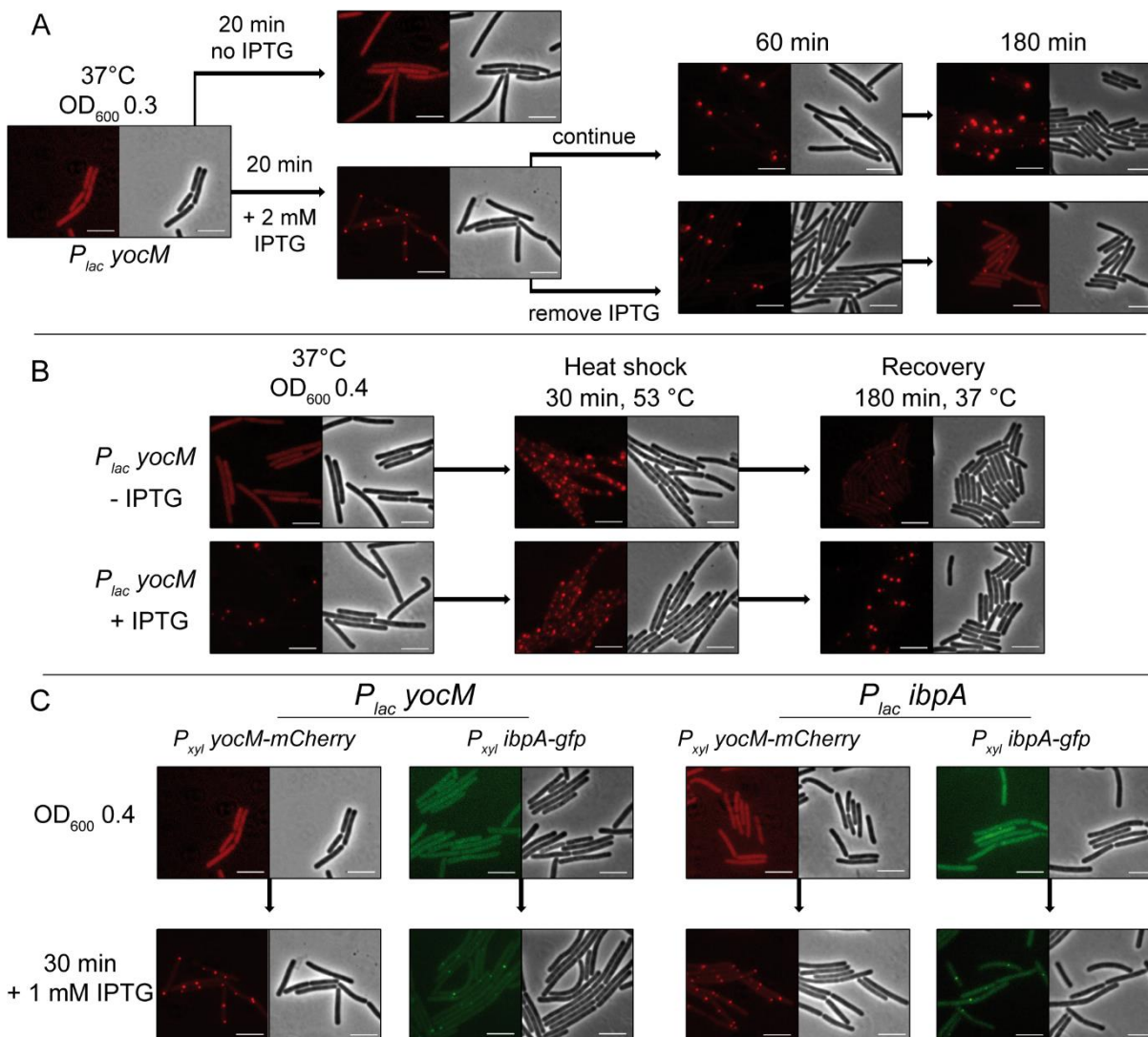
Figure 18: Overexpression of *yocM* leads to formation of polar fluorescent clusters in the presence of YocM-mCherry.

A) Strain P_{lac} *yocM* P_{xyl} *yocM-mcherry* (BIH629) was grown in LB + 0.5 % xylose until treated at OD_{600} 0.3 ± 2 mM IPTG for 20 min. Cells were harvested by centrifugation and resuspended in medium ± IPTG for recovery at 37 °C for 3 h. B) Strain P_{lac} *yocM* P_{xyl} *yocM-mcherry* (BIH629) was grown in LB + 0.5 % xylose ± 1 mM IPTG until treated OD_{600} 0.4 ± heat shock at 53 °C for 30 min. Cells were then shifted to 37 °C for 3 h to recovery. C) Strains P_{lac} *ibpA* P_{xyl} *yocM-mcherry* (BIH610), P_{lac} *yocM* P_{xyl} ibpA-*gfp* (BIH631), P_{lac} *yocM* P_{xyl} *yocM-mcherry* (BIH629) and P_{lac} *ibpA* P_{xyl} *ibpA-gfp* (BIH634) were grown in LB + 0.5 % xylose and treated with 1 mM IPTG at OD_{600} 0.4 for 30 min. Grey: phase contrast; red: mCherry; green: gfp (standard mCherry/gfp filter). Scale bar: 5 µm

Collectively, the data underline the YocM-mCherry fusion protein as a useful tool to investigate protein aggregate formation *in vivo*. However, studying the effect of sHsp in stress response by using a sHsp based marker protein requires specific attention.

3.1.2. The effect of salt stress on protein aggregation

Exposure to salt leads to changes in turgor pressure, cell size and intracellular ion composition, which can concurrently result in protein unfolding and potential protein aggregation (Bourot et al., 2000; Ignatova and Gierasch, 2006; Stadmiller et al., 2017). YocM was detected in the enriched aggregate fraction after exposure to severe salt stress and, when overexpressed, also observable in the cellular extract (Figure 19). However, in protein aggregate preparations only minor amounts of protein aggregates were observed after a salt shock compared to heat treated cells suggesting that the effect of heat stress on protein unfolding and aggregation is substantially different from the influence of salt stress (Figure 19) (Hantke et al., 2018; Runde et al., 2014). Though, the aggregate marker protein malate dehydrogenase (Mdh) still appeared to be associated with the salt induced aggregated protein fraction (Runde et al., 2014). The amount of Mdh in this fraction increased during severe salt exposure, while being decreased in the IPTG-induced P_{lac} *yocM* strain, suggesting that YocM can prevent Mdh aggregation during severe salt shock (Figure 19). IPTG per se had no significant influence on amount of aggregates at used concentrations (Hantke et al., 2018).
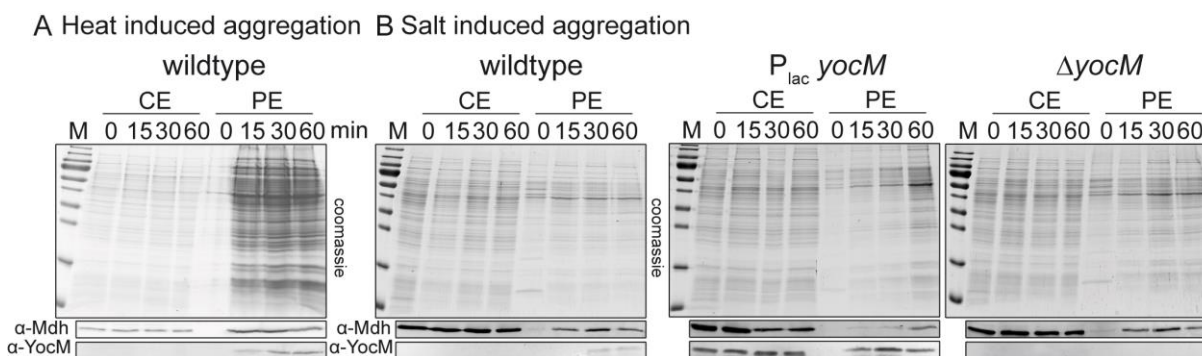
**Figure 19: Aggregate preparations reveal minor aggregate formation after salt compared to heat shock.**

Time-resolved aggregate preparations after A) 54 °C heat shock and B) 15% salt stress with SDS-page and α-YocM/α-Mdh western blotting of *B. subtilis* wt, P_{lac} *yocM* (BIH182, + 1 mM IPTG) and Δ*yocM* (BIH2). 2.5 µg of whole cell extract was analyzed. CE: cellular extract, PE: enriched pellet/aggregate fraction.

Moreover, the YocM-mCherry marked foci after salt stress appeared much more heterogeneous and fragmented compared to more distinct ones after heat stress (Figure 16). The YocM-mCherry fusion protein obviously co-localizes with all aggregated proteins. However, the salt shock induced and potentially more fragile aggregates might be more prone to be removed during the stringent washing steps of the aggregate preparation protocol which could explain the different results of fluorescence microcopy and aggregate preparations (Figure 16 and Figure 19).

To further elucidate the different nature of heat and salt stress mediated unfolding, it was hypothesized that while heat stress affects all proteins in the cell, salt stress might especially influence the folding of nascent polypeptide chains and structurally sensitive proteins. To test this hypothesis, chloramphenicol was used to arrest translation and reduce the number of nascent chains. As speculated, chloramphenicol resulted in a significant 20 % reduction of cells bearing YocM-mCherry marked subcellular protein aggregates following salt shock (Figure 20A). Furthermore, the amount of intracellular protein aggregates after heat shock did not differ from cells that were previously treated with chloramphenicol (Figure 20BC). At the same time it is important to note that the addition of chloramphenicol per se did not affect the total amount of protein aggregates and/or levels of YocM-mCherry (Figure 20DE).
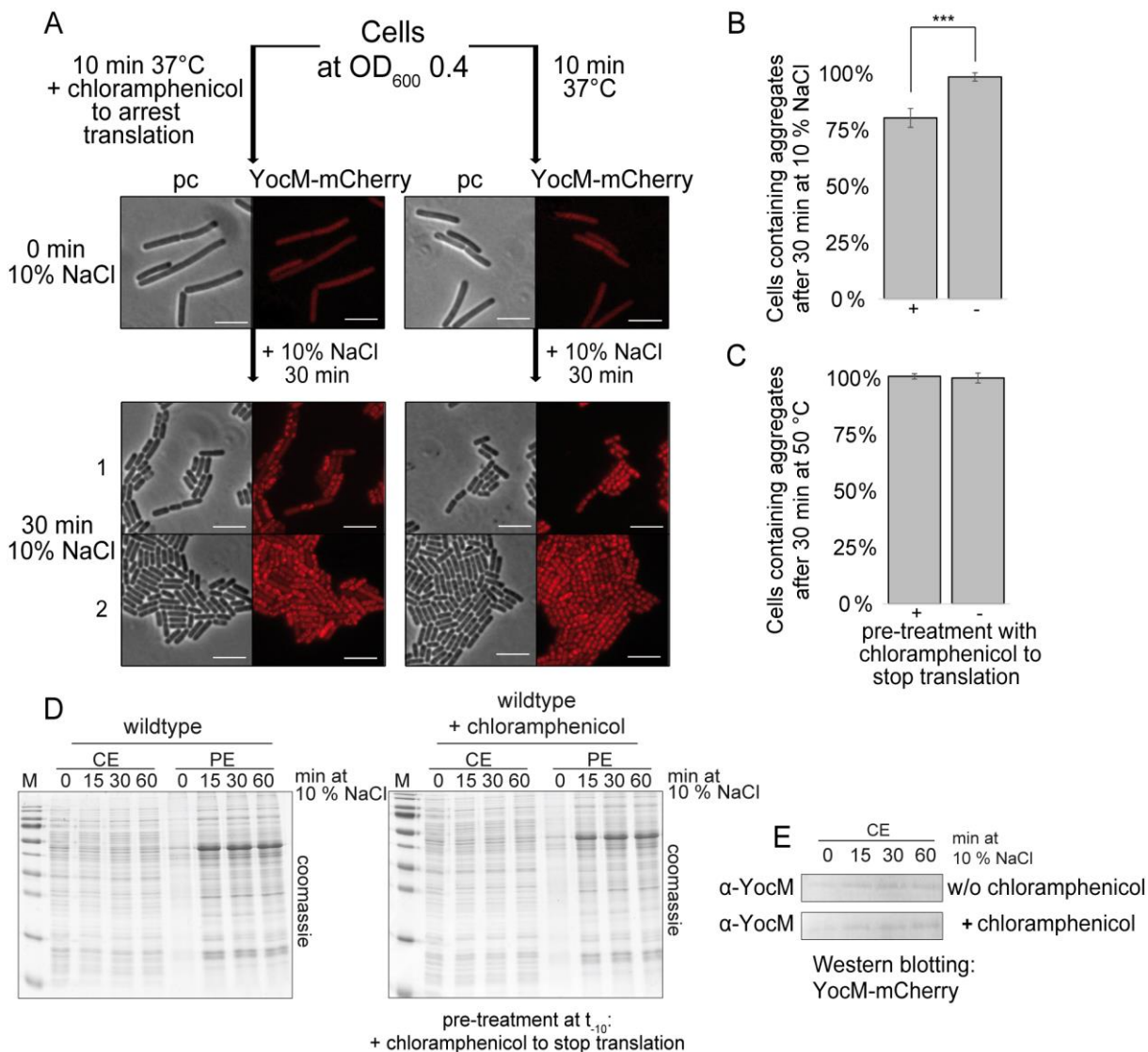
Figure 20: Impaired translation causes reduced protein aggregation after salt shock.

Strain P_{xyl} *yocM-mCherry* (BIH369) was grown in BMM + 0.5 % xylose and treated ± with final 25 µg · mL^{-1} chloramphenicol at OD$_{600}$ 0.4 for 10 min (LB medium for heat shock in C). After subsequent addition of 10 % NaCl cells were analyzed at t_{30}. Two analogous examples of salt shocked cells are shown (1/2). Grey: phase contrast; red: mCherry. Scale bar: 5 µm. Error bars indicate standard deviations calculated from three biological replicates (***: p<0.001, Welch's test). D) SDS-PAGE analysis of aggregate preparations at indicated time points after treatment with 10 % NaCl according to materials and methods with α-YocM western blotting (E) to detect levels of YocM-mCherry. 5 µg of whole cell extract was analyzed. CE: cellular extract, PE: enriched pellet/aggregate fraction.

3.1.3. Interplay of YocM with the PQC

A synergistic interplay of sHsps with the PQC network has been observed e.g. in *E. coli* when the combination of an *ibpA* deletion with Δ*dnaK* and Δ*clpB* deletion mutants resulted in an enhanced phenotype towards heat stress (Kitagawa et al., 2000; Mogk et al., 2003a, 2003b; Thomas and Baneyx, 1998). To determine the relation of YocM with the PQC in *B. subtilis*, the Δ*yocM* strain and additional deletions of *dnaK* and *clpC* were investigated regarding an enhanced phenotype upon heat and salt stress. First it has to be noted that despite a Δ*dnaK*Δ*clpC* double deletion mutant displayed severely impaired thermoresistance and thermotolerance, the sensitivity towards salt stress was not as affected, suggesting a negligible role of ClpC or DnaK in salt stress response in general (Figure 21). Additional deletion of *yocM* did not result in any obvious synergistic phenotype. However, whereas a Δ*yocM* deletion and the wildtype strain were indistinguishable regarding heat sensitivity, a triple Δ*yocM*Δ*dnaK*Δ*clpC* mutant strain was more impaired in thermoresistance than a Δ*dnaK*Δ*clpC* double mutant (Figure 21C). Furthermore, the induction of P$_{lac}$ *yocM* did not influence the cellular level of various chaperones indicating an independent and non-regulatory role in PQC network (Figure 21E).
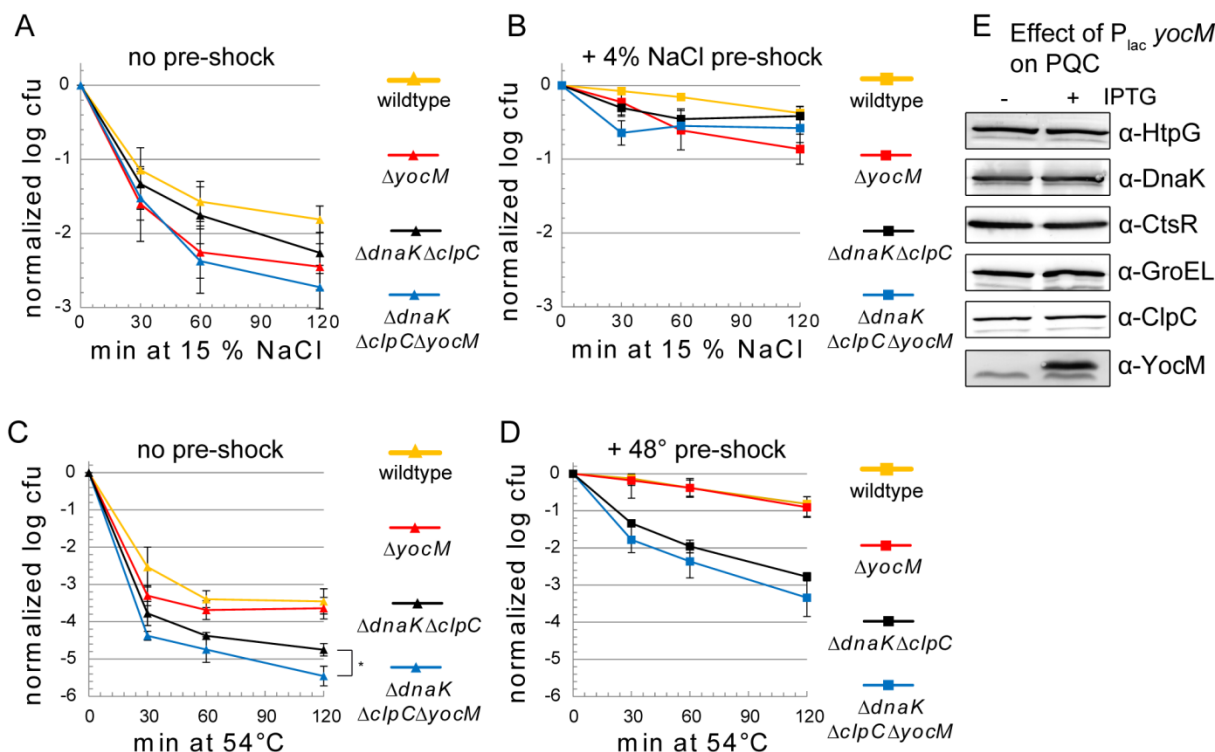
Figure 21: YocM potentially interacts with protein quality control system in *B. subtilis*.

A)-D) Wildtype (yellow), Δ*yocM* (BIH2, red), Δ*dnaK*Δ*clpC* (BIH79, black) and the triple Δ*dnaK*Δ*clpC*Δ*yocM* mutant strain (BIH121, blue) were treated with (A) a 15% NaCl salt shock (B after 30 min 4% NaCl) or (C) a 54 °C heat shock (D after 15 min 48°C) and survival was measured by *cfu* at indicated time points. Log$_{10}$-values were normalized and error bars indicate standard deviations (*: p<0.05, Welch's test). E) Induction of P_{lac} *yocM* (BIH182) by 1 mM IPTG for 30 min at OD$_{600}$ 0.4. 5 µg of whole cell extract was analyzed by western blotting.

3.1.4. CotM and CotP do not play a role in the PQC

Next it was investigated whether the other sHsp paralogs (CotM and CotP) played a role in stress response. Hence, all combinatorial single, double and triple deletion mutant strains of Δ*yocM*, Δ*cotM* and Δ*cotP* were tested, respectively. Thereby, thermotolerance development and thermoresistance were unaffected under tested conditions in all strains examined (Figure 22ABC). However, when testing salt sensitivity, all strains lacking *yocM* were less salt resistant, independent of the presence of *cotM* and *cotP*, suggesting that CotM and CotP play no significant role in PQC and that their apparent function is possibly restricted to their known role in proteinaceous coat formation during spore development (Figure 22DEF)

(McKenney et al., 2013). Moreover, both CotM-mCherry and CotP-mCherry did not interact with heat or salt stress generated protein aggregates as well as the YocM-mCherry fusion protein (Hantke et al., 2018). Collectively the data suggests that out of the three *B. subtilis* sHsp paralogs, only YocM fulfils a role in PQC.
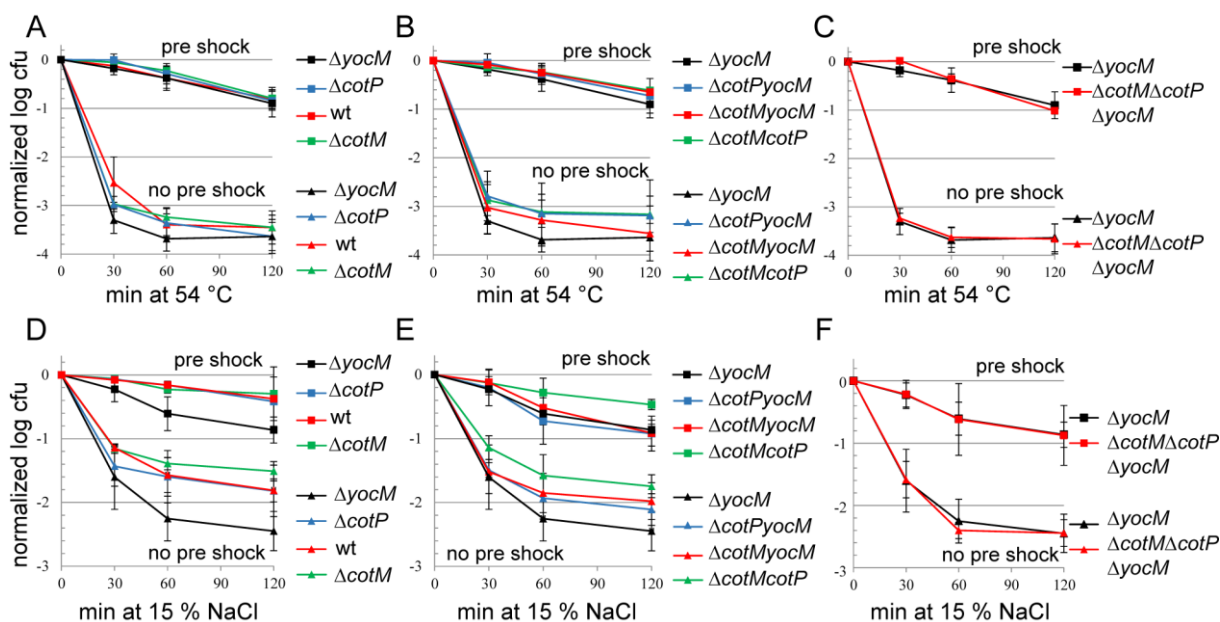
Figure 22: CotM and CotP are not involved in salt and heat stress response.

A)-F) Δ*yocM* (BIH2), Δ*cotM* (BIH339) and Δ*cotP* (BIH331) were compared to wt in a salt and thermotolerance experiment according to materials and methods. A)/D) Black: Δ*yocM* (BIH2); blue: Δ*cotP* (BIH331); red: wt (BIH1); green: Δ*cotM* (BIH339). B)/E) Black: Δ*yocM* (BIH2); blue: Δ*cotP*Δ*yocM* (BIH333); red: Δ*cotM*Δ*yocM* (BIH348); green: Δ*cotM*Δ*cotP* (BIH351). C)/F) Red: Δ*cotM*Δ*cotP*Δ*yocM* (BIH352); black: Δ*yocM* (BIH2). Squares (A/B/C): + 15 min pre-shock at 48 °C; triangles (A/B/C): no pre-shock. Squares (D/E/F): + 30 min pre-shock at 4 % NaCl; triangles (D/E/F): no pre-shock. Log$_{10}$-values of viable cell count were normalized and experiment was performed at least three times. Standard deviations are indicated as error bars.

3.1.5. YocM accelerates protein aggregation *in vitro*

To gain biochemical evidence for the obtained phenotype *in vivo*, YocM was purified and analyzed *in vitro*. Since sHsps usually occur in an equilibrium of various oligomeric structures, YocM (~18 kDa as a monomer) was tested in size exclusion chromatography and native PAGE. Both approaches indicated the existence of distinct higher oligomeric structures of YocM *in vitro* (~580-650 kDa / ~32-36 mer) (Figure 23AB). However, the fusion protein

YocM-mCherry was impaired in that characteristic structural feature with a potential tetramer (~175 kDa) as the highest oligomer observed in both approaches, although it was not the predominant species in the native PAGE (Figure 23AB). In addition, the underlying structure of YocM appeared to be a dimer (~36 kDa) or tetramer (~72 kDa), which is common for sHsp.
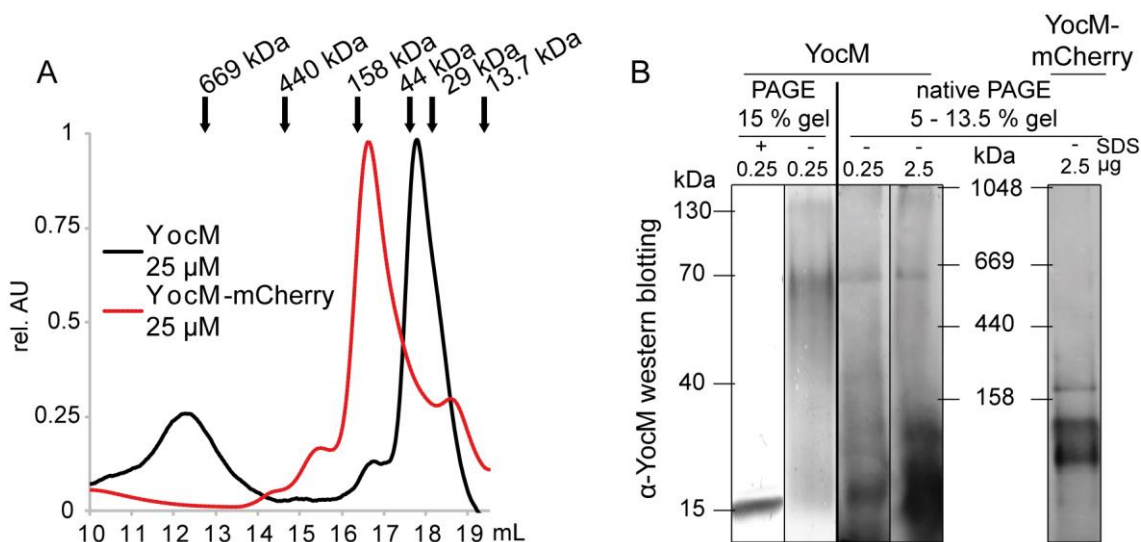
Figure 23: YocM forms higher oligomeric structures *in vitro*.

A) YocM (black, monomer: 18 kDa) and YocM-mCherry (red, monomer: 44 kDa) (25 µM each) were analyzed by size exclusion chromatography on a Superose6 Increase 10/300 column according to materials and methods. B) α-YocM western blotting of purified YocM after SDS-PAGE (15 % gel) and native PAGE (5 – 13.5 % gradient gel). Common native protein markers and their respective sizes are indicated in both approaches: IgM pentamer/ 1048 kDa, Thyroglobulin/ 669 kDa, Ferritin/ 440 kDa, Aldolase/ 158 kDa, Ovalbumin/ 44 kDa, carbonic anhydrase/29 kDa and Ribonuclease/ 13.7 kDa.

For further characterization of YocM as a sHsp, *in vitro* experiments using light scattering to follow the aggregation and refolding of model substrates were performed. First, chemically denatured firefly luciferase was used to determine the ability of YocM to prevent its aggregation upon dilution. Unexpectedly, addition of YocM accelerated the aggregation of chemically denatured luciferase instead of preventing it (Figure 24A).

Consistently, addition of YocM accelerated the aggregation of heat denatured Mdh at 47 °C, while YocM alone did not aggregate under these conditions (Figure 24B). However, only a minor protective effect of YocM on Mdh inactivation was observed during denaturation (Figure 24B). By contrast, lysozyme *per se* aggregated to a certain extent at 47 °C but did not impact the heat mediated enzyme inactivation (Figure 24C). As the *yocM* overexpressing strain displayed an improved growth at salt stress, it had to be determined whether the *in vitro* activity of YocM is influenced by higher salt concentrations. However, there was no significant difference in the Mdh activity loss and aggregation at 47 °C in the presence of YocM when 0.25 or 0.5 M NaCl was added (Figure 24D).
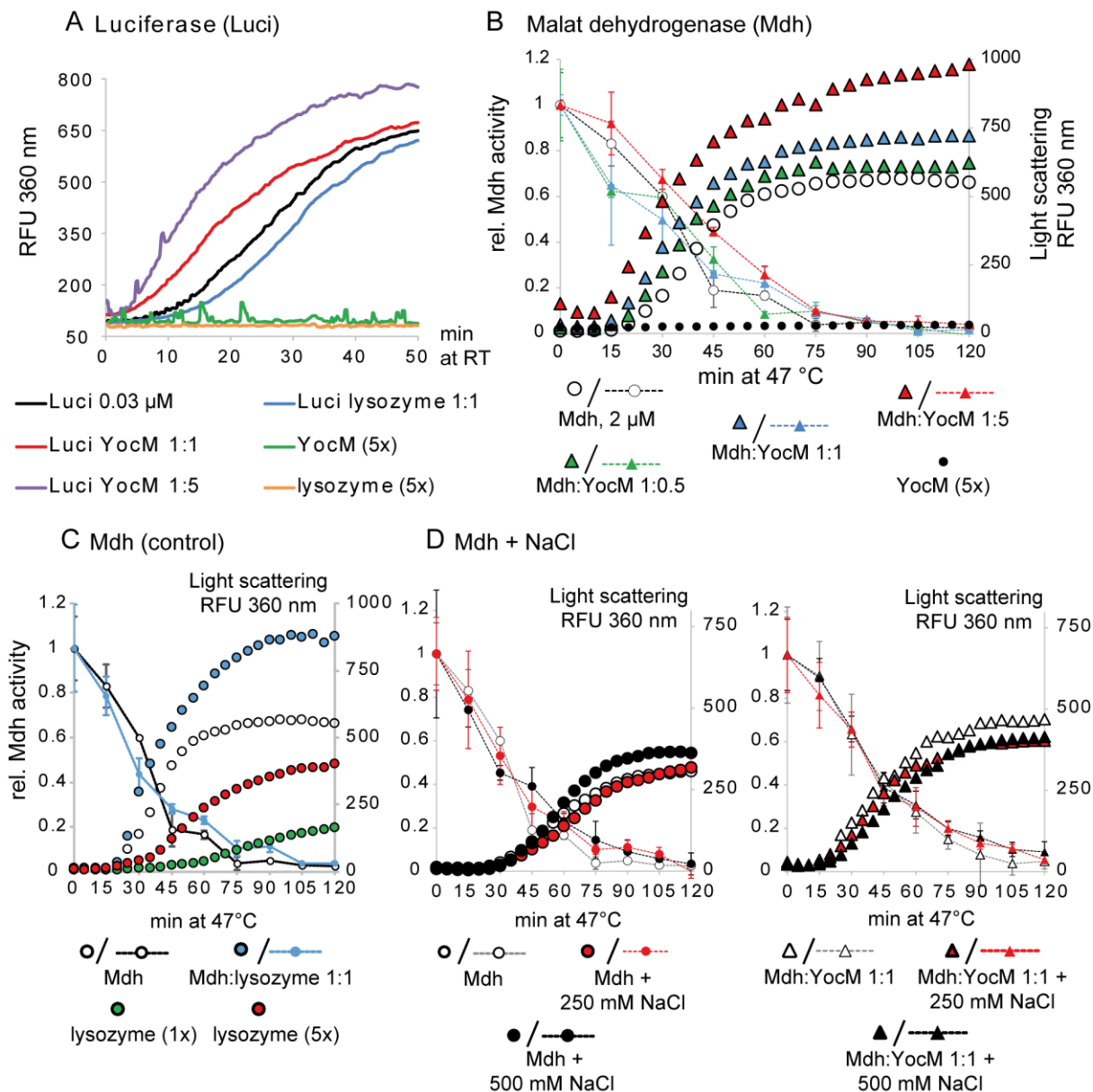
Figure 24: YocM accelerates aggregation of model substrates *in vitro*.

A) GuHCl denatured firefly luciferase (luci) was diluted into refolding buffer containing indicated amounts of YocM or lysozyme (luci final 0.03 µM). Dilution induced aggregation was measured by light scattering in a Jasco FP6500 spectrofluorometer. B)-C) Malate dehydrogenase (Mdh, final 2 µM) was incubated (B/C) ± lysozyme or ± YocM at indicated concentrations at 47 °C to induce unfolding and subsequent aggregation. D) Mdh (final 1µM) was incubated ± 250/500 mM NaCl at 47 °C. Light scattering was measured at 360/360 nm in a Jasco FP6500 spectrofluorometer and samples were taken at indicated time points to measure the loss of Mdh activity. Error bars indicate standard deviations and significant improvements are indicated (*: p<0.05, Welch's test).

As a defense mechanism upon salt stress, many cells accumulate compatible solutes, which protect protein function and prevent protein aggregation. Additionally, it was demonstrated several times that these chemical chaperones, in particular glycine betaine (GB) and proline, improved the survival of heat shocked *E. coli* or *B. subtilis* cells *in vivo* (Bashir et al., 2014b, 2014a; Caldas et al., 1999; Chattopadhyay et al., 2004; Diamant et al., 2003; Holtmann and Bremer, 2004). Hence, the effect of GB and proline was examined in the *in vitro* chaperone aggregation and refolding assays in combination with YocM or lysozyme as control. At that, 0.25 and 0.5 M GB or proline were used, as it was estimated that the intracellular concentration of GB reaches 0.6 M upon salt stress (Record et al., 1998; Stadmiller et al., 2017; Whatmore et al., 1990; Whatmore and Reed, 1990). In general, the addition of 0.5 M proline or 0.5 M GB reduced the rate and extent of Mdh aggregation at 47 °C (Figure 25 AB). Simultaneously, in the presence of 0.5 M GB, the addition of YocM retained significantly higher Mdh activity at 47 °C after 120 min (Figure 25A). A similar but minor effect was observed when 0.25 M proline or 0.25 M GB was used. Lysozyme as control did not positively affect Mdh activity under tested conditions (Figure 24C and Figure 25C). Those results were first hints towards a synergistic relationship between the sHsp YocM and chemical chaperones in *B. subtilis*, whereby the interplay of YocM with GB appeared to have the strongest protective effect.
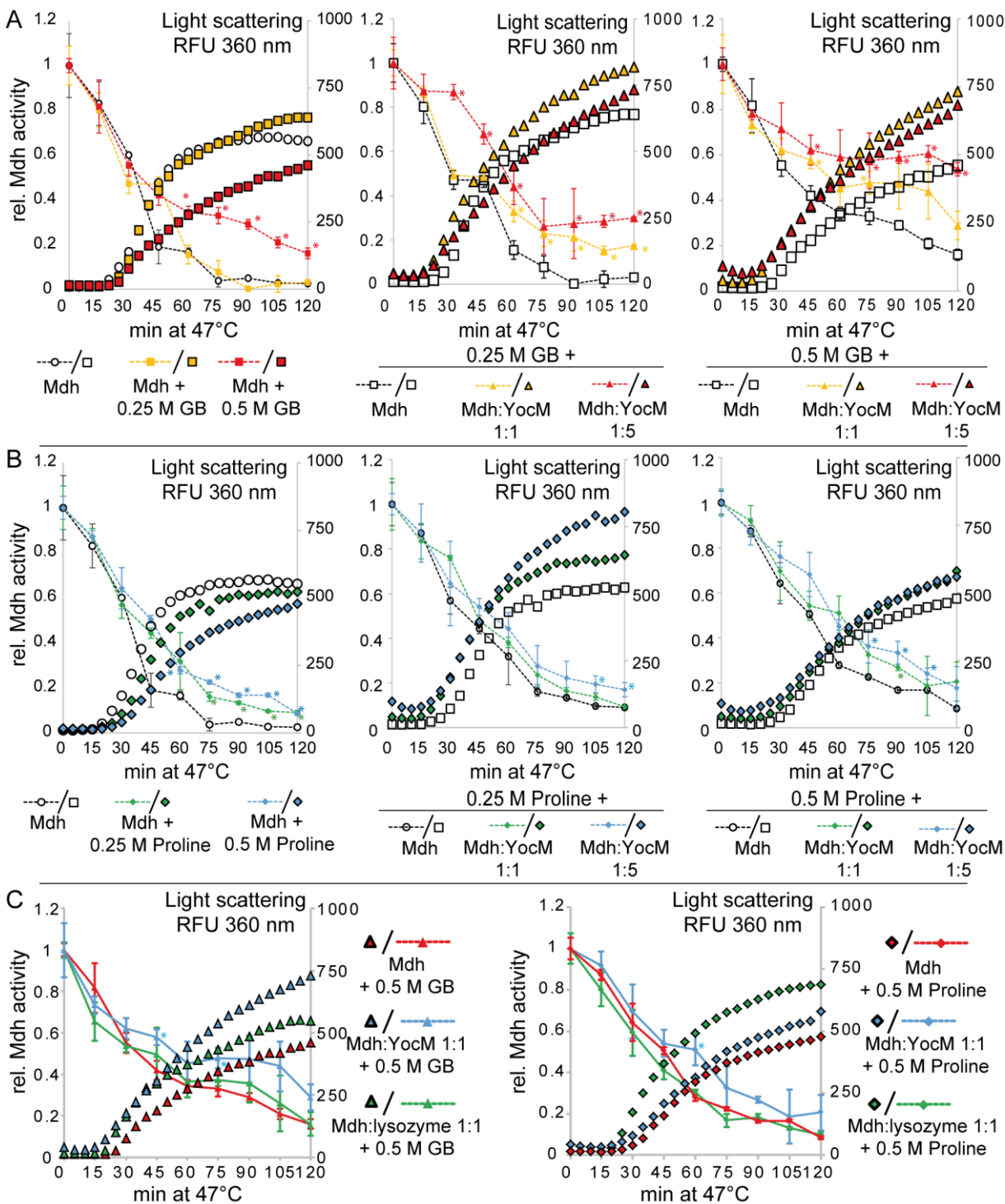
Figure 25: YocM and the chemical chaperone glycine betaine synergistically protect malate dehydrogenase activity at 47 °C.

Malate dehydrogenase (Mdh, final 2 μM) was incubated ± YocM and A) ± glycine betaine (GB), B) ± proline at concentrations of 0.25 or 0.5 M or C) ± lysozyme at 47 °C to induce unfolding and subsequent aggregation. Light scattering was measured at 360/360 nm in a Jasco FP6500 spectrofluorometer and samples were taken at indicated time points to measure the loss of Mdh activity. Error bars indicate standard deviations with significance indicated with respect to base line (Mdh ± GB/proline: white) indicated (*: p<0.05, Welch's test).

To confirm the observed aggregase-like and protective character of YocM, it was added at a later time point ($t_{45 \text{ min}}$) instead of supplementing it before starting the reaction. As anticipated, the addition of YocM resulted in an increase in light scattering and a decrease in the loss of Mdh activity from the moment it was added to the reaction mixture (Figure 26AB).
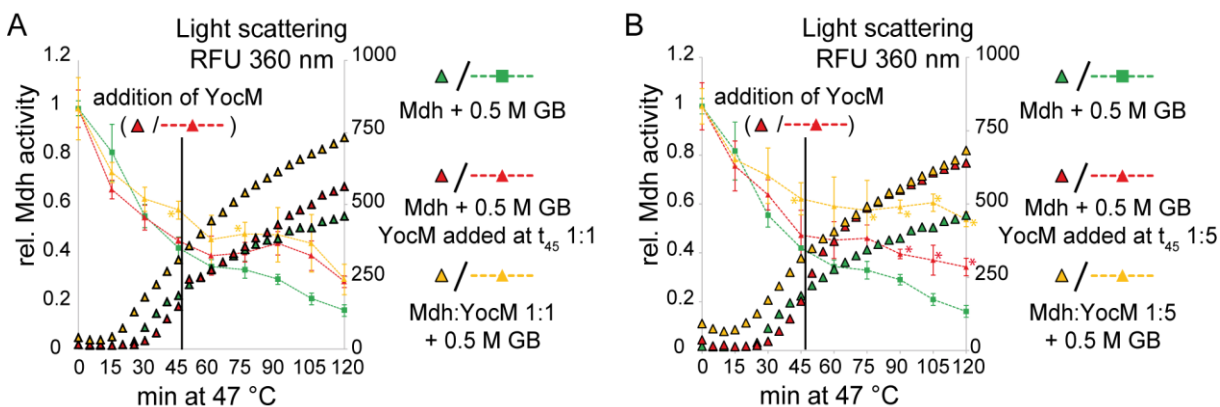
Figure 26: When added at a later time point, YocM maintains malate dehydrogenase activity at 47 °C to a lesser extent.

Malate dehydrogenase (Mdh, final 2 μM) was incubated with 0.5 M glycine betaine (GB) and ± YocM A) in a 1:1 ratio or B) in a 1:5 ratio. Samples were taken at indicated time points to measure the loss of Mdh activity. Error bars indicate standard deviations with significant improvements compared to the respective base line (Mdh ± GB/proline: white) indicated (*: $p<0.05$, Welch's test).

After chemical denaturation by using 6 M guanidinium hydrochloride, firefly luciferase instantly aggregated upon dilution into refolding buffer (Figure 24A). On the contrary, when Mdh was chemically denatured and subsequently diluted, it spontaneously refolded without detectable aggregation in light scattering (Figure 27). Next, the effect of YocM was investigated and an accelerated refolding process of Mdh was observed when YocM was added in a 5:1 ratio, which was not possible when lysozyme was used as control. Furthermore, refolding of Mdh was also positively influenced by the presence of chemical chaperones GB or proline *per se* (Figure 27). Simultaneously adding YocM slightly enhanced this effect.
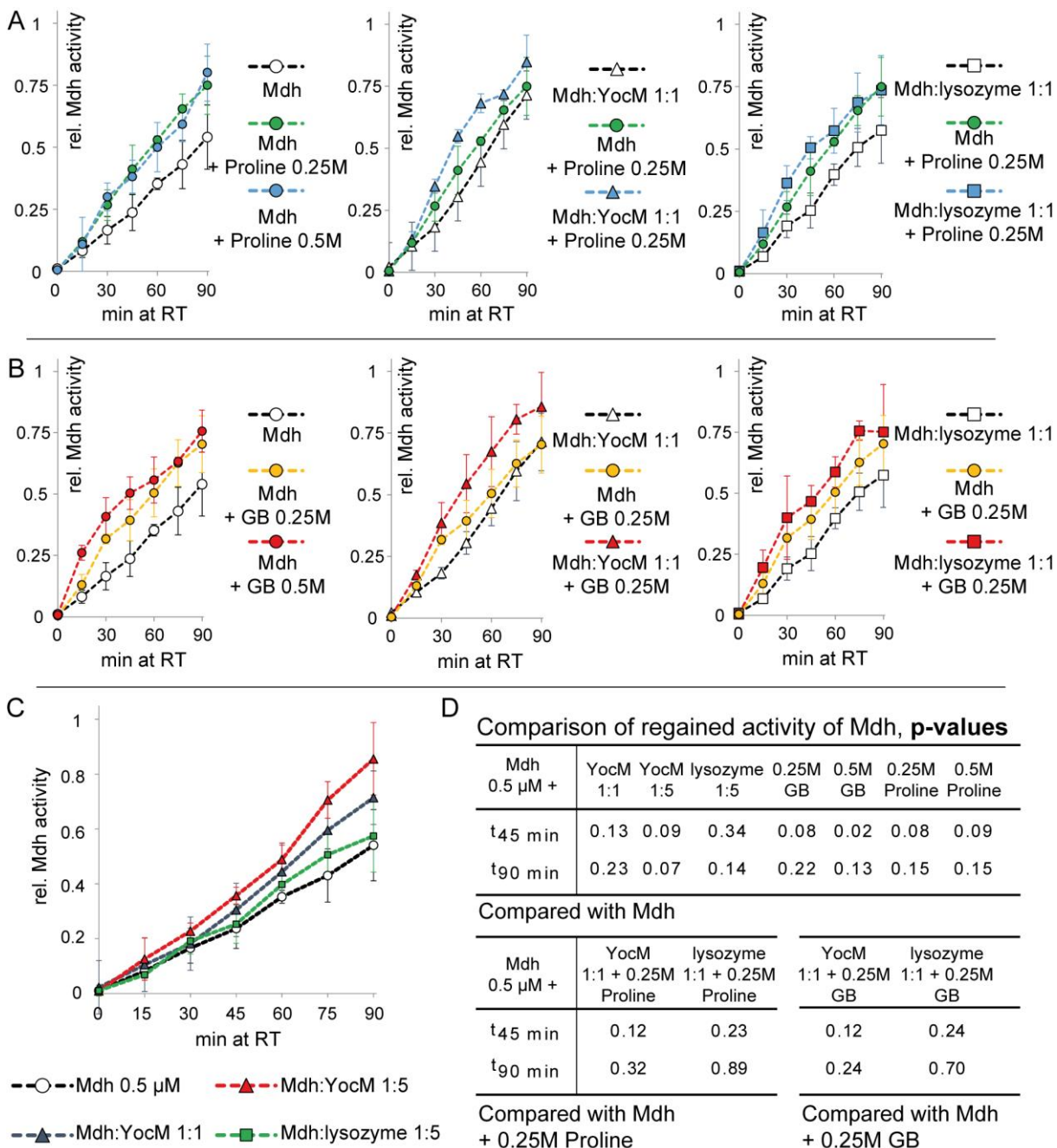
Figure 27: Refolding of GuHCl denatured malate dehydrogenase is slightly accelerated by chemical chaperones and YocM.

Malate dehydrogenase (Mdh) was denatured with 6 M GuHCl and refolding was initiated by dilution 1:100 (final 0.5 μM) in buffer ± YocM and ± lysozyme (as control) containing A) 0.25/0.5 M proline, B) 0.25/0.5 M glycine betaine (GB) or C) no further additives. Samples were taken for activity measurement at indicated time points to follow refolding process. No increasing light scattering at 360/360 nm was observed under any tested conditions. Standard deviations of three biological replicates are shown. p-values indicating significance are shown in D (Welch's test).

The refolding process of GuHCl denatured Mdh could be monitored by measuring the restored enzymatic activity upon dilution into an adequate buffer (Figure 27). Unsurprisingly, when Mdh was examined in an assay buffer with 6 M NaCl (close to saturation), no activity could be detected (Figure 28A). However, when Mdh was incubated in buffer containing additional 6 M NaCl prior to dilution into an assay buffer with adequate salt concentrations, the activity of Mdh was immediately restored (Figure 28BC). An ongoing refolding process as observed for GuHCl denatured Mdh was not detected (Figure 27). These results suggested that the treatment of Mdh with high salt concentrations did not lead to unfolding of Mdh, but abolished its enzyme activity possibly by interference with its substrates (oxaloacetate and NADH) and/or disturbance of Mdh dimerization (Dévényi et al., 1966).
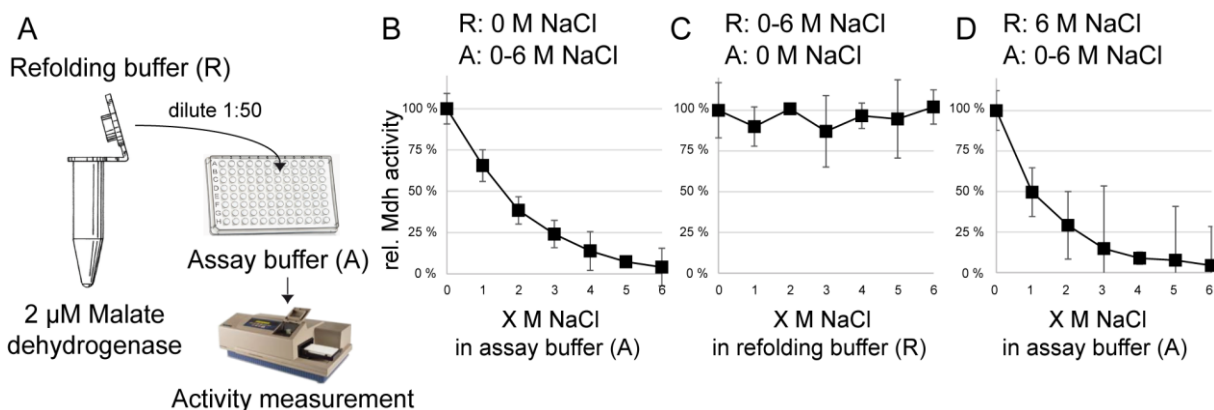
Figure 28: High NaCl concentrations abolish Mdh activity, which is immediately restored upon dilution into physiological buffer.

A) Malate dehydrogenase (2 µM) was incubated in refolding buffer (R) and diluted (1:50) into assay buffer (A) to measure its activity according to materials and methods. Error bars indicate standard deviations. B) The amount of NaCl was varied in assay buffer (0-6 M NaCl), while kept at constant 0 M NaCl in refolding buffer. C) The amount of NaCl was varied in refolding buffer (0-6 M NaCl), while kept at constant 0 M NaCl in assay buffer. D) The amount of NaCl was varied in assay buffer (0-6 M NaCl), while kept at constant 6 M NaCl in refolding buffer.

In contrast to Mdh, chemically denatured citrate synthase (CS) aggregated and regained only ~1 % of its activity within 50 min when diluted into refolding buffer (Figure 29A). Chemical chaperones proline and glycine betaine enhanced that refolding rate to final ~5 and 3 % of original citrate synthase activity under tested conditions, respectively (Figure 29BC). In addition, proline prevented the aggregation of CS to a certain extent (Figure 29C). The simultaneous addition of YocM further enhanced that effect. Importantly, addition of lysozyme as control did not influence the aggregation of CS.

In summary, addition of YocM in the presence of chemical chaperones resulted in enhanced protection of Mdh during heat mediated aggregation *in vitro* (Figure 25 and Figure 26). However, refolding of chemically denatured Mdh and CS was only slightly affected by YocM in the presence of GB or proline (Figure 27 and Figure 29). In the cases of heat mediated aggregation of Mdh as well as dilution induced aggregation of chemically denatured luciferase, addition of YocM resulted in accelerated aggregation (Figure 24). This aggregase-like activity has been observed for partially heat unfolded Mdh (at 41°C), which did not aggregate *per se*, but prevented the aggregation of completely heat unfolded Mdh (at 47°C) (Ungelenk et al., 2016). In contrast, the aggregase-like activity of YocM could only be observed using completely heat unfolded Mdh.
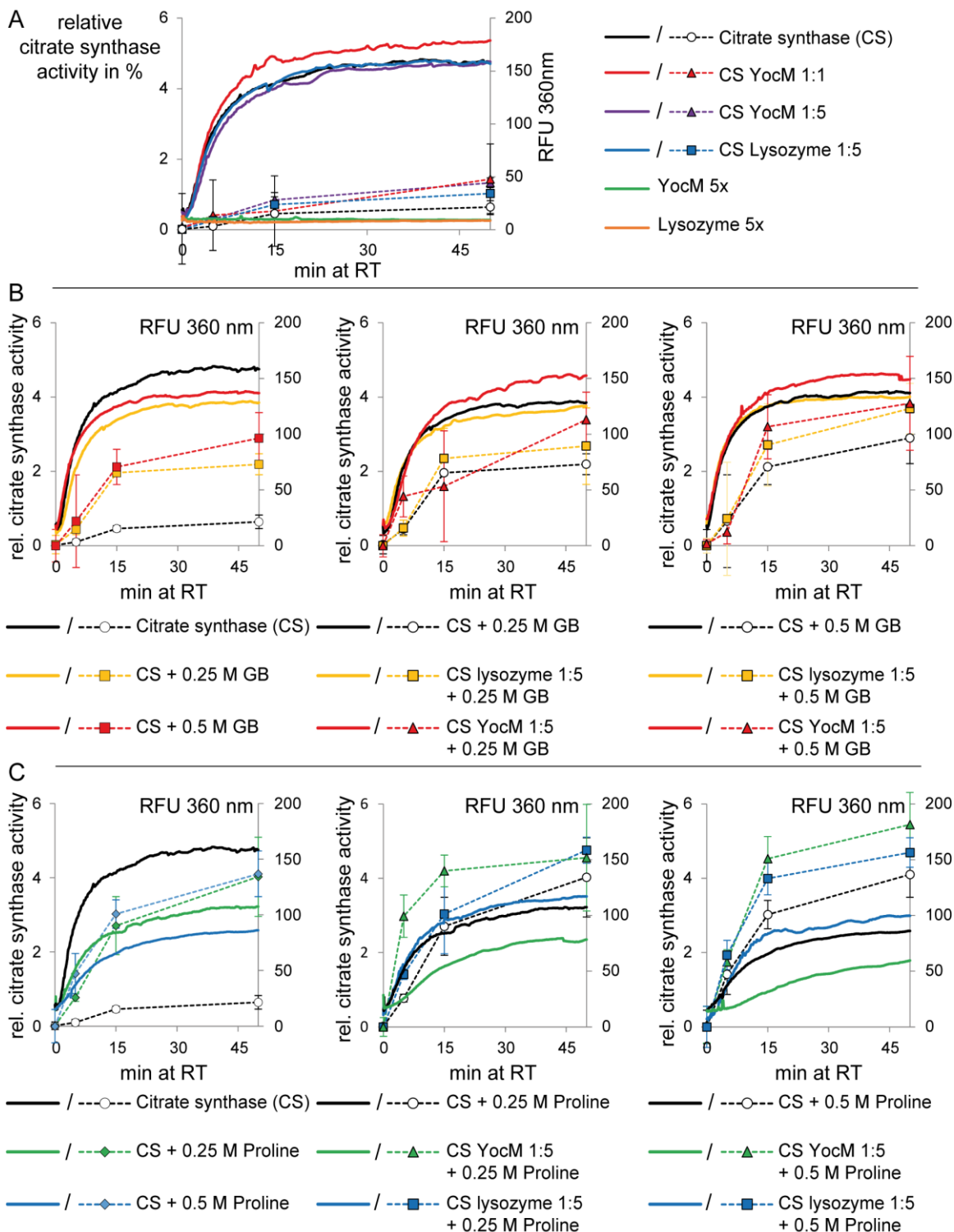
Figure 29: Proline and glycine betaine support refolding of GuHCl denatured citrate synthase.

Aggregation and refolding of GuHCl denatured Citrate synthase was induced by dilution 1:100 (final 0.1 μM) into buffer A) ± YocM or lysozyme at indicated ratios, B) + additional 0.25/0.5 M glycine betaine and C) + additional 0.25/0.5 M proline. Light scattering was measured at 360/360 nm and samples were taken at indicated time points for activity test in a SpectraMaxM3 at 30 °C at 412 nm. Error bars display standard deviations.

Collectively, YocM was identified to play a supportive role during salt stress in *B. subtilis*. While the expression of *yocM* was upregulated at elevated salt concentrations, the Δ*yocM* mutant was identified to be more sensitive towards salt stress (Figure 12, Figure 13 and Figure 14). Furthermore, YocM displayed the sHsp characteristic formation of higher oligomeric structures *in vitro*, which was impaired when a YocM-mCherry fusion protein was examined (Figure 23). However, this YocM-mCherry fusion still targeted protein aggregates *in vivo* and thus was established as a non-invasive protein aggregate marker (Figure 16 and Figure 18). Thereby the different nature of the rather insoluble heat stress induced protein aggregates and potentially more fragile salt stress originated protein aggregates was visualized *in vivo* (Figure 16, Figure 19, Figure 20 and Figure 21). Furthermore, it allowed the visualization and subsequent characterization of ClpC and McsB mediated protein disaggregation *in vivo* (see 3.2, Figure 32).

3.2.   *Interplay of ClpC and McsB in vivo*

Small heat shock proteins like YocM are members of the protein quality control system, which act ATP independently. Larger molecular chaperones like the Hsp100/Clp proteins rely on their ATPase activity to fulfill their function in protein degradation and disaggregation. In *B. subtilis*, the ATPase activity of the chaperone ClpC is predominantly dependent on its adaptor proteins (Kirstein et al., 2006, 2009b). In order to evaluate the specific roles of the three known adaptor proteins of ClpC, the increase in levels of MecA, McsB and YpbH was examined during heat stress and under thermotolerance conditions (Figure 30A). Thermotolerance describes the phenomenon of surviving a normally lethal heat shock (54 °C) when primed by a milder pre-shock (48 °C). In contrast to YpbH and MecA, McsB was not

detected at 37 °C (Figure 30B). At elevated temperatures and especially under thermotolerance conditions a distinct upshift of McsB levels was observed, whereas YpbH and in particular MecA did not follow this profile. In addition, raised levels of ClpC and ClpP were also observed during heat shock conditions with a peak at 50 °C (Figure 30B). This was consistent with transcriptomic data with only *clpC*, *mcsB* and *clpP* being upregulated upon heat shock (Nicolas et al., 2012). Besides from their regulatory role in e.g. competence development, *mecA* and *ypbH* were identified as part of the Spx Regulon, thereby part of the oxidative stress response (M. Nakano et al., 2002; Persuh et al., 2002; Rochat et al., 2012).
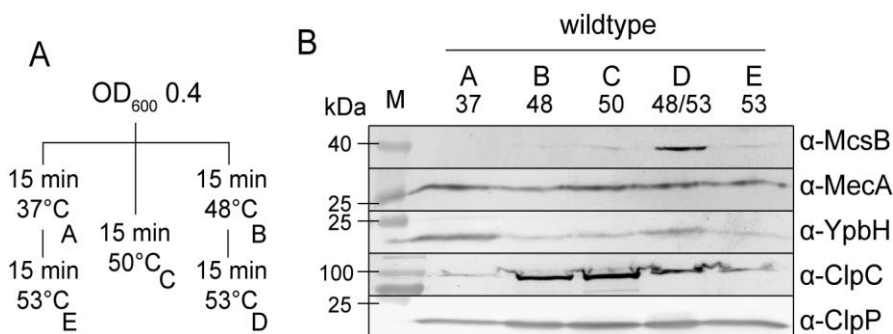
Figure 30: Levels of McsB display a strong bias towards thermotolerance and heat stress.

B. subtilis wildtype strain was in grown in LB medium with samples taken for western blotting according to the scheme in A). B) Western blotting to visualize levels of adaptor proteins McsB, MecA and YpbH, as well as ClpC and ClpP with 5 µg of cellular extract.

3.2.1. McsB is the main ClpC adaptor protein regarding heat stress

To further assess the importance of McsB during heat shock conditions, a strain lacking all genes for the adaptor proteins *mecA*, *ypbH* and *mcsB* was generated. That triple adaptor mutant strain (TAM) was in general more sensitive towards heat stress and significantly impaired in its ability to develop thermotolerance with a drop in cellular survival of about two orders of magnitude (Figure 31A). In order to determine the individual impact of each adaptor protein *per se*, each gene was re-introduced into the TAM strain in the *amy* locus *in trans*

under the control of an IPTG inducible promotor (P_{lac}). Thereby it was possible to investigate each adaptor protein individually in a TAM background strain lacking the other two. It was observed that when *mcsB* was expressed, the thermotolerance deficient phenotype of the TAM strain was restored (Figure 31B). However, neither expression of *mecA* nor expression of *ypbH* affected the heat sensitivity of the TAM strain significantly (Figure 31CD).

During a severe heat shock *B. subtilis* cells accumulate subcellular protein aggregates, which can be prevented by priming through a moderate pre-shock (Runde et al., 2014). Since an aggregate marker protein was established during the characterization of the sHsp YocM (3.1.1, Figure 16), the formation and clearance of protein aggregates during heat shock and subsequent recovery could be followed by fluorescence microscopy. Consistent with the above findings, only expression of *mcsB* during recovery from a 50 °C heat shock led to the complete removal of fluorescent foci (representing YocM-mCherry marked protein aggregates) (Figure 31E). To prove the synthesis of the respective adaptor protein, western blotting was performed after heat shock and recovery (Figure 31F). As MecA and YpbH are paralogs, the additional detection of MecA with the α-YpbH antibody was not surprising (Figure 31F).
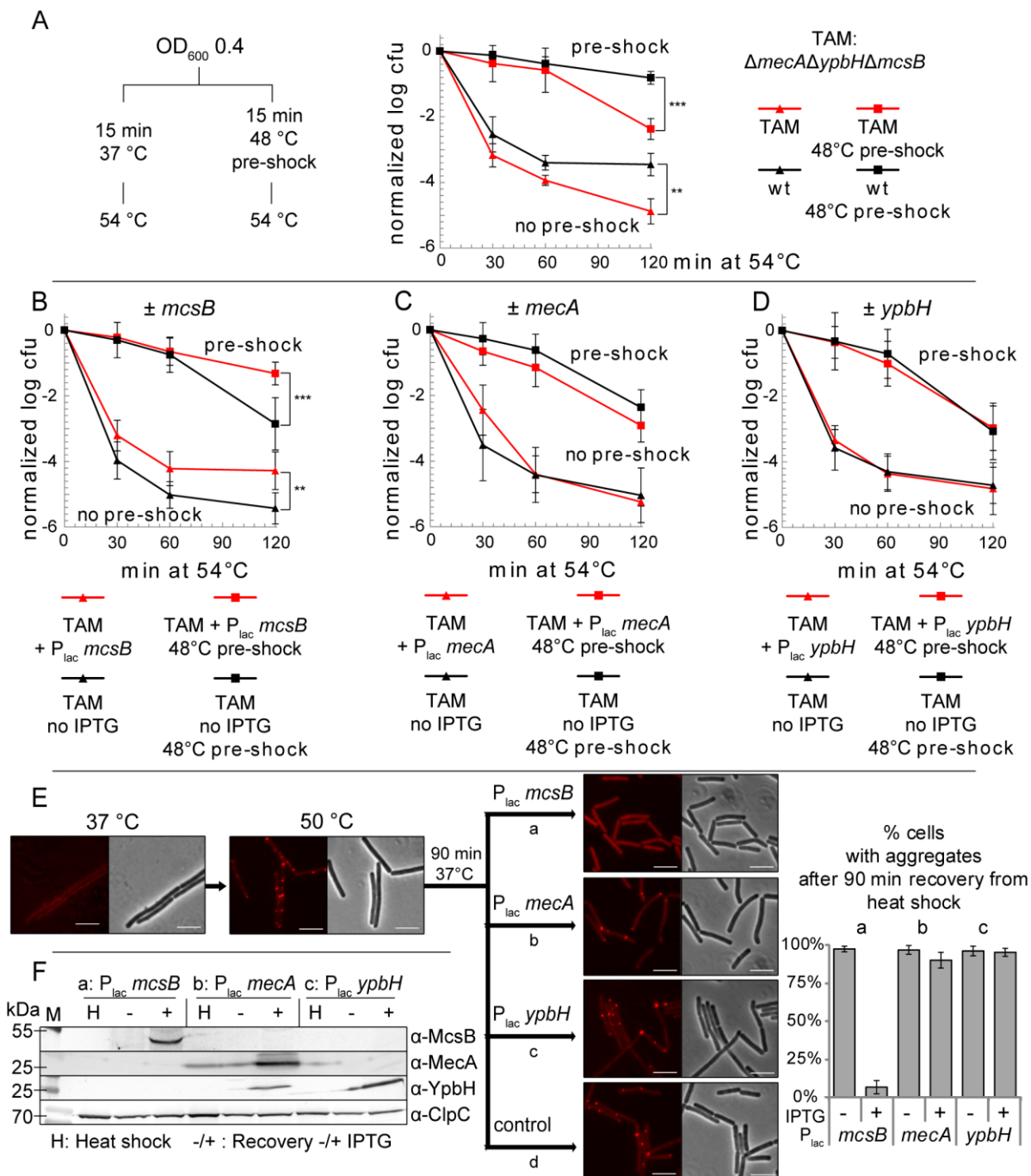
Figure 31: Only expression of *mcsB* restores thermotolerance deficient phenotype of Δ*mcsB*Δ*mecA*Δ*ypbH*.

A) *B. subtilis* wt (black) and Δ*mcsB*Δ*mecA*Δ*ypbH* (TAM, BIH737, red) were treated according to scheme ± pre-shock and subsequent heat shock at 54 °C. Survival was measured by *cfu* at indicated time points. B-D) TAM + P_{lac} *mcsB* / *mecA* / *ypbH* (BIH739/740/741) strains were analyzed as in A without IPTG (black) and with 2 mM IPTG (red). Squares: with 15 min pre-shock at 48 °C; triangles: without pre-shock. Log_{10}-values of viable cell count were normalized and standard deviations (indicated error bars) were calculated from three biological replicates (*: $p<0.05$, **: $p<0.01$, ***: $p<0.001$, Welch's test). E) Strains from B-D) were treated at OD_{600} 0.3 with 30 min at 50 °C and shifted to recover at 37 °C for 90 min ± 2 mM IPTG to express a: *mcsB*, b: *mecA* or c: *ypbH*, respectively (d: control: no IPTG). Samples for fluorescence microscopy and western blotting (F, 5 µg cellular extract) were taken at indicated time points.

3.2.2. McsB targets protein aggregates *in vivo*

To gain more insights into the observed McsB mediated clearance of subcellular aggregates (Figure 31E), a Δ*mcsB* deletion mutant had to be investigated individually. This mutant strain displayed a raised amount of YocM-mCherry marked protein aggregates, in particular after heat shock (Figure 32A). Importantly, the additional synthesis of McsB complemented that phenotype and resulted in the formation of fewer aggregates (Figure 32A). Hence, a m*csB-gfp* fusion was cloned to investigate the potential aggregate-targeting character of McsB. As expected, when *mcsB-gfp* was expressed, YocM-mCherry marked protein aggregates were also targeted by McsB-GFP (Figure 32B). It is important to note that a kinase inactive McsB C167S-GFP fusion protein was not impaired in its aggregate localizing character (Figure 32B) (Kirstein et al., 2005).

It must be kept in mind that in these experiments heat stress was applied when McsB-GFP was already present in the cell due to induction of P_{lac} *mcsB-gfp* at the very beginning. Thus, it had to be ruled out that McsB-GFP is localized to the subcellular aggregate fraction due to heat induced unfolding of McsB *itself*. As anticipated, the McsB-GFP fusion protein was also co-localized with protein aggregates when P_{lac} *mcsB-gfp* was induced later during the recovery without having sensed the actual heat shock (Figure 32C). Comparing clearance of aggregates by McsB and its GFP-fusion protein, McsB-GFP appeared to be only partially active (Figure 31E and Figure 32C). Therefore, both proteins were tested regarding their ability to activate ClpC ATPase *in vitro*. Consistently, McsB-GFP displayed only 20 % ClpC ATPase activation showing the importance of testing GFP-fusion proteins for their functionality and complementation (Figure 32D).
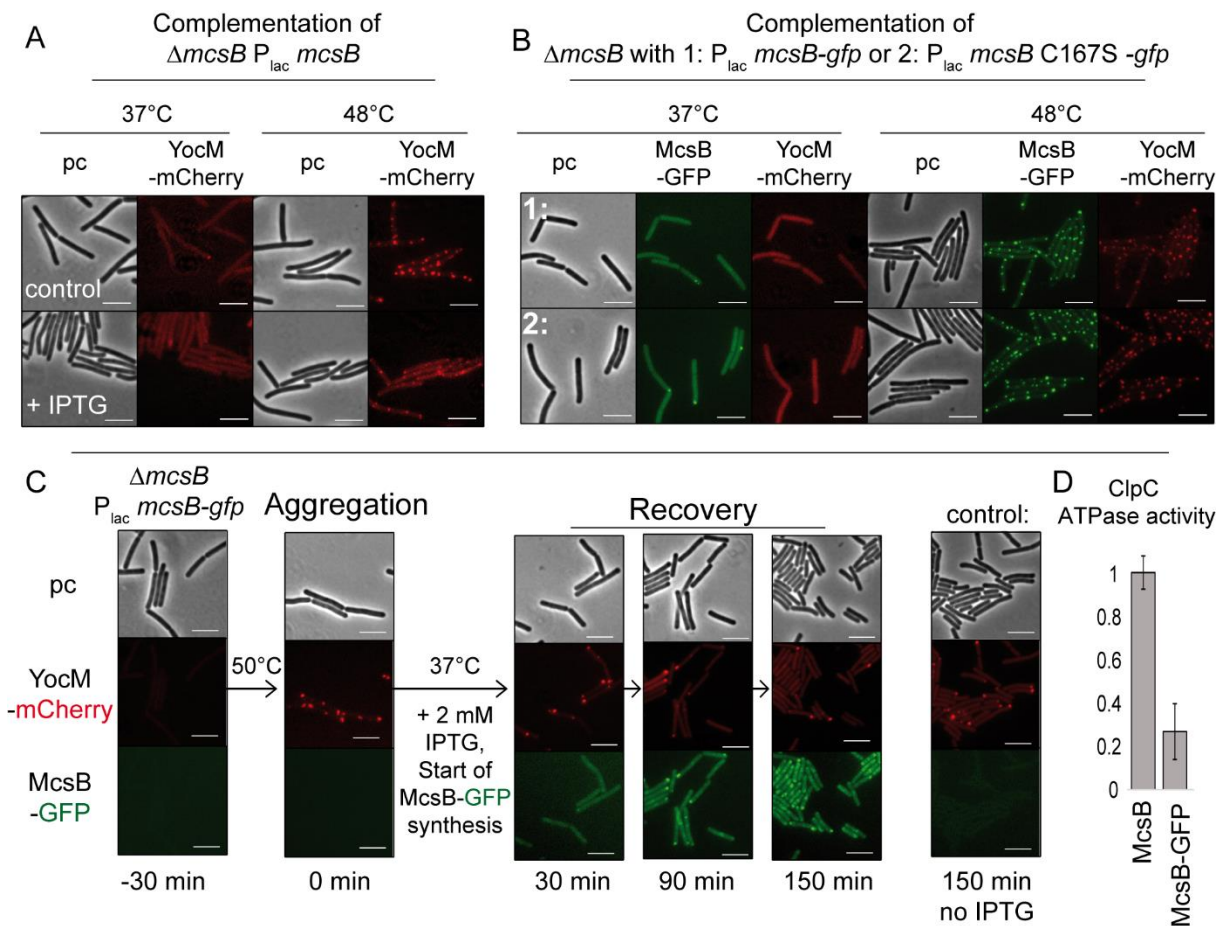
Figure 32: McsB targets protein aggregates *in vivo*.

A) The Δ*mcsB* P$_{lac}$ *mcsB* strain (BIH414) was grown in LB + 0.5 % xylose to induce P$_{xyl}$ *yocM-mcherry* and treated with 15 min 48 °C heat shock at OD$_{600}$ 0.4 with samples taken for fluorescence microscopy. B) The Δ*mcsB* P$_{lac}$ *mcsB*-(±C167S)-*gfp* strains (BIH677/678) were grown in LB + 0.5 % xylose to induce P$_{xyl}$ *yocM-mcherry* with additional 1 mM IPTG and treated with 15 min 48 °C heat shock at OD$_{600}$ 0.4 with samples taken for fluorescence microscopy. C) Strain Δ*mcsB* P$_{lac}$ *mcsB-gfp* (BIH677) was treated with a 50 °C heat shock for 30 min and afterwards shifted to 37 °C, before 2 mM IPTG was added to induced P$_{lac}$ *mcsB-gfp* during recovery. Samples were taken at indicated time points. All scale bars indicate 5 µm. One representative example is shown. D) Activation of ClpC ATPase by McsB and McsB-GFP was tested with a malachite green ATPase assay *in vitro*. Error bars indicate standard deviations.

3.2.3. Disaggregation by ClpCP is dependent on kinase active McsB *in vivo*

As the arginine kinase of McsB is crucial for its function but its exact role is not completely understood, a kinase inactive McsB C167S mutant was analyzed (Elsholz et al., 2010; Kirstein et al., 2005). Thus, a Δ*mcsB* mutant strain was complemented either by P$_{lac}$ *mcsB* or *mcsB* C167S, respectively. Monitoring the protein aggregates during 50 °C heat shock and

subsequent recovery at 37 °C demonstrated a severely impaired aggregate clearance when the kinase inactive McsB C167S was synthesized instead of fully active McsB (Figure 33A). However, the synthesis of McsB C167S during recovery phase still reduced the number of cells containing aggregates by 20 % indicating a potential impact non-related to its kinase activity (Figure 33A). Comparable amounts of McsB and McsB C167S were verified by α-McsB western blotting after heat shock and during recovery process (Figure 33B).
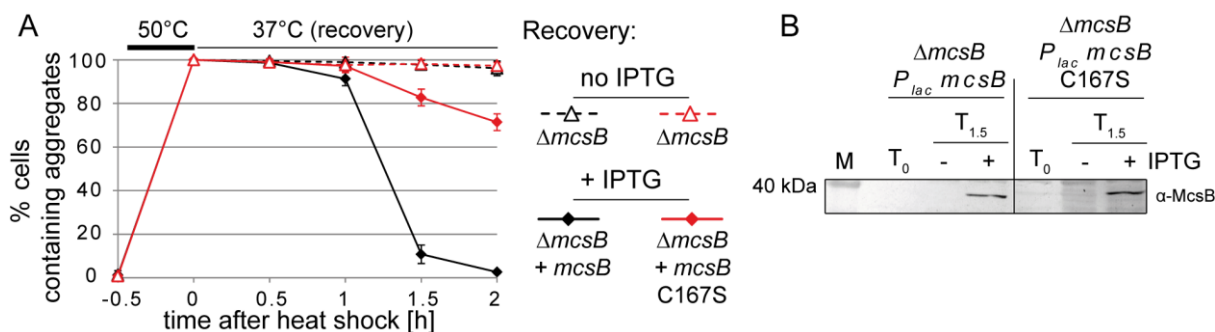
Figure 33: Clearance of aggregates requires kinase active McsB *in vivo*.

A) The Δ*mcsB* P$_{lac}$ *mcsB* (BIH414) and Δ*mcsB* P$_{lac}$ *mcsB* C167S (BIH439) strains were treated at OD$_{600}$ 0.3 in LB + 0.5 % xylose with a 50 °C heat shock for 30 min before ± 2 mM IPTG was added during recovery at 37 °C. Samples were taken for western blotting (B, 5 µg cell extract) and fluorescence microscopy at indicated time points to determine the ratio of cells containing YocM-mCherry marked protein aggregates. Error bars indicated standard deviations from at least three biological replicates.

The arginine kinase of McsB is indirectly regulated by its corresponding phosphatase YwlE, which de-phosphorylates phosphorylated arginine-residues on proteins, hence acting as counterpart of McsB (Elsholz et al., 2010; Kirstein et al., 2005). Consequently, the influence of YwlE on protein aggregation was investigated. A Δ*ywlE* mutant strain was complemented *in trans* either by IPTG inducible P$_{lac}$ *ywlE* or its inactive *ywlE* C7S mutant (Fuhrmann et al., 2013). It was speculated, that a less restricted McsB arginine kinase in a Δ*ywlE* mutant would result in a decreased formation of protein aggregates, whereas overexpression of *ywlE* would counter McsB dependent arginine phosphorylation and thereby led to an increased heat sensitivity as seen for Δ*mcsB* (Figure 31 and Figure 32A) (Elsholz et al., 2012).

During the investigation of heat stress it was observed, that aggregate clearance was substantially improved in a Δ*ywlE* mutant when compared to wildtype (Figure 34A). That phenotype could be complemented by expression of *ywlE* under control of P_{lac} promoter on a construct located *in trans*. As expected, a complementation was not observed when the inactive YwlE C7S mutant was synthesized. To rule out any indirect effect of YwlE, the effect of *ywlE* expression was tested in a strain with the inactive McsB C167S as an additional control (Figure 34A). As elevated levels of YwlE did not display any difference in this kinase inactive *mcsB* C167S mutant, YwlE did not directly affect aggregate clearance but relied on the indirect regulation of McsB activity (Figure 34A).

In addition to aggregate clearance, the formation of aggregates was analyzed under thermotolerance conditions. Consistent with the above findings, a Δ*ywlE* mutant accumulated a substantially reduced number of aggregates under thermotolerance conditions (48 °C pre shock + 53 °C heat shock) when compared to wildtype (Figure 34B). When complementing this phenotype by synthesis of YwlE *in trans*, the low induction of P_{lac} *ywlE* with 10 µM IPTG was already sufficient to lead to the minor formation of protein aggregates, whereas using 2 mM IPTG resulted in massive occurrence of protein aggregates in all cells (Figure 34B). This suggests that even small amounts of YwlE can have a substantial impact on the physiology of the cell regarding heat stress.
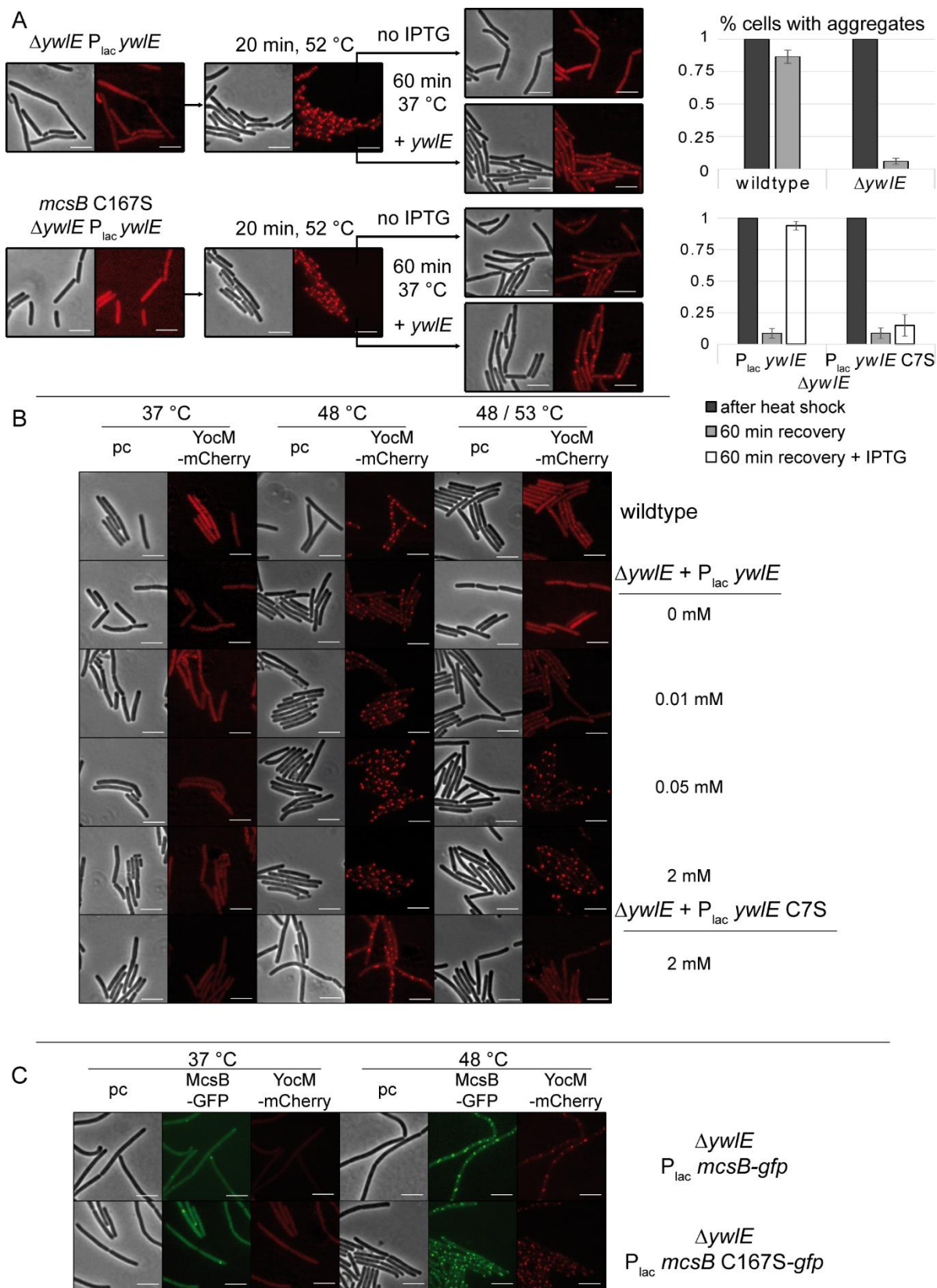
Figure 34: McsB dependent aggregate clearance after heat shock is accelerated in a Δ*ywlE* mutant.

A) The Δ*ywlE* (BIH819), Δ*ywlE* P$_{lac}$ *ywlE* (BIH828), Δ*ywlE* P$_{lac}$ *ywlE* C7S (BIH829) and *mcsB* C167S Δ*ywlE* P$_{lac}$ *ywlE* (BIH824) strains were treated at OD$_{600}$ 0.3 in LB + 0.5 % xylose with a 52 °C heat shock for 20 min before ± 2 mM IPTG was added during recovery at 37 °C for 60 min. Samples were taken for fluorescence microscopy at indicated time points to determine the ratio of cells containing YocM-mCherry marked protein aggregates. Error bars indicate standard deviations from three biological replicates. B) Wildtype (BIH369), Δ*ywlE* P$_{lac}$ *ywlE* (BIH828) and Δ*ywlE* P$_{lac}$ *ywlE* C7S (BIH829) strains were analyzed under standard thermotolerance conditions in LB + 0.5 % xylose and increasing IPTG concentrations to induce P$_{lac}$ *ywlE* according to materials and methods. C) Strains Δ*ywlE* P$_{lac}$ *mcsB-gfp* (BIH681) and Δ*ywlE* P$_{lac}$ *mcsB* C167S-*gfp* (BIH682) were grown in LB + 0.5 % xylose and treated with a 15 min 48 °C heat shock at OD$_{600}$ 0.4 with samples taken for fluorescence microscopy. One representative example is shown.

In addition, when examining the localization of the McsB-GFP fusion protein in a Δ*ywlE* mutant strain, distinct fluorescent foci of McsB-GFP were formed at the polar region of the cell (Figure 34C). It is important to note that the formation of these polar clusters in a Δ*ywlE* mutant was independent of the kinase activity of McsB (Figure 34C). In the wildtype strain, McsB-GFP clusters were only observed after heat shock and/or in a Δ*mcsB* deletion background strain (Figure 32BC). This localization pattern of McsB fused to a fluorescent protein had been observed before (Kirstein et al., 2008).

The obtained results demonstrated that the absence of YwlE enhances McsB activity leading to less aggregate formation upon heat shock (Figure 34B) and accelerated disaggregation in recovery (Figure 34A). In order to determine whether a Δ*ywlE* mutant strain would also be more resistant towards heat stress, a thermotolerance survival assay was performed.

First, the survival regarding heat stress of the Δ*mcsB* mutant strain was compared to the kinase inactive *mcsB* C167S strain. Both strains displayed a comparably and significantly elevated sensitivity towards heat stress and were both impaired in thermotolerance development (Figure 35A), suggesting that the arginine kinase activity of McsB is essential for its impact in heat stress response (Figure 35A). Surprisingly, a Δ*ywlE* mutant strain, which accumulated less aggregates than the wildtype strain during heat shock, was observed to be more affected by heat stress (Figure 35B and Figure 34AB). Moreover, besides from the *ywlE*

deletion, the overexpression of *ywlE* also led to significantly impaired heat resistance in a dose dependent manner (Figure 35B). Next, a Δ*ywlE* mutant was complemented *in trans*, but even though no IPTG was added to induce P$_{lac}$ *ywlE*, the previously diminished heat resistance was restored probably due to leakiness of P$_{lac}$ promotor (Figure 35B). To prove that hypothesis, the Δ*ywlE* mutant strain was complemented with P$_{lac}$ *ywlE* C7S, which is an inactive variant of the phosphatase and leakiness of the promotor would consequently not lead to restored heat resistance (Fuhrmann et al., 2013). As anticipated, the complemented Δ*ywlE* P$_{lac}$ *ywlE* C7S strain and the Δ*ywlE* strain were both affected by heat stress in a comparable manner (Figure 35C). These observations suggest that indeed the leakiness of the P$_{lac}$ promotor of P$_{lac}$ *ywlE* is sufficient for complementation of the Δ*ywlE* mutant strain and physiological levels of YwlE are marginal. Notably, overexpression of *ywlE* did not change levels of ClpC at 37 °C or under tested thermotolerance conditions (Figure 35DEFG). As already observed before, McsB was only detectable at heat shock conditions (Figure 30 and Figure 35DEFG). Remarkably, elevated levels of YwlE appeared to result in decreased amounts of McsB at 54 °C (Figure 35F) but not at thermotolerance conditions (48/54 °C) (Figure 35G).
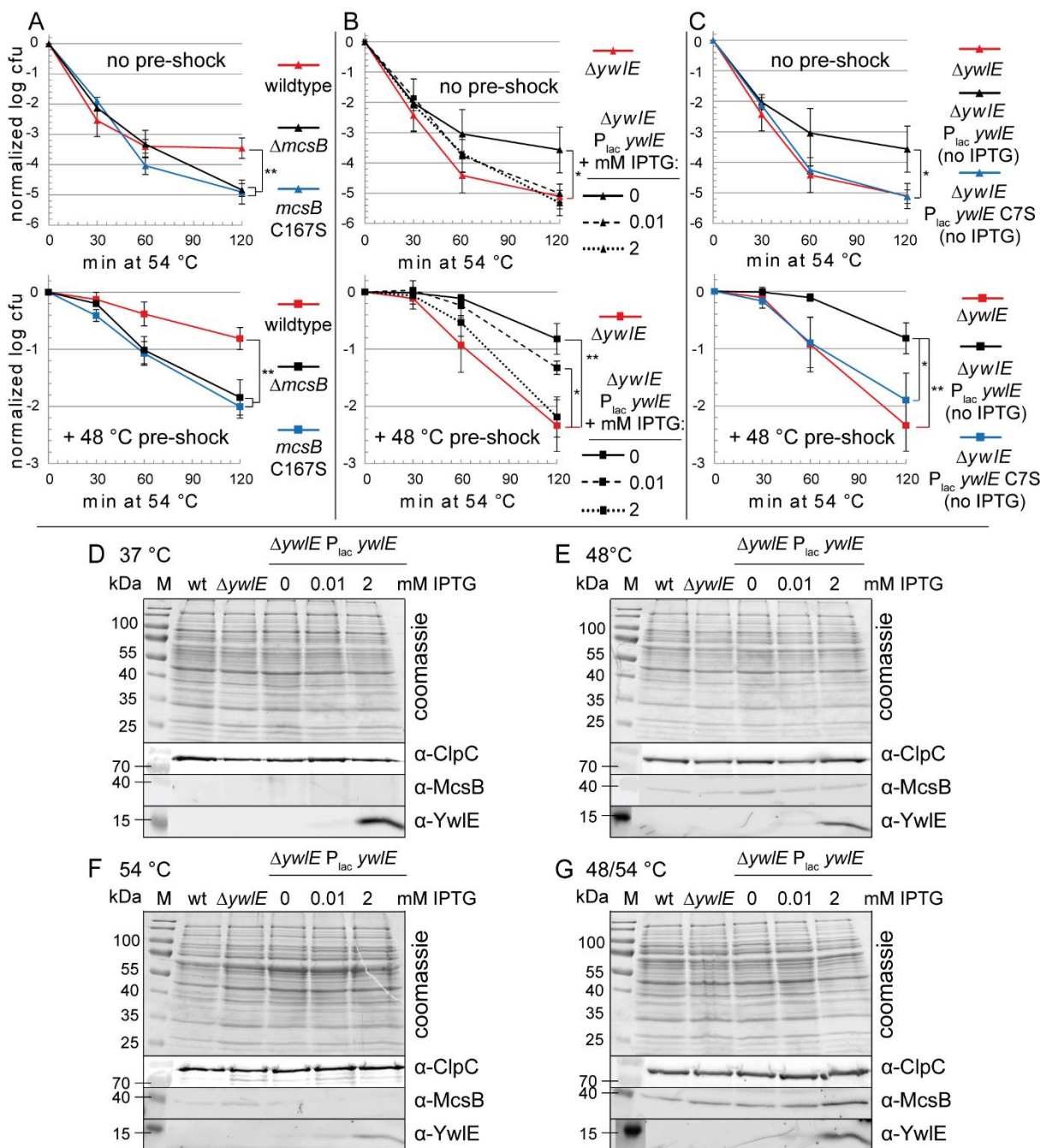
Figure 35: Deletion and overexpression of *ywlE* leads to increased heat sensitivity in *B. subtilis*.

A standard thermotolerance survival assay was performed with strains A) Δ*mcsB* (BIH69), *mcsB* C167S (BIH694) and wildtype, B) Δ*ywlE* (BIH819) and Δ*ywlE* P$_{lac}$ *ywlE* (BIH828) + indicated concentrations of IPTG and C) Δ*ywlE* (BIH819), Δ*ywlE* P$_{lac}$ *ywlE* (BIH828), Δ*ywlE* P$_{lac}$ *ywlE* C7S (BIH829) according to materials and methods. Cfu was normalized at indicated time points. Error bars indicate standard deviations based on three biological replicates. Significance is illustrated by *: $p<0.05$ and **: $p<0.01$ (Welch's test). D/E/F/G) The strains Δ*ywlE* (BIH819), Δ*ywlE* P$_{lac}$ *ywlE* (BIH828) and wildtype were treated ± 15 min 48 °C at OD$_{600}$ 0.4 (samples D/E) and afterwards shifted to 54 °C for 30 min (samples F/G). Samples for SDS-PAGE and western blotting (α-ClpC/ α-McsB/ α-YwlE) as well as Coomassie staining were taken at every step. D/E/F: 5 µg of cellular extract and G: 10 µg of cellular extract.

To prove the successful synthesis of YwlE after IPTG addition in the P_{lac} *ywlE* strain, western blotting was performed at standard thermotolerance conditions. Surprisingly, although overexpression of *ywlE* was confirmed by α-YwlE western blotting, YwlE was not detected in the wildtype strain at all tested temperatures (Figure 35DEFG). The physiological levels of YwlE were probably below the detection limit of the performed ECL (enhanced chemoluminescence, see Materials & Methods) for visualization of proteins after western blotting. In order to still get an impression of the amounts of YwlE in the cell, α-ywlE western blotting was performed with purified YwlE in a defined standard curve from 0.2 – 200 ng (Figure 36A). The comparison of this standard curve with the amount of YocM in the Δ*ywlE* P_{lac} *ywlE* strain (total 5 µg) allowed an extrapolation towards approximately 135 or less molecules YwlE per cell in the wildtype, which fitted the already observed range of 90 – 250 molecules YwlE (Muntel et al., 2014) (Figure 36BC).
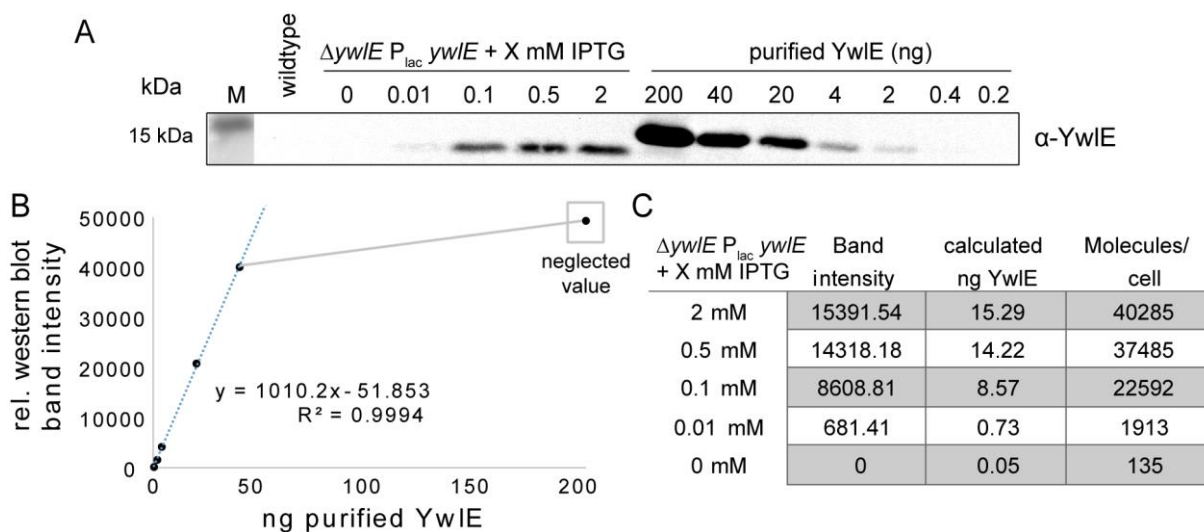
Figure 36: Quantitative α-YwlE western blotting.

A) The wildtype strain and the Δ*ywlE* P_{lac} *ywlE* (BIH828) strain were grown in the presence of indicated concentrations of IPTG in LB at 37 °C with samples for SDS-PAGE and α-YwlE western blotting (5 µg extract) taken at OD_{600} 0.5 and compared with indicated amounts of purified YwlE (His-tagged). Concentrations were obtained by Bradford test. B) Relative western blot band intensity was obtained with ImageJ software and plotted against the respective sample concentrations. Linear calibration was performed resulting in the equation y=1010.2x – 51.853, which was used to calculate the molecules YwlE per cell with cfu: $8.3 * 10^7$ cells/mL, $1.38 * 10^7$ cells in 5 µg extract and the size of YwlE, 16.6 kDa (C).

3.2.4. Toxicity of ClpC F436A depends on McsB

Recently it was observed that the F436A linker variant of *Staphylococcus aureus* ClpC displayed enhanced basal ATPase activity *in vitro* and that a *clpC* F436A expressing mutant strain was severely impaired in growth (Carroni et al., 2017). This toxic phenotype was suspected to be a direct consequence of the hyperactivity and simultaneous loss of physiological function of ClpC F436A. In order to gain more insight into the activation mechanism of ClpC, the ClpC F436A linker mutant was investigated in *B. subtilis*.

A markerless *clpC* F436A mutant *in cis* (strain BIH400) was impaired in growth at 37 °C and 50 °C (not shown). Unfortunately, the extent of impairment was hardly reproducible, which was probably based on the accumulation of suppressor mutation during the long-lasting procedure of the markerless transformation protocol (Arnaud et al., 2004). Therefore, the *clpC* F436A gene was cloned under the control of an IPTG inducible P_{lac} promoter to sustain reproducibility and allow a controllable expression. Surprisingly, the expression of *clpC* F436A in *B. subtilis* resulted in dramatic protein aggregation and the formation of bulges in the membrane, which were not exceptionally co-localized with the marked protein aggregates (Figure 37A). Moreover, the severely impaired growth of a *clpC* F436A expressing *S. aureus* was also observed in *B. subtilis* (Figure 37B) (Carroni et al., 2017). That effect was increased at elevated temperatures (Figure 37C).
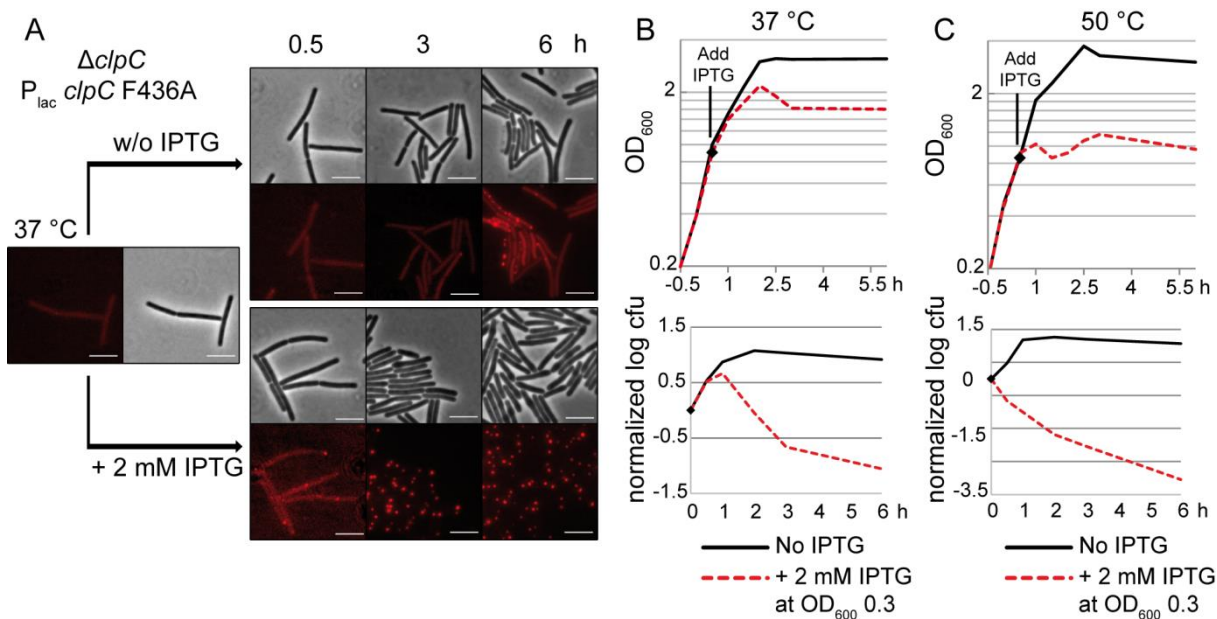
Figure 37: Expression of *clpC* F436A is toxic in *B. subtilis*.

Strain Δ*clpC* P$_{lac}$ *clpC* F436A (IH420) grown in LB + 0.5 % xylose at 37 °C was treated ± 2 mM IPTG at OD$_{600}$ 0.3. Samples were taken at indicated temperatures for A) fluorescence microscopy and B/C) OD measurement as wells as plating for cfu. One representative example is shown.

As *B. subtilis* ClpC is modulated by its adaptors, the effect of *clpC* F436A was examined in strains lacking the genes for each adaptor protein. Surprisingly, a Δ*mcsB* mutant completely abolished the toxicity and aggregation phenotype of the *clpC* F436A mutant (Figure 38A). In addition, a Δ*ypbH* mutant further increased the toxic effect of *clpC* F436A. Analyzing all combinations of single, double and triple adaptor deletion mutants demonstrated that whenever McsB was not present, the toxicity of ClpC F436A was severely decreased or abolished (Figure 38A). Remarkably, this was not observed in a Δ*mcsB* mutant strain with the *clpC* F436A analogue *clpE* Y344A, clearly indicating the importance of the adaptor protein McsB for activity of ClpC only (Figure 38B). As control, expression of *clpC* F436A and *clpE* Y344A was compared with the respective non-mutated strains P$_{lac}$ *clpC* and P$_{lac}$ *clpE* by western blotting (Figure 38C). In addition to that, neither overexpression of *clpC* nor overexpression of *clpE* negatively affected the viability of *B. subtilis* at 37 °C or 50 °C.
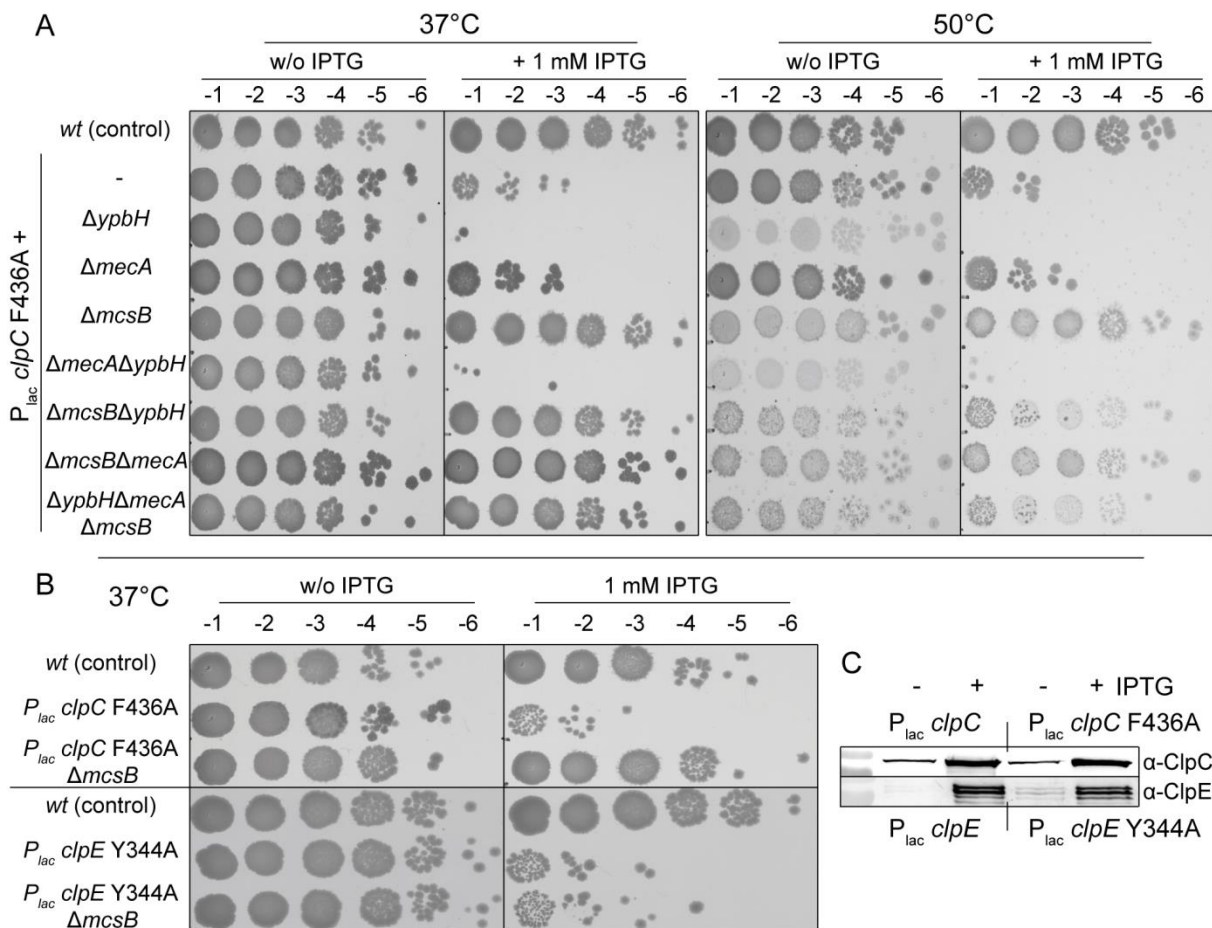
Figure 38: Toxicity of *clpC* F436A is dependent on the presence of McsB.

Strains A) wildtype, P$_{lac}$ *clpC* F436A (BIH384) + Δ*ypbH* (BIH613) + Δ*mecA* (BIH587) + Δ*mcsB* (BIH581) + Δ*mecA*Δ*ypbH* (BIH624) + Δ*mcsB*Δ*ypbH* (BIH619) + Δ*mcsB*Δ*mecA* (BIH589) + Δ*mcsB*Δ*mecA*Δ*ypbH* (BIH627) and B) P$_{lac}$ *clpE* Y344A (BIH383) and Δ*mcsB* P$_{lac}$ *clpE* Y344A (BIH647) were analyzed in a spot test according to materials and methods. Experiment was performed at least three times with one representative example shown. C) Strains P$_{lac}$ *clpC* (BIH151), P$_{lac}$ *clpC* F436A (BIH384), P$_{lac}$ *clpE* (BIH381) and P$_{lac}$ *clpE* Y344A (BIH383) were grown to OD$_{600}$ 0.3 in LB medium and treated ± 2 mM IPTG for 1 h to take samples for α-ClpC and α-ClpE western blotting (5 µg cellular extract).

Since the kinase activity of McsB was identified to be crucial for ClpC mediated disaggregation *in vivo*, its importance was examined regarding *clpC* F436A toxicity. Surprisingly, abolishing the kinase activity of McsB in either a *mcsB* C167S mutant strain or by deleting its activator *mcsA*, did not decrease the toxic effect of ClpC F436A (Figure 39). In addition, only the deletion of *mcsB* displayed a more translucent colony morphology at 50 °C. Both phenotypes suggested a role of McsB independent of its kinase activity.
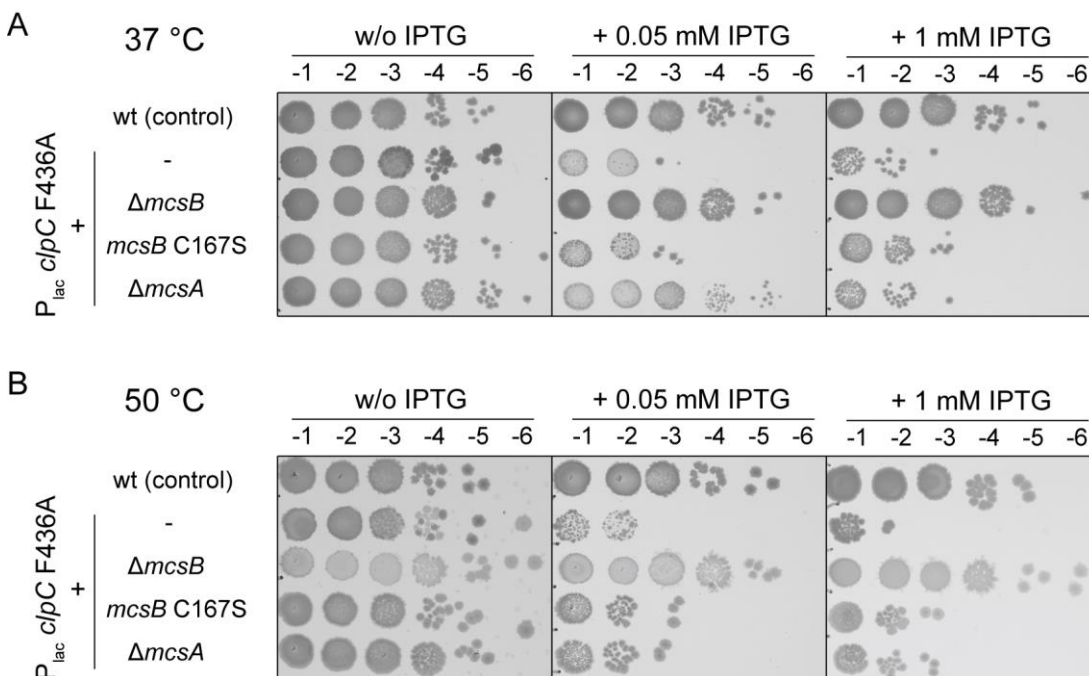
Figure 39: Toxicity of *clpC* F436A is decreased in Δ*mcsB*, but not in kinase inactive *mcsB* C167S.

The strains wildtype, P$_{lac}$ *clpC* F436A (BIH384) + Δ*mcsB* (BIH581) + *mcsB* C167S (BIH614) and + Δ*mcsA* (BIH622) were analyzed in a spot test according to materials and methods at A) 37 °C and B) 50 °C. Experiment was performed at least three times with one representative example shown.

To investigate the toxicity of ClpC F436A in more detail, a *clpC* F436A VGF::GGR (loop) mutant was created. A VGF::GGR mutant is incapable of forming the active ClpCP complex, allowing to differentiate between protein unfolding by ClpC and degradation by ClpCP (Figure 42) (Moliere, 2012). The *clpC* F436A VGF::GGR strain was not impaired in growth at 37 °C, however, a toxic phenotype was observed at elevated temperatures (Figure 40A). Strikingly, when analyzing all combinations of single, double and triple adaptor deletion mutants, all tested Δ*mcsB* mutant strains were more prone to the toxic effect of *clpC* F436A loop, which on first view contradicted the previous results, where the toxic effect of *clpC* F436A was abolished in a Δ*mcsB* mutant (Figure 40A).

However, while the toxicity of ClpC F436A was not abolished in a kinase inactive *mcsB* C167S mutant, expression of *clpC* F436A loop negatively affected the Δ*mcsB*, *mcsB* C167S and Δ*mcsA* strains, which all directly or indirectly lack kinase active McsB (Figure 40BC).
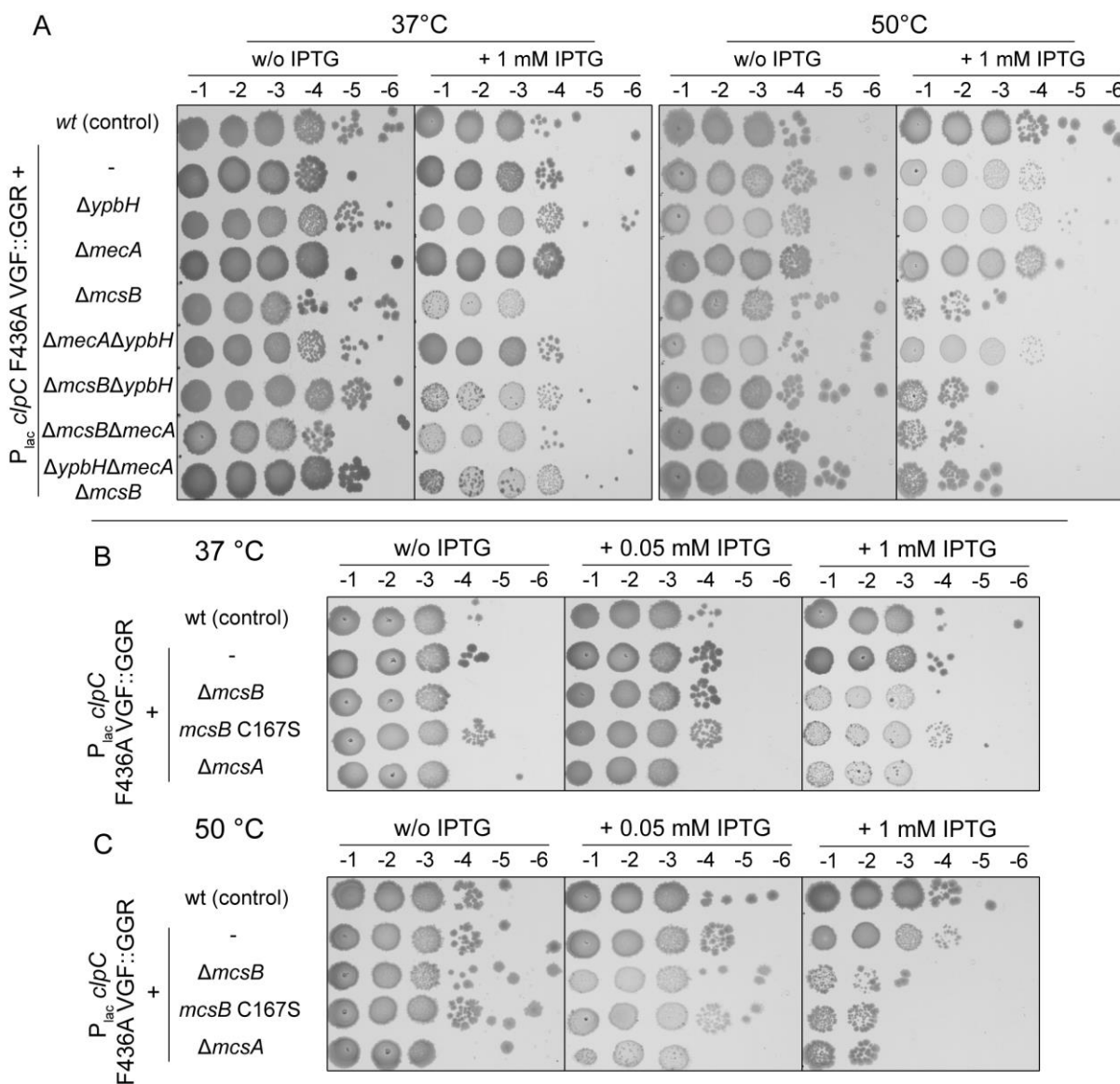
Figure 40: Absence of a kinase active McsB increases toxicity of *clpC* F436A VGF::GGR.

The strains A) wildtype, P$_{lac}$ *clpC* F436A VGF::GGR (BIH385) + Δ*ypbH* (BIH618) + Δ*mecA* (BIH588) + Δ*mcsB* (BIH582) + Δ*mecA*Δ*ypbH* (BIH625) + Δ*mcsB*Δ*ypbH* (BIH620) + Δ*mcsB*Δ*mecA* (BIH590) + Δ*mcsB*Δ*mecA*Δ*ypbH* (BIH628) and B)/C) + *mcsB* C167S (BIH615) and + Δ*mcsA* (BIH621) were analyzed in a spot test according to materials and methods at A/B) 37 °C and A/C) 50 °C. Experiment was performed at least three times with one representative example shown.

In addition to the toxic phenotype of *S. aureus clpC* F436A *in vivo*, an enhanced ATPase activity of ClpC$_{S.a.}$ F436A was observed *in vitro* (Carroni et al., 2017). To determine whether this is also true for *B. subtilis*, ClpC and its F436A variant were purified and an ATPase assay was performed. In accordance with the previous results, a significant ~three times enhanced basal ATPase activity of ClpC F436A was observed (Figure 41A). In addition, ClpC F436A was no longer activated by MecA indicating the necessity of this particular amino acid residue on the tip of the linker domain for interaction with MecA (Figure 41B). This was in line with the observations of ClpC$_{S.a.}$ F436A (Carroni et al., 2017).
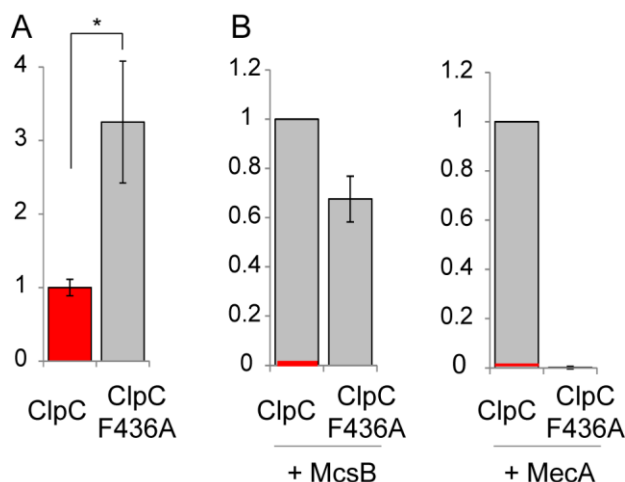
Figure 41: ClpC F436A displays enhanced basal ATPase activity *in vitro* and cannot be activated by MecA.

ClpC and ClpC F436A were compared in a malachite green ATPase assay at 37 °C with A) no adaptors or substrates (final 6 µM, 60 min, normalized to ClpC) or B) McsB or MecA added (final 1 µM, 15 min). Basal ClpC ATPase activity is indicated by red bar. All ATPase rates were calculated during phase of linear phosphate release according to materials and methods. Experiments were performed three times with standard deviation indicated as error bars. Significance is illustrated by *: $p<0.05$ and **: $p<0.01$ (Welch's test).

3.2.5. The impact of disaggregation vs. degradation in PQC

The protein quality control system consists of an intricate network of molecular chaperones and proteases. Heat stress leads to unfolding, misfolding and subsequent aggregation of proteins, which need to be degraded by proteases or disaggregated and refolded by

chaperones (Figure 1). ClpC as a AAA+ Clp ATPase was shown to disaggregate (alone) or degrade (in combination with ClpP) its substrate proteins *in vitro* (Kirstein et al., 2007; Schlothauer et al., 2003). As the clearance of heat induced protein aggregates was now observed *in vivo* (Figure 31, Figure 33 and Figure 34), the question arose whether it was the result of ClpC (±ClpP) mediated disaggregation or degradation. In order to distinguish between disaggregation and degradation, the ClpC VGF::GGR mutant was analyzed in more detail. This variant of ClpC is incapable of forming the active ClpCP proteolytic complex (Moliere, 2012). In order to assess the impaired degradation, a $\Delta clpC$ strain was complemented either with P_{lac} *clpC* or P_{lac} *clpC* VGF::GGR. Chloramphenicol was used to arrest translation and to subsequently follow the degradation of adaptor proteins MecA, McsB and YpbH, as re-synthesis was no longer possible. First it was observed that YpbH was degraded faster than MecA at 37 °C and 50 °C, while McsB was not detected at 37 °C at all (Figure 42A). In general, degradation was accelerated at 50 °C. As expected, the $\Delta clpC$ P_{lac} *clpC* VGF::GGR strain was incapable of degrading all three adaptor proteins at 37 °C and 50 °C (Figure 42B). The respective levels of ClpC and ClpC VGF::GGR were compared by western blotting (Figure 42C). *In vitro* degradation of β-casein was consistently not observed when the assay was performed with ClpC VGF::GGR instead of wildtype ClpC (Figure 42D).
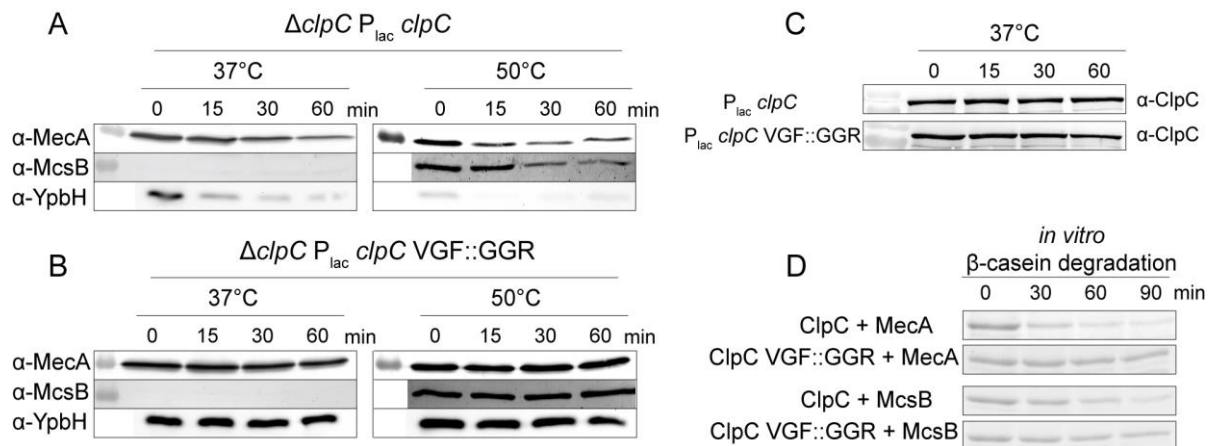
Figure 42: VGF::GGR mutation in ClpC prevents the degradation of target proteins.

Strain $\Delta clpC$ complemented by either A) P_{lac} *clpC* (BIH152) or B) P_{lac} *clpC* VGF::GGR (BIH504) was treated with 2 mM IPTG at OD_{600} 0.3 for 1 h. 25 µg/mL (final) chloramphenicol was added to arrest translation and samples were taken at indicated time points for western blotting (5 µg cellular extract). One representative example is shown. C) Control of A) / B) regarding ClpC levels during chloramphenicol treatment. D) *In vitro* degradation of β-casein at 37 °C according to materials and methods. All samples contain ClpP, β-casein, pyruvate kinase, PEP as well as indicated proteins ClpC, MecA and McsB. One representative result with band of β-casein is shown. Results in panel D) were generated in cooperation with Regina Kramer (IFMB / LUH).

As the ClpC VGF::GGR variant was not able to degrade of substrate proteins, the different impact of protein degradation and disaggregation by ClpC regarding thermoresistance, thermotolerance and aggregate clearance capacity was examined in a markerless *clpC* VGF::GGR mutant (where only disaggregation is possible) and compared with a complete $\Delta clpC$ mutant (where neither disaggregation nor degradation is possible).

Surprisingly, while a $\Delta clpC$ strain displayed impaired survival (Figure 43A) and increased protein aggregation at thermotolerance conditions (Figure 43B), a *clpC* VGF::GGR mutant was not observed to be heat sensitive under tested conditions. Additionally, McsB mediated removal of protein aggregates during recovery from heat shock was not impaired in this strain (Figure 43C). As a control, clearance of aggregates by McsB was not possible in an ATPase inactive *clpC* double walker mutant (DWB) strain (Figure 43C). This ClpC DWB variant fails to hydrolyze ATP and is considered a trapping mutant (Kirstein et al., 2006; Weibezahn et al., 2003), which demonstrated that the obtained phenotype is indeed based on a functional ClpC.

Figure 43: A *clpC* VGF::GGR mutant strain is not impaired in thermotolerance and aggregate clearance.

A) Wildtype (BIH369), Δ*clpC* (BIH432) and *clpC* VGF::GGR (BIH792) were examined in a standard thermotolerance experiment according to materials and methods with three biological replicates. Error bars indicate standard deviations with significance illustrated by *: $p<0.05$ and **: $p<0.01$ (Welch's test). Upper panel (squares) shows 48 °C pre-shocked cells, lower panel (triangles) shows survival of cells without former pre-shock. Additional samples were taken for fluorescence microscopy in B) to illustrate subcellular aggregation with YocM-mCherry. Scale bar indicates 5 μm. One representative example is shown. C) Strains Δ*mcsB* P_{lac} *mcsB* (BIH414), *clpC* VGF::GGR Δ*mcsB* P_{lac} *mcsB* (BIH485) and *clpC* E280A E618A (DWB) Δ*mcsB* P_{lac} *mcsB* (BIH488) were treated with at 50 °C heat shock for 30 min at OD_{600} 0.3. Cultures were split ± 2 mM IPTG to induce P_{lac} *mcsB* during recovery at 37 °C. Samples of at least three biological replicates were taken for fluorescence microscopy and ratio of cells containing YocM-mCherry marked aggregates was obtained by counting fluorescent foci. Results in panel A) were generated in cooperation with Regina Kramer (IFMB / LUH).

Protein degradation appeared to be less important than protein disaggregation regarding heat stress response. To further discriminate their respective impacts in protein stress, puromycin was applied as a different kind of stressor. Puromycin leads to impaired protein translation due to premature nascent chain termination and release of incomplete polypeptide chains (Pestka, 1971; Yarmolinsky and Haba, 1959). These incomplete peptide fragments represent misfolded proteins, which cannot be refolded. Hence it was hypothesized that removal of subcellular protein aggregates resulted from puromycin treatment rely on protein degradation.

The treatment with the antibiotic puromycin (25 µg/mL, 15 min) led to the formation of YocM-mCherry marked protein aggregates (Figure 44A). After centrifugation and removal of puromycin by resuspension of cells in fresh LB media, the clearance of YocM-mCherry marked protein aggregates was observed within 150 min when *mcsB* was expressed (Figure 44A, 1 vs 2). This suggests that McsB is in combination with ClpCP able to remove protein aggregates originated from different types of stress (Figure 44A, Figure 31 and Figure 33). During the inspection of the fluorescence microscopical images, some YocM-mCherry marked aggregates were observed outside of the cell suggesting previous cellular lysis (Figure 44E). These protein aggregates were excluded in the statistical evaluation in Figure 44C.

Remarkably, in contrast to clearance of heat based protein aggregates, the removal of protein aggregates resulted from puromycin treatment was not possible to a similar extent in the *clpC* VGF::GGR mutant as seen before (Figure 43C and Figure 44BC). Yet potential unfolding of incomplete, misfolded protein fragments by ClpC VGF::GGR might facilitate unspecific degradation by other concurrent proteases, which could explain the minor positive effect when *mcsB* was expressed in this *clpC* VGF::GGR strain (Figure 44C). Moreover, a *clpC* VGF::GGR mutant displayed a reduced removal of protein aggregates compared to the

wildtype after 150 min independent of the presence of McsB, indicating interactions with other adaptor proteins of ClpC (Figure 44C). As control, western blotting was performed to demonstrate comparable amounts of ClpC as well as the synthesis of McsB due to addition of IPTG (Figure 44D). These results suggested that protein degradation by McsB and an active ClpCP complex becomes important when disaggregation and refolding is not possible.
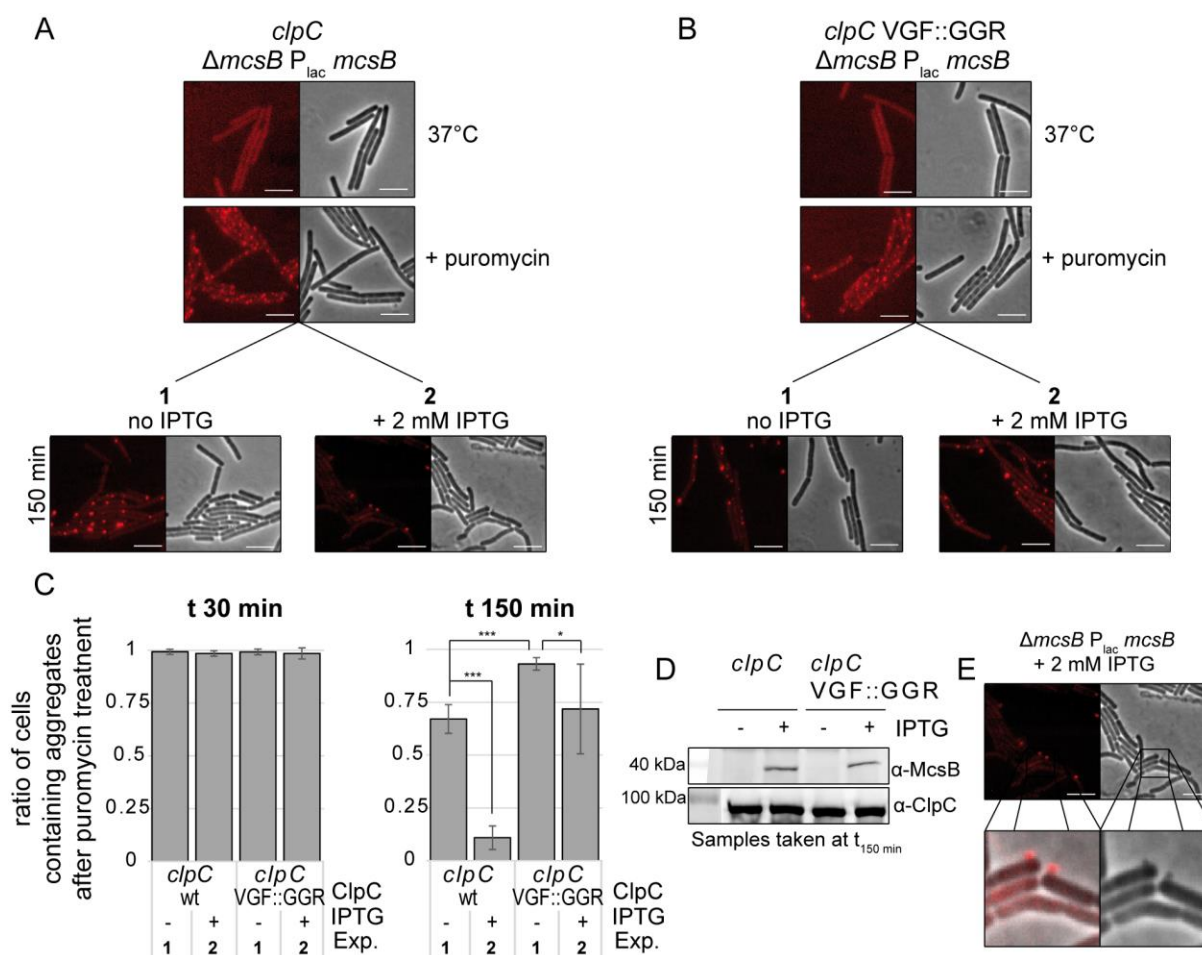
Figure 44: Clearance of subcellular aggregates resulted from puromycin treatment requires a functional ClpCP proteolytic complex.

The strains A/E) $\Delta mcsB$ P_{lac} $mcsB$ (BIH414) and B) $clpC$ VGF::GGR $\Delta mcsB$ P_{lac} $mcsB$ (BIH485) were grown in LB + 0.5 % xylose and treated with final 25 µg/mL puromycin at OD_{600} 0.4 for 15 min. Cells were harvested by centrifugation and resuspended in fresh LB + 0.5 % xylose without puromycin and ± 2 mM IPTG was added. Cultures were kept shaking at 37 °C for 150 min with samples taken at indicated time points for fluorescence microscopy (scale bar 5 µM) with one representative example shown. Ratios (C) were calculated from three biological replicates with error bars indicating standard deviations including significance indicated by *: $p<0.05$, **: $p<0.01$ and ***: $p<0.001$ (Welch's test). D) At t_{150min} after puromycin treatment, additional samples were taken for α-McsB and α-ClpC western blotting to allow comparability (5 µg cellular extract).

During the investigations regarding *in vivo* disaggregation after heat stress, it was demonstrated that kinase activity of McsB was essential for aggregate clearance (Figure 33). Furthermore, a deletion of *ywlE* substantially increased the removal of protein aggregates, which was only possible when McsB was present and kinase active (Figure 34). In order to elucidate the role of McsB kinase activity in targeting proteins for ClpCP degradation *in vivo*, the same experiments were performed with puromycin instead of heat stress.

As expected, when the kinase inactive McsB C167S was examined, aggregates clearance was abolished (Figure 45A). Furthermore, the $\Delta ywlE$ deletion mutant displayed accelerated clearance of puromycin induced aggregates within 150 min of recovery at 37 °C when compared to a strain with elevated levels of YwlE (Figure 44AB and Figure 45BC). That effect was not observed when a $\Delta ywlE$ strain was complemented with an inactive P_{lac} *ywlE* C7S variant *in trans* (Figure 45D). In addition, a kinase inactive *mcsB* C167S background mutation completely abolished aggregate removal regardless of the amount of YwlE present in the cell (Figure 45E). These observations indicated that kinase active McsB was essential for degradation of puromycin generated aggregates and were consistent with the previous experiments regarding aggregate removal after heat stress.
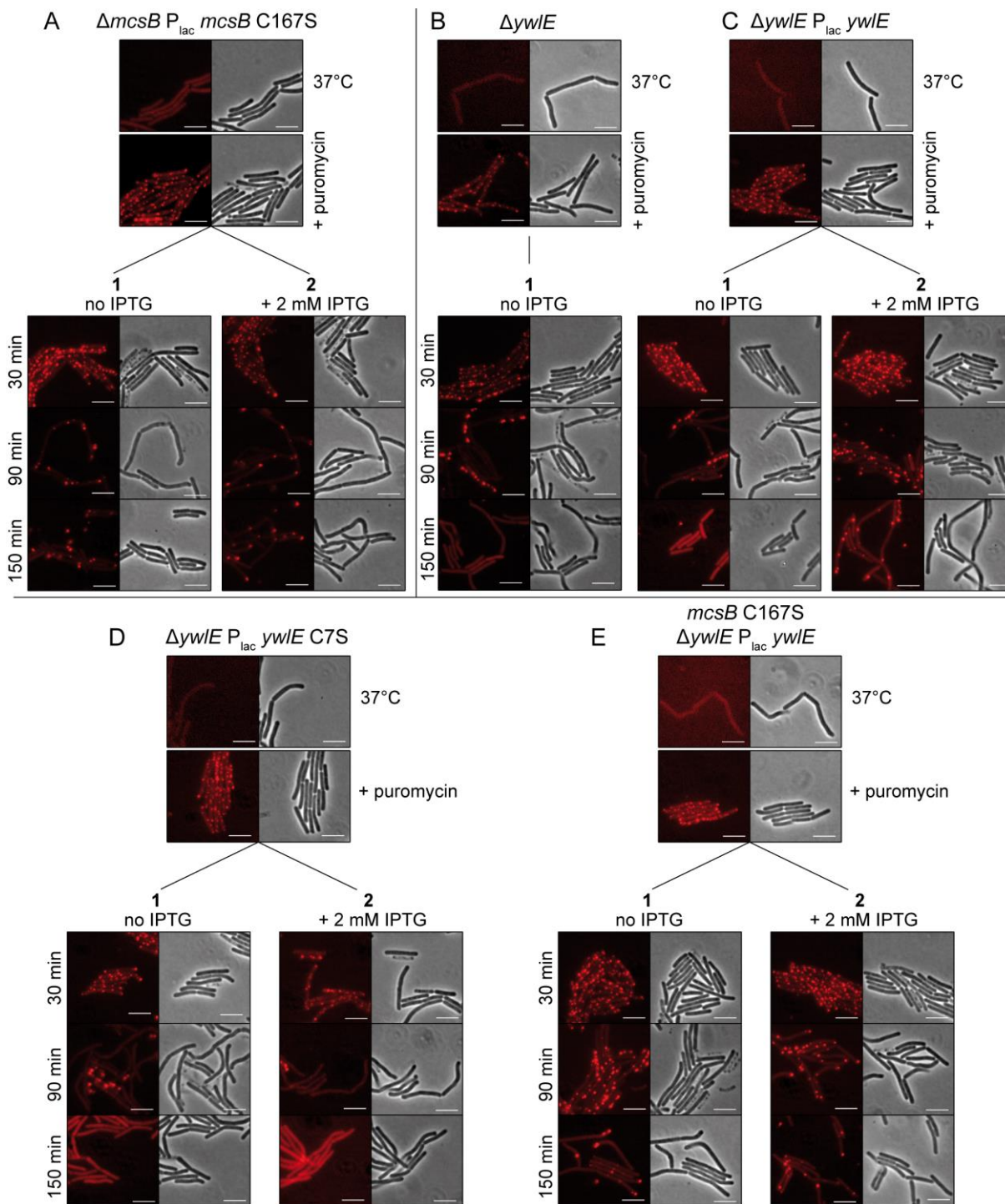
Figure 45: Kinase active McsB is essential to remove puromycin generated aggregates.

The strains A) Δ*mcsB* P*lac mcsB* C167S (BIH439) B) Δ*ywlE* (BIH819), C) Δ*ywlE* P*lac ywlE* (BIH828), D) Δ*ywlE* P*lac ywlE* C7S (BIH829) and E) *mcsB* C167S Δ*ywlE* P*lac ywlE* (BIH824) were grown in LB + 0.5 % xylose and treated with final 25 μg/mL puromycin at OD$_{600}$ 0.4 for 15 min. Cells were harvested by centrifugation at 5.000 xg for 5 min and resuspended in fresh LB + 0.5 % xylose without puromycin and ± 2 mM IPTG. Cultures were kept shaking at 37 °C for 150 min with samples taken at indicated time points for fluorescence microscopy (scale bar 5 μM) with one representative example shown.

3.3. Establishing a ClpC target-based screening system in B. subtilis

Recently, various compounds have been identified to target the NTD of ClpC resulting in cellular death of Gram-positive pathogenic bacteria like *M. tuberculosis* and *S. aureus*. Their non-pathogenic relative *B. subtilis* is often used as a general model organism and/or for proof of concept experiments since it is well studied, genetically accessible, fast growing and, as an S1 organism, does not need specific safety requirements.

In order to develop a ClpC target-based screening system, a suitable reporter had to be established. The underlying idea was to develop a fluorescent reporter fusion protein, which functions as a substrate for ClpCP and is therefore constantly degraded. Inhibition, competition or deregulation of ClpCP e.g. by natural compounds would result in a change of fluorescent signal possibly allowing for a fast high-throughput screening.

In *B. subtilis* the three known adaptor proteins MecA, YpbH and McsB are constantly degraded by the protease complex ClpCP (Figure 42A) (Kirstein et al., 2007; Persuh et al., 2002; Schlothauer et al., 2003; Trentini et al., 2016). McsB is 40 kDa in size and has, besides from its role as an adaptor protein in heat stress regulation by targeting CtsR for degradation by ClpCP, as a protein arginine kinase a major impact on cellular physiology and hence is a key player during heat stress response (see 3.2). Moreover there is no structure of McsB of the active ClpC-McsB complex known so far.

MecA is only 26 kDa in size and involved in e.g. competence development (Turgay et al., 1997). In contrast to McsB, a structure of the active ClpC-MecA complex has already been solved (Wang et al., 2011). Regarding its architecture it is known that both the NTD and CTD have distinct roles. While the NTD interacts with substrate proteins, the CTD binds and

activates ClpC (Persuh et al., 1999; Wang et al., 2011). In comparison to MecA, its paralog YpbH is not well studied (Persuh et al., 2002). Therefore, MecA was the first choice regarding the development of a ClpC reporter protein.

As expected, deletion of the NTD of MecA did not affect ClpC activation *in vitro* (Figure 41C). In addition it was observed that MecA$_{CTD}$ was degraded by ClpCP in a decelerated manner (Figure 46A). Consequently, the CTD was functional as a degradation tag without the NTD. Unsurprisingly, when the NTD as the putative substrate interaction site of MecA was deleted, degradation of the substrate α-casein by ClpCP was abolished (Figure 46B) suggesting that without the NTD, MecA$_{CTD}$ is not able to target proteins for ClpCP mediated degradation anymore.
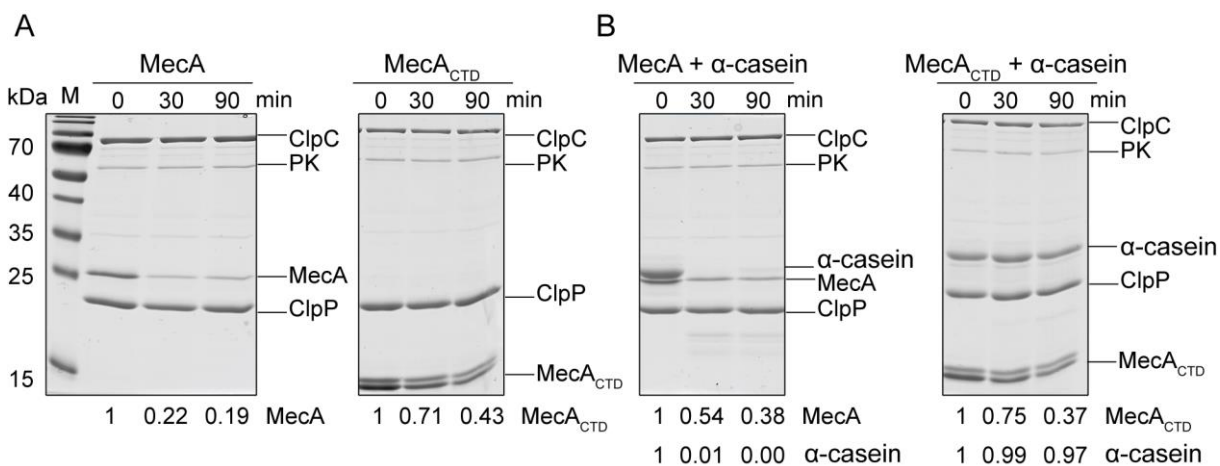
Figure 46: Deletion of NTD abolishes MecA mediated degradation of α-casein by ClpCP.

In vitro degradation assay was performed according to materials and methods at 37 °C with samples taken for SDS-PAGE and Coomassie staining at indicated time points after starting the reaction with ATP. Indicated proteins A) ClpC / MecA / ClpP / MecA$_{CTD}$ and B) ± α-casein were analyzed at a final concentration of 1 µM. Indicated ratios were calculated from band intensity using ImageJ and subsequently normalized to band intensity of ClpC. One representative example is shown. PK: pyruvate kinase.

To monitor the activity of ClpCP *in vivo*, the degradation tag MecA$_{CTD}$ was fused to a green fluorescent protein and examined regarding its degradation by ClpCP. The addition of GFP as well as its positioning on the C- or N-terminal end of MecA$_{CTD}$ did not significantly affect the

activation of the ClpC ATPase (Figure 47A). As ClpC F436A (see 3.2.4) was not activated by MecA or MecA$_{CTD}$, a MecA$_{CTD}$-GFP fusion protein was speculated to behave likewise (Figure 41). Surprisingly, when this fusion construct was analyzed regarding ClpC F436A ATPase activation, about 5 % of the abolished ClpC ATPase activity was regained (Figure 47B). However, that effect could not be observed when a GFP-MecA$_{CTD}$ fusion protein was investigated, suggesting a significant influence of the position of the GFP-tag during activation of ClpC F436A.
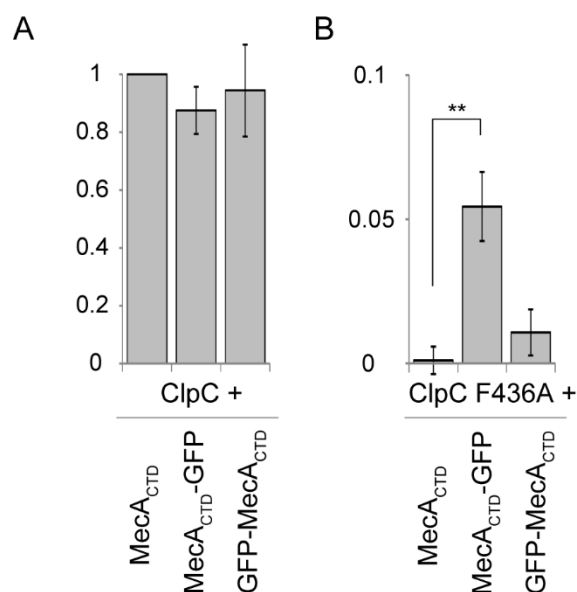
Figure 47: ATPase of ClpC F436A is slightly activated by MecA$_{CTD}$-GFP, but not by GFP-MecA$_{CTD}$.

ClpC (A) and ClpC F436A (B) were compared in a malachite green ATPase assay at 37 °C for 15 min with indicated MecA$_{CTD}$-fusion proteins (final 1 µM each). All ATPase rates were calculated during phase of linear phosphate release according to materials and methods. Experiments were performed three times with standard deviation indicated as error bars. Significance is illustrated by *: $p<0.05$ and **: $p<0.01$ (Welch's test).

Thus, the structure of active MecA-ClpC hexameric complex was analyzed regarding the positioning of the MecA$_{CTD}$ in more detail (Figure 48A). It has to be noted that GFP was fused to MecA$_{CTD}$ with an intermediary Gly-Ser-Ala linker region to allow flexibility and dynamics within substrate binding and unfolding by the ClpCP complex.
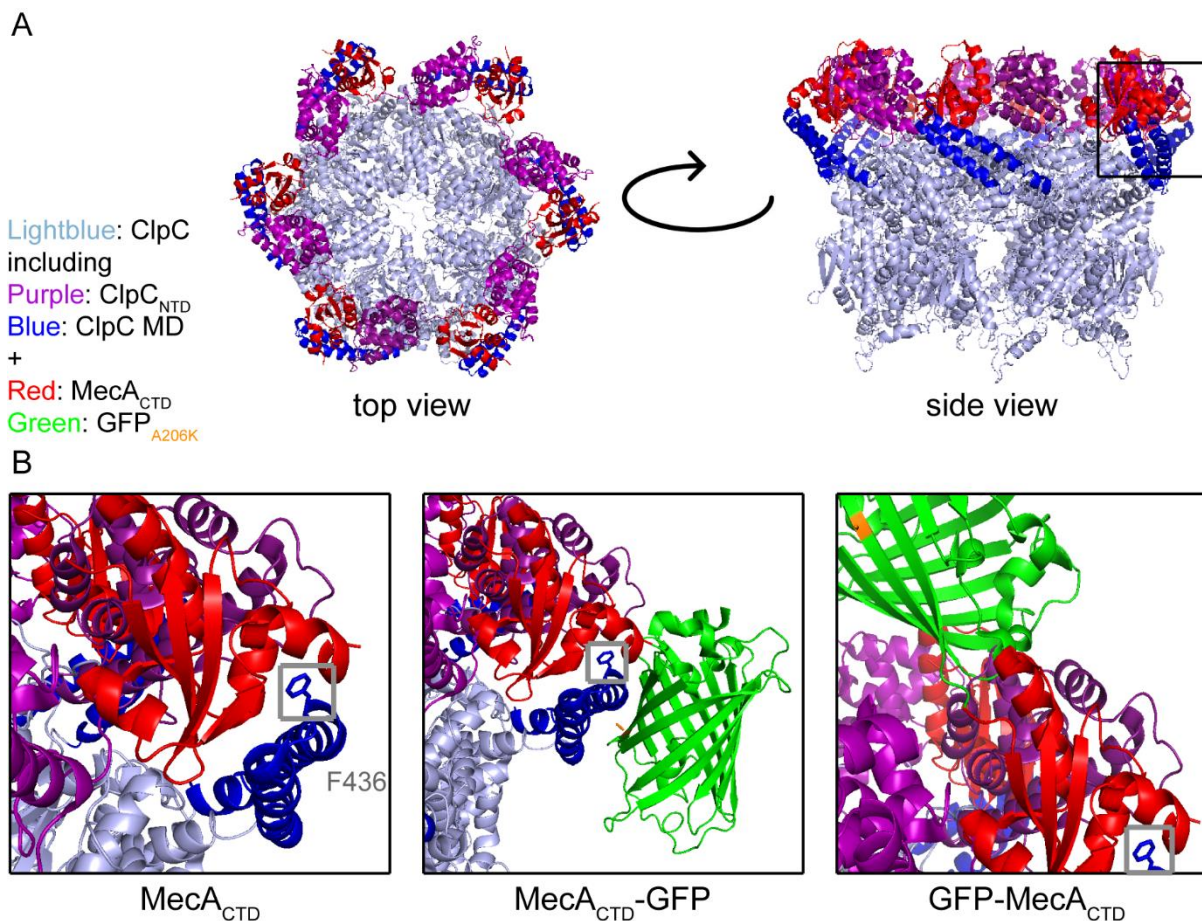
Figure 48: MecA$_{CTD}$-GFP fusion protein might restore ClpC F436A (+ MecA$_{CTD}$) activity by partially keeping the M-domain in its functional position.

A) Structure of hexameric ClpC-MecA complex obtained by cryo-electron microscopy (PDB: 3J3R, based on crystal structure PDB: 3PXG). The NTD of MecA is not shown because of low electron density due to high flexibility. B) Zoomed fraction of A): Phenylalanine F436 on tip of the M-domain (MD) is indicated (grey box). Crystal structure of GFP$_{A206K}$ (PDB: 2YE0) was added manually to actual structure of ClpC-MecA complex to illustrate hypothetical positioning at N- or C-terminal end of MecA$_{CTD}$. All experiments were performed with monomerized GFP A206K variant (orange) to prevent artifacts through dimerization. Color code: ClpC – lightblue, ClpC$_{NTD}$ – purple, ClpC$_{MD}$ – blue, MecA$_{CTD}$ – red, GFP$_{A206K}$ – green, A206K mutation of GFP – orange.

However, when examining the specific structural features on that position, it became evident that fusing GFP at the N-terminal end of MecA$_{CTD}$ would extend the active complex at its top region, whereas a C-terminal MecA$_{CTD}$-GFP fusion would rather lead to the positioning of GFP at the side of the complex next to the M-domain (Figure 48B). It is known that the positioning of the M-domain is essential for activity and regulation of ClpC or ClpB species

(Carroni et al., 2017, 2014; Haslberger et al., 2007). The loss of ClpC F436 abolishes the interaction of the M-domain with MecA (i.e. MecA$_{CTD}$). Hence, adding GFP might at least partially lead influence the position the M-domain by simple steric hindrance explaining the slightly restored activity in a ClpC F436A mutant with MecA$_{CTD}$-GFP as a modified adaptor protein (Figure 41C and Figure 48A).

As activation of ClpC was possible with all examined variants, the degradation of the GFP-fusion proteins was monitored by continuously measuring the fluorescence intensity in a plate reader during the reaction (Figure 49ABCD). Additionally, samples for SDS-PAGE were taken to compare the band intensity of the GFP-fusion protein in each reaction with the control sample (without ClpC) after 90 min (t$_{90\ min}$) (Figure 49EF).

Although both GFP-fusion proteins activated the ATPase of ClpC in a comparable manner, the N-terminal GFP-MecA$_{CTD}$ fusion protein was degraded faster than the C-terminal MecA$_{CTD}$-GFP fusion (Figure 49AB). As control, both fusion proteins were not processed when ClpC VGF::GGR or ClpC F436A was examined instead of the wildtype ClpC (Figure 49AB). Addition of MecA to the reaction mixture indicated a direct competition with the GFP-fusion proteins in a dose dependent manner (Figure 49CDEF).
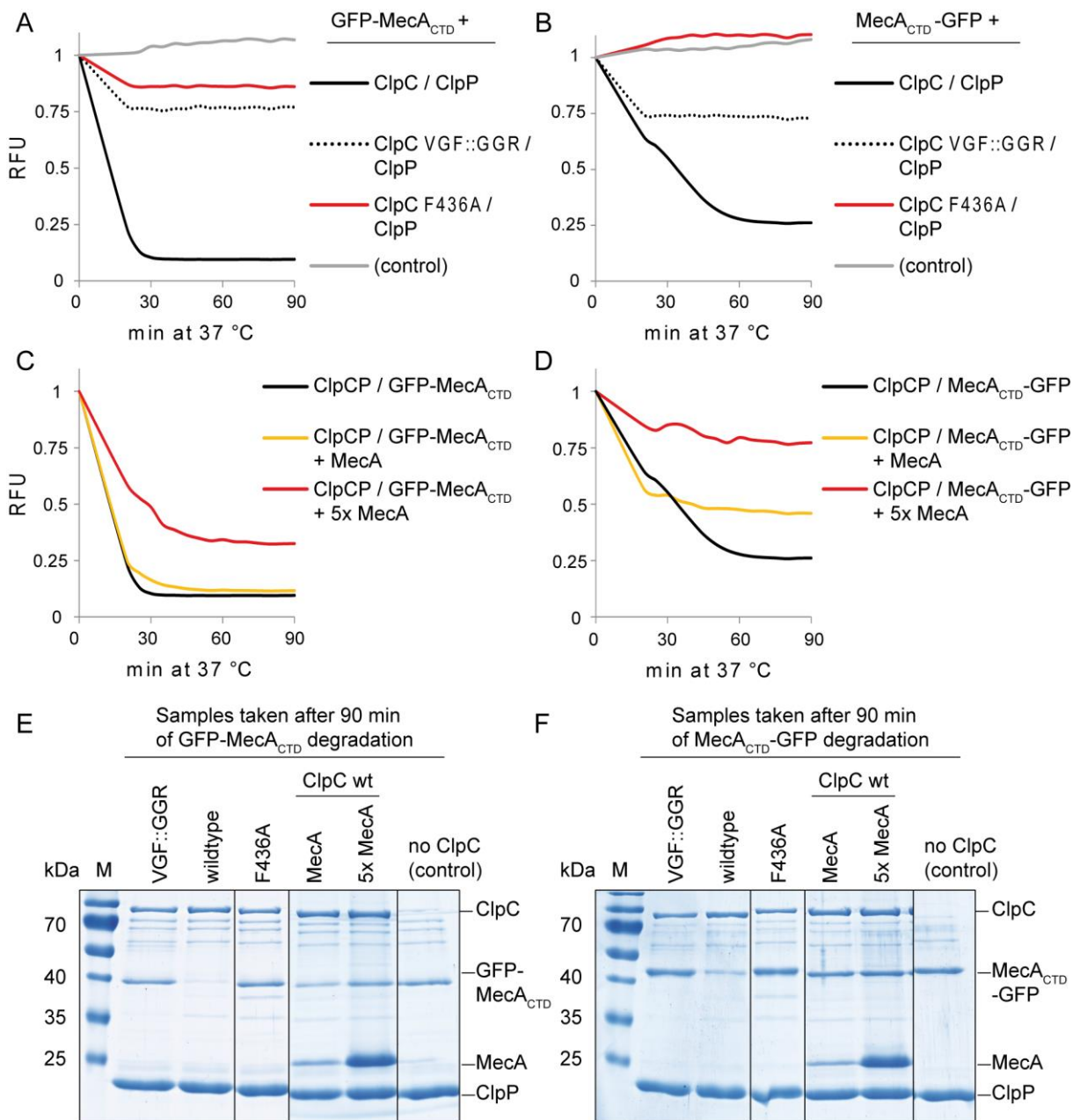
Figure 49: MecA$_{CTD}$-GFP and GFP-MecA$_{CTD}$ are degraded by ClpCP *in vitro*.

In vitro degradation assay was performed according to materials and methods in a SpectraMaxM3 plate reader at 37 °C. The breakdown of fluorescent A/C) GFP-MecA$_{CTD}$ and B/D) MecA$_{CTD}$-GFP was monitored at ex. 470 nm/em. 509 nm. All indicated proteins were diluted to a concentration of final 1 μM if not otherwise indicated. Samples were taken at t$_{90min}$ for SDS-PAGE and Coomassie staining (E/F) to compare the band intensity of the GFP-fusion protein in the respective sample with the control sample without ClpC. One representative example is shown. PK: pyruvate kinase.

Both MecA$_{CTD}$.GFP and GFP-MecA$_{CTD}$ fusion proteins were degraded *in vitro* (Figure 49). However, the MecA$_{CTD}$-GFP fusion was selected as the reporter for the construction of the screening strain as it was not degraded as efficiently and could therefore accumulate more easily upon disruption or deregulation of ClpC or ClpCP. Furthermore, a constitutive promotor (P$_{veg}$) was selected for synthesis of the reporter in the screening strain to avoid the requirement and possible influence of an inductor.

The strong P$_{veg}$ promotor resulted in sufficient synthesis of MecA$_{CTD}$-GFP as shown by western blotting (Figure 50A), which did not negatively affect growth of the screening strain. Furthermore, the α-MecA antibody detected the fusion protein as well as the regular levels of MecA as internal control (Figure 50A). As MecA was shown to compete with MecA$_{CTD}$-GFP *in vitro* (Figure 49F), the effect of a Δ*mecA* deletion regarding the P$_{veg}$ *mecA$_{CTD}$-gfp* strain was investigated *in vivo*. Deletion of *mecA* led to reduced band intensity of MecA$_{CTD}$-GFP in a western blotting experiment presumably due to lack of competition (Figure 50A). Nevertheless, *mecA* was not deleted in the final screening strain to minimize the genetic modifications compared to the wildtype strain, keeping the modifications as physiological as possible.

As anticipated, a Δ*clpC* deletion mutant led to accumulation of MecA$_{CTD}$-GFP indicated by augmented band intensity in western blotting (Figure 50A). On the contrary, elevated levels of ClpC decreased the amount of the fusion protein in the cell due to accelerated degradation (Figure 50B). Degradation of both MecA$_{CTD}$-GFP as well as untagged MecA was accelerated at 50 °C and only observed when ClpC was present in the cell (Figure 50C).
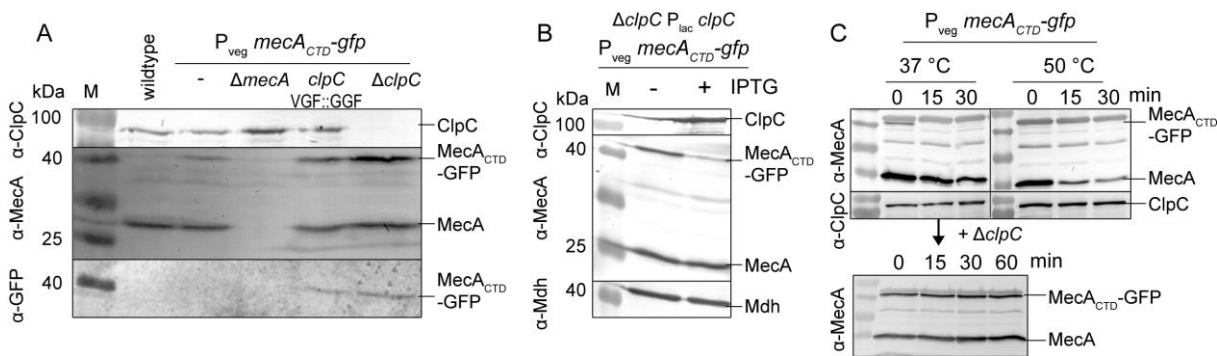
Figure 50: MecA$_{CTD}$-GFP is permanently degraded by ClpCP *in vivo*.

A) Strains P$_{veg}$ *mecA$_{CTD}$-gfp* (BIH11), + Δ*mecA* (BIH23), + *clpC* VGF::GGR (BIH24), + Δ*clpC* (BIH25) and wildtype were grown in LB medium to OD$_{600}$ 0.4 and samples were taken for α-ClpC, α-MecA and α-GFP western blotting (5 µg cellular extract). B) Strain Δ*clpC* P$_{lac}$ *clpC* P$_{veg}$ *mecA$_{CTD}$-gfp* (BIH186) was grown to OD$_{600}$ 0.4 and treated ± 2 mM IPTG for 1 h. Samples were taken for α-ClpC, α-MecA and α-Mdh western blotting (5 µg cellular extract). C) Strain P$_{veg}$ *mecA$_{CTD}$-gfp* (BIH11) and Δ*clpC* P$_{veg}$ *mecA$_{CTD}$-gfp* (BIH25) were treated with final 25 µg/mL chloramphenicol at OD$_{600}$ 0.4 to stop translation. Samples were taken at indicated time points for western blotting to follow breakdown of MecA and MecA$_{CTD}$-GFP, respectively.

Although MecA$_{CTD}$-GFP was detected by western blotting, when the strains were examined with fluorescence microscopy, no GFP signal was detected in the P$_{veg}$ *mecA$_{CTD}$-gfp* strain (Figure 51). A control strain expressing *gfp* without the *mecA$_{CTD}$* degradation tag displayed a strong fluorescent signal (Figure 51). As already observed in western blotting, exchange of wildtype *clpC* with *clpC* VGF::GGR or complete deletion of *clpC* resulted in accumulation of MecA$_{CTD}$-GFP and a substantial increase in GFP signal (Figure 50 and Figure 51). Additionally, the exchange of *clpC* with an ATPase inactive *clpC* DWB (double walker B) trap mutant resulted in a general increase in total GFP fluorescence signal and simultaneously in the formation of fluorescent foci at the cellular poles representing the trapped substrate MecA$_{CTD}$-GFP at ClpC (Figure 51).
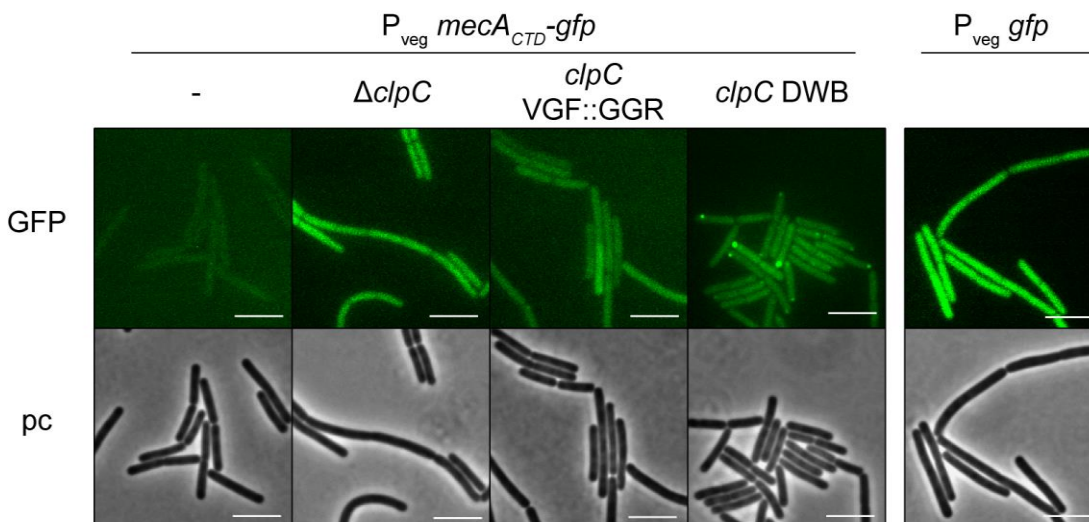
Figure 51: Impaired or deleted *clpC* leads to increase in MecA_{CTD}-GFP signal *in vivo*.

Strains P_{veg} $mecA_{CTD}$-*gfp* (BIH11), + $\Delta clpC$ (BIH25), + *clpC* VGF::GGR (BIH24), + *clpC* double walker B mutant (DWB, BIH143) and P_{veg} *gfp* (BIH27) were examined with fluorescence microscopy at OD_{600} 0.5. Phase contrast (pc) and standard gfp filters were used. Scale bar indicates 5 μm.

In order to allow high-throughput screening, the growth of the reporter strain had to be monitored in a plate reader and optimized regarding the fluorescent measurements. Growth curves were started at OD_{600} 0.1 with a volume up to 200 μL in a 96-well plate and incubated shaking at 30 °C while OD_{600} and fluorescence intensity (ex. 470 nm/ em. 485 nm) were tracked. As LB medium displayed severe background fluorescence and did not allow unimpeded monitoring of a possible accumulation of GFP signal, the screening strain was grown in the more transparent Belitsky minimal medium. In order to maintain fast growth of *B. subtilis* in this minimal medium, 0.01 % yeast extract was added. Additionally, enhanced GFP signal intensity could be achieved by an artificially raised cellular density due to evaporation of medium by incubating cells in 96-well plates without closing the lid. Due to low reproducibility of values after 18 h of growth, presumably because of unequal medium evaporation and oxygen distribution in the plate reader, growth curves were in general measured for 16 h.

Consistent with the pre-experiments (western blotting and fluorescence microscopy), the strain P_{veg} *mecA_CTD-gfp* did not display any fluorescent signal unless *clpC* was additionally impaired or completely deleted (Figure 52A). The obtained values are based on a normalization of the fluorescent signal divided by optical density, because in particular the $\Delta clpP$ mutant strain is severely impaired in growth in minimal media, which obviously results in a decreased total fluorescence (Figure 52B). Remarkably, in both strains *clpC* VGF::GGR and a complete $\Delta clpP$ deletion mutant, where only unfolding instead of degradation of substrate proteins and the reporter fusion MecA_CTD-GFP was possible, the signal intensity still reached about 40 % of positive control suggesting unspecific degradation after unfolding (Figure 52B).
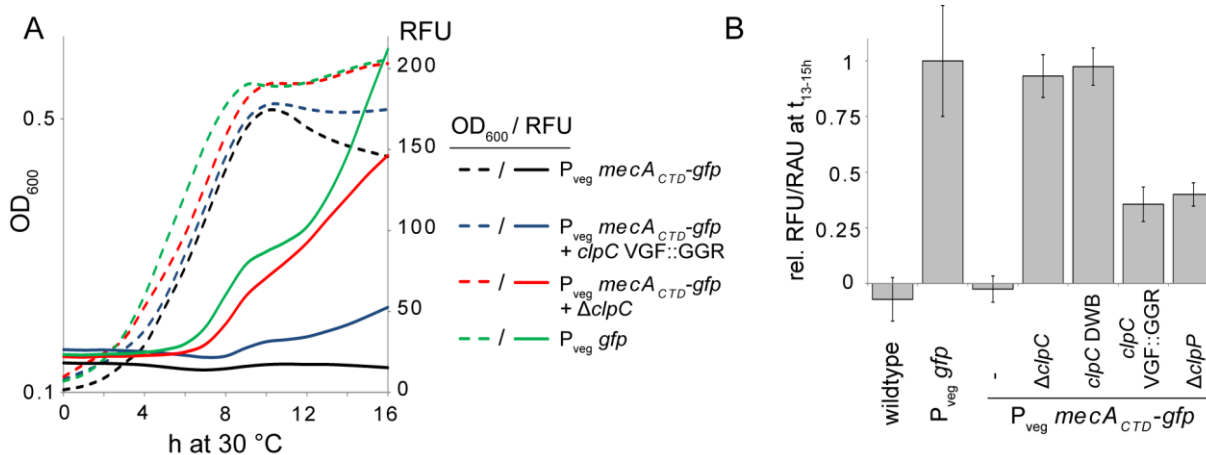
Figure 52: Accumulation of MecA_CTD-GFP in stationary phase leads to detectable GFP signal during growth in plate reader.

A) Strains P_{veg} *mecA_CTD-gfp* (BIH11), + $\Delta clpC$ (BIH25), + *clpC* VGF::GGR (BIH24) and P_{veg} *gfp* (BIH27) as well as B) $\Delta clpP$ P_{veg} *mecA_CTD-gfp* (BIH114) and *clpC* double walker B (DWB) P_{veg} *mecA_CTD-gfp* (BIH143) were grown in Belitsky minimal medium + 0.01 % yeast extract starting at OD_{600} 0.1 and kept shaking at 30 °C. OD_{600} and GFP signal (ex. 470 nm/ em. 485 nm) were monitored in a SpectraMax M3 plate reader with one representative example shown. B) Combined results of three biological replicates A). GFP signal intensity was normalized by cellular density. Results from time point 13-15 h are displayed. Error bars indicate standard deviation.

Next, different combinations of MecA$_{CTD}$ fused with mCherry instead of GFP were generated to support its applicability as a reporter *in vivo*. Additionally, the IPTG inducible P$_{lac}$ promoter instead of the constitutive P$_{veg}$ promoter was tested to generate alternatives regarding the screening strain. Obtained results in western blotting and fluorescence microscopy confirmed a comparable behavior of all tested MecA$_{CTD}$-mCherry and -GFP fusions *in vivo* (Figure 53BCD).

Moreover, besides from the established MecA$_{CTD}$ fusions as a reporter for ClpC activity, different other fusion proteins should be established to allow simultaneous screening for activity of other Clp proteins. The ssrA-tag is one example of a known marker for ClpXP mediated degradation (Wiegert and Schumann, 2001). In order to prevent false positive and superimposed signals with the GFP fusion protein, mCherry was selected for the second reporter. To this end *mcherry-ssrA* was integrated into the *lacA* site under the control of P$_{veg}$ promoter into the genome of *B. subtilis.* As P$_{veg}$ *mecA$_{CTD}$-gfp* was inserted into the *amyE* site, both reporter fusions could be produced simultaneously. As expected, expressing *mcherry-ssrA* did not result in a detectable mCherry signal in fluorescence microscopy (Figure 53A). However, when a strain lacking the ATPase ClpX was examined, an increase in fluorescence was observed (Figure 53A), which validated the mCherry-ssrA fusion protein as an adequate reporter for ClpX activity. It is important to note that a Δ*clpX* deletion mutant strain is severely impaired in motility and growth (Molière et al., 2016). Hence it was not possible to measure a growth curve (and fluorescence development) in the plate reader, where shaking and oxygen supply are only ensured to a certain extent.

Besides from compounds that address the unfoldases ClpC and ClpX, the attached protease ClpP has also been identified as a promising target for antibiotics (Lupoli et al., 2018). One prominent example are the acyldepsipeptides (ADEP), which trigger oligomerization of ClpP monomers and activate the proteolytic complex (Brötz-Oesterhelt et al., 2005; Kirstein et al., 2009a). Importantly, the ClpP complex is uncoupled from the corresponding ATPase and activated independently. This enhanced and unphysiological activation resulted in cellular death in different Gram-positive pathogens (Brötz-Oesterhelt et al., 2005; Ollinger et al., 2012). It was demonstrated that growth in ADEP treated cells is in particular impaired due to enhanced degradation of the cellular division protein FtsZ by ADEP activated ClpP complexes (Sass et al., 2011).

In order to further characterize potential antibiotic compounds that were identified by the screening strains, an FtsZ-mCherry and mCherry-FtsZ fusion protein was generated. Thereby a potential influence of the respective compound on activation of ClpP might be identified by a simple fluorescence microscopical analysis. In addition, in many organisms ClpX is involved in controlled proteolysis or at least in maintaining stability of FtsZ (Camberg et al., 2009; Dziedzic et al., 2010; Haeusser et al., 2009). Besides from the fluorescence intensity in total, the regular formation of Z-rings during cellular division could be investigated. Both FtsZ-mCherry and mCherry-FtsZ fusion proteins were investigated *in vivo* and additionally purified for potential *in vitro* testing. At 37 °C, the formation of the Z-ring was observed independent of the positioning of the mCherry-tag at the N- or C-terminal end of FtsZ (Figure 53E). A heat shock at 53 °C resulted in the dispersal of the Z ring and the localization of the fusion proteins to protein aggregates (Figure 53E).
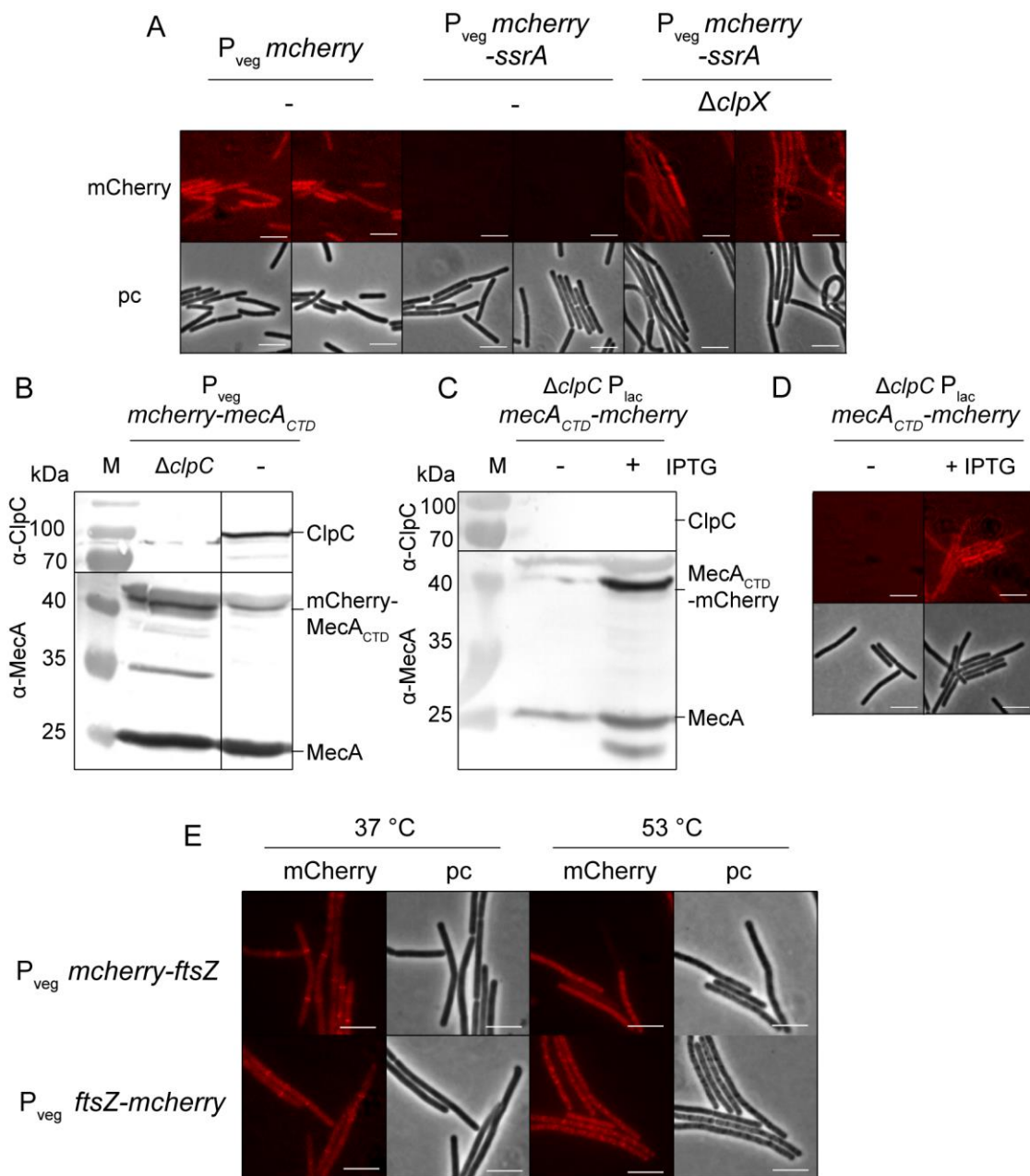
Figure 53: mCherry-ssrA is stabilized in a *clpX* mutant strain.

A) The strains P_{veg} *mcherry* (BIH239), P_{veg} *mcherry-ssrA* (BIH255) and $\Delta clpX$ P_{veg} *mcherry-ssrA* (BIH264) were grown to OD_{600} 0.5 and samples were taken for fluorescence microcopy with standard mcherry filter. Scale bar indicates 5 µm. B) Strains P_{veg} *mcherry-mecA$_{CTD}$* (BIH141) and $\Delta clpC$ P_{veg} *mcherry-mecA$_{CTD}$* (BIH133) were grown to OD_{600} 0.5 and samples were taken for α-ClpC and α-MecA western blotting (5 µg cellular extract). C) Strain $\Delta clpC$ P_{lac} *mecA$_{CTD}$-mcherry* (BIH154) were treated ± 1 mM IPTG for 1 h at OD_{600} 0.5 and samples were taken for α-ClpC and α-MecA western blotting (5 µg cellular extract) as well as fluorescence microscopy (D) with standard mcherry filter. Scale bar indicates 5 µm. E) The strains P_{veg} *mcherry-ftsZ* (BIH359) and P_{veg} *ftsZ-mcherry* (BIH360) were grown to OD_{600} 0.5 and treated with a 30 min heat shock of 53 °C. Samples were taken for fluorescence microcopy with standard mcherry filter. Scale bar indicates 5 µm.

After various potential reporter proteins have been tested and evaluated, eventually the final *Bacillus subtilis* screening strain constitutively expressed *mecA$_{CTD}$-gfp* and *mcherry-ssrA* to monitor activity of ClpC, ClpX and ClpP by measuring the levels of MecA$_{CTD}$-GFP and mCherry-ssrA, respectively (Figure 54).

Figure 54: Illustration of the established screening strain with reporter fusions and their corresponding Clp protease complexes.

A) The genes for *mecA$_{CTD}$-gfp* and *mcherry-ssrA* are under control of the constitutive promotor P$_{veg}$. Under normal conditions, both reporter protein fusions MecA$_{CTD}$-GFP and mCherry-ssrA are degraded by their corresponding protease complex ClpCP or ClpXP. No fluorescence is detectable.
B) Impaired or non-functional ClpC, ClpX and/or ClpP leads to diminished degradation and subsequent accumulation of reporter protein(s). Fluorescence can be measured.

3.3.1. Validation of the screening strain

Common targets for antibiotics are replication, transcription and translation. To exclude a false positive accumulation of a reporter fusion, e.g. due to a generally impaired translation and thus lower levels of the corresponding protease, the established screening strain had to be validated against standard antibiotics. Therefore, chloramphenicol, erythromycin, spectinomycin, kanamycin, phleomycin, ampicillin and ciprofloxacin were tested regarding their impact on the screening strain, a wildtype strain as negative control and a *gfp* expressing strain as a positive control. All compounds were tested in different concentrations ranging from 'no effect on growth' to 'substantial/complete inhibition of growth' upon addition from the beginning of the growth curve. Remarkably, none of the tested antibiotics resulted in a detectable fluorescent signal in the P_{veg} *mecA$_{CTD}$-gfp* strain at any concentration (Figure 55). Figure 55 displays two exemplary results of the two compounds erythromycin (A) and ampicillin (B) as well as a table containing the combined results of all analyzed compounds (C). As expected, the GFP signal of the positive control (P_{veg} *gfp*) was only decreased due to a general inhibition of growth at increased concentrations of antibiotics (Figure 55).
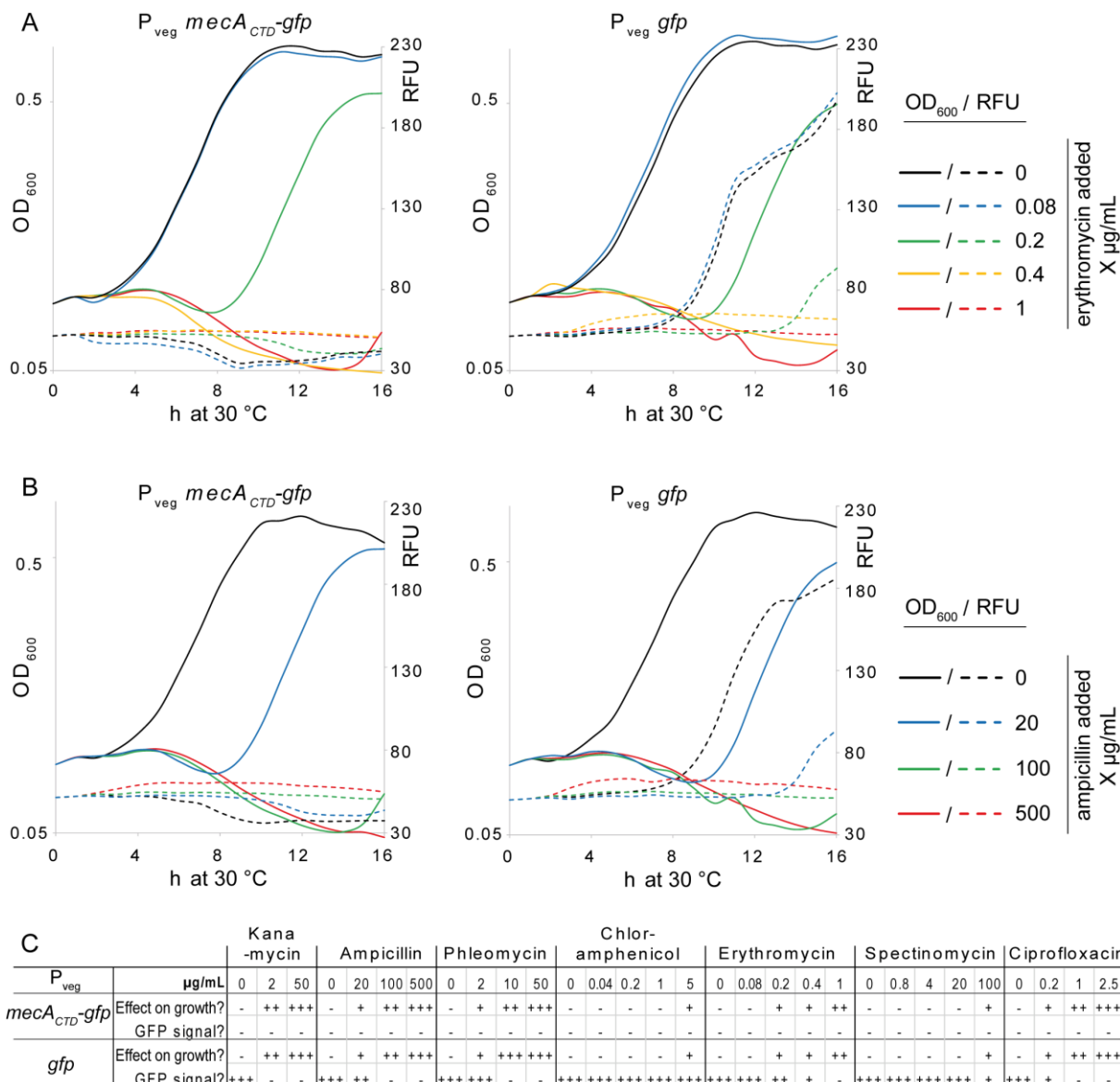
Figure 55: Selected standard antibiotics do not lead to accumulation of MecA$_{CTD}$-GFP.

Strains P$_{veg}$ *mecA$_{CTD}$-gfp* (BIH11) and P$_{veg}$ *gfp* (BIH27) were grown in SpectraMaxM3 plate reader in Belitsky minimal medium + 0.01 % yeast extract starting at OD$_{600}$ 0.1. Indicated antibiotics A) erythromycin and B) ampicillin were added to indicated final concentrations prior to incubation at 30 °C for at least 16 h. OD$_{600}$ and GFP signal (ex. 470 nm/ em. 509 nm) were continuously monitored. One representative example is shown. C) Combined results of all antibiotics tested according to procedure in A/B) and evaluated regarding effect on growth and detectable GFP signal of P$_{veg}$ *mecA$_{CTD}$-gfp* (BIH11) and P$_{veg}$ *gfp* (BIH27). Effect on growth: -: no effect, +: slightly inhibited, ++: severely impaired, +++: no growth. GFP signal: -: no detectable GFP signal, +: low GFP signal, ++: moderate GFP signal, +++: strong GFP signal.

In order to further evaluate the generated screening strain, two derivatives of the ClpC targeting cyclic peptide cyclomarin were analyzed regarding their respective impact on the reporter proteins. While cyclomarin C has a terminal double bond, cyclomarin A inherits an epoxide at that same position (Figure 56). Cyclomarin A was observed to deregulate and enhance ClpC1 activity e.g. in *M. tuberculosis*. However, *B. subtilis* was not affected, which was assumed to be predominantly based on the Tyr80 residue in ClpC (Schmitt et al., 2011; Vasudevan et al., 2013) (Figure 9). Hence, a *clpC* Y80F markerless point mutant was created in *B. subtilis* to approximate it to the *clpC1* Phe80 of *M. tuberculosis*.
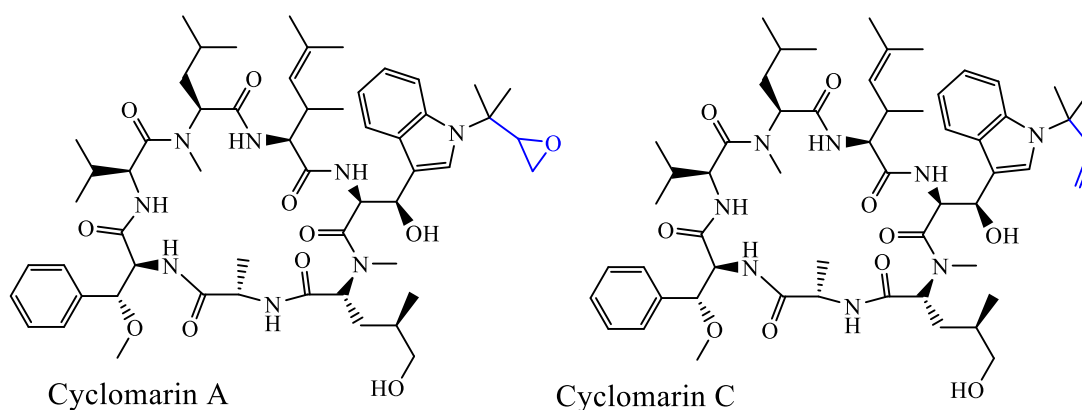
Figure 56: Structures of cyclomarin A and cyclomarin C.

Growth of *B. subtilis* was only slightly affected by elevated concentrations of cyclomarin A, whereas cyclomarin C did not lead to impaired growth (Figure 57AD). It is important to note that especially cyclomarin A itself absorbed at 600 nm, which caused problems at a final concentration of 10 µM and had to be subtracted from the total absorbance. Still, the normalization of relative fluorescence signal intensity (RFU) by optical density was error prone (Figure 57B). Therefore, as another normalization approach, the RFU of each strain was normalized by subtraction with RFU of a control strain without cyclomarin added (Figure 57C).

Only addition of 10 µM of cyclomarin A led to a minimal raise in GFP signal, corresponding to the accumulation of MecA$_{CTD}$-GFP in the screening strain P$_{veg}$ *mecA$_{CTD}$-gfp* P$_{veg}$ *mcherry-ssrA* (Figure 57C). This finding was expected as *B. subtilis* was observed to be resistant against cyclomarin (Schmitt et al., 2011). Remarkably, when the ClpC Y80F variant was introduced into the screening strain, it became more susceptible towards both cyclomarin A and cyclomarin C regarding accumulation of MecA$_{CTD}$-GFP (Figure 57CF). This effect was only observed at higher concentrations though. In addition, the measured GFP signal in the strain P$_{veg}$ *gfp*, which was used as positive control, was about 10 to 15 times higher when compared with the screening strains treated with the maximum concentration of cyclomarin A or C (10 µM) (Figure 57CFG). Although the detected amplitude in fluorescence upon cyclomarin addition was only marginal, these results still demonstrated that the established screening strain would have detected cyclomarin as a compound of interest. Even a minor raise in GFP signal indicates impaired degradation of MecA$_{CTD}$-GFP and could hint towards a promising candidate in antibiotic development.
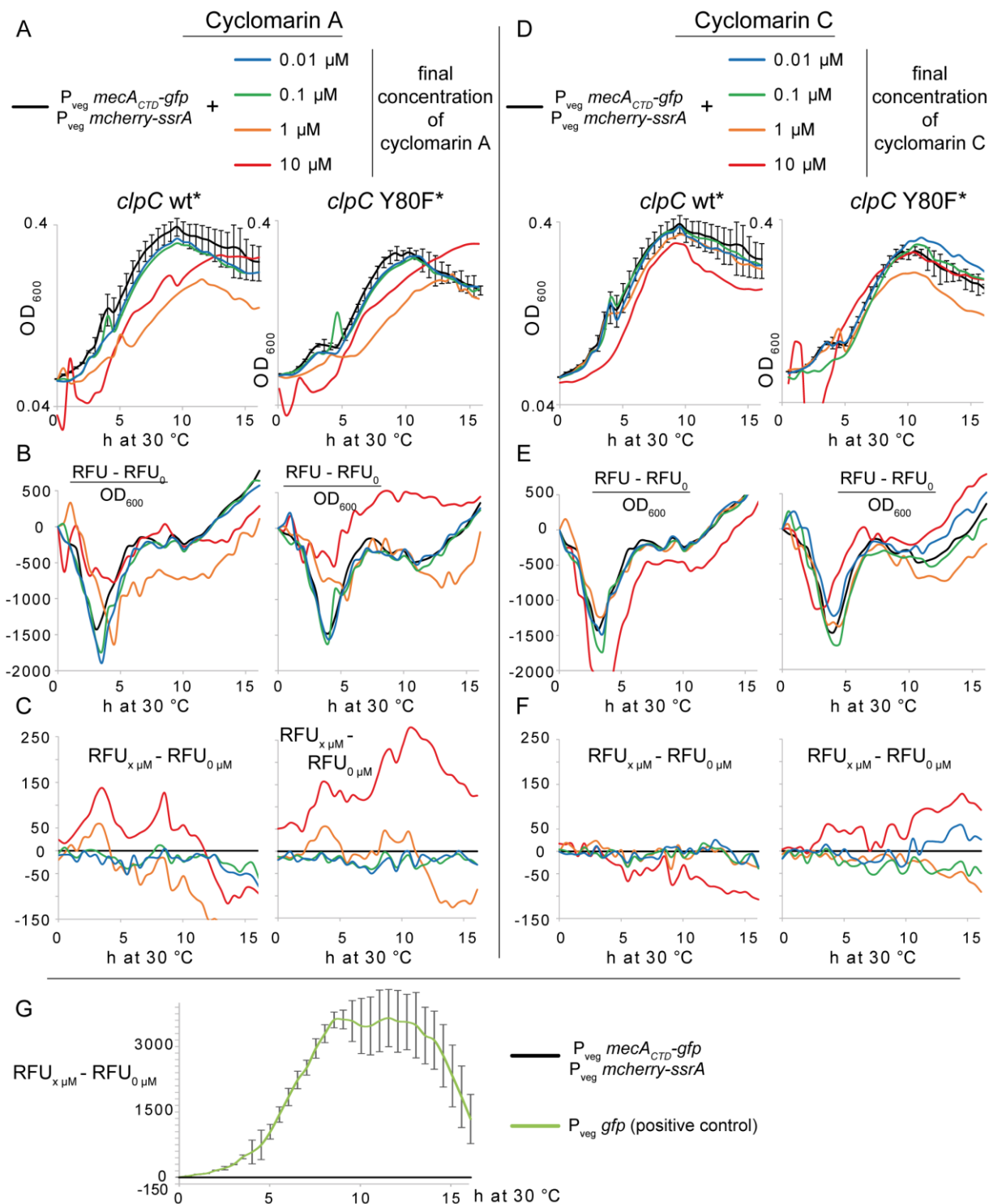
Figure 57: High concentrations of cyclomarin A or C lead to slight accumulation of MecA$_{CTD}$-GFP in *clpC* Y80F background strain.

The screening strains P$_{veg}$ *mecA$_{CTD}$-gfp* P$_{veg}$ *mcherry-ssrA* (BIH255) and *clpC* Y80F P$_{veg}$ *mecA$_{CTD}$-gfp* P$_{veg}$ *mcherry-ssrA* (BIH254) were grown in a TecanPro200 plate reader in Belitsky minimal medium + 0.01 % yeast extract starting at OD$_{600}$ 0.1. Indicated concentrations of A/B/C) cyclomarin A or D/E/F) cyclomarin C (dissolved in DMSO) were added from the beginning. Cells were grown shaking at 30 °C with OD$_{600}$, signal of

GFP (ex. 470 nm/ em. 509 nm) and mCherry (ex. 587 nm / em. 610 nm) monitored continuously. A/D) Optical density during growth in plate reader at 30 °C for at least 16 h. At 10 µM, cyclomarin *per se* absorbs light at 600 nm which was normalized by subtracting the base line signal. B/E) GFP signal was normalized by respective starting RFU and OD_{600} as indicated. C/F) RFU of control strain with no cyclomarin added was subtracted from RFU of each respective strain to illustrate positive and negative differences from baseline. G) Strain P_{veg} *gfp* (BIH27) was used as positive control for GFP signal and treated as described above (C/F). Addition of DMSO did not influence growth or GFP signal and mCherry signal was not detected under tested conditions. Unprocessed raw data were obtained by Victoria Schmitt and Dr. Jennifer Herrmann from HIPS (Helmholtz institute for pharmaceutical research).

3.3.2. Screening a myxobacterial compound library

Besides from the extensively exploited Gram-positive actinobacteria, the Gram-negative myxobacteria are among the top producers of natural products due to their rich secondary metabolism (Diez et al., 2012; Weissman and Müller, 2009; Xiao et al., 2011). As a screening strain to monitor ClpC, ClpX and ClpP activity as well as general growth of *B. subtilis* had been successfully established and validated, screening of a small myxobacterial compound library (~300 compounds) was performed during a two-week stay at the Helmholtz institute of pharmaceutical research (HIPS) in Saarbrücken in cooperation with Dr. Jennifer Herrmann.

In a first test, all 300 myxobacterial compounds were added to a final concentration of 10 µM (dissolved in DMSO) to the screening strain P_{veg} *mecA$_{CTD}$-gfp* P_{veg} *mcherry-ssrA* and its *clpC* Y80F counterpart producing the same reporter proteins. As controls, the strains P_{veg} *gfp* and P_{veg} *mcherry* as well as the wildtype strain and a DMSO sample were continuously examined. As a consequence of previous optimizations, all strains were grown shaking at 30 °C in a plate reader in Belitsky minimal medium + 0.01 % yeast extract. Many compounds were identified to inhibit growth of the screening strains, but did not lead to a raise in fluorescence. Promising compound candidates for a more detailed dose-dependent analysis are displayed in Table 8 and were chosen according to following characteristics:

- Enhanced GFP or mCherry signal in combination with impaired/inhibited growth

- Enhanced GFP or mCherry signal

- Impaired/inhibited growth while affecting either *clpC* Y80F or wildtype *clpC* strain

Table 8: Summarized results of selected compounds from screening ~300 myxobacterial compounds with strains P$_{veg}$ *mecA$_{CTD}$-gfp* P$_{veg}$ *mcherry-ssrA* ± *clpC* Y80F.

Screening and processing of obtained data were performed as described in materials and methods and Figure 57 with a final concentration of 10 µM. Model of screening strain and reporter proteins in Figure 54. OD$_{600}$/growth: ++: complete inhibition, +: growth impaired. Fluorescence signal: ++: strong signal, +: low signal 2.: 2nd dose-dependent test confirmed results (✓) or presumably false positive (X).

No.	Compound	Described activity, known target	Growth impaired?		GFP signal?		mCherry signal?		2.
			clpC	*clpC* Y80F	clpC	*clpC* Y80F	clpC	*clpC* Y80F	✓ / X
1	Carolacton	Folate-dep. C1 metabolism / FolD, anti-biofilm (Fu et al., 2017)	++	++	+	-	-	-	X
2	Myxopyronin B	RNA-Polymerase inhibitor (Belogurov et al., 2009)	++	++	+	-	-	-	✓
3	Myxopyronin A		+	+	+	+	-	-	✓
4	Saframycin Mx1 BCH	Potential anti-tumor drug (Arai et al., 1980)	+	++	-	-	+	-	X
5	Pinesin A	n.d.	+	+	-	+	-	-	n.d.
6	Disorazol A7	Microtubules polymeriz. inhibitor (Elnakady et al., 2004)	-	-	+	+	-	-	(✓)
7	Tubulysin Ar-672	Microtubules polymeriz. inhibitor (Khalil et al., 2006)	-	-	-	-	+	+	n.d.
8	Trichangion HZI	n.d.	-	-	-	-	+	-	n.d.
9	Haprolid	Cytotoxic (Steinmetz et al., 2016)	-	-	+	-	-	-	X
10	Chlorotonil	Antimalarial (Held et al., 2014)	++	-	-	-	-	-	X

n.d.: not determined.

Out of the 10 promising candidates from the pre-test (Table 8), carolacton (1), myxopyronin A & B (2/3), saframycin (4), disorazol A7 (6), haprolid (9) and chlorotonil (10) were selected for a second dose-dependent characterization.

Carolacton completely inhibited growth of the screening strains in a range of 0.125 µM – 128 µM. The lowest tested concentration of carolacton (62.5 nM) still led to substantially impaired growth. However, none of the conditions resulted in an evident raise in mCherry or GFP signal as seen in the pre-screen. In the first screen, chlorotonil failed to inhibit growth of *clpC* Y80F but completely prevented growth of the screening strain with wildtype *clpC*. In the dose-dependent test, that result could not be reproduced suggesting a pipetting error in the first assay. Haprolid and saframycin decelerated the growth of both screening strains at concentrations above 32 µM (haprolid) and 4 µM (saframycin), but did not result in a significant increase in GFP or mCherry as observed in the pre-screening.

Addition of disorazol A7 did not affect growth of *B. subtilis* but resulted in a minor raise in GFP signal during pre-testing, which was confirmed during 2nd screening (Figure 58 and Figure 59). However, the increase in GFP was not consistently dose dependent and reached only about 5 % of the positive control at concentration > 2 µM of disorazol (Figure 59B). At concentrations above 4 µM myxopyronin A, growth of *B. subtilis* was severely impaired in the screening strains. Furthermore, elevated concentrations above 32 µM led to complete inhibition. At 4 µM, the GFP signal reached ~ 20 % of the positive control suggesting an influence of myxopyronin A on accumulation of $MecA_{CTD}$-GFP in both screening strains (Figure 59C). Myxopyronin B affected the screening strains in slightly less intense manner (Table 8).

Collectively, the screening of 300 myxobacterial compounds in a pre-selection screening and 2nd dose dependent testing resulted in only two compounds (myxopyronin A and B) as potentially interesting regarding influence on ClpC activity (Figure 58 and Figure 59). Effects of other compounds that were at first glance selected for 2nd dose dependent screening could not be reproduced and were consequently evaluated as false positive results (Table 8, Figure 59 and Figure 57).
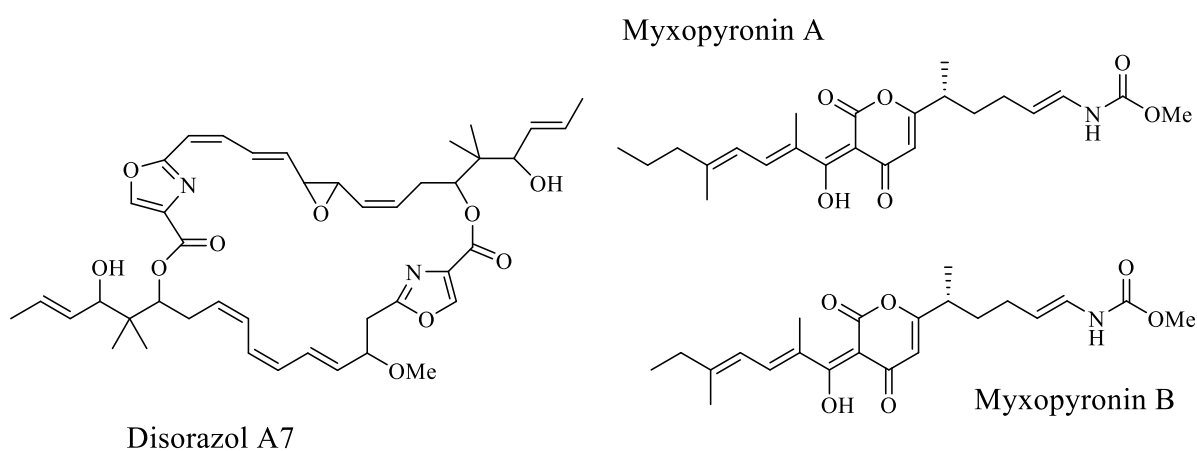
Figure 58: Structures of disorazol A7, myxopyronin A and myxopyronin B.

A

Normalization of RFU and OD_{600} to comparable RFU*: $RFU^* = \left(\dfrac{(RFU_i - RFU_{start})}{OD_i}\right)_{X\,\mu M} - \left(\dfrac{(RFU_i - RFU_{start})}{OD_i}\right)_{0\,\mu M}$

B Disorazol A7

Disorazol A7 did not affect growth of *B. subtilis* at tested concentrations

C Myxopyronin A

[X]Myxopyronin A impaired growth of *B. subtilis* at concentrations above 4 µM with complete inhibition > 32 µM
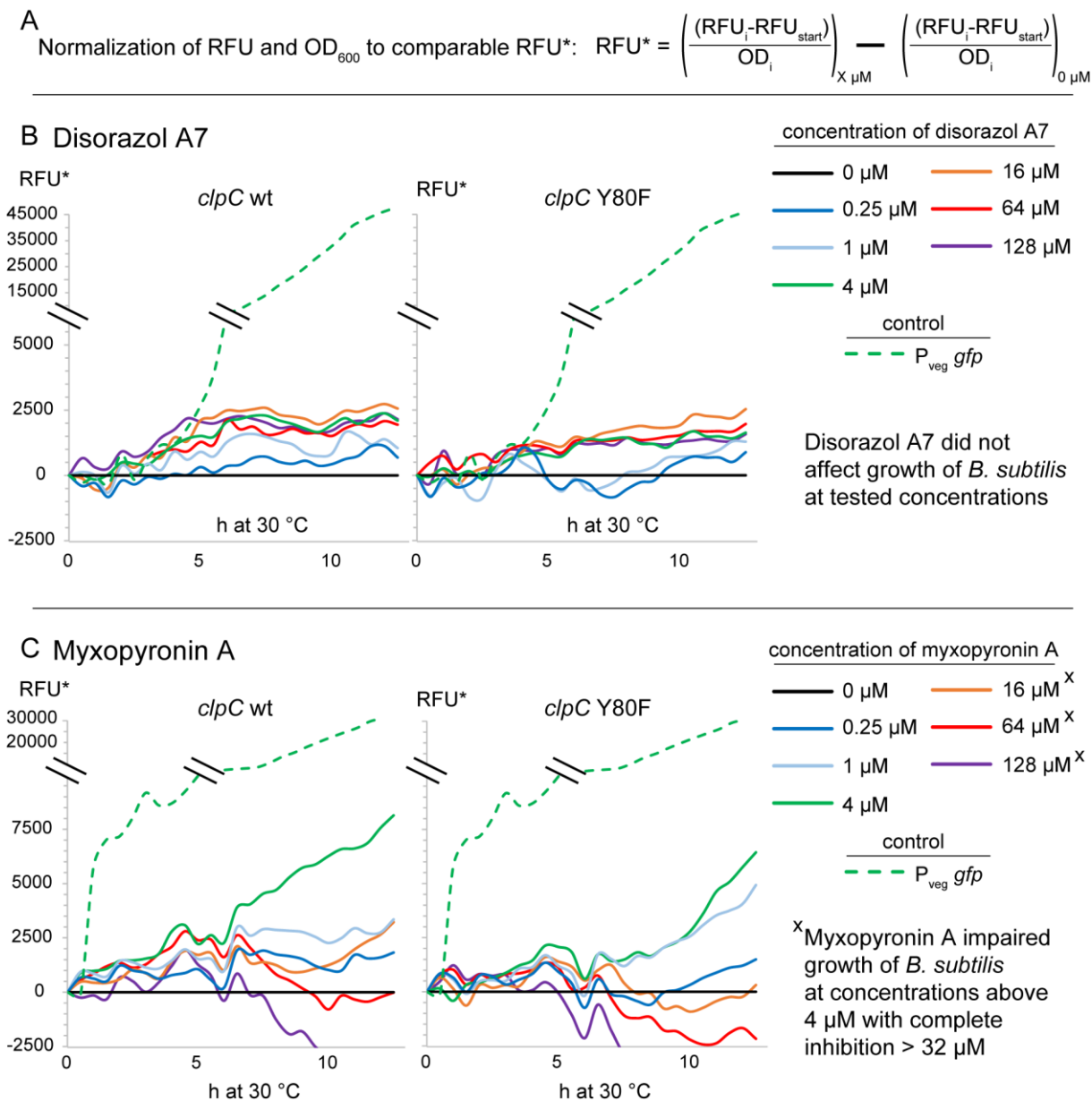
Figure 59: Dose dependent screening of disorazol A7 and myxopyronin A on P$_{veg}$ *mecA$_{CTD}$*-*gfp* P$_{veg}$ *mcherry-ssrA*.

A) Formula of normalization of relative fluorescence units (RFU) and OD_{600} to allow comparability. RFU_{start} was subtracted at each time point (RFU_i) and divided by OD_{600}. Obtained values from respective used concentrations (X µM) were further normalized with values from the samples without antibiotics added (0 µM). B/C) The screening strains P$_{veg}$ *mecA$_{CTD}$-gfp* P$_{veg}$ *mcherry-ssrA* (BIH255) and *clpC* Y80F P$_{veg}$ *mecA$_{CTD}$-gfp* P$_{veg}$ *mcherry-ssrA* (BIH254) were grown shaking at 30 °C in a TecanPro200 plate reader in Belitsky minimal medium + 0.01 % yeast extract starting at OD_{600} 0.1 with concentrations of 0.0625 – 128 µM disorazol A7 (B) and myxopyronin A (C) with only selected concentrations displayed to ensure clarity. OD_{600}, signal of GFP (ex. 470 nm/ em. 509 nm) and mCherry (ex. 587 nm / em. 610 nm) were monitored continuously. Strain P$_{veg}$ *gfp* (BIH27) was used as positive control for GFP signal. Addition of DMSO did not influence growth or GFP signal and mCherry signal was not detected under tested conditions. Unprocessed raw data were obtained by Victoria Schmitt and Dr. Jennifer Herrmann from HIPS (Helmholtz institute for pharmaceutical research).

3.3.3. The LCN-degradation tag

Besides from screening purposes, studying the MecA$_{CTD}$-GFP fusion protein in different *clpC* mutant strains gave more insight into the activation mechanism of ClpC and interaction sites with MecA (Figure 49, Figure 50, Figure 51 and Figure 52) demonstrating that studying degradational tags (degrons) with fused fluorescent proteins in different mutant strains can help to reveal their interaction partners. The sporulation factor SpoIIAB of *B. subtilis* contains a unique C-terminal LCN tag, which was shown to be essential for its degradation by ClpCP *in vivo* (Pan and Losick, 2003). Yet degradation of SpoIIAB was not achieved by ClpCP alone *in vitro* and additionally ClpC was not observed to interact with SpoIIAB in a direct manner. Both findings suggested the necessity of an adaptor protein for successful degradation of SpoIIAB by ClpCP (Pan and Losick, 2003). In order to reveal that missing adaptor protein, a strain producing the SpoIIAB specific LCN degradation on GFP was generated. In addition, a strep-tag was fused to the N-terminus of GFP-LCN to enable potential pull-down or specific interaction studies on a biotin matrix as downstream experiments.

In order to elucidate which adaptor protein was necessary for ClpCP mediated degradation of SpoIIAB, *strep-gfp*-LCN was transformed into *B. subtilis* under the control of a constitutive promotor P$_{veg}$ and investigated in a *clpC*, *mcsB*, *mecA* and/or *ypbH* deletion background. The strains were grown as established in 3.3 in a plate reader while continuously measuring optical density and fluorescence (Figure 60).
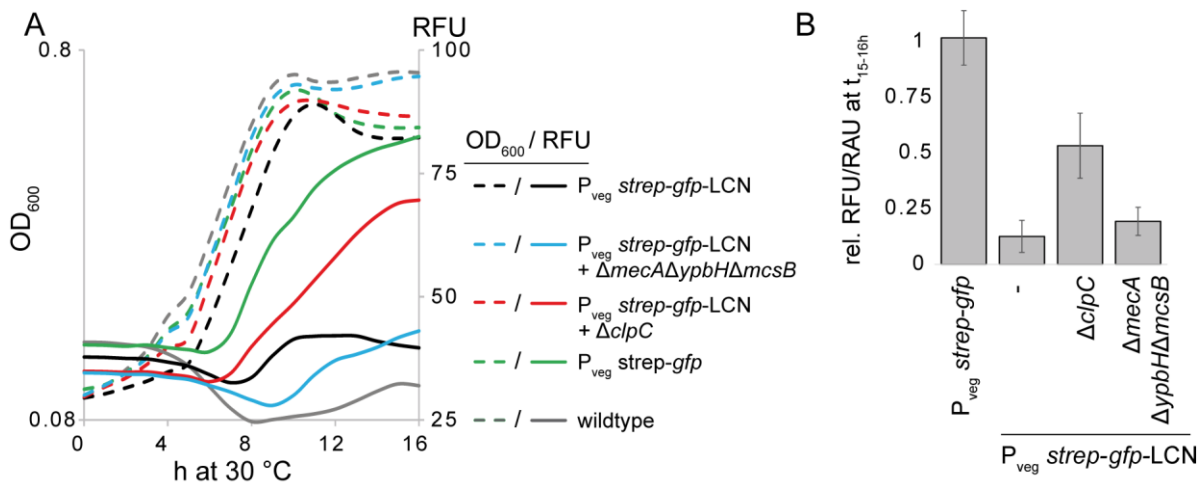
Figure 60: LCN-tagged GFP is stabilized in a Δ*clpC* mutant, but not in a Δ*mecA*Δ*mcsB*Δ*ypbH* mutant.

A) The strains P_{veg} *strep-gfp* (BIH38), P_{veg} *strep-gfp*-LCN (BIH35), Δ*clpC* P_{veg} *strep-gfp*-LCN (BIH246), Δ*mecA*Δ*mcsB*Δ*ypbH* P_{veg} *strep-gfp*-LCN (BIH39) and wildtype were grown shaking in a SpectraMax M3 plate reader in Belitsky minimal medium + 0.01 % yeast extract at 30 °C starting at OD_{600} 0.1. GFP (ex. 470 nm/ em. 509 nm) signal and optical density (600 nm) were monitored for at least 16 h with one representative example shown. B) Combined results of GFP signal intensity normalized by cellular density. Results from time point 15-16 h are displayed from at least three biological replicates. Error bars indicate standard deviation.

As expected, synthesis of Strep-GFP resulted in an increase in fluorescence during growth curve (Figure 60A). When the LCN tag was added, the fluorescence was significantly reduced to 10 % (Figure 60B). Subsequent deletion of *clpC* restored the fluorescent signal to 50 % of the positive control. However, deletion of *mecA*, *mcsB* and *ypbH* did not increase the fluorescence showing that GFP-LCN degradation by ClpCP is not dependent on one of the three known adaptor proteins (Figure 60). Additional *in vitro* experiments demonstrated that ClpC ATPase was not induced by mCherry-LCN *per se* and degradation of mCherry-LCN by ClpCP was not successful alone or in cooperation with MecA or McsB as adaptor proteins (data not shown).

Out of the three known adaptor proteins of ClpC, McsB was identified in 3.2 as the most important one regarding heat stress. However, the above results indicate the presence of a yet unknown adaptor protein for ClpCP mediated degradation of SpoIIAB.

4. Discussion

4.1.   The sHsp YocM protects B. subtilis during salt stress

Small heat shock proteins are present in all three domains of life. Although the name suggests that small *heat* shock proteins become important under heat stress conditions, sHsps have been identified to play a role in various other kinds of advers conditions such as salt and oxidative stress, and can additionally have a more specific function such as maintaining the refractive index in the eye lens (Haslbeck and Vierling, 2015; Horwitz et al., 1999).

In the Gram-positive model organism *B. subtilis*, three potential sHsp genes (*yocM*, *cotM*, *cotP*) encoding the sHsp-characteristic conserved α-crystallin domains were detected by sequence alignments (Reischl et al., 2001). More recent transcriptome studies revealed *yocM* to be generally induced by salt stress, which identified *yocM* as expressed in a substantially different way compared to the expression profiles of *cotM* and *cotP*, which were both identified to be upregulated upon sporulation conditions (Nicolas et al., 2012). However, it was not clear whether YocM is a small heat shock protein and, as such, part of the PQC system in *B. subtilis*.

The detailed analysis presented in this work demonstrated that *yocM* is upregulated upon salt shock (Figure 12). Consistently, the growth of the Δ*yocM* deletion mutant was impaired under salt shock conditions, which was not observed upon heat shock (Figure 13). Nevertheless, artificially raised levels of YocM conferred resistance towards elevated salt and heat stress conditions, indicating an underlying protective activity on protein homeostasis in general (Figure 13 and Figure 14). This generally increased resistance towards different types of stress upon heterologous and/or homologous overproduction of a sHsp has been observed

many times (Kim et al., 2013; Salas-Muñoz et al., 2012; Tian et al., 2012; Wang et al., 2017b) and is probably based on the general interaction of sHsps with substrate proteins, regardless of the origin of the potentially heterologous sHsp and the type of stress.

In comparison to *yocM*, *cotM* and *cotP* display a clear expression profile of sporulation genes and were not identified to have any impact regarding stress response (Figure 22) (Nicolas et al., 2012). Examining their evolutionary distance with a phylogenetic tree based on the amino acid sequence of the ACD domain (COG0071, EggNOG Database) also confirmed the distinct and diverse roles of the three paralogs YocM, CotM and CotP in *B. subtilis* (Huerta-Cepas et al., 2016). Remarkably, the asRNA S738 of *yocM* is also expressed under sporulation conditions and might prevent the efficient synthesis of YocM, indicating a potential evolutionary link to sporulation (Nicolas et al., 2012). Since bacteria are permanently exposed to different types of stress in their respective environments and the process of sporulation developed during evolution, it is tempting to speculate that in particular CotM and CotP evolved into sporulation specific sHsps (de Hoon et al., 2010; Paredes et al., 2005). However, one could also think of a sHsp involved in sporulation (e.g. as part of the spore coat), which evolved into a more salt specific sHsp, which could in the case of YocM derive from raised negative influence of a *cis*-acting asRNA (S738) (Nicolas et al., 2012). Nevertheless, YocM appeared to be the only sHsp that is involved in stress response of *B. subtilis*.

In general, the characteristic α-crystallin domain as well as the attenuated growth of the respective mutant strain during salt stress already indicated that YocM is a member of the sHsps that is involved in stress resistance. Furthermore, YocM displayed the typical aggregate targeting character of a sHsp. YocM as well as the YocM-mCherry fusion protein localized to

stress induced protein aggregates (Figure 16, Figure 19 and Figure 20). This characteristic feature was used to establish YocM-mCherry as a marker for subcellular protein aggregates, which enabled the visualization of protein aggregation upon different types of stress and subsequent disaggregation by the protein quality control machinery of *B. subtilis in vivo* (Figure 16, Figure 20, Figure 32, Figure 33 and Figure 61).

Previously, the *B. subtilis* malate dehydrogenase (Mdh) was fused to GFP to visualize protein aggregates upon heat shock due to unfolding and aggregation of Mdh *per se* (Runde et al., 2014). The now established YocM-mCherry aggregate marker provides various advantages compared to Mdh. A strain carrying the *mdh-gfp* fusion construct *in cis* had to be inoculated with a higher optical density to guarantee sufficient Mdh-GFP before heat treatment of the cells (Runde et al., 2014). Additionally, using YocM-mCherry is more reproducible since YocM *per se* did not aggregate upon comparable heat treatments (Figure 24), it also marks protein aggregate generated from other types of stress (while Mdh does not) (Figure 16) and synthesis of YocM-mCherry can be controlled by xylose (Figure 61).

It is important to note that fusing mCherry to YocM impaired the oligomerization abilities of YocM *in vitro*, which also diminished its protective character *in vivo* as overexpression of *yocM-mcherry*, in contrast to *yocM* alone, did not affect thermotolerance (Figure 17 and Figure 23). However, regarding the purpose of YocM-mCherry as a simple, non-invasive aggregate marker protein, this loss of function is beneficial (Figure 61).
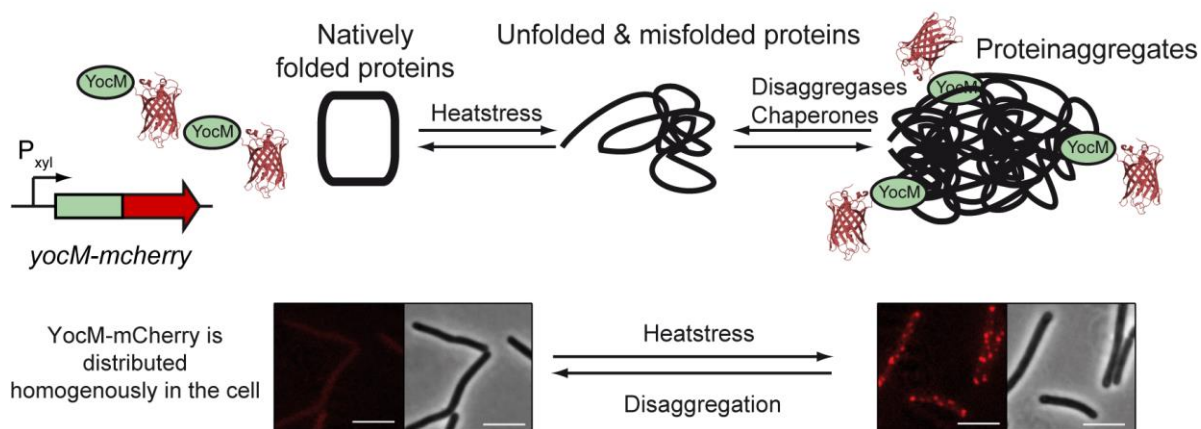
Figure 61: YocM-mCherry is a suitable marker for subcellular protein aggregates *in vivo*.

Under control of xylose inducible P_{xyl} promotor, *yocM-mcherry* is moderately expressed and YocM-mCherry is homogenously distributed in the cell. Heat stress leads to denaturation and misfolding of proteins, subsequently leading to the formation of protein aggregates, which are targeted by YocM-mCherry. Thereby, both formation and clearance of protein aggregates can be visualized by fluorescence microscopy. Representative pictures are shown.

When examined regarding protection of aggregation, YocM unexpectedly displayed an aggregation acceleration activity *in vitro* (Figure 24). Although aggregation e.g. of model substrate Mdh was accelerated at heat stress, the activity of Mdh was to certain extent protected and maintained (Figure 24 and Figure 25). These at first glance contradicting observations could be explained by specific sequestration of (partially) unfolded and misfolded protein species in a structural state where partial activity is preserved and/or spontaneous refolding is favored *in vitro*. This activity has been observed in yeast where Hsp42 displayed a similar aggregase activity with partially heat unfolded Mdh (41 °C) while still preventing aggregation at fully unfolding conditions (47 °C) (Ungelenk et al., 2016). The emerging picture of prevention of uncontrolled aggregation by specific aggregase-like sequestration of proteins that are prone to unfolding and aggregation adds new functional aspects to sHsps (Grousl et al., 2018; Ojha et al., 2011; Ungelenk et al., 2016).

Another considerable aspect is the mutual interplay of YocM with chemical chaperones. Since a) YocM contributed to salt resistance and b) salt stress leads to accumulation of

compatible solutes, GB and proline as the two major compatible solutes of *B. subtilis* were examined *in vitro* regarding their influence on YocM. Both proline and GB individually protected Mdh to certain extent regarding loss of activity upon heat treatment (Figure 25). In general, compatible solutes were observed to be able to provide thermoprotection to proteins (Bashir et al., 2014b, 2014a; Diamant et al., 2003, 2001; Holtmann and Bremer, 2004; Moses et al., 2012; Singer and Lindquist, 1998). It was observed that especially in combination with GB, the protective activities of YocM were enhanced (Figure 25). These results suggested a mutual, synergistic relationship, where the presence of chemical chaperones enhanced the protective abilities of a sHsp (and maybe vice versa). It had already been demonstrated that chemical chaperones such as GB can affect the chaperone activity of different *E. coli* chaperones such as DnaK, GroEL or ClpB *in vitro* (Diamant et al., 2001).

Furthermore, *yocM* was identified to be also upregulated upon cold shock (Nicolas et al., 2012). Remarkably, the chemical chaperone GB has been observed to be taken up by *B. subtilis* after cold stress conditions (Hoffmann and Bremer, 2011). These findings suggest that besides from their potential beneficial interplay in salt stress response, YocM could cooperate with GB also under cold stress conditions and further supports the hypothesis of a mutual relationship between a sHsp and chemical chaperones. However, since the actual experiments were performed *in vitro*, a specific interplay remains to be elucidated *in vivo*.

Apart from the potential interplay with chemical chaperones, sHsps have been observed to interact with other molecular chaperone systems, e.g. to facilitate protein disaggregation and refolding (Haslbeck and Vierling, 2015; Mogk et al., 2003a). Regarding YocM, this potential interplay with DnaK and/or ClpC was indicated when examining a Δ*dnaK*Δ*clpC*Δ*yocM* mutant strain *in vivo*, which was to certain extent more affected by heat stress when compared

to a Δ*dnaK*Δ*clpC* mutant strain (Figure 21). It had already been demonstrated that the lack of sHsps did not negatively affect the heat resistance of the cell as long as other chaperone systems such as DnaK and ClpB are still functionally present (Mogk et al., 2003a). Since YocM was identified as an aggregase-like protein, it is tempting to speculate that the specific sequestration of unfolding and misfolding proteins species facilitates active processing and refolding by other molecular chaperone systems such as ClpC and/or DnaK.

To sum up, YocM was characterized as a stress related sHsp in *B. subtilis*. Nevertheless, the experimental data suggested that its protective role is potentially limited to salt stress. Chemical chaperones such as GB accumulate upon salt stress and appeared to facilitate a synergistic effect with YocM regarding the protection of the folding state of model substrates *in vitro*. This indicated a functional relationship where uptake and synthesis of compatible solutes after salt stress provides a sHsp with an optimal environment to develop its full protective potential. This elaborated interplay adds an interesting aspect to the growing list of sHsp features and attributes.

4.1.1. The different nature of heat and salt stress

During the characterization of YocM as the first sHsp in *B. subtilis*, a YocM-mCherry aggregate marker protein was established and, among others, used to examine the different nature of salt and heat induced protein aggregates. In the respective environment, these different kinds of stress are not occurring in a strictly separate way. One example is the combination of heat and salt stress in a drought. In addition to that it was observed that in *B. subtilis* a mild salt-shock can cross-protect against a severe heat shock and vice versa, suggesting that both types of stress are connected (Völker et al., 1992). Especially plants have evolved numerous types of sHsp, which are not only expressed upon influence of a specific

stressor (e.g. heat stress), but also during multiple types of stress and during different developmental stages such as embryogenesis or pollen development (Mu et al., 2011; Muthusamy et al., 2017; Sun et al., 2002; Wehmeyer and Vierling, 2000; Zhao et al., 2018).

However, the folding stress experienced by cellular proteins is different upon heat and salt shock. Heat stress leads to unfolding and exposure of previously buried hydrophobic patches, which can interact and lead to misfolding and subsequent formation of insoluble protein aggregates. The removal of these insoluble aggregates requires functional molecular chaperones and protein disaggregases, which explains the severely impaired heat resistance when examining a Δ*clpC* and/or Δ*dnaK* mutant strain (Figure 21). The same mutant strains were not affected under salt stress conditions suggesting that both chaperone systems do not play a major role during salt stress (Figure 21). Consequently, the aggregate marker protein YocM-mCherry revealed more distinct protein aggregates after heat shock compared to a more heterogeneous distribution after salt stress (Figure 16 and Figure 20). In addition to fluorescence microscopy, protein aggregation was investigated by direct aggregate preparations. Here, the stringent washing steps during that experimental procedure guaranteed the removal of all soluble and membrane proteins and the enrichment of insoluble protein aggregates. The amount of protein aggregates obtained by aggregate preparations was substantially decreased when examining salt shocked cells in comparison to cells treated with heat stress (Figure 19). These results suggested differences in the properties of protein aggregates generated from these types of stress.

Upon a salt shock, water efflux causes a fast 2-3 fold reduction of cell size, thereby increasing the concentration of macromolecules and leading to an effect which is referred to as 'molecular crowding' (Stadmiller et al., 2017; Wang et al., 2012; Whatmore and Reed, 1990;

Zimmerman and Minton, 1993). Notably, molecular crowding was observed with ambiguous effects on protein stability. On one hand it was demonstrated that a crowded environment can enhance the stability of the native state of proteins (Cheung et al., 2005; Ebbinghaus et al., 2010; Monteith et al., 2015) while on the other hand protein-protein interactions in such an environment were identified to destabilize some model proteins (Ignatova et al., 2007; Schlesinger et al., 2011; Stadmiller et al., 2017). The complex influence of the cytoplasmic environment on protein folding and stability might therefore be more ambiguous and cannot be considered as generally favorable or unfavorable (Danielsson et al., 2015; Sarkar et al., 2013). Nevertheless, since smaller amounts of protein aggregates were formed after an osmotic shock (Figure 19), a fast reduction of cell size and simultaneous increase in molecular crowding appears to at least partially destabilize the overall folding state of the proteome (Stadmiller et al., 2017).

However, destabilization of proteins upon an osmotic upshift presumably also resulted from a change in turgor pressure and increased amounts of potassium ions. It was observed that an osmotic upshift leads to a decrease in turgor pressure in *B. subtilis* (Whatmore and Reed, 1990). The turgor pressure sustains the structural integrity of each cell by pressing the membrane to the cell wall and is thereby thought to drive growth in general (Cayley et al., 2000; Geitmann and Ortega, 2009). In order to prevent extensive water efflux and recover turgor pressure, K^+ are taken up as a first response to salt stress, albeit theses ions can also interfere with ionic inter- and intramolecular protein interactions (Hoffmann and Bremer, 2016; Höper et al., 2006; Whatmore and Reed, 1990). A moderate salt shock of 0.4 M NaCl led to an increase in K^+ levels up to 0.7 M within 1 h (Whatmore et al., 1990). Thus, it is questionable whether an intracellular protein would ever be in contact with substantially even

higher amounts of Na^+ and/or K^+. Nevertheless, the treatment of Mdh with NaCl (up to 6 M) decreased and subsequently abolished its enzyme activity (Figure 28) in a manner where it was presumably still at least partially folded, since the dilution into physiological buffer immediately restored full activity without an observable refolding process as seen with chemically denatured Mdh (Figure 27 and Figure 28). This suggested that only the dimerization of Mdh was impaired while the monomeric tertiary structure was still intact. However, one should keep in mind that these experiments were performed *in vitro* and do not take into account the combined effect of elevated salt concentrations, increased macromolecular crowding and reduced turgor pressure upon osmotic upshift *in vivo* (Cayley et al., 2000; Stadmiller et al., 2017; Whatmore and Reed, 1990).

It was further speculated that an osmotic upshift predominantly affects intermolecular protein interactions (e.g. Mdh dimerization), structurally sensitive proteins and in particular nascent peptide chains, which do not have correctly folded yet. To this end, chloramphenicol was used in order to arrest translation and reduce the apparent numbers of nascent chains before treatment with a salt shock. Remarkably, the significantly reduced formation of protein aggregates after salt stress was observed in cells pre-treated with chloramphenicol (Figure 20). As this was not observed during heat shock, one could speculate that heat stress affected all proteins in the cell while salt stress might be considered less severe regarding protein unfolding, potentially affecting in particular structurally sensitive proteins.

As a long term response during salt stress, compatible solutes are accumulated by synthesis or uptake (Kempf and Bremer, 1998; Roberts, 2005). They are thought to shield the protein surface and prevent aggregation by maintaining their hydration state without affecting cellular functions even at substantially high compatible solute concentrations (Arakawa and

Timasheff, 1985; Bourot et al., 2000; Cayley et al., 1992; Stadmiller et al., 2017). Since these compatible solutes protect protein activity in general, it is not surprising that they have been observed to provide a protective effect to native protein folding states during heat stress as well (Figure 25) (Bashir et al., 2014b; Holtmann and Bremer, 2004; Santoro et al., 1992).

Taken together, although salt and heat stress can be connected in the respective environment, they cause different types of protein unfolding stress. Heat stress leads to the formation of insoluble protein aggregates due to interaction of exposed hydrophobic patches. The experimental data suggests that salt stress can impair protein-protein interactions without unfolding of the protein, especially affecting nascent peptide chains at the ribosome and presumably structurally very sensitive proteins (Figure 19, Figure 20 and Figure 21). This appears to result in the formation of less and possibly more loose protein aggregates (Figure 16 and Figure 20), which do not require (and are maybe not even recognized by) protein disaggregation and degradation machineries (Figure 21). This could explain why a sHsp such as YocM and compatible solutes in general are more capable of counteracting the effects of salt stress, stabilizing protein structures in general by providing a more amenable environment upon an osmotic upshift (Kempf and Bremer, 1998; Stadmiller et al., 2017).

In the future, analyzing the specific composition of salt and heat stress generated protein aggregates by mass spectrometry could help to gain further evidence regarding the different behavior of proteins towards either type of stress.

4.2. *McsB is the main adaptor for ClpC mediated disaggregation*

The various systems of protein quality control mechanisms form a broad network to repair or remove misfolded proteins. AAA+ protease complexes and disaggregases are key players

within these systems to remove potentially toxic insoluble protein aggregates (Sauer and Baker, 2011). These large machineries need to be tightly controlled as malfunction could severely affect the viability of the cell (Carroni et al., 2017). This is true for their activity and in particular regarding their substrate recognition, which can be enabled by adaptor proteins or other chaperone systems (Haslberger et al., 2007; Kirstein et al., 2009b; Seyffer et al., 2012).

In *B. subtilis* both activity and substrate recognition of Hsp100/Clp proteins is modulated by their respective adaptor proteins. There are three adaptor proteins known for *B. subtilis* ClpC: MecA, McsB and YpbH. All of them have been identified to play different roles in regulatory proteolytic networks including ClpCP as the central protease (Elsholz et al., 2010, 2011a; Fuhrmann et al., 2009; Persuh et al., 2002; Schlothauer et al., 2003; Turgay et al., 1998). However, apart from degradation of specific substrate proteins in regulatory proteolysis, it has not been investigated whether one of them is in particular responsible for general protein homeostasis by facilitating ClpCP dependent unfolding and/or degradation of unspecific unfolded and misfolded proteins e.g. after a heat shock.

To this end, the different adaptor proteins MecA, YpbH and McsB had to be investigated regarding their respective roles in protein homeostasis after heat shock *in vivo*. Translational levels of McsB indicated a clear heat stress related profile, which was not observed for MecA and YpbH (Figure 30). Furthermore, although *mecA* and *ypbH* were identified as part of the Spx Regulon, which links them to the oxidative and heat stress response, only elevated levels of McsB resulted in the functional complementation of a thermotolerance deficient triple adaptor mutant strain Δ*ypbH*Δ*mecA*Δ*mcsB* (Figure 31) (Nakano et al., 2002; Persuh et al., 2002; Rochat et al., 2012; Runde et al., 2014). Consistently, using the previously established

aggregate marker protein fusion YocM-mCherry, it was observed that again only McsB facilitated the clearance of heat induced protein aggregates during recovery at 37 °C, which was dependent on active ClpC (Figure 31, Figure 32 and Figure 43C). It is important to mention that in previous studies MecA had been observed to disaggregate and refold the model substrate Mdh *in vitro*, albeit a Δ*mecA* mutant was not identified as thermosensitive (Schlothauer et al., 2003). The presumably less important role of MecA regarding heat stress *in vivo* was confirmed (Figure 30 and Figure 31) (Schlothauer et al., 2003).

Furthermore, it should be kept in mind that there are presumably more adaptor proteins of ClpC existent in *B. subtilis*. The degradation of LCN-tagged GFP (degron of the sporulation factor SpoIIAB) by ClpCP was observed to be independent of the three known adaptor proteins *in vivo* indicating the presence of an unknown adaptor protein for ClpC (Figure 60) (Pan and Losick, 2003). A potential novel adaptor protein of ClpC called 'MicA' was characterized to be relevant under sporulation conditions and toxic upon overexpression during vegetative growth (cooperation with Dr. Amy Hitchcock Camp, Mt. Holyoke College, unpublished). Moreover, a phage-encoded protein GP53, which is produced during infection of *B. subtilis* with phage SPO1, was identified to stimulate ClpC ATPase activity *in vitro* and promoted cell death when *gp53* was expressed in *B. subtilis* (Mulvenna et al., 2019) (cooperation with Prof. Ramesh Wigneshweraraj and Nancy Mulvenna, Imperial College London). These observations underline the yet not fully explored spectrum of ClpC modulating (adaptor) proteins for *B. subtilis*.

In contrast to the paralogs YpbH and MecA, McsB is a protein arginine kinase (Fuhrmann et al., 2009). As a) McsB had already been identified to target the transcriptional repressor CtsR for degradation by ClpCP in the regulation of the heat shock response and b) it was exhibited

in this work that McsB is the main adaptor protein to maintain protein homeostasis and remove protein aggregates after e.g. heat stress, it was intended to separately assess its arginine kinase activity and its role as an adaptor protein.

The aggregate targeting character of McsB was identified to be unaffected in the kinase inactive McsB C167S variant, suggesting that the roles as an arginine kinase and an adaptor protein are at least partially independent (Figure 32). On the other hand, a thermotolerance assay demonstrated that a kinase-inactive *mcsB* C167S mutant and a complete Δ*mcsB* mutant were comparably impaired when treated with a severe heat shock (regardless of a prior pre shock) (Figure 35). Furthermore, when comparing aggregate clearance in *mcsB* and kinase inactive *mcsB* C167S mutant strains, the *mcsB* C167S mutant exhibited a reduced aggregate clearance activity of about 10 % compared to active McsB (Figure 33). That observation was supported by the fact that kinase inactive McsB was observed to be still able to repress CtsR-DNA interactions by binding to CtsR (Elsholz et al., 2011a; Kirstein et al., 2005). Preventing the interaction of CtsR with the DNA binding sites in the class III heat shock genes results in their subsequent upregulation and thus could explain the slightly enhanced aggregate clearance (Figure 7 and Figure 33). Nevertheless, the arginine kinase activity of McsB was identified as crucial regarding its protective roles to maintain protein homeostasis after heat shock, e.g. by facilitating the removal of protein aggregates by ClpC and/or ClpCP.

Remarkably, arginine phosphorylation sites of McsB have been identified proteome-wide in *B. subtilis*, severely affecting gene expression in various developmental pathways and regulatory networks (Elsholz et al., 2012; Schmidt et al., 2014; Trentini et al., 2016), suggesting a broad and unspecific substrate spectrum of McsB. Therefore, it is obviously

difficult to strictly distinguish between the nature of McsB as an adaptor protein and an arginine kinase.

Theoretically, substrates could be bound by McsB *per se* and by McsB in a phosphorylated state, as seen for CtsR, albeit their interaction was increased when McsB was phosphorylated (Elsholz et al., 2010; Kirstein et al., 2005). However, since both kinase inactive and active McsB variants were observed to target protein aggregates, the recognition of substrate proteins is presumably independent of its arginine kinase activity (Figure 32). Furthermore, substrates could be phosphorylated at arginine residues and simultaneously need McsB to be targeted to ClpCP. A variant of CtsR lacking all arginine residues was still targeted by kinase active McsB for ClpCP dependent degradation (Elsholz et al., 2010). Moreover, substrates could be phosphorylated at arginines without the need of McsB for the targeting to ClpC (Elsholz et al., 2010, 2011a, 2012; Trentini et al., 2016). As a model substrate, the degradation of arginine phosphorylated β-casein by ClpCP was observed in the absence of McsB *in vitro* and was abolished in the presence of the phosphatase YwlE (Kirstein et al., 2007; Trentini et al., 2016). However, one should keep in mind that on one hand β-casein represents a special fully unfolded model substrate which might not require an adaptor protein like McsB for recognition by the ClpCP complex and on the other hand it was demonstrated that the degradation of CtsR is dependent on the presence of McsB (Elsholz et al., 2010).

One explanation of these at first glance contradicting results could be the special role of CtsR as a specific regulator of heat stress response, thus presumably being a special substrate for McsB and ClpCP. It was observed that the C-terminal domain of CtsR and McsB share structural similarities regarding a pArg binding motif (Suskiewicz et al., 2019), further supporting this hypothesis. Since CtsR degradation by ClpCP relies on the additional presence

of phosphorylated and active McsB, this interplay could guarantee the degradation of CtsR in order to prevent accumulation and maintain the regulatory negative feedback loop in heat stress response (Derré et al., 1999; Elsholz et al., 2010; Fuhrmann et al., 2009). These observations suggest a different role of arginine phosphorylation by McsB as part of general stress response (e.g. targeting and removal of unspecific protein aggregates) and in regulatory proteolysis of CtsR to control the heat stress response.

4.2.1. The dual role of arginine phosphorylation in disaggregation

The exact role of McsB dependent phosphorylation of arginine residues regarding targeting of substrates to ClpCP is still not clear. Nevertheless, phosphorylation of arginine residues *per se* has a major impact on proteins. It changes a positive into a negative charge, while phosphorylation of serine or threonine just adds one negative charge. This obviously affects protein stability and protein-protein interactions. In addition to that it was demonstrated that raised negative charges increased solubility of overproduced proteins, whereas insolubility was often associated with positively charged patches (Chan et al., 2013). This could hint towards a stabilizing and thus beneficial effect of protein arginine phosphorylation regarding heat stress in general, although substantially affecting the physiology of the respective protein. Supporting this hypothesis, arginine phosphorylated proteins were identified to be enriched in protein aggregates after heat stress and 25 % of the proteins degraded by ClpP were substrates of arginine phosphorylation by McsB (Trentini et al., 2016).

It is important to note that compared to e.g. phosphoester bonds, phosphoramidate bonds like pArg are thermodynamically unfavored and therefore transient, especially in the additional presence of the respective phosphatase. Thus, detection of arginine phosphorylation sites in the proteome of *B. subtilis* was only possible in either a *ywlE* mutant strain or in the presence

of a specific inhibitor (Elsholz et al., 2012; Schmidt et al., 2014). YwlE dephosphorylates McsB and its substrates, consequently counteracting McsB activity (Elsholz et al., 2011a; Hahn et al., 2009; Kirstein et al., 2005). Moreover, McsB can be inhibited by binding to ClpC (Elsholz et al., 2011a; Kirstein et al., 2005). A double deletion mutant of *clpC* and *ywlE* displayed a severely impaired growth in *B. subtilis*, which was restored by additionally deleting *mcsB* or abolishing its kinase activity (*mcsB* C167S) (Elsholz et al., 2011a). These observations suggested that although the lack of McsB impaired aggregate clearance, thermoresistance and thermotolerance (Figure 31, Figure 32 and Figure 33), a non-restricted, hyperactive McsB (e.g. due to lack of *ywlE*) could also perturb the viability of the cell.

In order to characterize this apparent balance between positive and negative effects of active McsB, its counterpart YwlE was examined in a dose dependent way. When *ywlE* was deleted, aggregate clearance during recovery from heat shock was significantly increased (Figure 34A). When examining a kinase inactive McsB (C167S) or a YwlE protein lacking its phosphatase ability (C7S) on the other hand, aggregate clearance was no longer accelerated, suggesting that enhanced aggregate clearance resulted from less restricted activity of McsB (Figure 34A). Accordingly, overexpression of *ywlE* led to substantially raised aggregate formation upon thermotolerance conditions in a dose dependent way (Figure 34B).

However, when the same strains were examined in a survival assay, both deletion and overexpression of *ywlE* led to severely impaired thermoresistance and thermotolerance (Figure 35). The leakiness of the P$_{lac}$ promoter appeared to be sufficient to complement a *ywlE* deletion in a Δ*ywlE* P$_{lac}$ *ywlE* strain. Extrapolation of quantitative western blotting pointed towards less than 135 molecules YwlE per cell (Figure 36), suggesting that low amounts of catalytically active YwlE are sufficient to keep McsB in an optimal state where

adequate activation is guaranteed, but hyperactivation and subsequent overphosphorylation of the proteome is prevented. Deletion of *ywlE* would lead to enhanced arginine kinase activity of McsB which would result in accelerated clearance of aggregates (Figure 62), which at first glance is beneficial for the survival of the cell. However, there are presumably also negative effects of uncontrolled arginine phosphorylation, since arginine phosphorylation sites have been observed to occur in a Δ*ywlE* mutant strain in the whole *B. subtilis* proteome (Elsholz et al., 2012).

Furthermore, the absence of YwlE might also be detrimental in the refolding process of substrates after disaggregation by ClpC. After translocation of an arginine phosphorylated peptide chain through the ClpC barrel, the arginine residues of the now unfolded protein presumably remain phosphorylated. Although these phosphorylated arginine residues potentially stabilized the unfolded state preventing re-aggregation to a certain extent, they could concurrently prevent refolding of the unfolded substrate into the native structure (Figure 62). Hence, in addition to unspecific and uncontrolled hydrolysis of the pArg bond, refolding could be induced by the phosphatase YwlE (Figure 62). This effect has already been observed *in vitro* where refolding of unfolded substrates after disaggregation was substantially improved when YwlE was added only in low amounts (unpublished results, Regina Kramer).

On the contrary, elevated levels of YwlE keep McsB in a restricted state where phosphorylation of its substrates and McsB itself is diminished. Since McsB is permanently dephosphorylated, CtsR cannot be targeted by McsB for ClpCP degradation (Elsholz et al., 2010; Kirstein et al., 2005). However, it was demonstrated that a strict degradation of CtsR is not essential in order to de-repress the heat shock response of *B. subtilis*, since CtsR possesses a glycine-rich loop, which can act as a molecular thermometer *per se*, abolishing CtsR-DNA

interactions upon heat treatment and resulting in de-repression of its target genes (Elsholz et al., 2010). More importantly, it was demonstrated that a mutated variant of ClpC with a decreased ability to bind pArg residues resulted in impaired survival during heat stress (Trentini et al., 2016). Assuming that arginine phosphorylation is an important signal for ClpCP dependent targeting of substrates, overexpression of *ywlE* would prevent functional targeting of unfolded and/or aggregated proteins and thus explain why protein aggregate clearance after heat shock was substantially impaired (Figure 33).

These hypotheses could explain the impaired viability of the cells regarding heat stress due to both deletion and overexpression of *ywlE* and underline the importance of a strict regulation of the arginine kinase activity of McsB in general (Figure 35 and Figure 62).
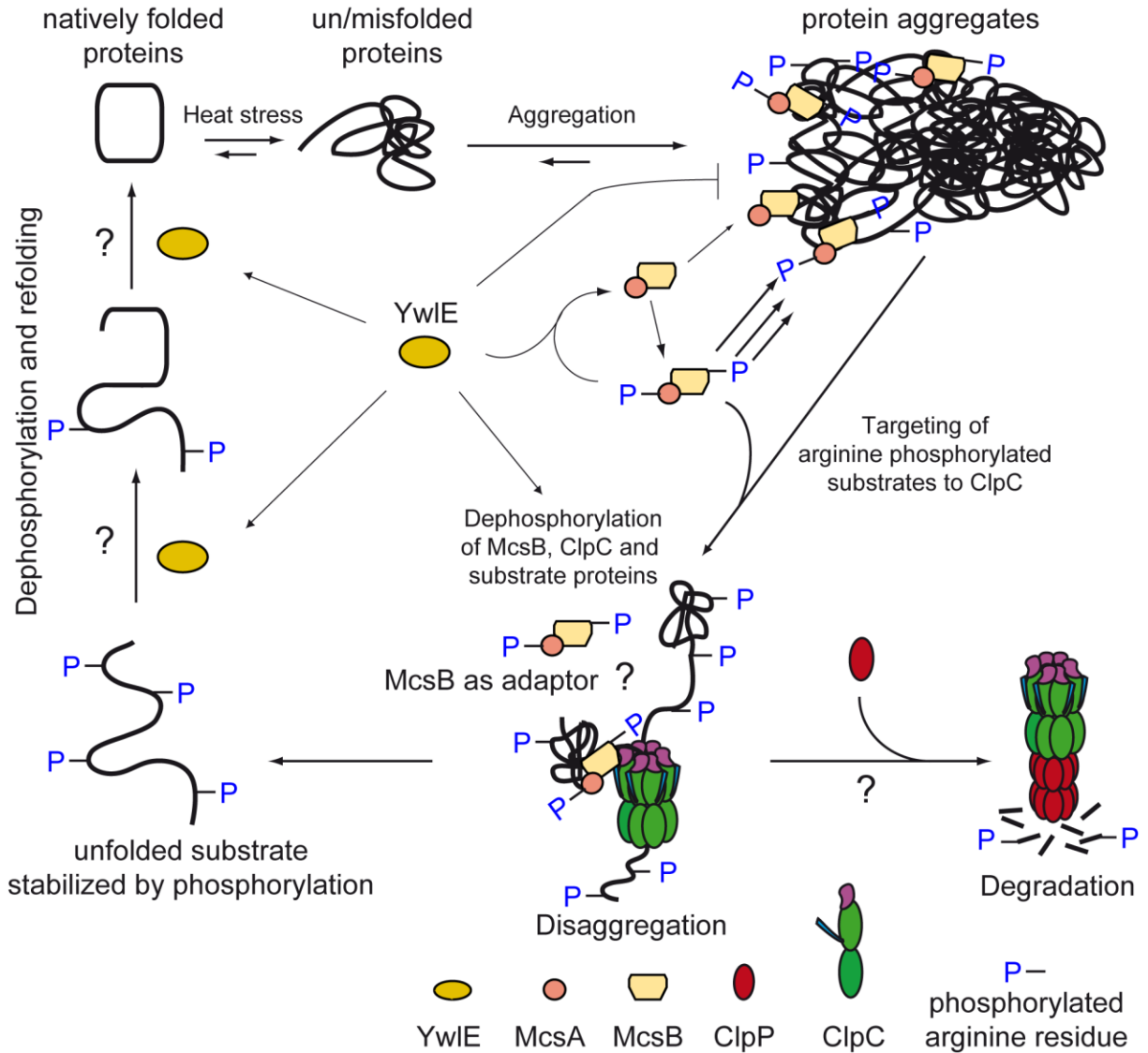
Figure 62: Simplified model of the impact of McsB arginine kinase activity and YwlE dephosphorylation events on protein disaggregation and refolding.

Native proteins can unfold due to heat stress and subsequently form insoluble potential toxic aggregates. Heat stress leads to activation of McsB by its activator McsA and autophosphorylation (Figure 7). While not activated McsB possesses a low aggregate targeting character, active McsB strongly targets and phosphorylates protein aggregates potentially improving its solubility in general and facilitating disaggregation by ClpC or degradation by ClpCP. Thereby it remains elusive whether McsB is, besides from its arginine kinase activity, essential as an adaptor protein (as proven for CtsR, Figure 7). The phosphatase YwlE dephosphorylates all phosphorylated arginine residues on proteins, including ClpC and McsB. Hence, elevated amounts of YwlE inhibit the activity of McsB due to dephosphorylation of McsB *per se*. However, dephosphorylation of unfolded and still arginine phosphorylated proteins by YwlE is presumably important to trigger refolding events due to reversion of charge. Additionally it is still unclear whether arginine phosphorylation is involved in determining the fate of a substrate protein regarding unfolding by ClpC or degradation by ClpCP.

One should keep in mind that some close relatives of *B. subtilis* lack McsB. Since CtsR was observed to be present regardless of the absence of McsB, it is assumed that ClpE inactivates CtsR in these strains (Elsholz et al., 2010). During disulfide stress, CtsR is also inactivated in *B. subtilis* without the need of kinase active McsB (Elsholz et al., 2011b). In addition, overexpression of *clpE* (from *Lactobacillus lactis*, lacking *mcsAB*) resulted in inactivation of CtsR upon oxidative stress (Elsholz et al., 2011b). These observations suggest differently evolved ClpE species, which sense oxidative stress by its zinc finger binding domain when McsAB is not present (Figure 6) (Elsholz et al., 2011b, 2010). Although protein arginine phosphorylation appears to have a major impact e.g. on removal of protein aggregates upon heat stress in *B. subtilis*, this protein modification system to sense proteotoxic stress and maintain protein homeostasis might therefore not be ubiquitously distributed.

4.2.2. ClpC is the major disaggregase in *B. subtilis*

While most organism possess stand-alone disaggregases such as ClpB in *E. coli* or Hsp104 in yeast, which are incapable of forming a functional proteolytic complex by association with a protease, *B. subtilis* lacks such a dedicated player (Molière and Turgay, 2013; Tessarz et al., 2008; Weibezahn et al., 2004). However, the stand-alone disaggregases ClpB or Hsp104 still needs to interact with other chaperone systems (DnaK/DnaJ/GrpE) to facilitate protein disaggregation and subsequent refolding (Mogk et al., 2015, 2003a; Seyffer et al., 2012; Zolkiewski, 1999). This interplay of ClpC with the DnaK system has not been observed in *B. subtilis*. It is important to note that the protein quality control system of *B. subtilis* diverges in various other aspects, e.g. in the control of *dnaK* and *groEL* transcription, from the *E. coli* system (Mogk et al., 1997). The *dnaK* mutant strain displays a moderate phenotype in *B. subtilis* while it is substantially involved in modulating *E. coli* heat shock response (Straus

et al., 1990). Nevertheless, all the highly conserved Hsp60, Hsp70, Hsp90 and Hsp100 homologs as well as the ribosome associated chaperone trigger factor and many other redox chaperones are present in both organisms (Elsholz et al., 2017; Kirstein et al., 2009b; Moliere and Turgay, 2009; Turgay, 2017).

The AAA+ unfoldase ClpC of *B. subtilis*, which is structurally similar to ClpB (Figure 6), possesses a peptide binding loop for interaction with the protease ClpP (Kirstein et al., 2009b). These observations raised the question whether especially ClpC as a key player in protein quality control would have a role besides its unfoldase activity in the proteolytic ClpCP complex as a stand-alone disaggregase, and if so, how this switch from disaggregation towards degradation is controlled and regulated.

To address these questions, it was examined whether unfolding of substrate proteins by ClpC without subsequent degradation by an associated ClpP protease was a) possible and b) physiologically relevant *in vivo*. To this end, the wildtype strain was compared to a strain, where the association of ClpC and ClpP was prevented by a mutated ClpC VGF tripeptide sequence (*clpC* VGF::GGR) (Kim et al., 2001; Moliere, 2012). Both strains were compared to either a full *clpC* deletion or a strain carrying an ATPase inactive *clpC* variant (DWB). Remarkably, the prevention of the association of ClpC and ClpP did not negatively affect thermoresistance, thermotolerance development, aggregate formation and McsB mediated aggregate clearance while a Δ*clpC* mutant and a *clpC* DWB strain were always at least partially impaired (Figure 42 and Figure 43). These results demonstrated that the absence of ClpCP dependent protein degradation was not detrimental under tested conditions. Hence, protein disaggregation appeared to be more important than protein degradation during general stress response. Nevertheless one should keep in mind that concerning specific developmental

pathways, unfolding of a substrate by ClpC is not sufficient and degradation by ClpCP is crucial. During the positive autoregulatory feedback loop in competence development of *B. subtilis* (see 1.4.3), the number of ComK molecules is substantially increasing (Persuh et al., 1999; Turgay et al., 1998, 1997). Degradation by MecA and ClpCP is essential to remove the elevated levels of ComK during the escape of the competent state (Turgay et al., 1998). However, regarding general proteolysis and protein homeostasis, protein disaggregation obviously saves cellular resources since the peptide chain may refold and does not require re-synthesis. These results suggested that degradation of misfolded substrates in general proteolysis could be favored when disaggregation and refolding is not possible due to e.g. damaged proteins or broken peptide chains.

In order to assess this hypothesis, puromycin was used to generate fragmentary protein species by inducing premature chain termination during protein synthesis, which subsequently misfold and generate protein aggregates (Figure 44). Thus, these aggregates had to be degraded as disaggregation and refolding was not possible. As expected, when the association of ClpC and ClpP was abolished, the clearance of protein aggregates was significantly decelerated compared to wildtype (Figure 44). Furthermore, when *mcsB* was expressed, the degradation of puromycin based aggregates was substantially accelerated. These observations additionally demonstrated that McsB is able to target protein aggregates for disaggregation or degradation (Figure 32, Figure 33, Figure 44 and Figure 62).

Taken together, protein disaggregation by ClpC was observed to be a major protective process regarding stress response of *B. subtilis*, unless refolding of the respective proteins was not possible. Nevertheless one has to keep in mind that protein degradation by ClpCP is important in regulatory proteolysis, where specific substrates, such as the transcription factor ComK in

competence development, have to be removed to close the feedback loop and prevent uncontrolled accumulation of ComK (Persuh et al., 1999; Turgay et al., 1998, 1997).

Taken together, the presented results imply a functional switch between ClpC and ClpCP where ClpP might not be generally attached to ClpC, although the numbers of ClpP tetradecamers are sufficient to occupy all corresponding unfoldases (Gerth et al., 2004). Remarkably, arginine phosphorylation sites have been detected in ClpP (Elsholz et al., 2012; Schmidt et al., 2014). As McsB was identified to be the essential adaptor protein for ClpC, regardless of association with ClpP, arginine phosphorylation could be involved in the switch between disaggregation and degradation.

Nevertheless, ClpC was identified as the main disaggregase in protein quality control of *B. subtilis* with the ability of attach to the ClpP protease complex, if necessary.

4.2.3. ClpC F436A causes protein aggregation and cellular death

Recently, the structure of a distinct and unique decameric state of ClpC$_{S.a.}$ formed by head to head interactions of the linker domains (MD) was solved for *S. aureus* (Carroni et al., 2017). While the formation of this complex was abolished when a F436A amino acid exchange was introduced at the tip of the linker domain, ClpC$_{S.a.}$ F436A concurrently displayed enhanced ATPase activity and FITC-casein degradation without the need of adaptor proteins *in vitro* (Carroni et al., 2017). Lack of the M-domain or suppression of resting state formation by F436A resulted in severely impaired survival *in vivo* (Carroni et al., 2017). Although such a decameric state has not been observed for *B. subtilis* ClpC$_{B.s.}$, an analogous ClpC$_{B.s.}$ F436A mutant was investigated in *B. subtilis* to examine the impact of this amino acid exchange on

its activity and to elucidate whether it is a conserved mechanism of Hsp100/Clp proteins or specific to *S. aureus*.

As observed for *S. aureus*, expression of *clpC* F436A led to cellular death in *B. subtilis* (Figure 37). Simultaneously, using the established YocM-mCherry aggregate marker protein, the severe formation of protein aggregates was observed upon expression of *clpC* F436A (Figure 16 and Figure 37). Remarkably, the toxicity of ClpC$_{S.a.}$ F436A was further enhanced in *S. aureus* when the N-terminal domain was deleted (Carroni et al., 2017). However, production of a ClpC$_{B.s.}$ F436A mutant lacking its N-terminal domain did not affect growth (Master's thesis Jana Theilmann, 03/2018-09/2018, supervised). Thus, in contrast to *S. aureus*, toxicity of ClpC F436A in *B. subtilis* appeared to be dependent on the interaction with adaptor proteins.

In order to elucidate which adaptor protein is the reason for ClpC F436A mediated toxicity, all combinations of Δ*mecA*, Δ*mcsB* and Δ*ypbH* gene deletions were analyzed regarding their respective impact. Remarkably, all negative impacts were abolished when a Δ*mcsB* mutant was introduced into the *clpC* F436A expressing strain (Figure 38). This was neither observed with the other known adaptor proteins nor with ClpE, which displayed a comparable phenotype when the analogous Y344A mutant was examined (Figure 38). Consistently it was demonstrated that ClpC F436A is still activated by McsB, but not MecA *in vitro* (Figure 41). These results strongly suggest that the toxicity of ClpC F436A is based on its interaction with its adaptor protein McsB.

In *B. subtilis* the oligomerization and activation of ClpC appears to be dependent on the presence of adaptor proteins (Kirstein et al., 2006). In *S. aureus*, McsB is also present, but since the lack of the N-terminal domain of ClpC F436A did not abolish but further enhanced

its phenotype, the interaction with McsB is not important for ClpC F436A toxicity in this strain (Carroni et al., 2017; Wozniak et al., 2012). When assuming an underlying similar mechanism, this observation would indicate that the toxic effect of ClpC F436A simply relies on active $ClpC_{F436A}P$ species, which can form in *S. aureus* without the need of adaptor proteins while *B. subtilis* ClpC requires McsB (since interaction with MecA is abolished in a F436A mutant (Figure 41)). Surprisingly, although the arginine kinase activity was observed to be essential for McsB activity in nearly all previous experiments (Figure 32, Figure 33, Figure 34 and Figure 35), the toxicity of a *clpC* F436A strain was not abolished in a kinase inactive *mcsB* C167S strain (Figure 39). These observations suggest that in the absence of a kinase active McsB, the ClpC F436A variant is already activated. Consequently, both kinase inactive and kinase active McsB could target substrate proteins to the activated $ClpC_{F436A}P$ protease complex in an uncontrolled manner. Based on this hypothesis, the toxicity of ClpC F436A would derive from (unphosphorylated) McsB targeting e.g. essential proteins for $ClpC_{F436A}P$ mediated degradation.

To this end, a ClpC F436A VGF::GGR variant which lacks the ability to associate with ClpP was investigated (Figure 40 and Figure 42). As expected, expression of *clpC* F436A VGF::GGR was not toxic at 37 °C, suggesting that indeed the uncontrolled degradation of an essential protein is the underlying reason for ClpC F436A toxicity (Figure 40). However, growth of the *clpC* F436A VGF::GGR expressing strain was slightly attenuated at 50 °C (Figure 40). Moreover, when *mcsB* was deleted, the fast formation of suppressor mutants was observed at 37 °C and growth became even more impaired at 50 °C. This was unexpected due to the fact that an additional Δ*mcsB* had abolished the toxicity of *clpC* F436A in the first place (Figure 39). Notably, a Δ*mcsB*, a *mcsB* C167S and a Δ*mcsA* mutant strain displayed a

comparably attenuated growth when *clpC* F436A VGF::GGR was expressed, suggesting that this effect was dependent on the kinase activity of McsB, which is impaired or completely abolished in all these strains (Figure 40) (Kirstein et al., 2005).

The opposing effects of a Δ*mcsB* mutant on a *clpC* F436A and a *clpC* F436A VGF::GGR expressing strain were at first glance contradictory. It is tempting to speculate that a direct and immediate effect of *clpC* F436A expression is degradation of at least one essential protein by $ClpC_{F436A}P$ using McsB as an adaptor (regardless of its phosphorylation state (Figure 39)), which then results in impaired growth and cellular death. As this is prevented in a *clpC* F436A VGF::GGR mutant, the observed minor toxic effect of ClpC F436A VGF::GGR at 50 °C might be of more indirect nature. ClpC F436A VGF::GGR could unfold intact (or even essential) proteins, abolish the formation of regular ClpCP complexes and/or perturb regulatory networks as interaction with (at least) MecA is no longer possible. Consequently, expression of *clpC* F436A VGF::GGR could lead to a generally occupied and impaired protein quality control system. This would also explain the increased susceptibility of the *clpC* F436A VGF::GGF mutant regarding the additional lack of kinase active McsB as an identified key player in aggregate clearance *in vivo* (Figure 38 and Figure 40).

In order to gain a better understanding of the toxic effect, an ATPase inactive ClpC F436A substrate trapping (DWB) mutant could be investigated in the future to identify potential target proteins and help to further elucidate the direct and indirect effects that cause the severe growth defect in *clpC* F436A expressing cells (Weibezahn et al., 2003).

Collectively, the experimental data suggests (and further confirms with respect to 3.2.1) that McsB is the most important adaptor protein for ClpC mediated disaggregation of protein aggregates in stress response. At the same time, McsB certainly plays an at least minor role

without its arginine kinase activity. Regarding Hsp100/Clp proteins, the M-domain was re-confirmed as an important regulatory feature (Oguchi et al., 2012; Seyffer et al., 2012). Impairing its function (e.g. due to specific amino acid exchange) resulted in a drastic change of a beneficial unfoldase towards a toxic aggregase (Figure 37 and Figure 38). This toxic effect was observed in different species (*B. subtilis* and *S. aureus*, (Carroni et al., 2017)) and in different Hsp100/Clp proteins (ClpC and ClpE, Figure 38), suggesting a general underlying principle, which is beneficial regarding future research in targeting Hsp100/Clp proteins in antimicrobial therapy.

4.3.   *ClpC is a suitable target for antibiotic screening*

During the last centuries, antibiotics have saved millions of lives. Unfortunately, especially due to overuse, inappropriate prescribing and excessive agricultural use, antibiotic resistant bacteria are emerging worldwide pointing towards a currently often called 'post-antibiotic era' (Kåhrström, 2013). Simultaneously, the number of approved, novel antibiotics is constantly declining, among other reasons, due to fading interest of pharmaceutical industry, as research has become less profitable (Edwards et al., 2018; Nathan and Goldberg, 2005).

The traditional targets of antibiotics are major cellular physiological processes such as translation, transcription, cell wall synthesis and replication. The underlying similarity regarding these targets is the assumption that bacterial cells are growing and proliferating e.g. during infection. However, a dormant, non-growing cell does not rely on e.g. active replication and translation and hence can survive the treatment with gyrase inhibitors like ciprofloxacin or translation inhibitors like tetracycline without genetic changes (Lewis, 2012). Hence, these persister cells are a major threat regarding antibiotic tolerance (Fisher et al., 2017; Mandal et al., 2019). In order to overcome these problems, novel targets for antibiotics

have been evaluated in the last years that do not depend on actively growing bacterial cells. These targets include, among others, signal transduction, biofilm formation and protein quality control (Brötz-Oesterhelt et al., 2005; Gotoh et al., 2010; Rice et al., 2002; Worthington et al., 2012).

Recently, various compounds, in particular from actinobacteria, have been identified to target the Hsp100/Clp protease complex ClpCP within the protein quality control network of different Gram-positive pathogenic bacteria (Brötz-Oesterhelt et al., 2005; Gao et al., 2014; Gavrish et al., 2014; Schmitt et al., 2011). Often these findings were originally based on previous screens for antibiotic activity (Cheng et al., 2007; Gao et al., 2014; Ozeki et al., 2015). Based on these promising observations, a ClpC target based screening system should be established in the S1 model organism *B. subtilis* to screen a myxobacterial compound library as proof of concept in cooperation with Dr. Jennifer Herrmann (HIPS) in Saarbrücken.

It is important to note that during characterization of the linker domain of ClpC, the *clpC* F436A mutant was identified to be toxic *in vivo* (Figure 37 and Figure 38). Exchanging one amino acid was already sufficient to deregulate the beneficial chaperone ClpC into a toxic and uncontrolled aggregase-like machinery, which concurrently loses its physiological function (Figure 37, Figure 39, Figure 41, Figure 43 and chapter 4.2). This fact clearly demonstrated that the chaperone ClpC is indeed a suitable target for antimicrobial therapy. In addition, all recently identified compounds that target and deregulate ClpC were found to interact with the N-terminal domain of the respective ClpC species e.g. in *M. tuberculosis* (Gao et al., 2015; Gavrish et al., 2014; Vasudevan et al., 2013). However, the F436A mutation is located on the tip of the linker domain (Figure 48). This finding suggested that besides from the N-terminal domain, the M-domain might also be a suitable target for drug development. This idea is

certainly not limited to ClpC, but could also apply to ClpB, where the M-domain is also an important regulatory element, albeit it is doubled in size (Carroni et al., 2017, 2014; Haslberger et al., 2007).

The established screening strain constitutively produced a GFP fusion of the MecA adaptor protein, MecA$_{CTD}$-GFP, to monitor ClpC activity as well as an ssrA-tagged mCherry to follow ClpX activity, respectively (Figure 54). As expected, the permanent synthesis and subsequent degradation of the fusion proteins did not affect growth of the screening strain and the CTD of MecA is not able to interfere with substrate proteins (Figure 46). MecA can present a substrate protein without MecA being degraded by ClpCP, which is not possible for the MecA$_{CTD}$-GFP fusion protein, possibly explaining the much faster degradation of the fusion protein especially at elevated temperatures *in vivo* (Figure 42, Figure 46, Figure 49 and Figure 50) (Schlothauer et al., 2003). Certainly one could speculate that MecA$_{CTD}$-GFP would still affect MecA dependent regulatory pathways such as competence development, as it competes with MecA for the binding site at ClpC (Figure 48 and Figure 49). However, these specific developmental pathways are not relevant during compound screening, albeit they could certainly help to further characterize compounds of interest by examining the way they affect these pathways. The influence of a compound on a specific ClpC dependent developmental pathway could e.g. suggest an overlapping binding site with a ClpC adaptor protein.

In general, it is important to note that growth of the *B. subtilis* strains in a shaking 96-well plate differed substantially from a shaking flask, as e.g. the Δ*clpX* mutant strain, which already displayed attenuated growth, did not grow under tested conditions in a 96-well plate (Figure 53). This is presumably due to inefficient oxygen distribution. The strains were

always examined in different wells in the 96-well plate to prevent and decrease false negative results.

Screening a smaller myxobacterial library of 300 compounds resulted in a pre-selection of ten interesting compounds after a first test, which were subsequently examined in a more specific dose-dependent screen (Figure 59 and Table 8). Unfortunately, the majority of the previously obtained results could not be reproduced and, hence, identified as false positive. Only myxopyronin A and B were observed to lead to an accumulation of MecA$_{CTD}$-GFP at elevated concentrations (Figure 59 and Table 8). At even higher concentrations ($> 4\ \mu M$) they substantially attenuated or completely abolished growth and consequently did not lead to accumulation of MecA$_{CTD}$-GFP anymore. However, as known RNA-polymerase inhibitors, the myxopyronins potentially affected the bacterial cell in a pleiotropic way (Belogurov et al., 2009). To exclude that myxopyronin based transcription deficiency of *clpC* instead of direct interaction of myxopyronin with ClpCP is responsible for the accumulation of MecA$_{CTD}$-GFP, a northern blotting or qPCR experiment accompanied by western blotting would certainly reveal the impact on levels of *clpC* and ClpC, respectively.

Despite the results of the actual screening, validation of the screening strain with various common antibiotics (Figure 55), known ClpC targeting compounds such as cyclomarin (Figure 56 and Figure 57), different background mutations (Figure 51, Figure 52 and Figure 53) and positive/negative controls in western blotting and fluorescence microscopy (Figure 49, Figure 50, Figure 51, Figure 52 and Figure 53) successfully demonstrated the functionality of the established screening strain to identify compounds that target the protein quality control system in *B. subtilis*.

Collectively, targeting Hsp100/Clp complexes in antimicrobial therapy is a reasonable approach. Firstly, a defect within these systems was observed to result in impaired virulence and/or pathogenicity (Gaillot et al., 2000; Kwon et al., 2004; Ollinger et al., 2012; Rouquette et al., 1998, 1996; Sassetti et al., 2003; Wozniak et al., 2012). Secondly, a bacterium with an impaired protein quality control system is presumably more sensitive towards the general immune response of the host (e.g. reactive oxygen/ROS and nitrogen species/RNS) during infection. Next, as already stated above, non-growing persister cells still possess an active protein quality control system while other processes such as replication or cell-wall synthesis are highly downregulated or completely shut down (Fisher et al., 2017; Lewis, 2012). Finally, when comparing the recently identified $ClpC_{NTD}$ targeting compounds lassomycin, cyclomarin and ecumicin, it becomes evident that all are either ribosomal or non-ribosomal cyclic peptides (Figure 8). ClpC, as part of the ClpCP protease complex, is designed to bind to adaptor and/or substrates proteins with its N-terminal domain, and hence obviously more suited to bind peptide chains than e.g. polyketide chains. This observation could help to guide and optimize screening of natural compound libraries.

In addition to natural products, in the last years novel approaches have been established such as genetically engineered phages, modified antibodies and CRISPR/Cas systems, which all contributed to progress in antimicrobial therapies (Citorik et al., 2014; Mariathasan and Tan, 2017; Trigo et al., 2013). Despite these innovative approaches, the classic target based screening systems are regaining attention due to identification of novel antibiotic compounds from uncultivable microorganisms by improved cultivation techniques or genome mining of metagenomics data without the necessity of cultivation (Medema and Fischbach, 2015; Ziemert et al., 2016). It became possible to sequence the genome from one single cell, which

is of particular interest because the majority of bacteria are assumed to be uncultivable (Amann et al., 1995; Raghunathan et al., 2005; Streit and Schmitz, 2004). Collectively, the fast increasing number of sequenced genomes and compiled metagenomics data provide a constantly raising amount of information regarding novel drugs and their respective active or cryptic gene clusters. To this end, specific target-based or general screening systems remain irreplaceable.

4.4.   *Summary and outlook*

During this work, YocM was identified as the first stress-related small heat shock protein of *B. subtilis*, ensuring survival of cells during salt shock presumably in a synergistic relationship with accumulated chemical chaperones. Although occurring in all domains of life, such a potential relationship has not been observed before and broadens the repertoire of sHsp functions. A better understanding of sHsp might ultimately help regarding a number of human diseases connected to mutated sHsps or malfunction of their respective regulation, such as a cataract, myopathy and neurological disorders (Sun and MacRae, 2005).

The established YocM-mCherry aggregate marker protein allowed the visualization of protein disaggregation and degradation *in vivo*. Thereby, protein disaggregation by ClpC was observed to be the favored way to deal with protein aggregates accumulated during heat stress in *B. subtilis*. Furthermore, McsB was identified as the most relevant adaptor protein for disaggregation of subcellular protein aggregates by the Hsp100/Clp protein ClpC during heat stress, which was in particular dependent on its protein arginine kinase activity. At that, levels of arginine phosphorylation appeared to be strictly controlled since elevated or decreased levels of the phosphatase YwlE severely affected the viability of the cell. On the one hand, these findings demonstrated the substantial influence of protein arginine phosphorylation in

PQC and heat stress regulation, albeit its precise and presumably target-specific role still needs to be addressed in the future. On the other hand, these insights into the PQC system of *B. subtilis* also demonstrate the intricate connection of regulatory proteolysis and general proteolysis in general and provide a better understanding of the bacterial cell since the underlying mechanism are conserved within all domains of life.

A better understanding of the PQC system may also help to find and characterize novel antibiotics. Exchanging only one amino acid in the linker domain of ClpC resulted in at least partial loss of physiological function, formation of subcellular aggregates and general toxicity *in vivo*. These observations proved ClpC to be a suitable target for antimicrobial therapy. To this end, a ClpC target based screening system was successfully established, validated and tested in *B. subtilis* with a myxobacterial compound library. This proof of concept forms the basis for high-throughput screening of larger compound libraries towards the development of antibiotics aiming at ClpC, a promising target for antimicrobial therapy.

List of figures

List of tables

References

Amann, R.I., Ludwig, W., Schleifer, K.H., 1995. Phylogenetic identification and in situ detection of individual microbial cells without cultivation. Microbiol. Rev. 59, 143–169.

Anagnostopoulos, C., Spizizen, J., 1961. REQUIREMENTS FOR TRANSFORMATION IN BACILLUS SUBTILIS. J. Bacteriol. 81, 741–746.

Andréasson, C., Fiaux, J., Rampelt, H., Mayer, M.P., Bukau, B., 2008. Hsp110 Is a Nucleotide-activated Exchange Factor for Hsp70. J. Biol. Chem. 283, 8877–8884. https://doi.org/10.1074/jbc.M710063200

Arai, T., Takahashi, K., Ishiguro, K., Mikami, Y., 1980. Some chemotherapeutic properties of two new antitumor antibiotics, saframycins A and C. Gan 71, 790–796.

Arakawa, T., Timasheff, S.N., 1985. The stabilization of proteins by osmolytes. Biophys. J. 47, 411–414. https://doi.org/10.1016/S0006-3495(85)83932-1

Arnaud, M., Chastanet, A., Débarbouillé, M., 2004. New vector for efficient allelic replacement in naturally nontransformable, low-GC-content, gram-positive bacteria. Appl. Environ. Microbiol. 70, 6887–6891. https://doi.org/10.1128/AEM.70.11.6887-6891.2004

Balaban, N.Q., Helaine, S., Lewis, K., Ackermann, M., Aldridge, B., Andersson, D.I., Brynildsen, M.P., Bumann, D., Camilli, A., Collins, J.J., Dehio, C., Fortune, S., Ghigo, J.-M., Hardt, W.-D., Harms, A., Heinemann, M., Hung, D.T., Jenal, U., Levin, B.R., Michiels, J., Storz, G., Tan, M.-W., Tenson, T., Van Melderen, L., Zinkernagel, A., 2019. Definitions and guidelines for research on antibiotic persistence. Nat. Rev. Microbiol. https://doi.org/10.1038/s41579-019-0196-3

Basha, E., Friedrich, K.L., Vierling, E., 2006. The N-terminal arm of small heat shock proteins is important for both chaperone activity and substrate specificity. J. Biol. Chem. 281, 39943–39952. https://doi.org/10.1074/jbc.M607677200

Basha, E., Jones, C., Blackwell, A.E., Cheng, G., Waters, E.R., Samsel, K.A., Siddique, M., Pett, V., Wysocki, V., Vierling, E., 2013. An unusual dimeric small heat shock protein provides insight into the mechanism of this class of chaperones. J. Mol. Biol. 425, 1683–1696. https://doi.org/10.1016/j.jmb.2013.02.011

Basha, E., O'Neill, H., Vierling, E., 2012. Small heat shock proteins and α-crystallins: dynamic proteins with flexible functions. Trends Biochem. Sci. 37, 106–117. https://doi.org/10.1016/j.tibs.2011.11.005

Bashir, A., Hoffmann, T., Kempf, B., Xie, X., Smits, S.H.J., Bremer, E., 2014a. Plant-derived compatible solutes proline betaine and betonicine confer enhanced osmotic and temperature stress tolerance to Bacillus subtilis. Microbiol. Read. Engl. 160, 2283–2294. https://doi.org/10.1099/mic.0.079665-0

Bashir, A., Hoffmann, T., Smits, S.H.J., Bremer, E., 2014b. Dimethylglycine provides salt and temperature stress protection to Bacillus subtilis. Appl. Environ. Microbiol. 80, 2773–2785. https://doi.org/10.1128/AEM.00078-14

Battesti, A., Gottesman, S., 2013. Roles of adaptor proteins in regulation of bacterial proteolysis. Curr. Opin. Microbiol. 16, 140–147. https://doi.org/10.1016/j.mib.2013.01.002

Belogurov, G.A., Vassylyeva, M.N., Sevostyanova, A., Appleman, J.R., Xiang, A.X., Lira, R., Webber, S.E., Klyuyev, S., Nudler, E., Artsimovitch, I., Vassylyev, D.G., 2009. Transcription

inactivation through local refolding of the RNA polymerase structure. Nature 457, 332–335. https://doi.org/10.1038/nature07510

Benaroudj, N., Raynal, B., Miot, M., Ortiz-Lombardia, M., 2011. Assembly and proteolytic processing of mycobacterial ClpP1 and ClpP2. BMC Biochem. 12, 61. https://doi.org/10.1186/1471-2091-12-61

Bepperling, A., Alte, F., Kriehuber, T., Braun, N., Weinkauf, S., Groll, M., Haslbeck, M., Buchner, J., 2012. Alternative bacterial two-component small heat shock protein systems. Proc. Natl. Acad. Sci. U. S. A. 109, 20407–20412. https://doi.org/10.1073/pnas.1209565109

Boch, J., Kempf, B., Schmid, R., Bremer, E., 1996. Synthesis of the osmoprotectant glycine betaine in Bacillus subtilis: characterization of the gbsAB genes. J. Bacteriol. 178, 5121–5129.

Bourot, S., Sire, O., Trautwetter, A., Touzé, T., Wu, L.F., Blanco, C., Bernard, T., 2000. Glycine betaine-assisted protein folding in a lysA mutant of Escherichia coli. J. Biol. Chem. 275, 1050–1056.

Brötz-Oesterhelt, H., Beyer, D., Kroll, H.-P., Endermann, R., Ladel, C., Schroeder, W., Hinzen, B., Raddatz, S., Paulsen, H., Henninger, K., Bandow, J.E., Sahl, H.-G., Labischinski, H., 2005. Dysregulation of bacterial proteolytic machinery by a new class of antibiotics. Nat. Med. 11, 1082–1087. https://doi.org/10.1038/nm1306

Buchner, J., Schmidt, M., Fuchs, M., Jaenicke, R., Rudolph, R., Schmid, F.X., Kiefhaber, T., 1991. GroE facilitates refolding of citrate synthase by suppressing aggregation. Biochemistry 30, 1586–1591. https://doi.org/10.1021/bi00220a020

Bukau, B., Weissman, J., Horwich, A., 2006. Molecular chaperones and protein quality control. Cell 125, 443–451. https://doi.org/10.1016/j.cell.2006.04.014

Caldas, T., Demont-Caulet, N., Ghazi, A., Richarme, G., 1999. Thermoprotection by glycine betaine and choline. Microbiol. Read. Engl. 145 (Pt 9), 2543–2548. https://doi.org/10.1099/00221287-145-9-2543

Camberg, J.L., Hoskins, J.R., Wickner, S., 2009. ClpXP protease degrades the cytoskeletal protein, FtsZ, and modulates FtsZ polymer dynamics. Proc. Natl. Acad. Sci. 106, 10614–10619. https://doi.org/10.1073/pnas.0904886106

Carroni, M., Franke, K.B., Maurer, M., Jäger, J., Hantke, I., Gloge, F., Linder, D., Gremer, S., Turgay, K., Bukau, B., Mogk, A., 2017. Regulatory coiled-coil domains promote head-to-head assemblies of AAA+ chaperones essential for tunable activity control. eLife 6. https://doi.org/10.7554/eLife.30120

Carroni, M., Kummer, E., Oguchi, Y., Wendler, P., Clare, D.K., Sinning, I., Kopp, J., Mogk, A., Bukau, B., Saibil, H.R., 2014. Head-to-tail interactions of the coiled-coil domains regulate ClpB activity and cooperation with Hsp70 in protein disaggregation. eLife 3. https://doi.org/10.7554/eLife.02481

Cayley, D.S., Guttman, H.J., Record, M.T., 2000. Biophysical characterization of changes in amounts and activity of Escherichia coli cell and compartment water and turgor pressure in response to osmotic stress. Biophys. J. 78, 1748–1764.

Cayley, S., Lewis, B.A., Record, M.T., 1992. Origins of the osmoprotective properties of betaine and proline in Escherichia coli K-12. J. Bacteriol. 174, 1586–1595.

Chan, P., Curtis, R.A., Warwicker, J., 2013. Soluble expression of proteins correlates with a lack of positively-charged surface. Sci. Rep. 3, 3333.

Chattopadhyay, M.K., Kern, R., Mistou, M.-Y., Dandekar, A.M., Uratsu, S.L., Richarme, G., 2004. The chemical chaperone proline relieves the thermosensitivity of a dnaK deletion mutant at 42 degrees C. J. Bacteriol. 186, 8149–8152. https://doi.org/10.1128/JB.186.23.8149-8152.2004

Chen, J., Feige, M.J., Franzmann, T.M., Bepperling, A., Buchner, J., 2010. Regions outside the alpha-crystallin domain of the small heat shock protein Hsp26 are required for its dimerization. J. Mol. Biol. 398, 122–131. https://doi.org/10.1016/j.jmb.2010.02.022

Cheng, L., Naumann, T.A., Horswill, A.R., Hong, S.-J., Venters, B.J., Tomsho, J.W., Benkovic, S.J., Keiler, K.C., 2007. Discovery of antibacterial cyclic peptides that inhibit the ClpXP protease. Protein Sci. Publ. Protein Soc. 16, 1535–1542. https://doi.org/10.1110/ps.072933007

Cheung, M.S., Klimov, D., Thirumalai, D., 2005. Molecular crowding enhances native state stability and refolding rates of globular proteins. Proc. Natl. Acad. Sci. 102, 4753–4758. https://doi.org/10.1073/pnas.0409630102

Citorik, R.J., Mimee, M., Lu, T.K., 2014. Sequence-specific antimicrobials using efficiently delivered RNA-guided nucleases. Nat. Biotechnol. 32, 1141–1145. https://doi.org/10.1038/nbt.3011

Clardy, J., Walsh, C., 2004. Lessons from natural molecules. Nature 432, 829–837. https://doi.org/10.1038/nature03194

Conlon, B.P., Nakayasu, E.S., Fleck, L.E., LaFleur, M.D., Isabella, V.M., Coleman, K., Leonard, S.N., Smith, R.D., Adkins, J.N., Lewis, K., 2013. Activated ClpP kills persisters and eradicates a chronic biofilm infection. Nature 503, 365–370. https://doi.org/10.1038/nature12790

Csonka, L.N., 1989. Physiological and genetic responses of bacteria to osmotic stress. Microbiol. Rev. 53, 121–147.

Culp, E., Wright, G.D., 2017. Bacterial proteases, untapped antimicrobial drug targets. J. Antibiot. (Tokyo) 70, 366–377. https://doi.org/10.1038/ja.2016.138

Danielsson, J., Mu, X., Lang, L., Wang, H., Binolfi, A., Theillet, F.-X., Bekei, B., Logan, D.T., Selenko, P., Wennerström, H., Oliveberg, M., 2015. Thermodynamics of protein destabilization in live cells. Proc. Natl. Acad. Sci. 112, 12402–12407. https://doi.org/10.1073/pnas.1511308112

de Hoon, M.J.L., Eichenberger, P., Vitkup, D., 2010. Hierarchical Evolution of the Bacterial Sporulation Network. Curr. Biol. 20, R735–R745. https://doi.org/10.1016/j.cub.2010.06.031

Delbecq, S.P., Klevit, R.E., 2013. One size does not fit all: the oligomeric states of αB crystallin. FEBS Lett. 587, 1073–1080. https://doi.org/10.1016/j.febslet.2013.01.021

DeMartino, G.N., Slaughter, C.A., 1999. The Proteasome, a Novel Protease Regulated by Multiple Mechanisms. J. Biol. Chem. 274, 22123–22126. https://doi.org/10.1074/jbc.274.32.22123

Derré, I., Rapoport, G., Msadek, T., 1999. CtsR, a novel regulator of stress and heat shock response, controls clp and molecular chaperone gene expression in gram-positive bacteria. Mol. Microbiol. 31, 117–131.

Dévényi, T., Rogers, S.J., Wolfe, R.G., 1966. Structural studies of pig heart malate dehydrogenase. Nature 210, 489–491.

Diamant, S., Eliahu, N., Rosenthal, D., Goloubinoff, P., 2001. Chemical chaperones regulate molecular chaperones in vitro and in cells under combined salt and heat stresses. J. Biol. Chem. 276, 39586–39591. https://doi.org/10.1074/jbc.M103081200

Diamant, S., Rosenthal, D., Azem, A., Eliahu, N., Ben-Zvi, A.P., Goloubinoff, P., 2003. Dicarboxylic amino acids and glycine-betaine regulate chaperone-mediated protein-disaggregation under stress. Mol. Microbiol. 49, 401–410.

Diez, J., Martinez, J.P., Mestres, J., Sasse, F., Frank, R., Meyerhans, A., 2012. Myxobacteria: natural pharmaceutical factories. Microb. Cell Factories 11, 52. https://doi.org/10.1186/1475-2859-11-52

Dziedzic, R., Kiran, M., Plocinski, P., Ziolkiewicz, M., Brzostek, A., Moomey, M., Vadrevu, I.S., Dziadek, J., Madiraju, M., Rajagopalan, M., 2010. Mycobacterium tuberculosis ClpX Interacts with FtsZ and Interferes with FtsZ Assembly. PLoS ONE 5, e11058. https://doi.org/10.1371/journal.pone.0011058

Ebbinghaus, S., Dhar, A., McDonald, J.D., Gruebele, M., 2010. Protein folding stability and dynamics imaged in a living cell. Nat. Methods 7, 319.

Edwards, S., Morel, C., Busse, R., Harbarth, S., 2018. Combatting Antibiotic Resistance Together: How Can We Enlist the Help of Industry? Antibiotics 7, 111. https://doi.org/10.3390/antibiotics7040111

Ehrnsperger, M., Gräber, S., Gaestel, M., Buchner, J., 1997. Binding of non-native protein to Hsp25 during heat shock creates a reservoir of folding intermediates for reactivation. EMBO J. 16, 221–229. https://doi.org/10.1093/emboj/16.2.221

Elnakady, Y.A., Sasse, F., Lünsdorf, H., Reichenbach, H., 2004. Disorazol A 1 , a highly effective antimitotic agent acting on tubulin polymerization and inducing apoptosis in mammalian cells. Biochem. Pharmacol. 67, 927–935. https://doi.org/10.1016/j.bcp.2003.10.029

Elsholz, A.K.W., Birk, M.S., Charpentier, E., Turgay, K., 2017. Functional Diversity of AAA+ Protease Complexes in Bacillus subtilis. Front. Mol. Biosci. 4, 44. https://doi.org/10.3389/fmolb.2017.00044

Elsholz, A.K.W., Hempel, K., Michalik, S., Gronau, K., Becher, D., Hecker, M., Gerth, U., 2011a. Activity Control of the ClpC Adaptor McsB in Bacillus subtilis. J. Bacteriol. 193, 3887–3893. https://doi.org/10.1128/JB.00079-11

Elsholz, A.K.W., Hempel, K., Pöther, D.-C., Becher, D., Hecker, M., Gerth, U., 2011b. CtsR inactivation during thiol-specific stress in low GC, Gram+ bacteria: Dual activity control of CtsR. Mol. Microbiol. 79, 772–785. https://doi.org/10.1111/j.1365-2958.2010.07489.x

Elsholz, A.K.W., Michalik, S., Zühlke, D., Hecker, M., Gerth, U., 2010. CtsR, the Gram-positive master regulator of protein quality control, feels the heat. EMBO J. 29, 3621–3629. https://doi.org/10.1038/emboj.2010.228

Elsholz, A.K.W., Turgay, K., Michalik, S., Hessling, B., Gronau, K., Oertel, D., Mäder, U., Bernhardt, J., Becher, D., Hecker, M., Gerth, U., 2012. Global impact of protein arginine phosphorylation on the physiology of Bacillus subtilis. Proc. Natl. Acad. Sci. U. S. A. 109, 7451–7456. https://doi.org/10.1073/pnas.1117483109

Faloona, G.R., Srere, P.A., 1969. Escherichia coli citrate synthase. Purification and the effect of potassium on some properties. Biochemistry 8, 4497–4503.

Famulla, K., Sass, P., Malik, I., Akopian, T., Kandror, O., Alber, M., Hinzen, B., Ruebsamen-Schaeff, H., Kalscheuer, R., Goldberg, A.L., Brötz-Oesterhelt, H., 2016. Acyldepsipeptide antibiotics kill mycobacteria by preventing the physiological functions of the ClpP1P2 protease. Mol. Microbiol. 101, 194–209. https://doi.org/10.1111/mmi.13362

Fetzer, C., Korotkov, V.S., Thänert, R., Lee, K.M., Neuenschwander, M., von Kries, J.P., Medina, E., Sieber, S.A., 2017. A Chemical Disruptor of the ClpX Chaperone Complex Attenuates the Virulence of Multidrug-Resistant Staphylococcus aureus. Angew. Chem. Int. Ed Engl. 56, 15746–15750. https://doi.org/10.1002/anie.201708454

Fisher, R.A., Gollan, B., Helaine, S., 2017. Persistent bacterial infections and persister cells. Nat. Rev. Microbiol. 15, 453.

Fu, C., Sikandar, A., Donner, J., Zaburannyi, N., Herrmann, J., Reck, M., Wagner-Döbler, I., Koehnke, J., Müller, R., 2017. The natural product carolacton inhibits folate-dependent C1 metabolism by targeting FolD/MTHFD. Nat. Commun. 8. https://doi.org/10.1038/s41467-017-01671-5

Fuhrmann, J., Mierzwa, B., Trentini, D.B., Spiess, S., Lehner, A., Charpentier, E., Clausen, T., 2013. Structural Basis for Recognizing Phosphoarginine and Evolving Residue-Specific Protein Phosphatases in Gram-Positive Bacteria. Cell Rep. 3, 1832–1839. https://doi.org/10.1016/j.celrep.2013.05.023

Fuhrmann, J., Schmidt, A., Spiess, S., Lehner, A., Turgay, K., Mechtler, K., Charpentier, E., Clausen, T., 2009. McsB Is a Protein Arginine Kinase That Phosphorylates and Inhibits the Heat-Shock Regulator CtsR. Science 324, 1323–1327. https://doi.org/10.1126/science.1170088

Fujisawa, M., Ito, M., Krulwich, T.A., 2007. Three two-component transporters with channel-like properties have monovalent cation/proton antiport activity. Proc. Natl. Acad. Sci. 104, 13289–13294. https://doi.org/10.1073/pnas.0703709104

Gaillot, O., Pellegrini, E., Bregenholt, S., Nair, S., Berche, P., 2000. The ClpP serine protease is essential for the intracellular parasitism and virulence of Listeria monocytogenes. Mol. Microbiol. 35, 1286–1294.

Gamba, P., Jonker, M.J., Hamoen, L.W., 2015. A Novel Feedback Loop That Controls Bimodal Expression of Genetic Competence. PLOS Genet 11, e1005047. https://doi.org/10.1371/journal.pgen.1005047

Gao, W., Kim, J.-Y., Anderson, J.R., Akopian, T., Hong, S., Jin, Y.-Y., Kandror, O., Kim, J.-W., Lee, I.-A., Lee, S.-Y., McAlpine, J.B., Mulugeta, S., Sunoqrot, S., Wang, Y., Yang, S.-H., Yoon, T.-M., Goldberg, A.L., Pauli, G.F., Suh, J.-W., Franzblau, S.G., Cho, S., 2015. The cyclic peptide ecumicin targeting ClpC1 is active against Mycobacterium tuberculosis in vivo. Antimicrob. Agents Chemother. 59, 880–889. https://doi.org/10.1128/AAC.04054-14

Gao, W., Kim, J.-Y., Chen, S.-N., Cho, S.-H., Choi, J., Jaki, B.U., Jin, Y.-Y., Lankin, D.C., Lee, J.-E., Lee, S.-Y., McAlpine, J.B., Napolitano, J.G., Franzblau, S.G., Suh, J.-W., Pauli, G.F., 2014. Discovery and characterization of the tuberculosis drug lead ecumicin. Org. Lett. 16, 6044–6047. https://doi.org/10.1021/ol5026603

Gavrish, E., Sit, C.S., Cao, S., Kandror, O., Spoering, A., Peoples, A., Ling, L., Fetterman, A., Hughes, D., Bissell, A., Torrey, H., Akopian, T., Mueller, A., Epstein, S., Goldberg, A., Clardy, J., Lewis, K., 2014. Lassomycin, a ribosomally synthesized cyclic peptide, kills mycobacterium tuberculosis by targeting the ATP-dependent protease ClpC1P1P2. Chem. Biol. 21, 509–518. https://doi.org/10.1016/j.chembiol.2014.01.014

Geitmann, A., Ortega, J.K.E., 2009. Mechanics and modeling of plant cell growth. Trends Plant Sci. 14, 467–478. https://doi.org/10.1016/j.tplants.2009.07.006

Gerth, U., Kirstein, J., Mostertz, J., Waldminghaus, T., Miethke, M., Kock, H., Hecker, M., 2004. Fine-tuning in regulation of Clp protein content in Bacillus subtilis. J. Bacteriol. 186, 179–191.

Giese, K.C., Vierling, E., 2002. Changes in oligomerization are essential for the chaperone activity of a small heat shock protein in vivo and in vitro. J. Biol. Chem. 277, 46310–46318. https://doi.org/10.1074/jbc.M208926200

Gotoh, Y., Eguchi, Y., Watanabe, T., Okamoto, S., Doi, A., Utsumi, R., 2010. Two-component signal transduction as potential drug targets in pathogenic bacteria. Curr. Opin. Microbiol. 13, 232–239. https://doi.org/10.1016/j.mib.2010.01.008

Grimaud, R., Kessel, M., Beuron, F., Steven, A.C., Maurizi, M.R., 1998. Enzymatic and structural similarities between the Escherichia coli ATP-dependent proteases, ClpXP and ClpAP. J. Biol. Chem. 273, 12476–12481.

Grousl, T., Ungelenk, S., Miller, S., Ho, C.-T., Khokhrina, M., Mayer, M.P., Bukau, B., Mogk, A., 2018. A prion-like domain in Hsp42 drives chaperone-facilitated aggregation of misfolded proteins. J. Cell Biol. 217, 1269–1285. https://doi.org/10.1083/jcb.201708116

Gundlach, J., Herzberg, C., Kaever, V., Gunka, K., Hoffmann, T., Weiß, M., Gibhardt, J., Thürmer, A., Hertel, D., Daniel, R., Bremer, E., Commichau, F.M., Stülke, J., 2017. Control of potassium homeostasis is an essential function of the second messenger cyclic di-AMP in Bacillus subtilis. Sci. Signal. 10. https://doi.org/10.1126/scisignal.aal3011

Haeusser, D.P., Lee, A.H., Weart, R.B., Levin, P.A., 2009. ClpX Inhibits FtsZ Assembly in a Manner That Does Not Require Its ATP Hydrolysis-Dependent Chaperone Activity. J. Bacteriol. 191, 1986–1991. https://doi.org/10.1128/JB.01606-07

Hahn, J., Kramer, N., Briley, K., Dubnau, D., 2009. McsA and B mediate the delocalization of competence proteins from the cell poles of Bacillus subtilis: Delocalization of competence proteins. Mol. Microbiol. 72, 202–215. https://doi.org/10.1111/j.1365-2958.2009.06636.x

Hahne, H., Mader, U., Otto, A., Bonn, F., Steil, L., Bremer, E., Hecker, M., Becher, D., 2010. A comprehensive proteomics and transcriptomics analysis of Bacillus subtilis salt stress adaptation. J Bacteriol 192, 870–82. https://doi.org/10.1128/JB.01106-09

Hantke, I., Schäfer, H., Janczikowski, A., Turgay, K., 2018. YocM a small heat shock protein can protect *Bacillus subtilis* cells during salt stress. Mol. Microbiol. https://doi.org/10.1111/mmi.14164

Hartl, F.U., Hayer-Hartl, M., 2009. Converging concepts of protein folding in vitro and in vivo. Nat. Struct. Mol. Biol. 16, 574–581. https://doi.org/10.1038/nsmb.1591

Hartl, F.U., Hayer-Hartl, M., 2002. Molecular chaperones in the cytosol: from nascent chain to folded protein. Science 295, 1852–1858. https://doi.org/10.1126/science.1068408

Haslbeck, M., Franzmann, T., Weinfurtner, D., Buchner, J., 2005a. Some like it hot: the structure and function of small heat-shock proteins. Nat. Struct. Mol. Biol. 12, 842–846. https://doi.org/10.1038/nsmb993

Haslbeck, M., Kastenmüller, A., Buchner, J., Weinkauf, S., Braun, N., 2008. Structural dynamics of archaeal small heat shock proteins. J. Mol. Biol. 378, 362–374. https://doi.org/10.1016/j.jmb.2008.01.095

Haslbeck, M., Miess, A., Stromer, T., Walter, S., Buchner, J., 2005b. Disassembling protein aggregates in the yeast cytosol. The cooperation of Hsp26 with Ssa1 and Hsp104. J. Biol. Chem. 280, 23861–23868. https://doi.org/10.1074/jbc.M502697200

Haslbeck, M., Vierling, E., 2015. A first line of stress defense: small heat shock proteins and their function in protein homeostasis. J. Mol. Biol. 427, 1537–1548. https://doi.org/10.1016/j.jmb.2015.02.002

Haslbeck, M., Walke, S., Stromer, T., Ehrnsperger, M., White, H.E., Chen, S., Saibil, H.R., Buchner, J., 1999. Hsp26: a temperature-regulated chaperone. EMBO J. 18, 6744–6751. https://doi.org/10.1093/emboj/18.23.6744

Haslberger, T., Weibezahn, J., Zahn, R., Lee, S., Tsai, F.T.F., Bukau, B., Mogk, A., 2007. M domains couple the ClpB threading motor with the DnaK chaperone activity. Mol. Cell 25, 247–260. https://doi.org/10.1016/j.molcel.2006.11.008

Hayer-Hartl, M., Bracher, A., Hartl, F.U., 2016. The GroEL–GroES Chaperonin Machine: A Nano-Cage for Protein Folding. Trends Biochem. Sci. 41, 62–76. https://doi.org/10.1016/j.tibs.2015.07.009

Hecker, M., Pane-Farre, J., Völker, U., 2007. SigB-dependent general stress response in Bacillus subtilis and related gram-positive bacteria. Annu Rev Microbiol 61, 215–36.

Held, J., Gebru, T., Kalesse, M., Jansen, R., Gerth, K., Müller, R., Mordmüller, B., 2014. Antimalarial Activity of the Myxobacterial Macrolide Chlorotonil A. Antimicrob. Agents Chemother. 58, 6378–6384. https://doi.org/10.1128/AAC.03326-14

Henriques, A.O., Beall, B.W., Moran, C.P., 1997. CotM of Bacillus subtilis, a member of the alpha-crystallin family of stress proteins, is induced during development and participates in spore outer coat formation. J. Bacteriol. 179, 1887–1897.

Hershko, A., Heller, H., Elias, S., Ciechanover, A., 1983. Components of ubiquitin-protein ligase system. Resolution, affinity purification, and role in protein breakdown. J. Biol. Chem. 258, 8206–8214.

Hesterkamp, T., Hauser, S., Lutcke, H., Bukau, B., 1996. Escherichia coli trigger factor is a prolyl isomerase that associates with nascent polypeptide chains. Proc. Natl. Acad. Sci. 93, 4437–4441. https://doi.org/10.1073/pnas.93.9.4437

Hinnerwisch, J., Fenton, W.A., Furtak, K.J., Farr, G.W., Horwich, A.L., 2005. Loops in the central channel of ClpA chaperone mediate protein binding, unfolding, and translocation. Cell 121, 1029–1041. https://doi.org/10.1016/j.cell.2005.04.012

Hochberg, G.K.A., Ecroyd, H., Liu, C., Cox, D., Cascio, D., Sawaya, M.R., Collier, M.P., Stroud, J., Carver, J.A., Baldwin, A.J., Robinson, C.V., Eisenberg, D.S., Benesch, J.L.P., Laganowsky, A., 2014. The structured core domain of αB-crystallin can prevent amyloid fibrillation and associated toxicity. Proc. Natl. Acad. Sci. U. S. A. 111, E1562-1570. https://doi.org/10.1073/pnas.1322673111

Hoffman, L., Rechsteiner, M., 1996. Nucleotidase Activities of the 26 S Proteasome and Its Regulatory Complex. J. Biol. Chem. 271, 32538–32545. https://doi.org/10.1074/jbc.271.51.32538

Hoffmann, T., Bremer, E., 2016. Management of Osmotic Stress by *Bacillus Subtilis*: Genetics and Physiology, in: de Bruijn, F.J. (Ed.), Stress and Environmental Regulation of Gene Expression and Adaptation in Bacteria. John Wiley & Sons, Inc., Hoboken, NJ, USA, pp. 657–676. https://doi.org/10.1002/9781119004813.ch63

Hoffmann, T., Bremer, E., 2011. Protection of Bacillus subtilis against Cold Stress via Compatible-Solute Acquisition. J. Bacteriol. 193, 1552–1562. https://doi.org/10.1128/JB.01319-10

Holtmann, G., Bakker, E.P., Uozumi, N., Bremer, E., 2003. KtrAB and KtrCD: two K+ uptake systems in Bacillus subtilis and their role in adaptation to hypertonicity. J. Bacteriol. 185, 1289–1298.

Holtmann, G., Bremer, E., 2004. Thermoprotection of Bacillus subtilis by exogenously provided glycine betaine and structurally related compatible solutes: involvement of Opu transporters. J. Bacteriol. 186, 1683–1693.

Homuth, G., Masuda, S., Mogk, A., Kobayashi, Y., Schumann, W., 1997. The dnaK operon of Bacillus subtilis is heptacistronic. J. Bacteriol. 179, 1153–1164.

Höper, D., Bernhardt, J., Hecker, M., 2006. Salt stress adaptation of Bacillus subtilis: a physiological proteomics approach. Proteomics 6, 1550–1562. https://doi.org/10.1002/pmic.200500197

Höper, D., Völker, U., Hecker, M., 2005. Comprehensive Characterization of the Contribution of Individual SigB-Dependent General Stress Genes to Stress Resistance of Bacillus subtilis. J. Bacteriol. 187, 2810–2826. https://doi.org/10.1128/JB.187.8.2810-2826.2005

Horwitz, J., 1992. Alpha-crystallin can function as a molecular chaperone. Proc. Natl. Acad. Sci. U. S. A. 89, 10449–10453.

Horwitz, J., Bova, M.P., Ding, L.-L., Haley, D.A., Stewart, P.L., 1999. Lens α-crystallin: Function and structure. Eye 13, 403–408. https://doi.org/10.1038/eye.1999.114

Hristozova, N., Tompa, P., Kovacs, D., 2016. A Novel Method for Assessing the Chaperone Activity of Proteins. PloS One 11, e0161970. https://doi.org/10.1371/journal.pone.0161970

Huerta-Cepas, J., Szklarczyk, D., Forslund, K., Cook, H., Heller, D., Walter, M.C., Rattei, T., Mende, D.R., Sunagawa, S., Kuhn, M., Jensen, L.J., von Mering, C., Bork, P., 2016. eggNOG 4.5: a hierarchical orthology framework with improved functional annotations for eukaryotic, prokaryotic and viral sequences. Nucleic Acids Res. 44, D286–D293. https://doi.org/10.1093/nar/gkv1248

Ignatova, Z., Gierasch, L.M., 2006. Inhibition of protein aggregation in vitro and in vivo by a natural osmoprotectant. Proc. Natl. Acad. Sci. U. S. A. 103, 13357–13361. https://doi.org/10.1073/pnas.0603772103

Ignatova, Z., Krishnan, B., Bombardier, J.P., Marcelino, A.M.C., Hong, J., Gierasch, L.M., 2007. From the test tube to the cell: Exploring the folding and aggregation of a β-clam protein. Biopolymers 88, 157–163. https://doi.org/10.1002/bip.20665

Jaspard, E., Hunault, G., 2016. sHSPdb: a database for the analysis of small Heat Shock Proteins. BMC Plant Biol. 16. https://doi.org/10.1186/s12870-016-0820-6

Jiang, C., Xu, J., Zhang, H., Zhang, X., Shi, J., Li, M., Ming, F., 2009. A cytosolic class I small heat shock protein, RcHSP17.8, of Rosa chinensis confers resistance to a variety of stresses to Escherichia coli, yeast and Arabidopsis thaliana. Plant Cell Environ. 32, 1046–1059. https://doi.org/10.1111/j.1365-3040.2009.01987.x

Kåhrström, C.T., 2013. Entering a post-antibiotic era? Nat. Rev. Microbiol. 11, 146.

Kappes, R.M., Kempf, B., Bremer, E., 1996. Three transport systems for the osmoprotectant glycine betaine operate in Bacillus subtilis: characterization of OpuD. J. Bacteriol. 178, 5071–5079.

Kappes, R.M., Kempf, B., Kneip, S., Boch, J., Gade, J., Meier-Wagner, J., Bremer, E., 1999. Two evolutionarily closely related ABC transporters mediate the uptake of choline for synthesis of the osmoprotectant glycine betaine in Bacillus subtilis. Mol. Microbiol. 32, 203–216.

Kempf, B., Bremer, E., 1998. Uptake and synthesis of compatible solutes as microbial stress responses to high-osmolality environments. Arch. Microbiol. 170, 319–330.

Kempf, B., Bremer, E., 1995. OpuA, an osmotically regulated binding protein-dependent transport system for the osmoprotectant glycine betaine in Bacillus subtilis. J. Biol. Chem. 270, 16701–16713.

Khalil, M.W., Sasse, F., Lünsdorf, H., Elnakady, Y.A., Reichenbach, H., 2006. Mechanism of Action of Tubulysin, an Antimitotic Peptide from Myxobacteria. ChemBioChem 7, 678–683. https://doi.org/10.1002/cbic.200500421

Khaskheli, G.B., Zuo, F., Yu, R., Chen, S., 2015. Overexpression of Small Heat Shock Protein Enhances Heat- and Salt-Stress Tolerance of Bifidobacterium longum NCC2705. Curr. Microbiol. 71, 8–15. https://doi.org/10.1007/s00284-015-0811-0

Kim, D.H., Xu, Z.-Y., Hwang, I., 2013. AtHSP17.8 overexpression in transgenic lettuce gives rise to dehydration and salt stress resistance phenotypes through modulation of ABA-mediated signaling. Plant Cell Rep. 32, 1953–1963. https://doi.org/10.1007/s00299-013-1506-2

Kim, R., Kim, K.K., Yokota, H., Kim, S.H., 1998. Small heat shock protein of Methanococcus jannaschii, a hyperthermophile. Proc. Natl. Acad. Sci. U. S. A. 95, 9129–9133.

Kim, Y.I., Levchenko, I., Fraczkowska, K., Woodruff, R.V., Sauer, R.T., Baker, T.A., 2001. Molecular determinants of complex formation between Clp/Hsp100 ATPases and the ClpP peptidase. Nat. Struct. Biol. 8, 230–233. https://doi.org/10.1038/84967

Kirstein, J., Dougan, D.A., Gerth, U., Hecker, M., Turgay, K., 2007. The tyrosine kinase McsB is a regulated adaptor protein for ClpCP. EMBO J. 26, 2061–2070. https://doi.org/10.1038/sj.emboj.7601655

Kirstein, J., Hoffmann, A., Lilie, H., Schmidt, R., Rübsamen-Waigmann, H., Brötz-Oesterhelt, H., Mogk, A., Turgay, K., 2009a. The antibiotic ADEP reprogrammes ClpP, switching it from a regulated to an uncontrolled protease: Mechanism of ClpP targeting antibiotic. EMBO Mol. Med. 1, 37–49. https://doi.org/10.1002/emmm.200900002

Kirstein, J., Molière, N., Dougan, D.A., Turgay, K., 2009b. Adapting the machine: adaptor proteins for Hsp100/Clp and AAA+ proteases. Nat. Rev. Microbiol. 7, 589–599. https://doi.org/10.1038/nrmicro2185

Kirstein, J., Schlothauer, T., Dougan, D.A., Lilie, H., Tischendorf, G., Mogk, A., Bukau, B., Turgay, K., 2006. Adaptor protein controlled oligomerization activates the AAA+ protein ClpC. EMBO J. 25, 1481–1491. https://doi.org/10.1038/sj.emboj.7601042

Kirstein, J., Strahl, H., Moliere, N., Hamoen, L.W., Turgay, K., 2008. Localization of general and regulatory proteolysis in Bacillus subtilis cells. Mol Microbiol 70, 682–94. https://doi.org/10.1111/j.1365-2958.2008.06438.x

Kirstein, J., Zühlke, D., Gerth, U., Turgay, K., Hecker, M., 2005. A tyrosine kinase and its activator control the activity of the CtsR heat shock repressor in B. subtilis. EMBO J. 24, 3435–3445. https://doi.org/10.1038/sj.emboj.7600780

Kitagawa, M., Matsumura, Y., Tsuchido, T., 2000. Small heat shock proteins, IbpA and IbpB, are involved in resistances to heat and superoxide stresses in Escherichia coli. FEMS Microbiol. Lett. 184, 165–171.

Koo, B.-M., Kritikos, G., Farelli, J.D., Todor, H., Tong, K., Kimsey, H., Wapinski, I., Galardini, M., Cabal, A., Peters, J.M., Hachmann, A.-B., Rudner, D.Z., Allen, K.N., Typas, A., Gross, C.A., 2017. Construction and Analysis of Two Genome-Scale Deletion Libraries for Bacillus subtilis. Cell Syst. 4, 291-305.e7. https://doi.org/10.1016/j.cels.2016.12.013

Koul, A., Vranckx, L., Dendouga, N., Balemans, W., Van den Wyngaert, I., Vergauwen, K., Göhlmann, H.W.H., Willebrords, R., Poncelet, A., Guillemont, J., Bald, D., Andries, K., 2008. Diarylquinolines are bactericidal for dormant mycobacteria as a result of disturbed ATP homeostasis. J. Biol. Chem. 283, 25273–25280. https://doi.org/10.1074/jbc.M803899200

Krajewski, S.S., Joswig, M., Nagel, M., Narberhaus, F., 2014. A tricistronic heat shock operon is important for stress tolerance of Pseudomonas putida and conserved in many environmental bacteria. Environ. Microbiol. 16, 1835–1853. https://doi.org/10.1111/1462-2920.12432

Kress, W., Mutschler, H., Weber-Ban, E., 2009. Both ATPase Domains of ClpA Are Critical for Processing of Stable Protein Structures. J. Biol. Chem. 284, 31441–31452. https://doi.org/10.1074/jbc.M109.022319

Kress, W., Mutschler, H., Weber-Ban, E., 2007. Assembly pathway of an AAA+ protein: tracking ClpA and ClpAP complex formation in real time. Biochemistry 46, 6183–6193. https://doi.org/10.1021/bi602616t

Krüger, E., Zühlke, D., Witt, E., Ludwig, H., Hecker, M., 2001. Clp-mediated proteolysis in Gram-positive bacteria is autoregulated by the stability of a repressor. EMBO J. 20, 852–863. https://doi.org/10.1093/emboj/20.4.852

Kuang, J., Liu, J., Mei, J., Wang, C., Hu, H., Zhang, Y., Sun, M., Ning, X., Xiao, L., Yang, L., 2017. A Class II small heat shock protein OsHsp18.0 plays positive roles in both biotic and abiotic defense responses in rice. Sci. Rep. 7. https://doi.org/10.1038/s41598-017-11882-x

Kurthkoti, K., Amin, H., Marakalala, M.J., Ghanny, S., Subbian, S., Sakatos, A., Livny, J., Fortune, S.M., Berney, M., Rodriguez, G.M., 2017. The Capacity of Mycobacterium tuberculosis To Survive Iron Starvation Might Enable It To Persist in Iron-Deprived Microenvironments of Human Granulomas. mBio 8. https://doi.org/10.1128/mBio.01092-17

Kwon, H.-Y., Ogunniyi, A.D., Choi, M.-H., Pyo, S.-N., Rhee, D.-K., Paton, J.C., 2004. The ClpP protease of Streptococcus pneumoniae modulates virulence gene expression and protects against fatal pneumococcal challenge. Infect. Immun. 72, 5646–5653. https://doi.org/10.1128/IAI.72.10.5646-5653.2004

Laemmli, U.K., 1970. Cleavage of structural proteins during the assembly of the head of bacteriophage T4. Nature 227, 680–685.

Laksanalamai, P., Robb, F.T., 2004. Small heat shock proteins from extremophiles: a review. Extrem. Life Extreme Cond. 8, 1–11. https://doi.org/10.1007/s00792-003-0362-3

Lanyi, J.K., 1974. Salt-dependent properties of proteins from extremely halophilic bacteria. Bacteriol. Rev. 38, 272–290.

Lelj-Garolla, B., Mauk, A.G., 2006. Self-association and Chaperone Activity of Hsp27 Are Thermally Activated. J. Biol. Chem. 281, 8169–8174. https://doi.org/10.1074/jbc.M512553200

Lewis, K., 2012. Persister Cells: Molecular Mechanisms Related to Antibiotic Tolerance, in: Coates, A.R.M. (Ed.), Antibiotic Resistance. Springer Berlin Heidelberg, Berlin, Heidelberg, pp. 121–133. https://doi.org/10.1007/978-3-642-28951-4_8

Lewis, P.J., Marston, A.L., 1999. GFP vectors for controlled expression and dual labelling of protein fusions in Bacillus subtilis. Gene 227, 101–110.

Li, Z.-Y., Long, R.-C., Zhang, T.-J., Yang, Q.-C., Kang, J.-M., 2016. Molecular cloning and characterization of the MsHSP17.7 gene from Medicago sativa L. Mol. Biol. Rep. 43, 815–826. https://doi.org/10.1007/s11033-016-4008-9

Lindner, A.B., Madden, R., Demarez, A., Stewart, E.J., Taddei, F., 2008. Asymmetric segregation of protein aggregates is associated with cellular aging and rejuvenation. Proc. Natl. Acad. Sci. U. S. A. 105, 3076–3081. https://doi.org/10.1073/pnas.0708931105

Liu, J., Mei, Z., Li, N., Qi, Y., Xu, Y., Shi, Y., Wang, F., Lei, J., Gao, N., 2013. Structural Dynamics of the MecA-ClpC Complex: A TYPE II AAA $^+$ PROTEIN UNFOLDING MACHINE. J. Biol. Chem. 288, 17597–17608. https://doi.org/10.1074/jbc.M113.458752

Livak, K.J., Schmittgen, T.D., 2001. Analysis of relative gene expression data using real-time quantitative PCR and the 2(-Delta Delta C(T)) Method. Methods San Diego Calif 25, 402–408. https://doi.org/10.1006/meth.2001.1262

Low, P.S., 1985. Molecular Basis of the Biological Compatibility of Nature's Osmolytes, in: Gilles, R., Gilles-Baillien, M. (Eds.), Transport Processes, Iono- and Osmoregulation. Springer Berlin Heidelberg, Berlin, Heidelberg, pp. 469–477. https://doi.org/10.1007/978-3-642-70613-4_39

Lupoli, T.J., Vaubourgeix, J., Burns-Huang, K., Gold, B., 2018. Targeting the Proteostasis Network for Mycobacterial Drug Discovery. ACS Infect. Dis. 4, 478–498. https://doi.org/10.1021/acsinfecdis.7b00231

Maaroufi, H., Tanguay, R.M., 2013. Analysis and Phylogeny of Small Heat Shock Proteins from Marine Viruses and Their Cyanobacteria Host. PLoS ONE 8, e81207. https://doi.org/10.1371/journal.pone.0081207

Machiels, B.M., Henfling, M.E.R., Gerards, W.L.H., Broers, J.L.V., Bloemendal, H., Ramaekers, F.C.S., Schutte, B., 1997. Detailed analysis of cell cycle kinetics upon proteasome inhibition. Cytometry 28, 243–252. https://doi.org/10.1002/(SICI)1097-0320(19970701)28:3<243::AID-CYTO9>3.0.CO;2-E

MacMicking, J.D., North, R.J., LaCourse, R., Mudgett, J.S., Shah, S.K., Nathan, C.F., 1997. Identification of nitric oxide synthase as a protective locus against tuberculosis. Proc. Natl. Acad. Sci. U. S. A. 94, 5243–5248.

Mandal, S., Njikan, S., Kumar, A., Early, J.V., Parish, T., 2019. The relevance of persisters in tuberculosis drug discovery. Microbiology 165, 492–499. https://doi.org/10.1099/mic.0.000760

Mariathasan, S., Tan, M.-W., 2017. Antibody–Antibiotic Conjugates: A Novel Therapeutic Platform against Bacterial Infections. Trends Mol. Med. 23, 135–149. https://doi.org/10.1016/j.molmed.2016.12.008

Marsee, J.D., Ridings, A., Yu, T., Miller, J.M., 2018. Mycobacterium tuberculosis ClpC1 N-Terminal Domain Is Dispensable for Adaptor Protein-Dependent Allosteric Regulation. Int. J. Mol. Sci. 19. https://doi.org/10.3390/ijms19113651

Martin, null, Ciulla, null, Roberts, null, 1999. Osmoadaptation in archaea. Appl. Environ. Microbiol. 65, 1815–1825.

Martin, A., Baker, T.A., Sauer, R.T., 2005. Rebuilt AAA + motors reveal operating principles for ATP-fuelled machines. Nature 437, 1115.

Mchaourab, H.S., Dodson, E.K., Koteiche, H.A., 2002. Mechanism of chaperone function in small heat shock proteins. Two-mode binding of the excited states of T4 lysozyme mutants by alphaA-crystallin. J. Biol. Chem. 277, 40557–40566. https://doi.org/10.1074/jbc.M206250200

McHaourab, H.S., Godar, J.A., Stewart, P.L., 2009. Structure and mechanism of protein stability sensors: chaperone activity of small heat shock proteins. Biochemistry 48, 3828–3837. https://doi.org/10.1021/bi900212j

McHaourab, H.S., Lin, Y.-L., Spiller, B.W., 2012. Crystal structure of an activated variant of small heat shock protein Hsp16.5. Biochemistry 51, 5105–5112. https://doi.org/10.1021/bi300525x

McKenney, P.T., Driks, A., Eichenberger, P., 2013. The Bacillus subtilis endospore: assembly and functions of the multilayered coat. Nat. Rev. Microbiol. 11, 33–44. https://doi.org/10.1038/nrmicro2921

McKenney, P.T., Driks, A., Eskandarian, H.A., Grabowski, P., Guberman, J., Wang, K.H., Gitai, Z., Eichenberger, P., 2010. A distance-weighted interaction map reveals a previously uncharacterized layer of the Bacillus subtilis spore coat. Curr. Biol. CB 20, 934–938. https://doi.org/10.1016/j.cub.2010.03.060

McKenney, P.T., Eichenberger, P., 2012. Dynamics of spore coat morphogenesis in Bacillus subtilis. Mol. Microbiol. 83, 245–260. https://doi.org/10.1111/j.1365-2958.2011.07936.x

Medema, M.H., Fischbach, M.A., 2015. Computational approaches to natural product discovery. Nat. Chem. Biol. 11, 639–648. https://doi.org/10.1038/nchembio.1884

Mevarech, M., Eisenberg, H., Neumann, E., 1977. Malate dehydrogenase isolated from extremely halophilic bacteria of the Dead Sea. 1. Purification and molecular characterization. Biochemistry 16, 3781–3785.

Miethke, M., Hecker, M., Gerth, U., 2006. Involvement of Bacillus subtilis ClpE in CtsR degradation and protein quality control. J. Bacteriol. 188, 4610–4619. https://doi.org/10.1128/JB.00287-06

Mogk, A., Deuerling, E., Vorderwülbecke, S., Vierling, E., Bukau, B., 2003a. Small heat shock proteins, ClpB and the DnaK system form a functional triade in reversing protein aggregation. Mol. Microbiol. 50, 585–595.

Mogk, A., Homuth, G., Scholz, C., Kim, L., Schmid, F.X., Schumann, W., 1997. The GroE chaperonin machine is a major modulator of the CIRCE heat shock regulon of Bacillus subtilis. EMBO J 16, 4579–90.

Mogk, A., Kummer, E., Bukau, B., 2015. Cooperation of Hsp70 and Hsp100 chaperone machines in protein disaggregation. Front. Mol. Biosci. 2. https://doi.org/10.3389/fmolb.2015.00022

Mogk, A., Schlieker, C., Friedrich, K.L., Schönfeld, H.-J., Vierling, E., Bukau, B., 2003b. Refolding of substrates bound to small Hsps relies on a disaggregation reaction mediated most efficiently by ClpB/DnaK. J. Biol. Chem. 278, 31033–31042. https://doi.org/10.1074/jbc.M303587200

Moliere, N., 2012. The Role of Bacillus subtilis Clp/Hsp100 Proteases in the Regulation of Swimming Motility and Stress Response. Leibniz Universität Hannover.

Molière, N., Hoßmann, J., Schäfer, H., Turgay, K., 2016. Role of Hsp100/Clp Protease Complexes in Controlling the Regulation of Motility in Bacillus subtilis. Front. Microbiol. 7. https://doi.org/10.3389/fmicb.2016.00315

Molière, N., Turgay, K., 2013. General and regulatory proteolysis in Bacillus subtilis. Subcell. Biochem. 66, 73–103. https://doi.org/10.1007/978-94-007-5940-4_4

Moliere, N., Turgay, K., 2009. Chaperone-protease systems in regulation and protein quality control in Bacillus subtilis. Res Microbiol 160, 637–44. https://doi.org/10.1016/j.resmic.2009.08.020

Monteith, W.B., Cohen, R.D., Smith, A.E., Guzman-Cisneros, E., Pielak, G.J., 2015. Quinary structure modulates protein stability in cells. Proc. Natl. Acad. Sci. 112, 1739–1742. https://doi.org/10.1073/pnas.1417415112

Moses, S., Sinner, T., Zaprasis, A., Stöveken, N., Hoffmann, T., Belitsky, B.R., Sonenshein, A.L., Bremer, E., 2012. Proline Utilization by Bacillus subtilis: Uptake and Catabolism. J. Bacteriol. 194, 745–758. https://doi.org/10.1128/JB.06380-11

Msadek, T., Kunst, F., Rapoport, G., 1994. MecB of Bacillus subtilis, a member of the ClpC ATPase family, is a pleiotropic regulator controlling competence gene expression and growth at high temperature. Proc. Natl. Acad. Sci. 91, 5788–5792. https://doi.org/10.1073/pnas.91.13.5788

Mu, C., Wang, S., Zhang, S., Pan, J., Chen, N., Li, X., Wang, Z., Liu, H., 2011. Small heat shock protein LimHSP16.45 protects pollen mother cells and tapetal cells against extreme temperatures during late zygotene to pachytene stages of meiotic prophase I in David Lily. Plant Cell Rep. 30, 1981–1989. https://doi.org/10.1007/s00299-011-1106-y

Mu, C., Zhang, S., Yu, G., Chen, N., Li, X., Liu, H., 2013. Overexpression of Small Heat Shock Protein LimHSP16.45 in Arabidopsis Enhances Tolerance to Abiotic Stresses. PLoS ONE 8, e82264. https://doi.org/10.1371/journal.pone.0082264

Mulvenna, N., Hantke, I., Burchell, L., Nicod, S., Turgay, K., Wigneshweraraj, S., 2019. Xenogeneic regulation of the ClpCP protease of Bacillus subtilis by a phage-encoded adaptor-like protein. bioRxiv. https://doi.org/10.1101/569657

Muntel, J., Fromion, V., Goelzer, A., Maaβ, S., Mäder, U., Büttner, K., Hecker, M., Becher, D., 2014. Comprehensive Absolute Quantification of the Cytosolic Proteome of *Bacillus subtilis* by Data Independent, Parallel Fragmentation in Liquid Chromatography/Mass Spectrometry (LC/MS ^{E}). Mol. Cell. Proteomics 13, 1008–1019. https://doi.org/10.1074/mcp.M113.032631

Muthusamy, S.K., Dalal, M., Chinnusamy, V., Bansal, K.C., 2017. Genome-wide identification and analysis of biotic and abiotic stress regulation of small heat shock protein (HSP20) family genes in bread wheat. J. Plant Physiol. 211, 100–113. https://doi.org/10.1016/j.jplph.2017.01.004

Nakano, M.M., Hajarizadeh, F., Zhu, Y., Zuber, P., 2001. Loss-of-function mutations in yjbD result in ClpX- and ClpP-independent competence development of Bacillus subtilis. Mol. Microbiol. 42, 383–394.

Nakano, M.M., Nakano, S., Zuber, P., 2002. Spx (YjbD), a negative effector of competence in Bacillus subtilis, enhances ClpC-MecA-ComK interaction. Mol. Microbiol. 44, 1341–1349.

Nakano, S., Zheng, G., Nakano, M.M., Zuber, P., 2002. Multiple pathways of Spx (YjbD) proteolysis in Bacillus subtilis. J. Bacteriol. 184, 3664–3670.

Namy, O., Mock, M., Fouet, A., 1999. Co-existence of *clpB* and *clpC* in the Bacillaceae. FEMS Microbiol. Lett. 173, 297–302. https://doi.org/10.1111/j.1574-6968.1999.tb13517.x

Nathan, C., 2011. Making space for anti-infective drug discovery. Cell Host Microbe 9, 343–348. https://doi.org/10.1016/j.chom.2011.04.013

Nathan, C., Cunningham-Bussel, A., 2013. Beyond oxidative stress: an immunologist's guide to reactive oxygen species. Nat. Rev. Immunol. 13, 349–361. https://doi.org/10.1038/nri3423

Nathan, C., Goldberg, F.M., 2005. The profit problem in antibiotic R&D. Nat. Rev. Drug Discov. 4, 887–891. https://doi.org/10.1038/nrd1878

Nau-Wagner, G., Boch, J., Le Good JA, null, Bremer, E., 1999. High-affinity transport of choline-O-sulfate and its use as a compatible solute in Bacillus subtilis. Appl. Environ. Microbiol. 65, 560–568.

Nelson, J.W., Sudarsan, N., Furukawa, K., Weinberg, Z., Wang, J.X., Breaker, R.R., 2013. Riboswitches in eubacteria sense the second messenger c-di-AMP. Nat. Chem. Biol. 9, 834–839. https://doi.org/10.1038/nchembio.1363

Nicolas, P., Mäder, U., Dervyn, E., Rochat, T., Leduc, A., Pigeonneau, N., Bidnenko, E., Marchadier, E., Hoebeke, M., Aymerich, S., Becher, D., Bisicchia, P., Botella, E., Delumeau, O., Doherty, G., Denham, E.L., Fogg, M.J., Fromion, V., Goelzer, A., Hansen, A., Härtig, E., Harwood, C.R., Homuth, G., Jarmer, H., Jules, M., Klipp, E., Le Chat, L., Lecointe, F., Lewis, P., Liebermeister, W., March, A., Mars, R.A.T., Nannapaneni, P., Noone, D., Pohl, S., Rinn, B., Rügheimer, F., Sappa, P.K., Samson, F., Schaffer, M., Schwikowski, B., Steil, L., Stülke, J., Wiegert, T., Devine, K.M., Wilkinson, A.J., van Dijl, J.M., Hecker, M., Völker, U., Bessières, P., Noirot, P., 2012. Condition-dependent transcriptome reveals high-level regulatory architecture in Bacillus subtilis. Science 335, 1103–1106. https://doi.org/10.1126/science.1206848

Nurminen, M., Butcher, S., Idänpään-Heikkilä, Ii., Wahlström, E., Muttilainen, S., Runeberg-Nyman, K., Sarvas, M., Mäkelä, P.H., 1992. The class 1 outer membrane protein of Neisseria meningitidis produced in Bacillus subtilis can give rise to protective immunity. Mol. Microbiol. 6, 2499–2506. https://doi.org/10.1111/j.1365-2958.1992.tb01426.x

Oguchi, Y., Kummer, E., Seyffer, F., Berynskyy, M., Anstett, B., Zahn, R., Wade, R.C., Mogk, A., Bukau, B., 2012. A tightly regulated molecular toggle controls AAA+ disaggregase. Nat. Struct. Mol. Biol. 19, 1338–1346. https://doi.org/10.1038/nsmb.2441

Ojha, J., Masilamoni, G., Dunlap, D., Udoff, R.A., Cashikar, A.G., 2011. Sequestration of Toxic Oligomers by HspB1 as a Cytoprotective Mechanism. Mol. Cell. Biol. 31, 3146–3157. https://doi.org/10.1128/MCB.01187-10

Ollinger, J., O'Malley, T., Kesicki, E.A., Odingo, J., Parish, T., 2012. Validation of the Essential ClpP Protease in Mycobacterium tuberculosis as a Novel Drug Target. J. Bacteriol. 194, 663–668. https://doi.org/10.1128/JB.06142-11

Oren, A., 2008. Microbial life at high salt concentrations: phylogenetic and metabolic diversity. Saline Syst. 4, 2. https://doi.org/10.1186/1746-1448-4-2

Ortega, J., 2002. Alternating translocation of protein substrates from both ends of ClpXP protease. EMBO J. 21, 4938–4949. https://doi.org/10.1093/emboj/cdf483

Ozeki, Y., Igarashi, M., Doe, M., Tamaru, A., Kinoshita, N., Ogura, Y., Iwamoto, T., Sawa, R., Umekita, M., Enany, S., Nishiuchi, Y., Osada-Oka, M., Hayashi, T., Niki, M., Tateishi, Y., Hatano, M., Matsumoto, S., 2015. A New Screen for Tuberculosis Drug Candidates Utilizing a Luciferase-Expressing Recombinant Mycobacterium bovis Bacillus Calmette-Guéren. PloS One 10, e0141658. https://doi.org/10.1371/journal.pone.0141658

Pan, Q., Garsin, D.A., Losick, R., 2001. Self-reinforcing activation of a cell-specific transcription factor by proteolysis of an anti-sigma factor in B. subtilis. Mol. Cell 8, 873–883.

Pan, Q., Losick, R., 2003. Unique degradation signal for ClpCP in Bacillus subtilis. J. Bacteriol. 185, 5275–5278.

Paredes, C.J., Alsaker, K.V., Papoutsakis, E.T., 2005. A comparative genomic view of clostridial sporulation and physiology. Nat. Rev. Microbiol. 3, 969–978. https://doi.org/10.1038/nrmicro1288

Paul, A., Rao, S., Mathur, S., 2016. The α-Crystallin Domain Containing Genes: Identification, Phylogeny and Expression Profiling in Abiotic Stress, Phytohormone Response and

Development in Tomato (Solanum lycopersicum). Front. Plant Sci. 7, 426. https://doi.org/10.3389/fpls.2016.00426

Persuh, M., Mandic-Mulec, I., Dubnau, D., 2002. A MecA paralog, YpbH, binds ClpC, affecting both competence and sporulation. J. Bacteriol. 184, 2310–2313.

Persuh, M., Turgay, K., Mandic-Mulec, I., Dubnau, D., 1999. The N- and C-terminal domains of MecA recognize different partners in the competence molecular switch. Mol. Microbiol. 33, 886–894.

Pestka, S., 1971. Inhibitors of Ribosome Functions. Annu. Rev. Microbiol. 25, 487–562. https://doi.org/10.1146/annurev.mi.25.100171.002415

Plaza del Pino, I.M., Sanchez-Ruiz, J.M., 1995. An osmolyte effect on the heat capacity change for protein folding. Biochemistry 34, 8621–8630.

Posner, M., Kiss, A.J., Skiba, J., Drossman, A., Dolinska, M.B., Hejtmancik, J.F., Sergeev, Y.V., 2012. Functional validation of hydrophobic adaptation to physiological temperature in the small heat shock protein αA-crystallin. PloS One 7, e34438. https://doi.org/10.1371/journal.pone.0034438

Prepiak, P., Dubnau, D., 2007. A peptide signal for adapter protein-mediated degradation by the AAA+ protease ClpCP. Mol. Cell 26, 639–647. https://doi.org/10.1016/j.molcel.2007.05.011

Radeck, J., Kraft, K., Bartels, J., Cikovic, T., Dürr, F., Emenegger, J., Kelterborn, S., Sauer, C., Fritz, G., Gebhard, S., Mascher, T., 2013. The Bacillus BioBrick Box: generation and evaluation of essential genetic building blocks for standardized work with Bacillus subtilis. J. Biol. Eng. 7, 29. https://doi.org/10.1186/1754-1611-7-29

Raghunathan, A., Ferguson, H.R., Bornarth, C.J., Song, W., Driscoll, M., Lasken, R.S., 2005. Genomic DNA Amplification from a Single Bacterium. Appl. Environ. Microbiol. 71, 3342–3347. https://doi.org/10.1128/AEM.71.6.3342-3347.2005

Record, M.T., Courtenay, E.S., Cayley, S., Guttman, H.J., 1998. Biophysical compensation mechanisms buffering E. coli protein-nucleic acid interactions against changing environments. Trends Biochem. Sci. 23, 190–194.

Reischl, S., Thake, S., Homuth, G., Schumann, W., 2001. Transcriptional analysis of three Bacillus subtilis genes coding for proteins with the alpha-crystallin domain characteristic of small heat shock proteins. FEMS Microbiol. Lett. 194, 99–103.

Rice, S.A., Givskov, M., Høiby, N., Parsek, M.R., Riedel, K., Heydorn, A., Eberl, L., Andersen, J.B., Hentzer, M., Molin, S., Kjelleberg, S., Rasmussen, T.B., 2002. Inhibition of quorum sensing in Pseudomonas aeruginosa biofilm bacteria by a halogenated furanone compound. Microbiology 148, 87–102. https://doi.org/10.1099/00221287-148-1-87

Roberts, M.F., 2005. Organic compatible solutes of halotolerant and halophilic microorganisms. Saline Syst. 1, 5. https://doi.org/10.1186/1746-1448-1-5

Rochat, T., Nicolas, P., Delumeau, O., Rabatinová, A., Korelusová, J., Leduc, A., Bessières, P., Dervyn, E., Krásny, L., Noirot, P., 2012. Genome-wide identification of genes directly regulated by the pleiotropic transcription factor Spx in Bacillus subtilis. Nucleic Acids Res. 40, 9571–9583. https://doi.org/10.1093/nar/gks755

Rouquette, C., de Chastellier, C., Nair, S., Berche, P., 1998. The ClpC ATPase of Listeria monocytogenes is a general stress protein required for virulence and promoting early bacterial escape from the phagosome of macrophages. Mol. Microbiol. 27, 1235–1245.

Rouquette, C., Ripio, M.-T., Pellegrini, E., Bolla, J.-M., Tascon, R.I., Vazquez-Boland, J.-A., Berche, P., 1996. Identification of a ClpC ATPase required for stress tolerance and in vivo survival of Listeria monocytogenes. Mol. Microbiol. 21, 977–987. https://doi.org/10.1046/j.1365-2958.1996.641432.x

Ruibal, C., Castro, A., Carballo, V., Szabados, L., Vidal, S., 2013. Recovery from heat, salt and osmotic stress in Physcomitrella patens requires a functional small heat shock protein PpHsp16.4. BMC Plant Biol. 13, 174. https://doi.org/10.1186/1471-2229-13-174

Runde, S., Molière, N., Heinz, A., Maisonneuve, E., Janczikowski, A., Elsholz, A.K.W., Gerth, U., Hecker, M., Turgay, K., 2014. The role of thiol oxidative stress response in heat-induced protein aggregate formation during thermotolerance in Bacillus subtilis. Mol. Microbiol. 91, 1036–1052. https://doi.org/10.1111/mmi.12521

Salas-Muñoz, S., Gómez-Anduro, G., Delgado-Sánchez, P., Rodríguez-Kessler, M., Jiménez-Bremont, J.F., 2012. The Opuntia streptacantha OpsHSP18 gene confers salt and osmotic stress tolerance in Arabidopsis thaliana. Int. J. Mol. Sci. 13, 10154–10175. https://doi.org/10.3390/ijms130810154

Sambrook, J., Russell, D.W., 2001. Molecular cloning: a laboratory manual, 3rd ed. ed. Cold Spring Harbor Laboratory Press, Cold Spring Harbor, N.Y.

Sandhu, D., Cornacchione, M.V., Ferreira, J.F.S., Suarez, D.L., 2017. Variable salinity responses of 12 alfalfa genotypes and comparative expression analyses of salt-response genes. Sci. Rep. 7, 42958. https://doi.org/10.1038/srep42958

Santoro, M.M., Liu, Y., Khan, S.M., Hou, L.X., Bolen, D.W., 1992. Increased thermal stability of proteins in the presence of naturally occurring osmolytes. Biochemistry 31, 5278–5283.

Sarkar, M., Li, C., Pielak, G.J., 2013. Soft interactions and crowding. Biophys. Rev. 5, 187–194. https://doi.org/10.1007/s12551-013-0104-4

Sarkar, N.K., Kim, Y.-K., Grover, A., 2009. Rice sHsp genes: genomic organization and expression profiling under stress and development. BMC Genomics 10, 393. https://doi.org/10.1186/1471-2164-10-393

Sass, P., Josten, M., Famulla, K., Schiffer, G., Sahl, H.-G., Hamoen, L., Brotz-Oesterhelt, H., 2011. Antibiotic acyldepsipeptides activate ClpP peptidase to degrade the cell division protein FtsZ. Proc. Natl. Acad. Sci. 108, 17474–17479. https://doi.org/10.1073/pnas.1110385108

Sassetti, C.M., Boyd, D.H., Rubin, E.J., 2003. Genes required for mycobacterial growth defined by high density mutagenesis. Mol. Microbiol. 48, 77–84.

Sauer, C., Syvertsson, S., Bohorquez, L.C., Cruz, R., Harwood, C.R., van Rij, T., Hamoen, L.W., 2016. Effect of Genome Position on Heterologous Gene Expression in Bacillus subtilis: An Unbiased Analysis. ACS Synth. Biol. 5, 942–947. https://doi.org/10.1021/acssynbio.6b00065

Sauer, R.T., Baker, T.A., 2011. AAA+ proteases: ATP-fueled machines of protein destruction. Annu. Rev. Biochem. 80, 587–612. https://doi.org/10.1146/annurev-biochem-060408-172623

Schägger, H., von Jagow, G., 1991. Blue native electrophoresis for isolation of membrane protein complexes in enzymatically active form. Anal. Biochem. 199, 223–231.

Schlesinger, A.P., Wang, Y., Tadeo, X., Millet, O., Pielak, G.J., 2011. Macromolecular Crowding Fails To Fold a Globular Protein in Cells. J. Am. Chem. Soc. 133, 8082–8085. https://doi.org/10.1021/ja201206t

Schlothauer, T., Mogk, A., Dougan, D.A., Bukau, B., Turgay, K., 2003. MecA, an adaptor protein necessary for ClpC chaperone activity. Proc. Natl. Acad. Sci. U. S. A. 100, 2306–2311. https://doi.org/10.1073/pnas.0535717100

Schmidt, A., Trentini, D.B., Spiess, S., Fuhrmann, J., Ammerer, G., Mechtler, K., Clausen, T., 2014. Quantitative Phosphoproteomics Reveals the Role of Protein Arginine Phosphorylation in the Bacterial Stress Response. Mol. Cell. Proteomics 13, 537–550. https://doi.org/10.1074/mcp.M113.032292

Schmitt, E.K., Riwanto, M., Sambandamurthy, V., Roggo, S., Miault, C., Zwingelstein, C., Krastel, P., Noble, C., Beer, D., Rao, S.P.S., Au, M., Niyomrattanakit, P., Lim, V., Zheng, J., Jeffery, D., Pethe, K., Camacho, L.R., 2011. The Natural Product Cyclomarin Kills Mycobacterium Tuberculosis by Targeting the ClpC1 Subunit of the Caseinolytic Protease. Angew. Chem. 123, 6011–6013. https://doi.org/10.1002/ange.201101740

Schmitz, K.R., Sauer, R.T., 2014. Substrate delivery by the AAA+ ClpX and ClpC1 unfoldases activates the mycobacterial ClpP1P2 peptidase. Mol. Microbiol. 93, 617–628. https://doi.org/10.1111/mmi.12694

Seyffer, F., Kummer, E., Oguchi, Y., Winkler, J., Kumar, M., Zahn, R., Sourjik, V., Bukau, B., Mogk, A., 2012. Hsp70 proteins bind Hsp100 regulatory M domains to activate AAA+ disaggregase at aggregate surfaces. Nat. Struct. Mol. Biol. 19, 1347–1355. https://doi.org/10.1038/nsmb.2442

Simard, C., Lemieux, R., Côté, S., 2001. Urea substitutes toxic formamide as destabilizing agent in nucleic acid hybridizations with RNA probes. Electrophoresis 22, 2679–2683. https://doi.org/10.1002/1522-2683(200108)22:13<2679::AID-ELPS2679>3.0.CO;2-L

Singer, M.A., Lindquist, S., 1998. Multiple effects of trehalose on protein folding in vitro and in vivo. Mol. Cell 1, 639–648.

Slager, J., Veening, J.-W., 2016. Hard-Wired Control of Bacterial Processes by Chromosomal Gene Location. Trends Microbiol. 24, 788–800. https://doi.org/10.1016/j.tim.2016.06.003

Specht, S., Miller, S.B.M., Mogk, A., Bukau, B., 2011. Hsp42 is required for sequestration of protein aggregates into deposition sites in Saccharomyces cerevisiae. J. Cell Biol. 195, 617–629. https://doi.org/10.1083/jcb.201106037

Spiegelhalter, F., Bremer, E., 1998. Osmoregulation of the opuE proline transport gene from Bacillus subtilis: contributions of the sigma A- and sigma B-dependent stress-responsive promoters. Mol. Microbiol. 29, 285–296.

Stadmiller, S.S., Gorensek-Benitez, A.H., Guseman, A.J., Pielak, G.J., 2017. Osmotic Shock Induced Protein Destabilization in Living Cells and Its Reversal by Glycine Betaine. J. Mol. Biol. 429, 1155–1161. https://doi.org/10.1016/j.jmb.2017.03.001

Stannek, L., Gunka, K., Care, R.A., Gerth, U., Commichau, F.M., 2015. Factors that mediate and prevent degradation of the inactive and unstable GudB protein in Bacillus subtilis. Front. Microbiol. 5. https://doi.org/10.3389/fmicb.2014.00758

Steil, L., Hoffmann, T., Budde, I., Völker, U., Bremer, E., 2003. Genome-Wide Transcriptional Profiling Analysis of Adaptation of Bacillus subtilis to High Salinity. J. Bacteriol. 185, 6358–6370. https://doi.org/10.1128/JB.185.21.6358-6370.2003

Steinmetz, H., Li, J., Fu, C., Zaburannyi, N., Kunze, B., Harmrolfs, K., Schmitt, V., Herrmann, J., Reichenbach, H., Höfle, G., Kalesse, M., Müller, R., 2016. Isolation, Structure Elucidation, and (Bio)Synthesis of Haprolid, a Cell-Type-Specific Myxobacterial Cytotoxin. Angew. Chem. Int. Ed. 55, 10113–10117. https://doi.org/10.1002/anie.201603288

Straus, D., Walter, W., Gross, C.A., 1990. DnaK, DnaJ, and GrpE heat shock proteins negatively regulate heat shock gene expression by controlling the synthesis and stability of sigma 32. Genes Dev. 4, 2202–2209. https://doi.org/10.1101/gad.4.12a.2202

Streit, W.R., Schmitz, R.A., 2004. Metagenomics – the key to the uncultured microbes. Curr. Opin. Microbiol. 7, 492–498. https://doi.org/10.1016/j.mib.2004.08.002

Stromer, T., Ehrnsperger, M., Gaestel, M., Buchner, J., 2003. Analysis of the interaction of small heat shock proteins with unfolding proteins. J. Biol. Chem. 278, 18015–18021. https://doi.org/10.1074/jbc.M301640200

Stülke, J., Hanschke, R., Hecker, M., 1993. Temporal activation of beta-glucanase synthesis in Bacillus subtilis is mediated by the GTP pool. J. Gen. Microbiol. 139, 2041–2045. https://doi.org/10.1099/00221287-139-9-2041

Sun, W., Van Montagu, M., Verbruggen, N., 2002. Small heat shock proteins and stress tolerance in plants. Biochim. Biophys. Acta 1577, 1–9.

Sun, Y., MacRae, T.H., 2005. The small heat shock proteins and their role in human disease: Small heat shock proteins and disease. FEBS J. 272, 2613–2627. https://doi.org/10.1111/j.1742-4658.2005.04708.x

Suskiewicz, M.J., Hajdusits, B., Beveridge, R., Heuck, A., Vu, L.D., Kurzbauer, R., Hauer, K., Thoeny, V., Rumpel, K., Mechtler, K., Meinhart, A., Clausen, T., 2019. Structure of McsB, a protein kinase for regulated arginine phosphorylation. Nat. Chem. Biol. 15, 510–518. https://doi.org/10.1038/s41589-019-0265-y

Tanner, A.W., Carabetta, V.J., Dubnau, D., 2018. ClpC and MecA, components of a proteolytic machine, prevent Spo0A-P-dependent transcription without degradation: ClpC and MecA prevent Spo0A-P-dependent transcription. Mol. Microbiol. 108, 178–186. https://doi.org/10.1111/mmi.13928

Tessarz, P., Mogk, A., Bukau, B., 2008. Substrate threading through the central pore of the Hsp104 chaperone as a common mechanism for protein disaggregation and prion propagation. Mol. Microbiol. 68, 87–97. https://doi.org/10.1111/j.1365-2958.2008.06135.x

Thomas, J.G., Baneyx, F., 1998. Roles of the Escherichia coli small heat shock proteins IbpA and IbpB in thermal stress management: comparison with ClpA, ClpB, and HtpG In vivo. J. Bacteriol. 180, 5165–5172.

Tian, H., Tan, J., Zhang, L., Gu, X., Xu, W., Guo, X., Luo, Y., 2012. Increase of stress resistance in Lactococcus lactis via a novel food-grade vector expressing a shsp gene from Streptococcus thermophilus. Braz. J. Microbiol. Publ. Braz. Soc. Microbiol. 43, 1157–1164. https://doi.org/10.1590/S1517-838220120003000043

Trentini, D.B., Suskiewicz, M.J., Heuck, A., Kurzbauer, R., Deszcz, L., Mechtler, K., Clausen, T., 2016. Arginine phosphorylation marks proteins for degradation by a Clp protease. Nature 539, 48–53. https://doi.org/10.1038/nature20122

Trigo, G., Martins, T.G., Fraga, A.G., Longatto-Filho, A., Castro, A.G., Azeredo, J., Pedrosa, J., 2013. Phage Therapy Is Effective against Infection by Mycobacterium ulcerans in a Murine Footpad Model. PLoS Negl. Trop. Dis. 7, e2183. https://doi.org/10.1371/journal.pntd.0002183

Turgay, K., 2017. General and Regulatory Proteolysis in Bacillus subtilis, in: Graumann, P.L. (Ed.), Bacillus Cellular and Molecular Biology. Caister Academic Press, Norfolk, UK, pp. 191–222.

Turgay, K., Hahn, J., Burghoorn, J., Dubnau, D., 1998. Competence in Bacillus subtilis is controlled by regulated proteolysis of a transcription factor. EMBO J. 17, 6730–6738. https://doi.org/10.1093/emboj/17.22.6730

Turgay, K., Hamoen, L.W., Venema, G., Dubnau, D., 1997. Biochemical characterization of a molecular switch involving the heat shock protein ClpC, which controls the activity of ComK, the competence transcription factor of Bacillus subtilis. Genes Dev. 11, 119–128.

Turgay, K., Persuh, M., Hahn, J., Dubnau, D., 2001. Roles of the two ClpC ATP binding sites in the regulation of competence and the stress response. Mol. Microbiol. 42, 717–727.

Ulaczyk-Lesanko, A., Hall, D.G., 2005. Wanted: new multicomponent reactions for generating libraries of polycyclic natural products. Curr. Opin. Chem. Biol. 9, 266–276. https://doi.org/10.1016/j.cbpa.2005.04.003

Ungelenk, S., Moayed, F., Ho, C.-T., Grousl, T., Scharf, A., Mashaghi, A., Tans, S., Mayer, M.P., Mogk, A., Bukau, B., 2016. Small heat shock proteins sequester misfolding proteins in near-native conformation for cellular protection and efficient refolding. Nat. Commun. 7, 13673. https://doi.org/10.1038/ncomms13673

van Montfort, R.L., Basha, E., Friedrich, K.L., Slingsby, C., Vierling, E., 2001. Crystal structure and assembly of a eukaryotic small heat shock protein. Nat. Struct. Biol. 8, 1025–1030. https://doi.org/10.1038/nsb722

Vasudevan, D., Rao, S.P.S., Noble, C.G., 2013. Structural Basis of Mycobacterial Inhibition by Cyclomarin A. J. Biol. Chem. 288, 30883–30891. https://doi.org/10.1074/jbc.M113.493767

Vaubourgeix, J., Lin, G., Dhar, N., Chenouard, N., Jiang, X., Botella, H., Lupoli, T., Mariani, O., Yang, G., Ouerfelli, O., Unser, M., Schnappinger, D., McKinney, J., Nathan, C., 2015. Stressed mycobacteria use the chaperone ClpB to sequester irreversibly oxidized proteins asymmetrically within and between cells. Cell Host Microbe 17, 178–190. https://doi.org/10.1016/j.chom.2014.12.008

Voges, D., Zwickl, P., Baumeister, W., 1999. The 26S Proteasome: A Molecular Machine Designed for Controlled Proteolysis. Annu. Rev. Biochem. 68, 1015–1068. https://doi.org/10.1146/annurev.biochem.68.1.1015

Völker, U., Mach, H., Schmid, R., Hecker, M., 1992. Stress proteins and cross-protection by heat shock and salt stress in Bacillus subtilis. J. Gen. Microbiol. 138, 2125–2135. https://doi.org/10.1099/00221287-138-10-2125

von Blohn, C., Kempf, B., Kappes, R.M., Bremer, E., 1997. Osmostress response in Bacillus subtilis: characterization of a proline uptake system (OpuE) regulated by high osmolarity and the alternative transcription factor sigma B. Mol. Microbiol. 25, 175–187.

Voskuil, M.I., Bartek, I.L., Visconti, K., Schoolnik, G.K., 2011. The response of mycobacterium tuberculosis to reactive oxygen and nitrogen species. Front. Microbiol. 2, 105. https://doi.org/10.3389/fmicb.2011.00105

Wang, F., Mei, Z., Qi, Y., Yan, C., Hu, Q., Wang, J., Shi, Y., 2011. Structure and mechanism of the hexameric MecA–ClpC molecular machine. Nature 471, 331–335. https://doi.org/10.1038/nature09780

Wang, K.H., Isidro, A.L., Domingues, L., Eskandarian, H.A., McKenney, P.T., Drew, K., Grabowski, P., Chua, M.-H., Barry, S.N., Guan, M., Bonneau, R., Henriques, A.O., Eichenberger, P., 2009. The coat morphogenetic protein SpoVID is necessary for spore encasement in Bacillus subtilis. Mol. Microbiol. 74, 634–649. https://doi.org/10.1111/j.1365-2958.2009.06886.x

Wang, M., Zou, Z., Li, Q., Sun, K., Chen, X., Li, X., 2017a. The CsHSP17.2 molecular chaperone is essential for thermotolerance in Camellia sinensis. Sci. Rep. 7, 1237. https://doi.org/10.1038/s41598-017-01407-x

Wang, M., Zou, Z., Li, Q., Xin, H., Zhu, X., Chen, X., Li, X., 2017b. Heterologous expression of three Camellia sinensis small heat shock protein genes confers temperature stress tolerance in yeast and Arabidopsis thaliana. Plant Cell Rep. 36, 1125–1135. https://doi.org/10.1007/s00299-017-2143-y

Wang, Y., Sarkar, M., Smith, A.E., Krois, A.S., Pielak, G.J., 2012. Macromolecular Crowding and Protein Stability. J. Am. Chem. Soc. 134, 16614–16618. https://doi.org/10.1021/ja305300m

Waters, E.R., 2013. The evolution, function, structure, and expression of the plant sHSPs. J. Exp. Bot. 64, 391–403. https://doi.org/10.1093/jxb/ers355

Waters, E.R., Aevermann, B.D., Sanders-Reed, Z., 2008. Comparative analysis of the small heat shock proteins in three angiosperm genomes identifies new subfamilies and reveals diverse evolutionary patterns. Cell Stress Chaperones 13, 127–142. https://doi.org/10.1007/s12192-008-0023-7

Wehmeyer, N., Vierling, E., 2000. The Expression of Small Heat Shock Proteins in Seeds Responds to Discrete Developmental Signals and Suggests a General Protective Role in Desiccation Tolerance. Plant Physiol. 122, 1099–1108. https://doi.org/10.1104/pp.122.4.1099

Weibezahn, J., Schlieker, C., Bukau, B., Mogk, A., 2003. Characterization of a trap mutant of the AAA+ chaperone ClpB. J. Biol. Chem. 278, 32608–32617. https://doi.org/10.1074/jbc.M303653200

Weibezahn, J., Tessarz, P., Schlieker, C., Zahn, R., Maglica, Z., Lee, S., Zentgraf, H., Weber-Ban, E.U., Dougan, D.A., Tsai, F.T.F., Mogk, A., Bukau, B., 2004. Thermotolerance Requires Refolding of Aggregated Proteins by Substrate Translocation through the Central Pore of ClpB. Cell 119, 653–665. https://doi.org/10.1016/j.cell.2004.11.027

Weinhäupl, K., Brennich, M., Kazmaier, U., Lelievre, J., Ballell, L., Goldberg, A., Schanda, P., Fraga, H., 2018. The antibiotic cyclomarin blocks arginine-phosphate-induced millisecond dynamics in the N-terminal domain of ClpC1 from Mycobacterium tuberculosis. J. Biol. Chem. 293, 8379–8393. https://doi.org/10.1074/jbc.RA118.002251

Weissman, K.J., Müller, R., 2009. A brief tour of myxobacterial secondary metabolism. Bioorg. Med. Chem. 17, 2121–2136. https://doi.org/10.1016/j.bmc.2008.11.025

Whatmore, A.M., Chudek, J.A., Reed, R.H., 1990. The effects of osmotic upshock on the intracellular solute pools of Bacillus subtilis. J. Gen. Microbiol. 136, 2527–2535. https://doi.org/10.1099/00221287-136-12-2527

Whatmore, A.M., Reed, R.H., 1990. Determination of turgor pressure in Bacillus subtilis: a possible role for K+ in turgor regulation. J. Gen. Microbiol. 136, 2521–2526. https://doi.org/10.1099/00221287-136-12-2521

Wickner, S., Maurizi, M.R., Gottesman, S., 1999. Posttranslational quality control: folding, refolding, and degrading proteins. Science 286, 1888–1893.

Wiegert, T., Schumann, W., 2001. SsrA-mediated tagging in Bacillus subtilis. J. Bacteriol. 183, 3885–3889. https://doi.org/10.1128/JB.183.13.3885-3889.2001

Wojtyra, U.A., Thibault, G., Tuite, A., Houry, W.A., 2003. The N-terminal Zinc Binding Domain of ClpX Is a Dimerization Domain That Modulates the Chaperone Function. J. Biol. Chem. 278, 48981–48990. https://doi.org/10.1074/jbc.M307825200

Wood, J.M., 2015. Bacterial responses to osmotic challenges. J. Gen. Physiol. 145, 381–388. https://doi.org/10.1085/jgp.201411296

Worthington, R.J., Richards, J.J., Melander, C., 2012. Small molecule control of bacterial biofilms. Org. Biomol. Chem. 10, 7457. https://doi.org/10.1039/c2ob25835h

Wozniak, D.J., Tiwari, K.B., Soufan, R., Jayaswal, R.K., 2012. The mcsB gene of the clpC operon is required for stress tolerance and virulence in Staphylococcus aureus. Microbiol. Read. Engl. 158, 2568–2576. https://doi.org/10.1099/mic.0.060749-0

Wu, Y., Luo, H., Kanaan, N., Wu, J., 2000. The proteasome controls the expression of a proliferation-associated nuclear antigen Ki-67. J. Cell. Biochem. 76, 596–604.

Xiao, Y., Wei, X., Ebright, R., Wall, D., 2011. Antibiotic Production by Myxobacteria Plays a Role in Predation. J. Bacteriol. 193, 4626–4633. https://doi.org/10.1128/JB.05052-11

Yarmolinsky, M.B., Haba, G.L., 1959. INHIBITION BY PUROMYCIN OF AMINO ACID INCORPORATION INTO PROTEIN. Proc. Natl. Acad. Sci. U. S. A. 45, 1721–1729.

Zaprasis, A., Bleisteiner, M., Kerres, A., Hoffmann, T., Bremer, E., 2015. Uptake of Amino Acids and Their Metabolic Conversion into the Compatible Solute Proline Confers Osmoprotection to Bacillus subtilis. Appl. Environ. Microbiol. 81, 250–259. https://doi.org/10.1128/AEM.02797-14

Zaprasis, A., Hoffmann, T., Stannek, L., Gunka, K., Commichau, F.M., Bremer, E., 2014. The -Aminobutyrate Permease GabP Serves as the Third Proline Transporter of Bacillus subtilis. J. Bacteriol. 196, 515–526. https://doi.org/10.1128/JB.01128-13

Zhao, P., Wang, D., Wang, R., Kong, N., Zhang, C., Yang, C., Wu, W., Ma, H., Chen, Q., 2018. Genome-wide analysis of the potato Hsp20 gene family: identification, genomic organization and expression profiles in response to heat stress. BMC Genomics 19, 61. https://doi.org/10.1186/s12864-018-4443-1

Ziemert, N., Alanjary, M., Weber, T., 2016. The evolution of genome mining in microbes – a review. Nat. Prod. Rep. 33, 988–1005. https://doi.org/10.1039/C6NP00025H

Zimmerman, S.B., Minton, A.P., 1993. Macromolecular Crowding: Biochemical, Biophysical, and Physiological Consequences. Annu. Rev. Biophys. Biomol. Struct. 22, 27–65. https://doi.org/10.1146/annurev.bb.22.060193.000331

Zolkiewski, M., 1999. ClpB Cooperates with DnaK, DnaJ, and GrpE in Suppressing Protein Aggregation: A NOVEL MULTI-CHAPERONE SYSTEM FROM *ESCHERICHIA COLI*. J. Biol. Chem. 274, 28083–28086. https://doi.org/10.1074/jbc.274.40.28083

Zweers, J.C., Nicolas, P., Wiegert, T., van Dijl, J.M., Denham, E.L., 2012. Definition of the σ(W) regulon of Bacillus subtilis in the absence of stress. PloS One 7, e48471. https://doi.org/10.1371/journal.pone.0048471

Żwirowski, S., Kłosowska, A., Obuchowski, I., Nillegoda, N.B., Piróg, A., Ziętkiewicz, S., Bukau, B., Mogk, A., Liberek, K., 2017. Hsp70 displaces small heat shock proteins from aggregates to initiate protein refolding. EMBO J. 36, 783–796. https://doi.org/10.15252/embj.201593378

Curriculum vitae

Ingo Hantke - 06.07.1991 in Stadthagen

Ausbildung

10/2015   **Leibniz Universität Hannover (LUH),** *Promotion in Biologie*
09/2019   Hannover, Deutschland
- Forschungsgebiete: Antibiotics, Gene regulation, Cloning, Protein quality control
- Hannover School for Biomolecular Drug Research (HSBDR) – Stipendium

10/2013 –   **LUH,** *Master of Science in Life Sciences* (Note: 1,0 mit Auszeichnung)
09/2015   - Schwerpunkte: Molekularbiologie, Bioprozesstechnik

10/2010 –   **LUH,** *Bachelor of Science in Life Sciences* (Note: 1,0 mit Auszeichnung)
09/2013

08/2003 –   **Wilhelm-Busch-Gymnasium, Stadthagen,** *Abitur* (Note: 1,3)
06/2010

Berufserfahrung

10/2015   **Institut für Mikrobiologie, Wissenschaftlicher Mitarbeiter**
06/2019   LUH, Hannover, Deutschland

03/2014 –   **Institute for Food Engineering, Praktikant**
04/2014   Technion, Haifa, Israel

01/2012 –   **Institut für Mikrobiologie, Hilfswissenschaftler**
03/2015   LUH, Hannover, Deutschland

List of publications

Data part of this work

Hantke, I., Schäfer, H., Janczikowski, A., Turgay, K., (**2018**). YocM a small heat shock protein can protect Bacillus subtilis cells during salt stress. Mol. Microbiol. https://doi.org/10.1111/mmi.14164

Carroni, M., Franke, K.B., Maurer, M., Jäger, J., Hantke, I., Gloge, F., Linder, D., Gremer, S., Turgay, K., Bukau, B., Mogk, A., (**2017**). Regulatory coiled-coil domains promote head-to-head assemblies of AAA+ chaperones essential for tunable activity control. eLife 6. https://doi.org/10.7554/eLife.30120

Not included

Schäfer, H, Beckert, B., Steinchen, W., Nuss, A., Beckstette, M., Hantke, I.,…, Bange, G., Wilson, D., Turgay, K. (**2019**). The alarmone (p)ppGpp is part of the heat shock response of Bacillus subtilis (bioRxiv: https://doi.org/10.1101/688689, submitted to PLoS Genetics)

Hantke, I., Schäfer, H., Kramer, R., Turgay, K. (**2019**). The stressful life of *Bacillus subtilis*. BIOspektrum 02/2019. doi: 10.1007/s12268-019-1023-0

Schäfer, H., Heinz, A., Sudzinová, P., Voß, M., Hantke, I.,…, Turgay, K. (**2018**). Spx, the central regulator of the heat- and oxidative stress response in B. subtilis, can directly repress transcription of translation-related genes. MolMicro. 2018 Nov 27. 10.1111/mmi.14171

Dougan, DA., Hantke, I., Turgay, K. (**2018**). Dysregulating ClpP: From Antibiotics to Anticancer? Cell Chem. Biol., Aug 16;25(8):929-930. doi: 10.1016/j.chembiol.2018.08.002

Manuscripts in preparation

Mulvenna, N., Hantke, I., Burchell, L., Nicod, S., Bell, D., Turgay, K., Wigneshweraraj, S. (**2019**). Modulation of the ClpCP protease of *Bacillus subtilis* by phage-encoded adaptor-like protein. (bioRxiv. https://doi.org/10.1101/569657, accepted Journal of Biological Chemistry)

Hantke, I.*, Kramer, R.*, Gunka, K., Turgay, K. (**2019**). McsB is the main adaptor protein for ClpC mediated disaggregation in *Bacillus subtilis*. (in preparation)

Acknowledgement

Zunächst möchte ich mich bei meinem Doktorvater Prof. Kürsad Turgay in aller Form für die tolle Betreuung während der Promotion bedanken. Die von dir gewährte Freiheit bei meinen Projekten war außerordentlich hilfreich und bildet die Grundlage für die gesamte Arbeit. Dabei standst du mir immer mit Rat und Erfahrung zur Seite. Du hast mir wirklich viel beigebracht. Danke für alles!

Ohne die tollen Kollegen und Kolleginnen im Institut für Mikrobiologie (Eike, Hendrik und Michael) und ganz speziell in der AG Turgay (Regina & Michelle) wäre die Promotion bei weitem nicht so erfolgreich und gleichzeitig unterhaltsam gewesen. Das trifft auch ganz besonders auf das Büro-Team 169 zu (Heinrich & Michael). Es war immer schön, zur Uni zu gehen (sogar am Sonntag, wenn es sein musste…). Insbesondere möchte ich mich ebenfalls bei den technischen Assistentinnen (Armgard & Katrin) für die tolle Unterstützung bedanken. Ihr habt mir sehr geholfen und eine beachtliche Menge Zeit erspart! Außerdem musste ich nicht so früh aufstehen, das mögen Doktoranden ja wirklich gar nicht.

Auch bei allen meinen Kooperationspartnern in Stockholm (Martha Carroni), Heidelberg (Axel Mogk), London (Nancy Mulvenna & Ramesh Wigneshweraraj), South Hadley (Amy Camp) und Berlin (Alex Elsholz & Emmanuelle Charpentier) möchte ich mich für die erfolgreiche Zusammenarbeit in den verschiedenen Projekten und die tolle Betreuung bei den Aufenthalten in Saarbrücken (Rolf Müller & Jennifer Herrmann) und Heidelberg (Nassos Typas & Alex Koumoutsi) bedanken.

Prof. Dr. Marcus Horn danke ich für die Übernahme des Prüfungsvorsitzes und die anregenden Diskussionen bei verschiedenen Vorträgen, sowie Prof. Dr. Jens Boch und PD Dr. Axel Mogk für die Anfertigung des zweiten bzw. dritten Gutachtens meiner Dissertation.

Ganz besonderer Dank gilt meiner Familie (die sich im Laufe der Promotion fast verdoppelt hat!): Ihr wart immer für mich da und habt mir damit sehr geholfen. Während der Promotionszeit war insbesondere die Unterstützung bei der Organisation der Hochzeit fantastisch. Ich wüsste wirklich nicht, wo ich ohne euch stehen würde!

Als letztes gilt mein größter Dank meiner Frau Verena. Du hast mich jederzeit zu 100 % unterstützt und hast mir immer geholfen, den Blick für das Wesentliche nicht zu verlieren. Ohne dich hätte ich die Arbeit niemals so anfertigen können. Danke! Go Team Veringo!